SCUOLA DI DOTTORATO
UNIVERSITÀ DEGLI STUDI DI MILANO-BICOCCA

Department of Biotechnology and Biosciences

PhD program in Science Cycle XXIX

Curriculum in Chemistry

Chemistry and renewable energy: DFT investigation on CO_2 reduction and H_2 oxidation/production catalyzed by transition metal biomimics.

Federica Arrigoni

Registration number: 718417

Tutor: Giuseppe Zampella

Coordinator: Maria Luce Frezzotti

ACADEMIC YEAR 2015/2016

Summary

Chemistry of life involves a huge number of reactions that needs bioinorganic catalysts, such as metalloenzymes, to occur. Metal ions, embedded in the active site of an enzyme, play an essential role in catalysis by virtue of their rich redox chemistry, that allows them to interact with, bind, activate the substrate(s) and also to stabilize possible intermediates along the turnovered reaction. Hence, metal ions provide accessible low energy paths for otherwise chemically demanding transformations. A striking feature of metalloenzymes reactivity is that it is often multi-faceted, including, sometimes, some of the most challenging reactions in chemistry. Indeed metalloenzymes often work with high rates, at room pressure and temperature and by means of only cheap and bioavailable metal ions (such as first row transition metals). Scientists devote intensive efforts in the study of metalloenzyme functioning, with two main scopes. The first is to uncover the basic principles of the reactivity of these natural devices, necessary to achieve such an outstanding efficiency. The second is to transfer these principles into the design of noble-metal-free synthetic devices, such as biomimetic catalysts, able to carry out the same transformations of the native systems. The so-called biomimetic approach is sometimes a necessity, since the direct utilization of metalloenzymes for the development of inexpensive and efficient technological devices, to perform on large scale the reactions of interest, is often prohibitive.

Catalytic cycles of both metalloenzymes and biomimetic compounds usually consist in multi-step processes that involve short-living and often highly reactive intermediates, that can undergo a variety of transformations along different scenarios. This poses serious challenges to the research focused on such systems, whose complexity is even increased by the presence of transition metal ions, intrinsically characterized by a highly versatile and thus complicated chemistry. Therefore, theoretical studies are extremely useful to unravel the main structure-function relationships associated with these systems, allowing to gain information that are out of reach for experimental techniques. In this context, quantum mechanical (QM) tools are particularly suited to address the detailed characterization and description of all species along the catalytic cycle, at both enzymes and homogenous catalysts metal sites, including labile transition states and short-living intermediates.

The focus of the present thesis is the QM investigation, in the Density Functional Theory (DFT) framework, of two specific iron-based metalloenzymes and their related biomimetic catalysts. Both systems under study, namely [FeFe]-hydrogenases and nitrogenases enzymes, are intriguing for their potential application in the biofuel production and energy storage fields. [FeFe]-

hydrogenases, which most of the thesis is dedicated to, catalyze the reversible formation of H_2 from protons and electrons, with surprising rates and close to the thermodynamic potential. They are thus an elegant and, at the same time, cheap solution that Nature has provided in order to store energy in the form of molecular hydrogen, a process that usually requires fossil fuels reforming processes or expensive platinum-based technologies. The interest in nitrogenases arises, instead, from their ability to activate and reduce highly inert substrates. Besides their "conventional" role in dinitrogen biological fixation, nitrogenases have also shown an interesting substrate promiscuity, being also able to reduce small organic unsaturated compounds, among which also carbon dioxide to hydrocarbons. CO_2 recycle through its chemical reduction is a task attracting more and more interest among worldwide scientific community. Indeed, its conversion could lead to value-added chemicals, that can be used as synthetic building-blocks or, remarkably, as fuels.

Both enzyme active sites are composed by iron-sulfur organometallic clusters, and several inorganic and organometallic chemists have been inspired by their structures in the design and synthesis of an ever-increasing number of biomimetic catalysts. Despite their similarity to the enzyme's active site, [FeFe]-hydrogenases biomimetic complexes cannot reach the enzyme efficiency. In the past few decades, extensive efforts in synthetizing H^+ reduction catalysts with improved activity have been done, and they are currently increasing. Several strategies have been followed in order to reproduce some key enzyme structural features that are difficultly conserved in synthetic compounds, but that are at the same time fundamental to guarantee high catalytic performances. By contrast, very few examples of nitrogenases active site analogues have been proposed, and none of them has been tested towards any substrate promiscuity e.g. towards CO_2 reduction.

In the first chapter of this thesis the main information about the functioning and the structure of both [FeFe]-hydrogenases and nitrogenases will be provided, together with a description of the state-of-the-art of related biomimetic compounds developments. Chapter 2 is instead a survey on the theoretical foundation of DFT and its role in the dissection of transition metal complexes chemistry. The investigation of several puzzling issues in the field of [FeFe]-hydrogenase biomimics is instead the subject of Chapter 3, which is organized in a series of subprojects. Some of them have been addressed purely from a computational point of view, while others have implied collaborations with experimental international research groups. Eventually, Chapter 4 regards the theoretical dissection of a class of nitrogenases functional analogues, with particular attention towards their role in carbon dioxide activation and possible conversion into either carbon monoxide or formic acid.

Contents

Chapter 1

Catalysis without precious metals: lessons from Nature

We have to remember that
what we observe is not nature herself,
but nature exposed to our method of questioning.

Werner Heisenberg

1.1 Metalloenzymes and biofuels production

Metalloenzymes are able to catalyze some of the most difficult and yet important reactions in Nature, being the role played by metal ions essential.[1, 2, 3] The discovery that metalloenzymes perform biotechnologically relevant transformations by means of organometallic chemistry principles has spontaneously triggered profitable interactions among scientists.[4, 5] In fact, recent progresses in metalloenzyme biochemistry and organometallic chemistry led to a stronger and stronger linkage between these two apparently distant disciplines. Among the different metals found in these enzymes, first row transition metals (e.g. Fe, Ni, Cu) are surely the most abundant, being involved in several key biological and metabolic processes such as electron transfer, activation and production of energy-related small molecules.[6]

Hydrogen gas is undoubtedly one the most interesting energy-related small molecules, by virtue of its extremely low volumetric energy density along with its clean combustion.[7] There is in fact the prospect that dihydrogen would become a major energy vector in the next future, towards a large scale hydrogen economy e.g. by means of fuel cells-like technologies.[8] Currently, the dominant process for direct generation of dihydrogen is steam reforming from fossil fuels, a well-established industrial scale technology which, however, is not free from drawbacks.[9] Two of the major advantages of the use of dihydrogen as fuel are that it allows to overcome the unsustainable abuse of fossil fuels, which are intrinsically non-renewable on human time scale, and that it could limit greenhouse gases emissions, which have devastating effects on our environment, climate and health. It is clear that, in this scenario, producing H_2 starting from hydrocarbons, through non

"green" industrial processes, appears counter-productive. A clean and promising alternative to steam reforming technologies is to generate dihydrogen from protons and electrons, the chemical conversion on which hydrogen fuel cells are based.[10] Such a reaction, however, requires an electrocatalyst to occur in both forward and backward direction without large overpotentials. The best catalyst for this transformation is platinum, as well as some of its alloys. Platinum is used, for example, in commercial proton exchange membrane (PEM) fuel cells in the form of adsorbed nanoparticles.[11] Unfortunately, being platinum a precious metal, its sustainability is unreliable for a growing hydrogen economy, in terms of both low abundancy and high costs.[12] Nature provides a very powerful strategy to perform the same reaction avoiding the need of noble metals. Hydrogenase enzymes, among which the [FeFe]-variant is the most active, are in fact able to convert protons and electrons into dihydrogen and vice versa, with efficiency approaching the one of platinum and at mild potentials (-0.1 to -0.5 V vs NHC).[13][14] It is not surprising that the discovery of the hydrogenase active site consists of an organometallic cluster has stimulated an intense interest through all the chemical community.[15]

The same general considerations can be made when dealing with nitrogenase enzymes. Nitrogenases are very fascinating from a chemical standpoint: they can efficiently activate and reduce small unsaturated substrates that show high thermodynamic and kinetic inertness.[16] Indeed, besides accomplishing the difficult task of N_2 fixation into ammonia at room temperature and pressure (in contrast with the harsh conditions necessary to perform the famous Haber-Bosh industrial process[17]), they can also convert carbon-containing molecules, such as CO_2, into hydrocarbons.[18, 19] This last reactivity is particularly interesting in the biofuel production/storage framework. Significant scientific and economic imperatives are driving, in fact, the development of CO_2 recycle, through its fixation and conversion into "high-energy" products, which can be used as both building blocks for synthesis and fuels (e.g. formic acid, methane) or energy reservoirs (e.g. for H_2 storage).[20] This valorization of CO_2 would lead to a switch from the present linear utilization of carbon based fuels to a cyclic one.[21] Hence, it is desirable that, in the future, the use of CO_2 as C1 building block will significantly increase, as a result of its lower toxicity and abundant availability in comparison with the widely employed CO.[22] Currently, the major obstacle preventing CO_2 efficient conversion is the lack of cheap and efficient catalysts.[5] Remarkably, whereas the most active homogeneous synthetic catalysts for CO_2 reduction (both chemical and electrochemical) contain noble metals[23], nitrogenases reactivity is ascribed to cheap and bioavailable metals, such as iron.

It is undeniable that finding a strategy to carry out the same transformations catalyzed by hydrogenases and nitrogenases in a practical, cheap and highly efficient way will be crucial to meet the ever-increasing worldwide energy demand. Many efforts have been devoted to understanding both structure and function of these metalloproteins. The ultimate test is to use this knowledge to design synthetic analogues reproducing structures and/or functions of native metalloprotein active sites.[24] In this way, it would be possible to supplant the use of traditional precious metals in favor of inexpensive and abundant ones. Interestingly, both [FeFe]-hydrogenase and nitrogenase cofactors are iron-sulfur organometallic clusters, whose minimal subunit, necessary for catalyzing both proton reduction and N_2/CO_2 fixation, is a Fe_2S_2 core.[13, 25] As a result, the

number of synthesized biomimetic catalysts (particularly featuring a Fe_2S_2 scaffold), as structural and functional models of both enzymes active site, has grown exponentially in recent years. However, several gaps yet need to be fixed, since none of these catalysts can reach the efficiency of the related natural system. Additionally, some questions naturally arise: how does the same chemical unit carry out so many different transformations? Is it possible to transfer the substrate selectivity/promiscuity performed by Nature into synthetic compounds? Since the answers to these interrogatives cannot exclude a deep knowledge of both natural systems, the following sections will provide an overview on both [FeFe]-hydrogenase and nitrogenase enzymes structure and function.

1.2 Nature and H_2 production: the [FeFe]-hydrogenases enzyme

1.2.1 Enzyme architecture and function

Nature has developed its own strategy to produce dihydrogen and to employ it as an energy source by means of a set of highly efficient catalysts: the hydrogenases enzyme.[26] This enzyme is found in a series of microorganisms, including anaerobic eukaryotes, anaerobic prokaryotes, anaerobic fungi and some green algae, where molecular hydrogen plays a central role in their life-sustaining transformations.[27, 28, 29] Three phylogenetically unrelated classes of hydrogenases are known, which are classified according to the metal ions composing their respective active site. In [FeFe]-hydrogenases and [NiFe]-hydrogenases dihydrogen is the only substrate or product, according to $H_2 \rightleftharpoons 2H^+ + 2e^-$, while in the third class, called [Fe]-hydrogenases or iron-sulfur-cluster-free hydrogenases, the hydrogen uptake is coupled to a second substrate (methenyltetrahydromethanopterin).[30, 31, 32] Among them, [FeFe]-hydrogenases feature the largest turnover frequency (up to $9x10^3$ s^{-1}), being approximately 10-100 times more active than [NiFe]-hydrogenases.[33] Most studied [FeFe]-hydrogenases are from green algae, *Clostridia* and *Desulfovibrio* species. Generally, the location of hydrogenases in the bacterial cell reflects the enzyme's function. [FeFe]-hydrogenase (DdH) from *Desulfovibrio desulfuricans* is a periplasmic enzyme involved in dihydrogen oxidation, which is thought to be coupled to ATP synthesis in the cytoplasm. The cytoplasmic *Clostridium pasteurianum* [FeFe]-hydrogenase I (CpI) is instead involved in dihydrogen generation, accepting electrons from ferredoxin, with protons as electrons acceptors.[27, 34] Molecular masses of [FeFe]-hydrogenases vary from 45 to 130 kDa. The majority of [FeFe]-hydrogenases is monomeric (in the cytoplasm), contrasting with the basically dimeric structure of [NiFe]-hydrogenases.[35] However, also dimeric, trimeric, and tetrameric enzymes are also known (in the periplasm).[28, 36]

Common feature of all [FeFe]-hydrogenases is the presence of a catalitically active site featuring the same molecular assembly, the so called H-cluster, which is hosted in the center of a highly functional protein matrix.[37] The hydrophobic pocket, in which the H-cluster is situated, is formed by a rather complex fold of four loops and four helices.[38] All of them exhibit an overall

high degree of conservation around the H-cluster in a multiple sequence alignment of 828 putative [FeFe]-hydrogenases.[35]

A consensus model of the H-cluster (Figure 1.2.1) consists of a di-iron core (hereafter to referred as $[2Fe]_H$) in which one of the two iron atoms is covalently linked to a typical cubane iron-sulfur cluster (referred to as $[4Fe4S]_H$) via a bridging cysteine residue. The other three cysteinates that coordinate the Fe sites of the $[4Fe4S]_H$ subcluster, form the only covalent contacts between protein and H-cluster. The two Fe atoms of $[2Fe]_H$ are usually referred as proximal (Fe_p) and distal (Fe_d) according to their relative position with respect to the$[4Fe4S]_H$ subunit. Most [FeFe]-hydrogenases also contain accessory 4Fe4S or 2Fe2S cofactors (F-clusters), which, together with the $[4Fe4S]_H$ subunit, create an electron transfer pathway between the protein surface and the buried $[2Fe]_H$ cluster (where catalysis occurs) and vice versa.[38, 37, 39] However, the existence of [FeFe]-hydrogenases lacking F-clusters (e.g. in green algae) indicates that the functionally essential domain to ensure catalysis is the sole H-cluster.[27] In the $[2Fe]_H$ subunit both Fe atoms are bound to two diatomic ligands, that have been assigned to one CO and one CN^- per each Fe according to their environment in the protein structure: the CO molecules are contained in hydrophobic pockets, while the CN^- are fixed to the protein, one through the backbone and the other via a lysine conserved in all [FeFe]-hydrogenases.[38, 36, 37, 40, 41] The importance of the key lysine anchoring one cyanide in Clostridium pasteurianum [FeFe]-hydrogenases is such that its replacement results in a complete loss of activity because of the missed anchoring of the H-cluster to the enzyme active site. These non-bonding interactions are not only fundamental for the active site integrity, but also for its functioning (vide infra).[42, 43]

The unusual non-protein CO and CN^-ligands stabilize low spin and low oxidation states of the iron ions.[41, 22] The two Fe centers are bridged by a third CO molecule and by a dithiolate bridge-head. The latter, was originally modeled as a propandithiolate (pdt)[38] molecule and only subsequently proved to be an azadithiolate (adt) ligand, by means of further spectroscopic, mechanistic and theoretical studies. Indeed, the presence of the adt is justified by the reactivity of the enzyme, since a secondary amine would easily drive (via Walden inversion) the proton transfers involved in the H_2 production/oxidation processes, acting as an intramolecular Brønsted acid/base cofactor.[44, 45]

The higher efficiency of [FeFe]-hydrogenases, with respect to the other enzyme's families, makes them extremely interesting candidates concerning the development of applications based on bio-hydrogen or semi-artificial H_2 production systems. As a consequence, many efforts (both experimental and theoretical) have been made in the past few decades, with the aim of i) dissecting H-cluster functioning at a molecular level and ii) finding a strategy for using it as a biological model for the development of new and efficient synthetic catalysts.[46, 15] In the next sections of the present chapter, the most relevant advancements and goals achieved to date in both fields will be presented, in order to provide a general picture of the state-of the-art of [FeFe]-hydrogenases research.

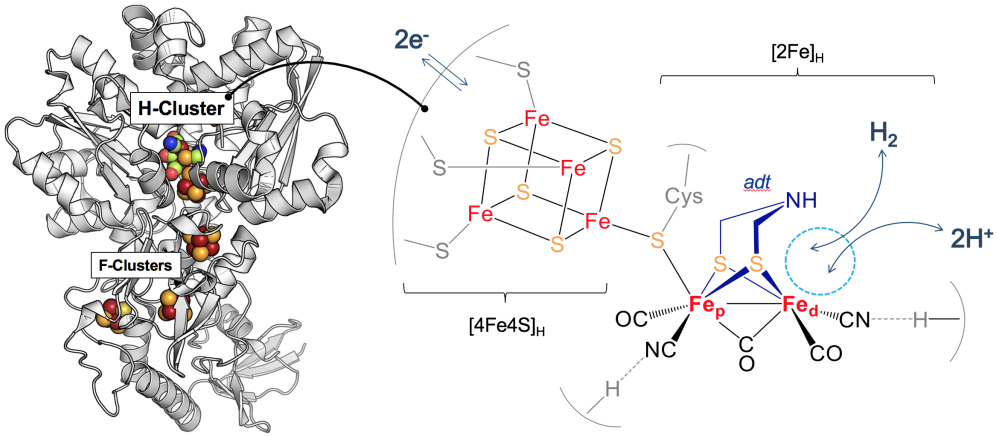

Figure 1.2.1: X-ray crystallographic [FeFe]-hydrogenase (DdH) (left) and structure of the H-cluster (right).

1.2.2 Redox states of the H-cluster and catalytic cycle

Catalysis for H_2 evolution comprises two electron and two proton transfers, during which the H-cluster varies its redox state and ligand coordination (Figure 1.2.2). Both $[2Fe]_H$ and $[4Fe4S]_H$ subunits are in fact redox active. The cubane part can be in the oxidized $[4Fe4S]^{2+}$ or reduced $[4Fe4S]^{+1}$ states. The binuclear part, instead, can be doubly oxidized $Fe^{II}Fe^{II}$, mixed-valence $Fe^{II}Fe^{I}$ or doubly reduced $Fe^{I}Fe^{I}$. The total number of possible redox states of the overall H-cluster is thus (at least in principle) six. However, FTIR experiments have revealed that only two of them can be assigned to critical resting states of the catalytic cycle: the paramagnetic active "oxidized" state (H_{ox}) and the diamagnetic active "reduced" state (H_{red}).[47, 48, 49] They both feature a +2 charged cubane (as indicated by Mössbauer studies) and differ for the redox state of the di-iron core, which has been assigned to $Fe^{II}Fe^{I}$ in H_{ox} and $Fe^{I}Fe^{I}$ in H_{red}.[50, 51, 52] The CO ligands are less firmly anchored to the protein environment with respect to CN^-, and can switch between different configuration states in the course of the catalytic process. In fact, a significant movement of the fully bridging CO to terminal position (but still remaining localized in the region of space between the iron ions) in H_{ox} is thought to take place upon enzyme reduction.[53] Very recently, an additional super-reduced state H_{sred}, earlier regarded as inactive or artificial[54], has been proposed as an intermediate of the catalytic process.[55, 56] The existence of this state suggests that also the redox activity of the cubane might play a role in catalysis, since the additional electron with respect to H_{red} leads to a $[4Fe4S]^{+1}$ unit. The stability of this super-reduced state is supposed to be strictly related to the presence of accessory 4Fe4S clusters in the protein. In fact, H_{sred} is quickly re-oxidized to H_{red} by the intimate electronic contacts between the H-cluster and the other iron-sulfur clusters, composing the electron transfer chain. Since in those enzyme varieties lacking F-clusters H_{sred} can be trapped as stable state, a model of the catalytic cycle including it as active intermediate has been proposed.[57] According to this model,

it is assumed that in H_{sred} the proton is associated to the H-cluster, presumably bound to a close amino acid residue (the exact binding site of the first proton is still unclear). At this stage, a hydride bound to the mixed valence H_{ox} state can be formed in a single step, which could react with a second proton (supplied by the adt cofactor) to form molecular hydrogen.

The characterization of catalysis intermediates has required extensive efforts, since the presence of the strong field diatomic ligands forces the Fe atoms into a low spin state and complicates the assignment of their oxidation states. In this context, a combined spectroscopic/computational approach in the study of binuclear iron complexes has been fundamental.[58, 59, 60] Computational studies in the field of [FeFe]-hydrogenase models, which have been mainly carried out in the framework of Density Functional Theory (DFT, see Chapter 2), have been reported for the first time in 1999 by Ian Dance, who investigated coordination compounds related to $[2Fe]_H$.[61] Cao and Hall, however, were the first to compare computed CO and CN^- vibrations of well-designed model complexes with FTIR spectra of the enzyme.[62] This powerful approach strongly indicated that low-valent $Fe^{II}Fe^{I}$ and $Fe^{I}Fe^{I}$ species better account for the electronic active states of the enzyme active site, a possibility that was not ruled out on the basis of previous Mössbauer spectra[63], that were originally interpreted in terms of a paramagnetic $Fe^{III}Fe^{II}$ redox level in the oxidized form, and diamagnetic $Fe^{II}Fe^{II}$ in the reduced form. The same strategy has been adopted in the following years, leading to remarkable results in the characterization of each intermediate structure. Computations confirmed in fact that the partially oxidized H_{ox} form corresponds to a $Fe^{II}Fe^{I}$ state that feature a vacant coordination site at Fe and a fully bridging CO. The unpaired electron is predicted to be mainly localized on Fe_d, in agreement with EPR data. The diamagnetic reduced H_{red} form has not been fully structurally characterized yet, since the apical site on Fed in this state is possibly occupied by a hydride ligand, giving a $Fe^{II}Fe^{II}$-H species, or, alternatively, the apical site could be vacant, giving a $Fe^{I}Fe^{I}$ form in which the adt is presumably protonated. These possibilities are not distinguished by available biophysical data and have not been unambiguously discerned by means of DFT tools. The fully oxidized form has been confirmed instead to be a $Fe^{II}Fe^{II}$species in which Fed is bound to an exogenous neutral substrate, such as water or H_2 [62] or to a OH^- ion[49], that can all compete with nitrogen coordination of the intramolecular adt cofactor.[64, 65]

1.2.3 The key active site features for catalysis

This section has the attempt to briefly summarize some of the main structural ingredients of the H-cluster, considered responsible for the incredible activity of [FeFe]-hydrogenases. First of all, it has to be mentioned that [FeFe]- and [NiFe]-hydrogenases, both highly efficient in processing H_2, feature Fe-CO/CN^--SR centers at their active sites. Since these two enzymes do not have any evolutionary linkage, it is clear that Fe-CO/CN^--SR units are particularly well suited to perform this kind of reactivity. Interestingly, several iron-sulfur clusters containing enzymes exist that do not show hydrogenase reactivity. A possible explanation is that metal-hydrides, whose formation is essential in the interconversion between H_2 and protons, are better stabilized by low-spin Fe

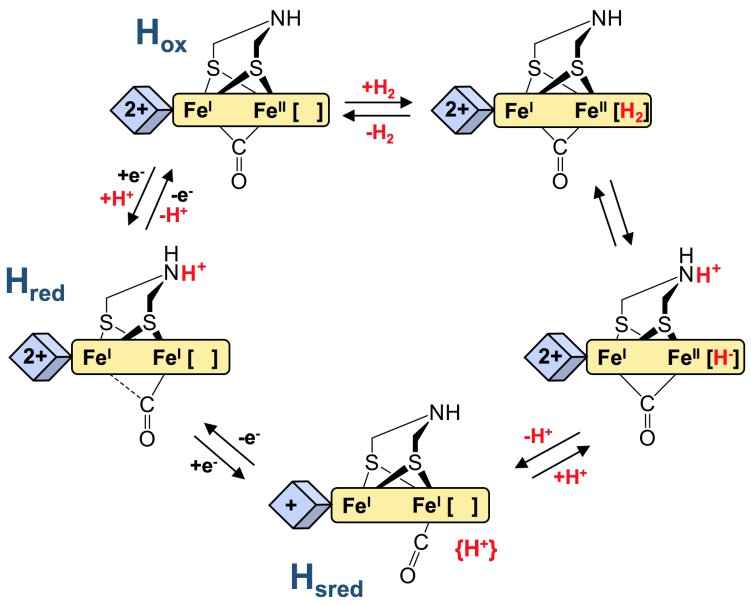

Figure 1.2.2: Proposed catalytic cycle of H_2 evolution/oxidation by [FeFe]-hydrogenases.

centers (as in the presence of carbonyl and cyanide ligands) with respect to high-spin alternatives (as in typical 4Fe4S clusters).[66]

The role of CO and CN^- is also highlighted by the nature of their interactions with the protein. The weak interactions between CO groups and hydrophobic pockets allow one CO to easily switch between fully bridging and semi-bridging/terminal position at Fe_d, concomitantly with the switches of active site redox state along the catalytic pathway. The function of this limited rearrangement is to guarantee electronic redistribution among the metal centers, a useful tool for tuning Fe redox properties in the course of catalysis. The strong H-bonds involving CN^- ligands (in particular the one at Fe_d) and the protein, instead, reduce ligand fluxionality and stabilize the so called "rotated" or "inverted" conformation of the H-cluster, which is surely one of the most important structural features of the active site. In this conformation, the diiron center is best described as a rotated form that possesses a square pyramid geometry at one iron atom (Fe_d) and is inverted with respect to the geometry of the other moiety (Fe_p).[67] As a consequence, the five-coordinated Fe_d shows a vacant coordination position in trans to the bridging CO, primed for both protonation and H_2 binding. It is intriguing that in many synthetic diiron dithiolates closely resembling the active site coordination environment of Fe ions, the "inverted" structure is not observed, as such compounds are exclusively characterized by an "eclipsed" conformation of the two square pyramidal ligand environment of Fe's. This last observation might be one of possible reasons at the origin of the minor catalytic activity (if any) of many synthetic models vs the enzyme. These observations could partly explain why Nature has selected such unusual and abiological ligands as component of the enzyme active site. Unfortunately, to make things further complicated, putting cyanides out of the catalytic pocket and incorporating them on synthetic scaffolds, turned out in a too large proton affinity globally hindering turnover of dihydrogen

production from acids.[68]

Adt was found to be an another indispensable feature for an effective hydrogenase related catalysis, being able to assist and modulate both protonation and H_2 activation. Since the binding of protons and dihydrogen at Fe_d, to form classical and non-classical metal-hydrides respectively, is the core of hydrogenase reactivity, it is clear that the presence of adt (Brønsted base) in proximity to the free coordination site at Fe_d (Lewis acid) is a strong requirement for efficient catalysis.[44, 69]

The hindering of ligand fluxionality, besides stabilizing the rotated structure, is also fundamental to impede eventual intramolecular hydrides isomerizations during catalysis. It is well known that, in the enzyme, the proton binds at the vacant apical position at Fe_d, forming a terminal hydride (t-H) which is much less stable (and thus much more reactive) with respect to its Fe-Fe bridging counterpart (μ-H). The latter, constitutes a real thermodynamic sink in the catalytic cycle. Remarkably, the enzyme architecture, by avoiding ligand rotation around Fe centers, is able to prevent interconversion pathway from t-H to μ-H intermediates,[70] whose formation has been so far observed (and computationally dissected) in any diiron dithiolate designed for modelling the [FeFe]-hydrogenase.[71]

1.3 Nitrogenases enzyme and CO_2 reduction

1.3.1 Enzyme architecture and function

Nitrogen is an essential element of most part of biomolecules, from DNA to proteins. Consequently, all organisms require this nutrient for their life and growth.[72] The main reservoir of elemental nitrogen is the Earth's atmosphere, whose 79% is formed by N_2. However, despite its abundance, N_2 is a highly inert molecule[73, 74] that need to be converted into a more reactive and bioavailable form (NH_3) to be usable for biosynthetic processes.[75, 76, 77] In Nature, as aforementioned, the capability to fix nitrogen is limited to a small but highly diversified group of diazotrophic microorganisms, distributed across both the bacterial and archaeal domains. Some of nitrogen fixing bacteria can be aerobic or anaerobic, phototropic or chemotropic. They can be free-living (non-symbiotic) or mutualistic bacteria (symbiotic).[78, 79] Despite their metabolic diversity, they all rely on the same system to accomplish nitrogen fixation: the nitrogenase enzyme.[80, 81] This complex metalloprotein, which clearly plays a central role in the nitrogen biogeochemical cycle[82], is able to fix about 10^8 tons of nitrogen per year.[83, 84]

The best studied and characterized member of this metalloenzyme family is the molibdenum (Mo)-nitrogenase, which is a Fe/Mo-dependent system.[85, 86, 87, 88] This is considered the "conventional" nitrogenase, being present in every nitrogen-fixing microorganism. However, also (V)-nitrogenase and the less common (Fe)-nitrogenase exist, in which Mo is replaced by vanadium or iron, respectively.[83, 87] These so-called alternative variants are found only in a limited set of diazotrophs and are present secondarily to (Mo)-nitrogenase, being expressed only when Mo concentrations are limiting. Additionally, they are less specific and efficient on binding N_2 and

reducing it into NH_3 (in the order (Mo) > (V) > (Fe)-nitrogenase).[89]

Nitrogenase consists of two component metalloproteins: the Fe-protein and the MoFe-protein (if considering (Mo)-nitrogenase).[90, 91] The former is an homodimeric protein with ATPase activity that features a 4Fe4S cluster and represents the only known source of electrons for the MoFe-protein, the nitrogenase catalytically active component. The latter, is an $\alpha_2\beta_2$-tetramer and contains the FeMo-cofactor (FeMo-co), which is the active site of substrate binding and reduction, and an auxiliary P-cluster, which is instead presumed to mediate the interprotein ATP-dependent electron transfer (from Fe-protein to the FeMo-co)[92]. The P-cluster is a di-cubane, in which the two 4Fe4S clusters share a sulfur atom (to give a Fe_8S_7 overall system), and is located at each a/b-subunit interface, while the FeMo-co is a $MoFe_7S_9C$-homocitrate complex and is positioned within each α-subunit.[93, 94, 95, 86, 96, 97]

Despite the first key advances in the disclosure of (Mo)-nitrogenase structure and function date back to 1990s[84], only recent studies have began to shed light on the order of events during catalysis (e.g. inter-clusters electron transfers and the nature of their coupling with ATP hydrolysis)[98, 99], on the identity of turnover intermediates and on various aspects of the very complicated N_2 fixation mechanism (mainly investigated through computational tools)[100, 101, 102, 103, 104, 105]. Less is known about the vanadium counterpart, especially from a mechanistically standpoint. In fact, in contrast to (Mo)-nitrogenase, a XRD solved structure of the vanadium variant is not available, making the disclosure of its structure-function relationships more complicated and challenging. A tentative explanation of this different behavior is that, despite the VFe-protein presents numerous similarities to MoFe-protein (from sequence homology to active site structure), its P-cluster is not a sole Fe_8S_7 cluster as in (Mo)-nitrogenase, where it acts as a covalent link between α and β subunits, but is formed instead by two separated 4Fe4S clusters. This apparently small difference weakens inter-subunits interactions, impeding protein crystallization.[16]

1.3.2 The FeMo-co: structure, activation and role in N_2 fixation

The FeMo-co (Figure 1.3.2) is an iron-sulfur cage which can be viewed as the union of a $[Fe_4S_3]$ and a $[MoFe_3S_3]$ subunit, linked by three sulfide ligands and an interstitial hexacoordinated carbide.[106, 107, 108, 109, 110] The central six Fe atoms are in a peculiar trigonal prismatic arrangement, while the remaining Fe has a tetrahedral geometry, binding three sulfides and a cysteine. The entire cluster is considered an organometallic cofactor because it features a small organic component, characterized by an homocitrate molecule coordinated to Mo.[95, 86] The latter is also bound to three sulfides and to the imidazole group of a histidine residue, leading to octahedral geometry. The active site is thus anchored to the protein through the side chains of only two residues, bound to Fe and Mo sites which are located at opposite ends of the cluster. The formal oxidation states of iron atoms are two Fe^{II} and five Fe^{III} , with an overall S = 3/2 resting state.[111, 112] The nature of the interstitial atom has been uncertain until recent years, when pulsed EPR spectroscopy revealed a central carbon atom by ^{13}C labeling, observation subsequently confirmed by the detection of 2p→1s carbon-iron transition by X-ray

emission spectroscopic studies.[106, 107, 108] FeMo-co and FeV-co feature the same structural and magnetic properties, although Mo^{IV} is replaced by V^{III}.[113, 18, 89, 114]

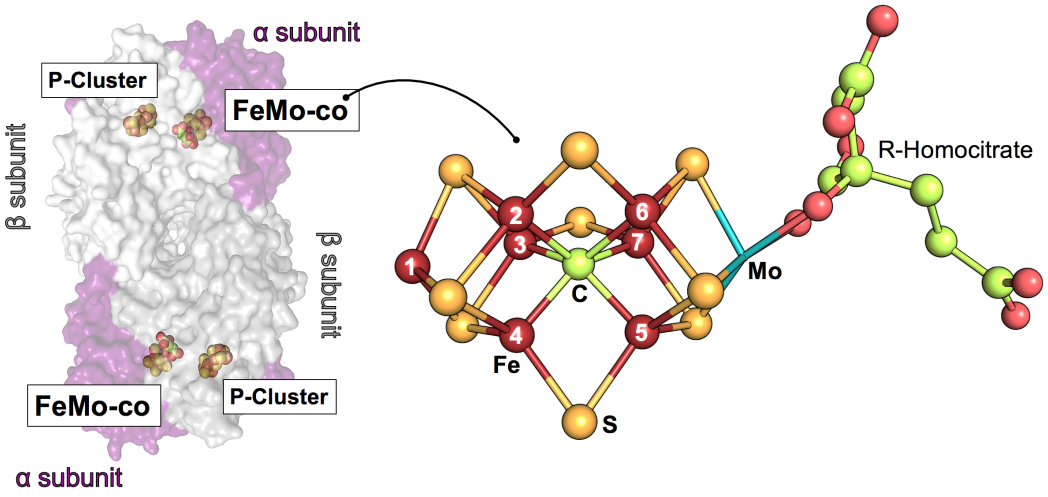

Figure 1.3.1: X-ray crystallographic MoFe-protein (left) and FeMo-co structures (right). Hydrogens have been omitted for clarity.

Recent advances in the studies of nitrogenases revealed that a valine residue has a fundamental steric control on substrate access to the active-site, while a nearby histidine was inferred to be involved in proton delivery to the FeMo-co. These residues are located over one FeS face of the FeMo-co, composed by Fe atoms 2, 3, 6, and 7. This observation has pinpointed that this FeS face can be considered the sole "active face", able to directly interact with both protons and dinitrogen, also implying that the main reactivity of the FeMo-co in binding and activating N_2 is ascribed to one (or more) of its iron centers.[115, 116, 117]

The first progresses in understanding the multistep N_2 reduction mechanism have been made in the 1970s and 1980s, especially by Lowe and Thorneley and their co-workers, who performed extensive kinetic studies to describe the transformation of FeMo-co during catalysis.[118, 84] Their measurements culminated in the formulation of the Lowe-Thorneley (LT) kinetic model for nitrogenase function, which describes the evolution of the active site intermediates "E_n", where n is the number of steps of proton/electron delivery to the MoFe-protein (Figure 1.3.2). A direct consequence of the LT model is that the enzymatic stoichiometry associated to N_2 fixation is not the one of a simple balanced reaction of N_2 conversion into NH_3, where 6 electrons/protons participate, but is given by:

$$N_2 + 8H^+ + 8e^- + 16ATP + 16H_2O \rightarrow 2NH_3 + H_2 + 16ADP + 16P_i$$

Interestingly, the overall reaction illustrates that the reduction of one mole of N_2 leads to the

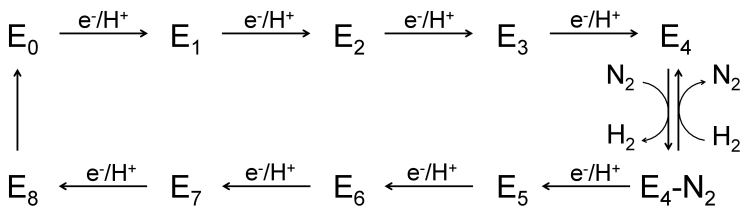

Figure 1.3.2: Highly simplified LT kinetic scheme, highlighting correlated electron/proton delivery in eight steps and N_2 binding/H_2 release at the E_4 level. LT also denote the protons added to FeMo-co (e.g., E_1H_1); for clarity, we have omitted this.

formation of a mole of H_2. This apparent "waste" of reducing equivalent, which becomes even larger in the case of V-nitrogenases (where the moles of H_2 released per mole of N_2 are three) has been interpreted as a sort of dihydrogen recycle, in order to allow recovery of some energy consumed during fixation (nitrogen-fixing organisms also contain, in fact, hydrogenase enzymes as active part of their metabolism).[84, 119]

Additionally, Hoffmann et al describe this obligatory formation of H_2 as functional for N_2 binding and activation. In fact, they proposed the occurrence of a concerted substitution of two hydrides, bound to the same Fe, with dinitrogen, following a reductive elimination process.[16] According to this mechanism, the departing H_2 carries two reducing equivalents stored in the cofactor, while the Fe that binds N_2 is formally doubly reduced, becoming highly activated towards N_2 activation. It is clear that such a process could not occur at the earlier stages of catalysis, since the arrival of at least two electrons and two protons is needed. In fact, the halfway intermediate E4, activated by the accumulation of four protons and four electrons, has proved to be the key intermediate in N_2 binding. This species is supposed to feature two bridging hydrides involving only two iron atoms of the active face of the FeMo-co.[120, 117] This suggests that a minimal unit composed by a di-iron core, with suitable basic protonation sites (e.g. two sulphides) would be, at least in principle, sufficient to perform N_2 activation and fixation. This observation has been used as guideline for the design of simple FeMo-co bioinspired compounds (vide infra).

1.3.3 Substrate promiscuity

Nitrogenases have the remarkable property of catalyzing the reduction of a series of substrates beside the physiological one (N_2). For example, as aforementioned, both Mo and V nitrogenases are able to reduce protons and form H_2 which is always a co-product in the nitrogen fixation process.[18] Notably, they can also reduce unsaturated hydrocarbons and CO to alkanes, a reactivity reminiscent of the one performed by late transition metals in the industrial Fischer-Tropsch process.[18, 89, 121, 122, 123] Nitrogenases are therefore in the spotlight as a biological setting where industrial milestones such as Haber-Bosch and Fischer-Tropsch processes surprisingly meet.

The most fascinating "alternative" nitrogenase reducing reactivity is surely that exerted towards CO_2, the more abundant greenhouse gas.[124, 125] The replacement of a single metal ion with another in the cofactor can modulate the catalytic activity of the system. Noteworthy is the enhanced substrate promiscuity when switching from Mo to V: V-nitrogenase is in fact 700-fold more active towards the reduction of CO, C_2H_2 and CO_2 into hydrocarbons of various lengths (even to methane) with respect to the Mo counterpart, which is instead more active towards N_2 fixation.[18, 126] Such a difference in substrate promiscuity has not been rationalized yet, and further studies are still needed in order to highlight the factors to which it could be ascribed.

1.4 The biomimetic approach

Both hydrogenase and nitrogenase, unfortunately, present several obstacles that inhibit their practical utilization as catalysts e.g. for biofuel production.[127] First, their high sensitivity to oxigen surely represents the major barrier to their direct incorporation into low-cost technological devices. Second, isolation of these enzymes in large quantities from natural sources is difficult, and there have been many difficulties in understanding the biosynthesis and maturation mechanism of both hydrogenases and nitrogenases, due to complexity of their gene expression and electron transfer system linked to the enzymes. Third, utilization of enzymes as electrocatalysts in bio-fuel cells requires high loadings on electrodes which may prove impossible to achieve. One promising strategy to overcome these inconveniences is to take inspiration from both enzyme active sites and to conceive new molecular devices that are able to mimic their function, performing the reactions of interest in a controlled and effective manner. This strategy is generally called "biomimetic approach" and has as its objective the design and the preparation of stable, noble-metal free and relatively small molecules that simulate or achieve the coordination sphere, composition, stereochemistry, and oxidation states of the native metal cofactor.[128, 129]

The starting point of the biomimetic approach is a deep knowledge of the native system, concerning both mechanistic and structural aspects. In this way, it is possible at a second stage, to dissect possible structure-function relationships, in order to disclose which ones are those fundamental for catalysis. The last step consists in using the up-to-now acquired information to design synthetic materials, which should preserve the chemistry of the natural systems but, at the same time, independently from them. This research field is very wide and interdisciplinary, since it involves different fields of expertise, from crystallography, to spectroscopy, enzymology, biochemistry, synthetic (bioinorganic, metallorganic) and computational chemistry.

In general, two main guidelines are followed in the synthesis of new active site analogues. The first one aims to reproduce the atomic content and connectivity of the active site, as well as its main structural features, in order to create new elegant structural biomimetics. The second one, instead, aims to replicate only the functional features of the enzyme active site, often through the use of different atomic content and connectivity than that found in the native system, in order to synthesize new bioinspired compounds, also referred to as functional mimics.[130] These two approaches can lead to extremely different results in terms of reactivity and catalysis turnover. In

this regard, [NiFe]-hydrogenases analogues provide a fascinating example.[131] Indeed, although several mimics of its active site were reported after its structure had been determined, construction of Ni-Fe heterobimetallic models with structural relevance able, at the same time, to perform enzymatic activity has been a great challenge for chemists.[15, 132] In fact, up to 2009 none of these structural mimics were shown to be catalytically active, and only the use of organometallic ruthenium moieties in place of the Fe fragment allowed for the preparation of active catalysts first for H_2 evolution and, later, for its oxidation.[133, 134, 135] Thus, only the synthesis of functional analogues of the active site allowed catalytic performances. Subsequently, Ogo and co-workers proposed the first active functional analogue with an iron-nickel binuclear core[136] while, remarkably, Bullock et al. and Du Bois et al. showed that even simple mononuclear functional analogues, containing Fe or Ni alternatively, could be highly efficient and bidirectional catalysts, also overcoming the performances of the enzyme.[69, 137] In particular, Ni-based systems with well-designed pendant amine ligands (acting as proton- transfer relay) and suitable experimental conditions can create more than 100,000 hydrogen molecules every second, while their natural inspiration clocks in at around 10,000 per second.

Since both [FeFe]-hydrogenase and nitrogenase active sites are iron-sulfur based coordination compounds, several inorganic and organometallic chemists have been inspired by their structures in the design and synthesis of an ever-increasing number of both structural and functional analogues.[127, 15] In the following sections, it will be briefly described how mimics of [FeFe]-hydrogenase and nitrogenase active sites have been developed and progressively refined during the last fifteen years.

1.4.1 [FeFe]-Hydrogenase active site analogues: background and challenges

1.4.1.1 Overview

The organometallics of diiron dithiolate-bridged hexacarbonyl complexes, resembling [FeFe]-hydrogenase active site, started in 1929, when Reihlen et al. described the synthesis of $Fe_2(CO)_6(\mu\text{-}SEt)_2$.[138] Later, in the 1980s, Seyferth[139], Hieber[140], and Poliblanc[141] extended the number of synthesized models of this class, also testing the introduction of chelating dithiolate ligands. Thus, when the structures of the H-cluster subsites were elucidated in 1998–1999[36, 38], the complex $Fe_2(CO)_6(\mu\text{-pdt})$, strikingly similar to $[2Fe]_H$, was already reported and it could be considered as the parent of a first generation of [FeFe]-mimics. In fact, this discovery inspired the development of numerous synthetic routes to better approach the active site of [FeFe]-hydrogenase. Three independent groups of (Rauchfuss, Pickett and Darensbourg) were the first to synthesize a real structural analogues of $[2Fe]_H$, by replacing two CO of $Fe_2(CO)_6(\mu\text{-pdt})$ (pdt = propandithiolate) with two cyanide ligands, to give the water-soluble dianion $[Fe_2(CO)_4(CN)_2(\mu\text{-pdt})]^{2-}$.[142, 143, 144] Later, other derivatives with pdt replaced by adt or odt (odt = oxodithiolate) have also been proposed.[145, 146] The number of reported systems bearing a [2Fe]-units has then grown exponentially, and up to now over 300 [FeFe]-hydrogenase mimics have been

described.[15] The thrust of this chemistry has been mainly to provide a wide set of complexes with different redox and electrocatalytic properties. However, of major importance is that it has enabled the reproduction of a series of active site features, through the preparation of H_{ox}-like mixed valence species, the stabilization of the rotated conformation with a bridging CO, hydride intermediates (both bridging and terminal) characterization, the synthesis of H-cluster model analogues (also including a cubane subunit) and H_2 oxidation studies. This kind of chemistry will be discussed in more detail below.

In general, there are two main differences between the enzyme active site and its analogues. The first one is purely structural, since the majority of the proposed biomimics does not feature a core that matches that of the enzyme subsite. In fact, in order to accomplish the above mentioned tasks, biologically relevant thioether groups, isocyanides or, alternatively, abiological phosphine, amine or carbene ligands are commonly adopted in place of cyanides.[147, 148, 149, 150, 151, 152, 153, 154, 155, 156, 157, 158, 159, 160]However, it has been argued that the use of these ligands provides electron density at the Fe centers at least partially approaching that of cyanide ligation, giving complexes that resemble the natural subsite in terms of valency and oxidation states. Consequently, and disappointingly, cyanide complexes have been quite under represented, especially when intended to electrocatalytic applications (vide infra). Indeed, the main problems in the use of cyanide complexes in proton reduction are related to their regiochemistry of protonation and their low robustness. The reactivity of the monosubsituited electron-rich $[Fe_2(CO)_5(CN)(\mu\text{-pdt})]^-$ is restricted to the cyanide, the protonation preferential (both kinetic and thermodynamic) site.[161] The disubstituted derivative, instead, is highly reactive and upon protonation results in sub-stoichiometric H_2 evolution with fast decomposition of the compound or undesired formation of unreactive polymeric derivatives.[161, 162] The second difference, instead, is that [2Fe] analogues usually tend to electrocatalytically reduce protons at large overpotentials, cycling through the Fe^IFe^I/ Fe^IFe^0 states, in contrast to what occurs in the enzyme mechanism.

Surrogate ligands have not been only used to approach the electron donating properties of cyanide, but also to modulate the chemical nature of the dithiolate bridge. This gave rise to a new plethora of models, in which Se and Si have been used as bridgeheads, while Te or other higher group chalcogens have been introduced in place of sulphur atoms.[163, 164, 165, 166, 167] Although the successes in overcoming intrinsic issues, such as large overpotential associated to proton reduction, have been scarce, this approach stimulated the development of new interesting organometallic compounds bearing novel features.

The presence of electron-rich phosphines or carbenes in place of CN^- ligands is important to make the $Fe_2(SR)_2$ core sufficiently basic to easily form Fe–H species. However, the enhancement of electron density at the diiron core also makes reduction potentials more unfavorable. Recently, Felton and co-workers highlighted that it is possible to lower the overpotential for catalysis without acting directly on Fe first coordination sphere, but just modifying the central chain of the dithiolate linker.[168] In particular, the inclusion of an aromatic dithiolate bridgehead suitably substituted with electron-withdrawing groups has proved to lower the potential for catalysis. Anyway, also this last strategy is not free from drawbacks, since the electron-richness of the dithiolate pendant also modulate its basicity, that must be sufficiently high to compensate for

otherwise slow rates of proton transfer at metals. In other words, the concomitant tuning of redox properties, basicity, catalytic performances, structural features and system robustness is extremely complex, since all of these factors are very sensitive even to small structural variations and may be in competition within each other, a fact that makes the improvement of [FeFe]-mimics activity a very difficult and challenging goal.

1.4.1.2 Mixed valency and rotated structures

The key features of the resting state structure of H_{ox} and its CO-inhibited form H_{ox}-CO are $Fe^{I}Fe^{II}$ mixed valency and the presence of a carbon monoxide ligand that bridges the two iron atoms.[169] In general, mixed-valent bridging carbonyl complexes are unstable.[15] Indeed, bridging carbonyls have been first synthetically achieved in diferrous systems.[170, 171] Later, the synthesis of mixed-valent $Fe^{I}Fe^{II}$ systems with a bridging CO has been achieved using subtle combinations of monophosphine, diphosphine, and carbene ligands and by the choice of non-coordinating solvents like CH_2Cl_2 in oxidation procedures. Remarkably, this strategy allowed the preparation of model systems with a rotated conformation, which neatly mimics the one of the enzyme. The introduction of electron-ligand allows both enhanced electron density at Fe and steric effects imparted by the bulky ligands, two factors that have proved to stabilize the rotated Fe unit. In particular, the steric bulk is presumably able to protect the five-coordinate site. The major contributions in this context derive from Rauchfuss and Darensbourg groups and in recent years the number of mixed-valence models has increased.[172, 150, 173, 174, 175, 157]

The next step has been the retention of the rotated form also at the $Fe^{I}Fe^{I}$stage. Also in this context, steric tricks have been adopted. Particularly, the use of bulky dithiolate ligands (plus a combination of coordination asymmetry of the two Fe's along with intramolecular formation of weak remote-agostic interactions) have been crucial for the stabilization of the coordination vacancy.[176, 177] This topic will be discussed in section 3.1 and, in more detail, in section 3.4.

1.4.1.3 Hydrides

In both directions of turnover, the formation of hydride intermediates is implicit in the chemistry of hydrogenases, and thus there is great interest in the protonation studies of diiron dithiolates. The protonation site of the active site is accepted to be the apical position at the rotated Fe_d moiety. However, at least in principle, there are other possible sites available at which protons could bind, such as the Fe–Fe bond, the amino bridge, dithiolate bridges and cyanide ligands. In synthetic models, all of these types of protonation have been detected, singly or in combination.[15] The simple $Fe_2(CO)_6(\mu\text{-pdt})$ does not protonate measurably with strong acids such as HBF_4 in polar solvents.[161] In order to observe protonation i) at least one CO must be replaced e.g. with a phosphine/CN^- ligand and/or ii) the nature of the dithiolate bridge must be modified to increase its protophilicity. Recently, also several examples of protonation at pendant basic functionality incorporated into phosphine ligands (acting as proton shuttle as adt) have been described.[178, 179, 180, 181] This kind of protonation, as well as the N-protonation of adt, are kinetlically favored, even in phosphine-substituted derivatives such as $Fe_2(CO)_4(PMe_3)_2(\mu\text{-adt})$,

where the FeFe bond is 1000× more basic than the amine.[182, 183]

The nature of Fe protonation is substantially controlled by the nature of the substituent on the di-iron dithiolate core. Bridging hydrides (μ-H) are surely the thermodynamic product of protonation, and so the majority of characterized hydride models has a bridging nature.[141, 151] The examples of terminal hydrides (t-H) are very limited in number. Rauchfuss and co-workers reported the first crystal structure of a t-H complex, namely $[Fe_2(\mu\text{-H})(CO)_4(PMe_3)_2(\mu\text{-edt})]^+$, but it was synthesized by direct addition of a hydride ligand.[184] Other t-H examples have mostly been detected as transient intermediates that rapidly rearrange to their bridging counterparts. Indeed, Schollammer and co-workers have shown, by NMR studies, that protonation of bis(diphosphines) asymmetrical substituted pdt complexes at low-temperature leads to the initial formation of a t-H, recognized as the kinetic product of protonation, which transforms to the thermodynamically stable μ-H at higher temperatures.[180] The same behavior has been observed later by Rauchfuss et al. on similar systems.[151] Additonally, it was discovered that terminal hydrides are more stable when the diiron dithiolato center is both electron-rich and has bulky ligands that hinder turnstile rotation, and isomerization to μ-H becomes slower. Also the presence of adt has proved to stabilize the terminal hydride.[151] Probably, the Fe-Fe bond is not the kinetic site for protonation because of the presence of bulky phosphines, that sterically restrict the approach of the acid molecule, or, alternatively, because of the formation of a terminal/bridging CO pre-equilibrium that exposes a vacant site for protonation in terminal position.[15] DFT investigation has suggested that in derivatives featuring bulky P ligands the terminal-axial Fe site is less encumbered respect to the Fe-Fe region and thus more susceptible of attack by the acid molecule.[185]

It would be desirable to slow down the t-H to μ-H rearrangement for two reasons: i) t-H is much more reactive towards H_2 release than μ-H ones (suggesting that t-H is more hydridic than the μ-H ligand.) and ii) the t-H is reduced at much positive potentials than the isomeric μ-H. This lowered reduction potential points to a thermodynamic advantage for terminal hydrides as precursors to H_2 . For instance, the t-H species $[Fe_2H(CO)_2$ $(dppv)_2$ $(\mu\text{-adt})]^{2+}$ electrochemically releases H_2 in trifluoroacetic acid in CH_2Cl_2 with a calculated TOF of 5000 s^{-1}, which substantially higher if compared to the TOF of its μ-H form (20 s^{-1}). All of these advantages of t-H forms (over μ-H ones) somehow justify why the enzyme would likely favor their formation as active intermediates.[186]

1.4.1.4 Redox properties and electrocatalysis

The design of new biomimics for the electrocatalytic hydrogen production/oxidation requires the understanding of their redox properties. Ciclic voltammetry is normally used to screen synthetic systems in terms of their oxidation and their reduction potentials, together with their efficiency in electrocatalysis. Most part of the studies have been carried out in the proton reduction framework, while oxidation of dihydrogen has been much less explored. Indeed, very few examples of mimics able to activate and oxidize dihydrogen are known.

As aforementioned, the redox potential of synthetic systems is very sensitive to iron first and second coordination spheres. Reduction potentials of a series of complexes, representing the most part of the types of structures examined to date, are collected in Table 1.4.1.4. As expected, the substitution of one CO with more basic ligands makes the reduction potential of the system more negative. Protonation of the complex, especially at N-based bridge-heads or ligands, can instead lead to easier reduction.[183]

Rauchfuss et al. described in 2001 the first example of electrocatalytic proton reduction catalyzed by $[Fe_2(CO)_4(CN)(PMe_3)(\mu\text{-pdt})]^-$, providing the first link between organometallics and [FeFe]-hydrogenase-like reactivity.[161] Subsequently, the number of active electrocatalysts has rapidly grown.

H_2 Evolution needs the reductive coupling of two protons. The sequence of protonation and reduction steps can vary according to the nature of the system. For example, in hexacarbonyl diiron dithiolates hydrogenesis the first step is always an electron-transfer and, usually, catalysis follows an ECEC mechanism (although exceptions, such as the involvement of a further reduction step, have been reported). In the absence of acid, most of them tend to undergo directly a double reduction, where the second reductive process occurs at a potential which is less negative than the first one.[187] This is usually indicative of an important structural rearrangement upon reduction, e.g. the break of a Fe-S bond.[154] For electron-richer complexes, instead, protonation can occur prior reduction, forming hydride species that are active catalysts.[162] Qualitative studies suggested that, for these systems, the rate determining step of turnover could be precisely the direct protonation of the diiron core, highlighting the high barriers associated to protonation of metal centers and indicating the possible advantages of cofactors that would facilitate protonation.[188]

Factors like solvent and proton source nature are decisive for the rate of dihydrogen evolution, since they could also affect the overpotential of catalysis.[160] The understanding of the mechanism at a molecular level is often difficult because of the formation of elusive intermediates, which can undergo important structural rearrangements. Thus CV techniques are usually complemented with modern digital simulations experiments, also in conjunction with computational (DFT) tools.[189]

1.4.1.5 Redox auxiliaries

Synthetic models with appended clusters and photosensitizers have also been proposed as catalysts for proton reduction.[194, 195, 196, 197] The linkage of a 4Fe4S subunit to a $Fe_2(SR)_2(CO)_5$ center (through a cysteinate residue) led to a model of the entire H-cluster, which, interestingly, shows activity towards proton reduction in the presence of 3,5-dimethylpyridinium as proton source, although affected by very high overpotentials.[198]

Also abiological redox cofactors have been adopted to modify diiron models, such as pendant ferrocene (Fc) groups[199, 200, 201], a diphosphine functionalized fullerene[202], non-innocent 2,3-bis (diphenylphosphine) maleic anhydride (BMA)[203] and light-harvesting chromophores like $[Ru(bipy)_3]^{2+}$[204] and Zn(TPP)[197] (with the long-range goal of developing a catalyst for light-

Compound	E_{pc}	Ref
$\mathbf{[Fe_2(CO)_6(\mu\text{-}pdt)]}$	-1.17	[190]
$\mathbf{[Fe_2(CO)_6(\mu\text{-}adt)]}$	-1.09	[147]
$\mathbf{[Fe_2(CO)_6(\mu\text{-}SCH_2OCH_2S)]}$	-1.10	[191]
$\mathbf{[Fe_2(CO)_6(\mu\text{-}bdt)]}$	-0.83	[154]
$\mathbf{[Fe_2(CO)_5(CN)(\mu\text{-}pdt)]^-}$	-1.35	[161]
$\mathbf{[Fe_2(CO)_4(CN)_2(\mu\text{-}pdt)]^{2-}}$	-1.84	[161]
$\mathbf{[Fe_2(CH_3(C(\mu\text{-}CH_2(S)_2(CH_2(SCH_3)(CO)_5]}$	-1.31	[192]
$\mathbf{[Fe_2(CH_3(C(\mu\text{-}CH_2(S)_2(CH_2(SCH_3)(CO)_4(CN)]^-}$	-1.88	[192]
$\mathbf{[Fe_2(\mu\text{-}SCH_2(NBn)CH_2S)(PMe_3)_2(CO)_4]}$	-1.69	[193]
$\mathbf{[Fe_2(\mu\text{-}SCH_2(NHBn)CH_2S)(PMe_3)_2(CO)_4]^+}$	-1.06	[193]

Table 1.4.1: Primary redox potentials of some {2Fe2S}-assemblies.

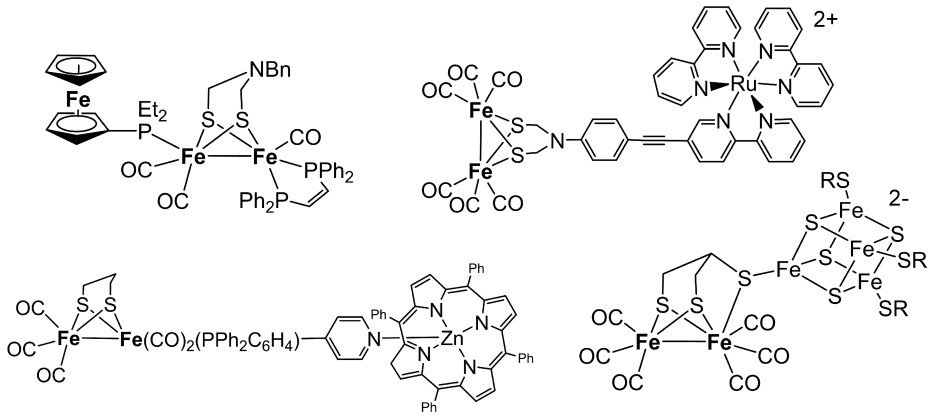

Figure 1.4.1: Examples of [FeFe]-hydrogenase biomimic compounds with redox/photochemical auxiliaries.

driven hydrogen production). They have been covalently linked to the azadithiolate cofactor and through phosphine ligands of simple biomimic compounds. Unfortunately, only the fullerene model exhibits any electronic communication between the the diiron core and the redox cofactor, while Fc functionalities have provided an electrochemical internal standard. Indeed, the only system in which the redox cofactor is able to promote intramolecular electron transfer processes is $[Fe_2(CO)_3(FcP^*)$ (dppv)μ-$\{(SCH_2)_2NBn\}]$ (FcP^* = Cp*Fe($C_5Me_4CH_2PEt_2$)) reported by Rauchfuss and Camara.[205] Remarkably, this is also one the few biomimic compounds able to oxidize H_2.

1.4.1.6 H_2 Oxidation and bidiretional catalysis

Hox is the crucial redox state in both H_2 binding and oxidation. However, the majority of synthetic mixed-valent diiron systems are completely inactive towards dihydrogen oxidation to protons, a failure which is surely in part due to their operation at potentials far from ther-

modynamic reversibility. The first experiments aimed to couple H_2 activation with oxidation represented a dramatic breakthrough in modelling the bidirectional functionality of the [FeFe]-hydrogenase enzyme. The system $[Fe_2(CO)_3(dppv)(PMe_3)(\mu\text{-adtR})]^+$, proposed by Rauchfuss et al., is able to activate 1 atm H_2 at room temperature in the presence of a mild oxidant in solution, e.g. decamethylferrocenium (Fc^{*+}).[206] Subsequently, the redox cofactor FcP* , a rough functional approximation of the cubane, has been directly incorporated into the system in order to achieve the catalytic oxidation of H_2.[205] Remarkably, catalysis occurs, although with very modest rates, which have been postulated to be connected with the low affinity of the H_{ox} model towards H_2. The key factor responsible for catalytic activity has been identified with a possible simultaneity of H_2 binding and intramolecular electron transfer (from the diiron core to FcP*), a process that would provide driving force for H_2 activation and heterolysis. These first results led to the conclusion that the attachment of an electron transfer relay should be a definite feature of biomimics, in order to achieve H_2 oxidation ability. However, very recently Sun and co-workers shown that systems simply bearing a proton relay functionality incorporated into a phosphine ligand (without intramolecular redox auxiliaries) are also able to perform bidirectional catalysis, even at slightly increased rates.[207]

Although these recent results represent a great step forward in the field of hydrogenase biomimic design, the turnover reached (in the order of 10^{-4} s^{-1}) are several orders of magnitude lower than the 28,000 s^{-1} of the natural system, a gap that must be fixed in view of the incorporation of these systems into future practical technological devices.

1.4.1.7 State-of-the-art of FeMo-co analogues

The subject area of nitrogenases mimic compounds has been much less explored in comparison with the hydrogenases one. Structurally relevant models, comprising multiple iron atoms and a sulfur environment, have been synthesized with the aim of gaining a fundamental understanding of the nitrogen binding and the subsequent ammonia synthesis mechanism.[208, 209, 210, 211, 212] In fact, there is a limited understanding of N_2 binding to the FeMo(V)-co, because of i) the complexity of the cofactor and ii) the difficulties in populating a 4-fold reduced complex resembling the E4 state (the stage at which N_2 binding is predicted to occur in Mo-nitrogenases) for spectroscopic characterization.[213] Unfortunately, these synthesized structural analogues do not show ability to bind N_2.[213] Hence, most part of the complexes proposed for dinitrogen fixation and conversion are structurally quite far from the entire FeMo-co.

After the discovery of the first transition metal-N_2 complex in 1965, $[Ru(N_2)(NH_3)_5]^{2+}$[214], it came the hope that an abiological N_2 fixation and chemical reduction would be forth-coming. Unfortunately, despite a variety of metal complexes coordinating N_2 has been isolated for almost all transition metals[215], also including Fe, Mo and V (the more biologically relevant ones), very few reports of catalytic N_2 conversion into ammonia have appeared. In 2003 Schrock and Yandulov presented the first well-established system, composed by a single Mo ion and a tetradentate abiological ligand, namely $[HIPTN_3N]Mo(N_2)$ (where $[HIPTN_3N]^{3-}$ is $[\{3,5\text{-}(2,4,6\text{-i-}Pr_3C_6H_2)_2C_6H_3NCH_2CH_2\}_3\ N]^{3-}$}), able to convert nitrogen into ammonia with an overall yield of 65%.[216, 217] This was the first coordination compounds that performed this reactivity in a

catalytic manner, under ambient conditions and in the presence of suitable proton and an electron sources. Hence, it represents a breakthrough in the development of homogeneous catalyst for N_2 fixation. This result, together with the knowledge of the structure of both FeMo-co and FeV-co, prompted the synthesis of novel Mo, Fe and V-based compounds with enhanced affinity towards N_2 or capable in reducing nitrogenase substrates e.g. N_2 (although with very drastic experimental protocols), hydrazine and derivatives. Among them, we find mononuclear complexes like MoCp*Me_3[218], Mo and V thiolate complexes[219, 220, 77, 221], MFe_3S_4 (M = Mo or V) cubanes[222, 223, 224], mononuclear Fe system with tetraphosphine[225, 226, 227, 228], N-heterocyclic carbenes[229], or PNP pincer ligands[230] and binuclear Fe compounds with SiP_2O or bulky β-diketiminate ligands[231]. However, these system cannot be considered real functional analogues of nitrogenase active site.

Producing functional and structural models of nitrogenases has proved to be exceptionally difficult. Very few bioinspired compounds composed by small portions of the entire FeMo-co have been reported. They include models bearing i) an Fe-N_2 interaction supported by a combination of sulfur and carbon ligands[232, 233, 234] ii) a dihydride Fe_2S_3MoO unit able to reduce acetylene to ethylene[235] or ii) a Fe_2S_2 scaffold with reductive activity towards hydrazine and derivatives.[236, 237, 238, 239] This last class of systems, introduced by Qu and colleagues, is of particular interest in the context of the present PhD thesis, since the Fe_2S_2 scaffold resemble the diiron dithiolate structure of hydrogenase biomimic compounds. Thus, it will be the topic of section 4.1.

Interestingly, the proposed FeMo(V)-co analogues has never been tested towards substrate promiscuity, in particular towards CO_2 activation and conversion. The dissection of this reactivity would luckily provide hints for the design of novel Fe-based compounds with catalytic activity towards CO_2 reduction. Indeed, non-bioinspired compounds based on cheap first row transition metals has been scarcely investigated compared to noble-metal-based alternatives. Some improvements have been recently achieved in the context of CO_2 hydrogenation to formate, as possible solution for secure and reversible dihydrogen storage. Beller et al. described the synthesis and the catalytic performances of both iron-based and cobalt-based tetraphosphine complexes. Milstein et al. proposed the most active iron-based homogeneous catalyst for CO_2 hydrogenation[240], containing pincer PNP ligands.[241] Very recently, Appel et al. synthesized instead an example of triphosphine copper system as active precursor for CO_2 conversion into formate.[242] Although these comforting results, generally the non-noble metal catalysts still show low activity. One promising strategy to overcome this gap would be combining the information gained from both bioinspired and non-bioinspired compounds, in order to highlight differences/common principles that could turn useful to drive the design of more and more efficient catalysts for CO_2 fixation.

Chapter 2

Theoretical background

2.1 Overview

Since the mid-1980's, computational chemistry has rapidly emerged as a subfield of theoretical chemistry, being surely one of the fastest growing areas of chemistry. This is due to the continuous technological development of CPUs, making computing power less and less expensive, and to the increase in the number of efficient high-performance computational algorithms. The chemical community has already accepted computational tools not as an addition to experimental ones, but instead as independent and reliable source of information, that can turn extremely useful to get insight into molecular processes, as well as to predict them.

The primary focus of computational chemistry is on solving chemically-related problems, whose nature determine which is the most suitable level of theory (i.e. computational approach) to address them. When dealing with the computational dissection of properties that directly depend on electrons within a chemical system, such as structural, spectroscopic and reactivity properties of molecules, an ab-initio Quantum Mechanical (QM) approach is mandatory. Indeed, the postulates and theorems of QM methodologies form the rigorous foundation for the prediction of observable chemical properties starting from first principles. In this context, a microscopic system is described by the wave function (Ψ), i.e the solution of the time-independent Schödinger equation that completely characterize all its chemical and physical properties. This function, which depends on one spin and three spatial coordinates for each electron (assuming nuclei as fixed, according to Born-Oppenheimer approximation), does not result particularly intuitive for multi-electrons systems. However, computational methods relying on wave function theory (WFT) have been intensively employed. The first steps to deal with the complex many-body Schrodinger equation, whose solution is represented by the wave function itself, have been achieved by Hartree and Fock. Indeed, they derived the Hartree-Fock (HF) theory, that consists in a set of self-consistent, wave function-based equations that allow an iterative calculation of energies and other parameters of interests.[243]

HF theory is the basis of every wave function electronic structure methods. However, it has its flaws. First of all, the high computational cost when modeling systems of large size, since WFT

implies the dependency on the 3N (or 4N if considering spin)-dimensional asymmetric wave function (with N the number of electrons in the system).[244] Another deficiency of the HF theory is the lack of electron correlation (both static and dynamical). This is due to the approximation of the wave function as a single Slater determinant (static correlation) and to the fact that the instantaneous repulsion of electrons is not covered by the HF effective potential, which treats the electrostatic interactions in only an average manner. More precisely, HF takes into account correlations between parallel-spin electrons only, i.e., it gives the exchange energy, but it does not take into account any correlations between opposite-spin electrons (dynamical correlation). The development of methods to determine accurately and efficiently the correlation contributions is still a highly active research subject in conventional quantum chemistry. Sophisticated approaches use the HF theory as starting point to develop "correlated" wave function methods, the so called post-HF methods, such as Møller-Plesset Perturbation Theory (MPn),[245], Configuration Interaction (Full-CI (FCI) or truncated-CI (CISD, CISDT..)), Coupled Cluster (CCD, CCSD ..))[246, 247] and multi-reference methods (CASSCF, MR-CI, MR-CC).[248, 249] However, they are too expensive in terms of computational costs to be practical for large chemical and biochemical systems. An approach to lower computational costs can therefore be the use of a less complex base object, instead of the wave function. The foundation of this approach has been provided in 1964 by Hohenberg and Kohn,[250] when they demonstrated that the electron density, which only depends on three spatial coordinates (or four, including the spin), in principle, provides all the ingredients necessary to describe the ground state properties of a system. This made possible the birth of Density Functional Theory (DFT), which, remarkably, also takes into account electronic correlation effects. It is thus clear why, in the past decades, DFT has made its way from a peripheral position to center stage among the available QM methodologies. Since DFT (and its application in the study of chemical systems) is the focus of the present PhD thesis, the salient points of its theoretical origin and background will be summarized in the following.

2.2 The Density Functional Theory

2.2.1 From the Thomas-Fermi model to the Hohenberg-Kohn theorems

The early attempts for gaining information about molecular systems by means of the electron density, rather than the wave function, date back well before 1964. In 1921, in fact, Thomas[251] and Fermi[252] proposed independently a quantum statistical model (the Thomas-Fermi model) which described for the first time the energy of a uniform gas in terms of its electron density, which integrates to the correct number of electrons in the system. Although this model is not suitable at all to be applied to any molecular system, its formulation provide conceptual roots for DFT, since for the first time a density functional was proposed that was able to map a density $\rho(\vec{r})$ onto an energy, without the need of any additional information.

The major breakthrough in DFT was in 1964 when Hohenberg and Kohn published their theorems, [250] providing a link between the electron density and the many-electron Schrodinger equation. The first one is a proof of existence and states:

"The external potential $V_{ext}(\overrightarrow{r})$ is (to within a constant) a unique functional of $\rho(\overrightarrow{r})$; since, in turn $V_{ext}(\overrightarrow{r})$ fixes $\hat{\mathrm{H}}$, we see that the full many particle ground state is a unique functional of $\rho(\overrightarrow{r})$"

where V_{ext} is the static Coulomb potential arising from the nuclei (as result of the Born-Oppenheimer approximation) and $\hat{\mathrm{H}}$ is the N-electron Hamiltonian operator. In other words, they demonstrated by reductio ad absurdum that the ground state electron density uniquely specifies the external potential V_{ext} and uniquely determines the number of electrons N (and vice versa), a statement that can be summarized as:

$$\rho_0 \Rightarrow \hat{\mathrm{H}} \Rightarrow \Psi_0 \Rightarrow \mathrm{E}_0(\text{and all other properties}). \tag{2.2.1}$$

Since the ground state energy is a functional of the ground state electron density, so must be its individual components:

$$\mathrm{E}_0[\rho] = \mathrm{T}[\rho_0] + \mathrm{E}_{ee}[\rho_0] + \mathrm{E}_{\mathbf{N}e}[\rho_0]. \tag{2.2.2}$$

Separating the energy expression into those parts that depend on the system (i.e. $\mathrm{E}_{\mathrm{N}e}[\varrho_0] = \int \varrho_0(\overrightarrow{r})\mathrm{V}_{\mathrm{N}e}\mathrm{d}\overrightarrow{r}$) and those which, instead, are universal (thus independent from N and nuclear coordinates/charge $\mathrm{R_A}$and $\mathrm{Z_A}$), and then collecting the system independent part into a new quantity, the Hohenberg-Kohn functional $\mathrm{F_{HK}}[\varrho_0]$, we obtain:

$$\mathrm{E}_0[\rho] = \int \rho_0(\overrightarrow{r})\mathrm{V}_{\mathrm{N}e}d\overrightarrow{r}) + \mathrm{F_{HK}}[\rho_0]. \tag{2.2.3}$$

$\mathrm{F_{HK}}[\rho]$ contains thus the functional for the kinetic energy $\mathrm{T}[\rho]$ and for the electron-electron interaction $\mathrm{E}_{ee}[\rho]$. This last term (apart from its classic Coulomb part) is given by the non-classical exchange and Coulomb electronic correlation effects. If $\mathrm{F_{HK}}[\rho]$ were exactly known, we would have been able to solve the Schrodinger equation without approximations. Unfortunately, Hohenberg and Kohn did not provide any explicit expression for their functional, whose search is the major limit, and at the same time the major challenge, in density functional theory.

The second theorem is a variational principle, and it states:

"*A universal functional for the energy in terms of the electron density can be defined, valid for any external potential. For any particular $V_{ext}(\overrightarrow{r})$, the exact ground state energy of the system is the global minimum value of this functional, and the electron density that minimizes the functional is the exact ground state density.*"

The original proof of the theorem was provided by variation calculus and subsequently by the so called *constraint-search* approach, introduced by Levy and Lieb (whose discussion is beyond the purpose of the present thesis). In other words, this theorem states that if we take a trial density

$\tilde{\rho}(\overrightarrow{r})$, associated with some external potential $\tilde{\mathrm{V}}_{ext}$, the energy obtained from the functional given in equation 2.2.2 represents an upper bound to the ground state energy E_0. If and only if the exact ground state density is inserted into equation 2.2.3 then E_0could turn out. Indeed, any trial density $\tilde{\rho}(\overrightarrow{r})$ defines its own Hamiltonian $\tilde{\hat{\mathrm{H}}}$and so its own wave function $\tilde{\Psi}$. The latter can also be considered the wave function of the Hamiltonian generating the true external potential V_{ext}, and thus we arrive at:

$$\left\langle \tilde{\Psi} \left| \hat{\mathrm{H}} \right| \tilde{\Psi} \right\rangle = T[\tilde{\rho}] + V_{ee}[\tilde{\rho}] + \int \tilde{\rho}(\overrightarrow{r}) \mathrm{V}_{ext} d\overrightarrow{r}) = \mathrm{E}[\tilde{\rho}] \geq \mathrm{E}_0[\rho_0] = \left\langle \Psi_0 \left| \hat{\mathrm{H}} \right| \Psi_0 \right\rangle \tag{2.2.4}$$

which is the desired result. Anyway, the major implication of this second theorem is that density functional theory is usually termed as "ground state theory". Indeed, the applicability of the variational approach 2.2.4 is only limited to ground state energy, and not transferable to electronically excited states. Indeed the HK theorems are restricted to non-degenerate ground states that are solution of the time-independent Schödinger equation.

The Hohenberg-Kohn theorems, although laid a rigorous foundation for DFT as it is known today, do not tell us how to calculate the total energy from electron density, since the exact form of the functional $\mathrm{F}_{\mathrm{HK}}[\rho]$ is not known and represent the major part of complexities of the many-electron problems.

2.2.2 The Kohn-Sham formalism

Hohenberg and Kohn with their theorems proofed that the electron density determines the external potential, which determines the Hamiltonian, which determines the wave function, so that the energy of the ground state can be determined variationally. However, only with Kohn and Sham[253] in 1965 the density functional theory became a practical tool for rigorous calculations. Indeed, they had the ingenious idea of referring the Hamiltonian to a non-interacting system of electrons. The crucial point of their methodology, which also provide a link to "reality", where electrons interact, is that the overall ground state density of their fictitious system of non-interacting electrons is exactly the *same* density of the real interacting system. In this approach, the Hamiltonian is thus expressed as a sum of one-electron operators, its eigenfunctions are Slater determinants[1] of the individual one-electron eigenfunctions, and the eigenvalues are the sum of the one-electron eigenvalues. If the Slater determinant enter in the HF scheme as an approximation of the true N-electron wave function, when dealing with non-interacting fermions it becomes the exact wave function of the system. Additionally, since the kinetic energy of a non-interacting system is known and it is exact, the KS approach allowed the determination of a large fraction of the entire kinetic energy of the actual system. Indeed, they separated the functional F[ρ] as

[1] A Slater determinant Φ_{SD} is used in HF and DFT theories to approximate to the electronic wave function as an antisymmetrized product of N one-electron wave functions $\chi_i(\overrightarrow{x}_i)$ (called spin-orbitals, being composed by a spatial orbital and a spin function (α or β), and is expressed as:

$$\Phi_{SD} = \frac{1}{\sqrt{N!}} det\{\chi_1(\overrightarrow{x}_1)\chi_2(\overrightarrow{x}_2)...\chi_N(\overrightarrow{x}_N)\}.$$

follows:

$$F[\rho(\overrightarrow{r})] = T_S[\rho(\overrightarrow{r})] + J[\rho(\overrightarrow{r})] + E_{XC}[\rho(\overrightarrow{r})] \tag{2.2.5}$$

where T_S is the kinetic energy in the non-interacting system, J is the classical Coulomb interaction, while E_{XC} is the so called exchange-correlation functional. It comprehends the non-classical effect of selfinteraction correction, the non-classical electronic correlation and exchange terms, together with a residual kinetic energy, T_C (driving from electrons interaction, so that the entire true kinetic energy $T = T_S + T_C$ is contained in the density functional). Thus, the only unknown part of F is limited to E_{XC}, whose formulation will be described later.

Interestingly HF and KS approaches show various similarities, among which the mathematical technology offered by a common variational principle, a same iterative approach for the optimization of molecular orbitals, expressed in implicit form (which has not be treated here for sake of brevity), and the description of the system ground state wave function by a single Slater determinant (they are in fact called "monodeterminantal methods"). This last point represents a limit in computational modeling, when the ground state of a system (in general open-shell) can not be represented as a single Slater determinant. However, HF and DFT have an important difference: HF is deliberately an approximate theory, whose approximations are introduced in order to solve the relevant equations exactly; by contrast, DFT is an exact theory, but its relevant equations need approximations in order to be solved, because the form of the key operator $E_{XC}$is unknown.[244]

2.2.3 The quest for approximate exchange-correlation functionals

The Kohn-Sham formalism allows the exact treatment of most of the contributions to the electronic energy of an atomic and molecular system, including a large fraction of kinetic energy.[253] The only unknown part is restricted to the non-classical exchange-correlation functional $E_{XC}[\rho]$.[254] Unlike conventional wave function based methods, in density functional theory there is not a systematic strategy to improve functionals approximation, which represents the major drawback of the DFT approach. Hereafter, the current state of art in the search of approximated $E_{XC}[\rho]$ will be briefly presented.

2.2.3.1 The Local Density and Local Spin-Density Approximations

The simplest concept used for the implementation of the exchange-correlation functional is the Local Density Approximation (LDA).[244] According to this approach, which is built on the uniform electron gas model, E_{XC} can be written in the simple form

$$E_{XC}^{LDA}[\rho] = \int \rho(\overrightarrow{r})\varepsilon_{XC}(\rho(\overrightarrow{r}))d\overrightarrow{r} \tag{2.2.6}$$

where $\varepsilon_{XC}(\rho(\overrightarrow{r}))$ is the exactly known exchange-correlation energy per particle of a uniform gas of electrons and is weighted with the probability $\rho(\overrightarrow{r})$ that there is in fact an electron in the considered position in space. $\varepsilon_{XC}(\rho(\overrightarrow{r}))$ can be written as sum of two terms, for exchange and correlation contributions, respectively

$$\varepsilon_{XC}(\rho(\overrightarrow{r})) = \varepsilon_X(\rho(\overrightarrow{r})) + \varepsilon_C(\rho(\overrightarrow{r})). \tag{2.2.7}$$

While the exchange part ε_X, representing the exchange energy of an electron in a uniform electron gas, is known and is expressed as

$$\varepsilon_X = -\frac{3}{4}\sqrt[3]{\frac{3\rho(\overrightarrow{r})}{\pi}}, \tag{2.2.8}$$

no explicit expression is known for the correlation part ε_C, but it can be approximated in several ways. For example, there are the PZ81[255], the VWN[256] and the PW92[257] LDA correlation functionals.

LDA can be extended to the unrestricted case, where the spin-α and the spin-β densities are not equal, arriving at the Local Spin Density Approximation (LSD) . The functional basic equation is almost equal to 2.2.5, except for the use of ρ_α and ρ_β in place of ρ, according to:

$$E_X^{LDA}[\rho_\alpha, \rho_\beta] = \int \rho(\overrightarrow{r})\varepsilon_{XC}(\rho_\alpha(\overrightarrow{r}), \rho_\beta(\overrightarrow{r}))d\overrightarrow{r}. \tag{2.2.9}$$

The main assumption of this model is clearly that the density ρ varies very slowly and locally with position. Thus, it could be a good physical model for an idealized metal, but it is very far from describing any realistic situation resembling a molecular system, where the electron density is not homogeneous and usually varies rapidly. To yield accurate chemical description, one usually has to add corrections by means of terms involving the gradient of ρ, as will be shown in the following.

2.2.3.2 The Generalized Gradient Approximation

The major failure in LDA is the incapability of describing non-homogeneous electron densities. One way to improve this approximation is consider not only the electron density but also its gradient. In the generalized gradient approximation (GGA), density gradient corrections are added to the LDA.[244] GGA exchange-correlation energy is the sum of GGA exchange energy (E_X^{GGA}) and GGA correlation energy (E_C^{GGA}), and the approximations for the two terms are sought individually. The exchange part can be written as

$$E_X^{GGA} = E_X^{LDA} - \sum_\sigma \int F(s_\sigma)\rho_\sigma^{4/3}(\overrightarrow{r})d\overrightarrow{r}. \tag{2.2.10}$$

It is thus derived from the LDA exchange with an additional correction term, where the argument of F is the *reduced density gradient* for spin σ

$$s_\sigma(\overrightarrow{r}) = \frac{|\nabla\rho_\sigma(\overrightarrow{r})|}{\rho_\sigma^{4/3}(\overrightarrow{r})}. \tag{2.2.11}$$

s_σ goes to zero in the bonding regions where the gradient is minimal, while getting more significant in low-density regions. For the function F formulation, two main lines have instead been followed. The first one is based on the GGA exchange functional developed by Becke in 1988, commonly denoted as B or B88[258]. The basic idea was to choose a flexible mathematical functional form, which depends on one or more parameters, and then to perform a numerical fitting of these parameters to molecular thermochemical data. Indeed, B functional incorporates a single parameter, whose value has been optimized by fitting to exactly known exchange energies of the six gas noble gases, from He to Rn. Other functionals which are related to this approach include the Perdew-Wang (PW)[257], the modified-Perdew-Wang (MPW)[259], OptX (O)[260] and X[261] exchange functionals, where X is a particular combination of B and PW to give improved performance over either. The second philosophy, instead, is the development of functional that are free from semiempirical parameters, and thus derived by quantum mechanics basic principles, including scaling relations, correct limits for high and low densities, correct LSD limit for slowly varying densities, and the fulfillment of exact relations on the exchange holes. In this context, representative are the functional proposed by Becke in 1986 (B86) and Perdew (P)[262], the one by Lacks and Gordon in 1993 (LG)[263] and the implementation of Perdew, Burke and Ernzerhof in 1996 (PBE and mPBE)[264, 262]. With respect to the corresponding gradient-corrected correlation functionals, among the most widely chosen we can find the commonly abbreviated P or P86[265], which is the correlation counterpart of 1986 Perdew exchange functional (and the gradient-based correction of its 1981 local correlation functional), the parameter-free Perdew-Wang functional (PW81)[255], and the popular Lee-Yang-Parr (LYP)[266] developed in 1988, which does not correct LDA expression, but instead is constructed from the correlated wave function of Colle and Salvetti, based on four empirical parameters fit to the helium atom.[267]

Typically, a complete label of a functional is given by the acronym of the exchange functional, followed by the one of the correlation functional. For instance, the GGA functional BP86, which has been the most-used in the present PhD research, consists in B (Becke's 1988 exchange functional) plus P86 (Perdew's 1986 correlation functional).

A recent improvement of GGA functionals has been achieved with the so called meta-GGA, or M-GGA, by means of two corrections proposed by Becke and Roussel in 1989. The first one consists in considering explicitly higher (generally second) order density gradients, thus including additional semi-local information, while the second is the inclusion of the kinetic energy density, which involves derivatives of the occupied Kohn-Sham orbitals. They both aim to describe the inhomogeneous distribution of electron density within a molecule more accurately. Although it is quite good in predicting e.g. atomization energies, generally, this class of functional suffers for

low numerical stability. Several exchange-correlation M-GGA functionals have been presented, such as TPSS[268], KCIS[269], and VSXC[270].

2.2.3.3 Hybrid functionals

Exchange contributions are significantly larger in absolute numbers than the corresponding correlation effects. Therefore, a prerequisite to extract reliable information from DFT is to dispose of an accurate expression for the exchange functional. Interestingly, in the HF theory framework, the exchange energy of a Slater determinant can be calculated exactly. From this observation, naturally derived the incorporation of a portion of exact exchange from HF theory in the formulation of the exchange–correlation energy functional, marking the birth of the so called "hybrid" functionals.[244]

Hybrid functional formulations has been inspired by the so called Adiabatic Connection Methods (ACM)[271], which aim to control somehow the extent of electron-electron interactions in a many-electron system. In other words, the idea is to smoothly convert the non-interacting KS reference system into a real fully interacting system. According to this approach, and following the Hellmann-Feynman theorem,[272] the exchange-correlation functional is given by the integral

$$\mathrm{E_{XC}} = \int_0^1 \langle \Psi(\lambda) | V_{XC}(\lambda) | \Psi(\lambda) \rangle \, d\lambda \tag{2.2.12}$$

where λ describes the extent of interelectronic interactions, which goes from zero (no interaction) to one (full interaction). In the non-interacting limit, $\mathrm{V_{XC}}$becomes $\mathrm{V_X}$, since the only contribution to V is exchange (deriving from wave function antisymmetry). Moreover, the Slater determinant of KS orbitals is the exact wave function for the non-interacting Hamiltonian. Thus, the corresponding expectation value is the exact exchange for a non-interacting system, and it can be computed following HF calculations (except that KS orbitals are used). The correlation contribution is instead introduced by means of computed values from appropriate DFT computations. Thus, $\mathrm{E_{XC}}$can be written as

$$\mathrm{E_{XC}} = (1-a)\mathrm{E_{XC}^{DFT}} + a\mathrm{E_X^{HF}} \tag{2.2.13}$$

where a is an empirical constant to be optimized. Actually, what happens in the design of hybrid functionals, is that additional emprical parameters could be introduced, in order to maximize the utility of the method. For instance, B3LYP[258, 266] functional (the only hybrid functional used in the present thesis) is an example of 3-parameter functional and is formulated as follows:

$$\mathrm{E_{XC}^{B3LYP}} = (1-a)\mathrm{E_X^{LSD}} + a\mathrm{E_X^{HF}} + b\Delta\mathrm{E_X^B} + (1-c)\mathrm{E_C^{LSD}} + c\mathrm{E_C^{LYP}} \tag{2.2.14}$$

where a, b, and c have optimized to 0.20, 0.72, and 0.81, respectively. It means that in B3LYP functional a 20% of HF exact exchange is introduced in the evaluation of the overall exchange-correlation energy.

Other functionals following this three-parameters scheme are B3PW91, O3LYP and X3LYP. However, also one-parameter models, just restricting themselves to adjust the percentage of HF exchange included in the functional, have been proposed. Examples are B1PW91 and B1LYP, B1B95, mPW1PW91 and PBE1PBE (usually referred to as PBE0, since the contribution of HF exchange (0.25) has not been empirically optimized but derived on the basis of perturbation theory argumentations, and thus is formally contains "zero" parameters). Also M-GGA hybrid functionals do exist. Among them, we find TPSSH, the hybrid counterpart of TPSS, and the very "young" family of M06-type functionals, proposed by Truhlar and Zhao, including M06-L (fully local and without HF exchange so actually it is a pure functional), M06 (27% of HF exchange), M06-2X (54% of HF exchange) and M06-HF (100% of HF exchange).[273, 244]

2.3 DFT and transition metal complexes

The important role of computational methods in modern inorganic/bioinorganic chemistry and the ubiquitous character of metal ions in both environment and living organisms led to the fast development of theoretical modeling of transition metal chemistry. Indeed, in some case of study the computational approach becomes fundamental. For instance, transition metal presence in metalloprotein active sites, although allowing a very rich biochemistry, makes the experimental disclosure of structure-activity relationships generally difficult, because of the intrinsically versatile, complex and (often) elusive chemistry of transition metals. Among the contemporary QM theoretical approaches, DFT investigations have proven to be an essential tool for the study of chemical reactions involving transition metal compounds, allowing the prediction of many important chemical and physical properties from first principles. DFT methods have become suitable for modeling even complex chemical systems, e.g. metalloproteins and relative biomimic compounds. As aforementioned, one of the main advantages of DFT is its positive trade-off between accuracy and computational efficiency. DFT computational costs scale more favorably with system size than the corresponding costs of other QM methods (such WFT-based ones), maintaining at the same a comparable accuracy. Indeed, the scaling behavior of DFT is no worse than N^3,where N is the number of basis functions used to represent KS orbitals.[244] This is better than HF by a factor of N, and much more better than all the other QM methodologies. However, when dealing with transition metals, the greatest advantage of DFT is that it intrinsically includes correlation effects, whose incorporation in a well-balanced way at a WFT level requires the use of highly costly (in terms of both computational power and time) post-HF methods. Correlation effects can not be neglected in modeling the electron distribution of transition metal compounds, since they could be very large even on ground state structures. Additionally, the implementation of several approximations, models and tools has allowed the treatment of crucial aspects of transition metal compounds chemistry, such as relativistic effects (by means of the introduction of relativistic effective core potentials (RECPs))[274], magnetic properties and spin couplings (with

the Broken Symmetry approximation (BS)[275], which allows the treatment of antiferromagnetic coupling in the monodeterminantal description), solvation effects (with solvation models such as PCM, COSMO, COSMO-RS..), dispersion corrections (e.g. with Grimme contributions in DFT-D)[276], photochemical properties (with TD-DFT) and so on, elevating the quality and the efficiency of the research in the DFT area. It is clear that the hardest task of DFT computations is the right choice of the exchange-correlation functional, among the variety of formulations proposed, as well as its conjunction with a suitable set of basis functions. Indeed, it must be underlined that *the best functional do not exist*, and that the performances of every functional are strictly related to the chemical problem which has to be addressed and to the chemical properties of the system under investigation. Thus, what is considered an "improved" functional may be less suitable than earlier generation functionals for the modeling of a particular phenomena or for the study of a particular property. Thus, literature, experience and benchmarking are always fundamental to drive the choice of the best functional for any given problem.

2.4 Computational methods employed in this thesis

The TURBOMOLE 7.0.1 suite of programs[277] has been used to perform all the computations described in the present thesis. The general information regarding the adopted computational methodologies are presented in the following, while additional details (if needed) are included in the specific sections of the next Chapters.

2.4.1 Geometry optimizations and functional choice

Stationary points of the energy hypersurface have been located by means of energy gradient techniques, and full vibrational analyses have been carried out to further characterize each pure energy minimum (no imaginary frequencies). The DFT grid-size was set to standard m3 value.

When dealing with [FeFe]-hydrogenase biomimic compounds (Sections 3.1-3.6), geometry optimizations have been always carried out using the BP86 pure GGA functional[258, 278], as implemented in the TURBOMOLE suite. Indeed, the adoption of BP86 functional, in conjunction with a triple-ζ basis set with polarization on all atoms (TZVP),[279] has proven to be most successful scheme in modeling H-cluster-like systems and their ground state properties, both structural and spectroscopic.[42, 280, 64, 65, 185, 281, 71] In some cases, a double functional approach has been adopted to further validate results (especially in the absence of experimental data to be matched). In particular, in Sections 3.4 and 3.6 geometry optimizations and vibrational analysis have been performed at both BP86/TZVP and B3LYP/TZVP level.

All the optimized ground state structures of the hydrogenases biomimics reported in the present thesis correspond to low spin states, as expected considering the characteristics of the ligands forming the coordination environment of the metal atoms and in agreement with available experimental data.

For what concerns nitrogenase biomimic compounds (Chapter 4), the TPSS pure M-GGA exchange-correlation functional has been used.[268, 279] The class of system investigated in Chapter 4 has

been subject of previous calculations (performed by Qu at al. [237]), which have been taken as reference for the choice of the level of theory. Indeed, we found that the computed spin multiplicity of the ground state of the unraveled class of systems, as well as the energy gap between low-spin and high-spin solutions, are highly affected by the functional choice. Since no experimental information related to the spin state of these catalysts is available, we decided to adopt the same theoretical approach previously followed.

The resolution of identity technique has been adopted in order to speed up BP86 and TPSS computations, since expensive four-center integrals (describing the classical electron-electron repulsive contribution to the total energy) are approximated through a combination of two three-center integrals.[282]Grimme empirical dispersion corrections[276] for density functional calculations have been also included when needed (Section 3.4).

2.4.2 Transition state search

The optimization of transition state structures has been carried out according to a procedure based on a pseudo Newton-Raphson method.[283] Initially, geometry optimization of a guess transition state structure is carried out constraining the distance corresponding to the reaction coordinate. Vibrational analysis (at the same level of theory) of the constrained minimum energy structures is then carried out and, if one negative eigenmode corresponding to the reaction coordinate is found, the curvature determined at such point is used as starting point in the transition state search. The location of the transition state structure is carried out using an eigenvector-following search: the eigenvectors in the hessian are sorted in ascending order, the first one being that associated to the negative eigenvalue. After the first step, however, the search is performed by choosing the critical eigenvector with a maximum overlap criterion, which is based on the dot product with the eigenvector followed at the previous step.

2.4.3 Solvent effects treatment

The COnductor-like Screening MOdel (COSMO)[284, 285] has been used to describe dielectric screening effects in solvents. According to this model, the solvent is represented implicitly by a dielectric continuum of permittivity ε. The solute molecule (or ion) thus forms an atom-centered polygonal cavity embedded in the dielectric medium. The charge distribution of the solute polarizes the dielectric medium, whose response is described by the generation of screening charges on the cavity surface. The solvent CH_2Cl_2 has been modeled with a continuum dielectric with $\varepsilon = 8.93$ (Sections 3.1, 3.2, 3.3, 3.5, 3.6), THF with $\varepsilon = 7.58$ (Section 3.3, Chapter 4), and MeCN with $\varepsilon = 37.5$ (Section 3.3). For what concerns active site models, ε was set equal to 4, a value commonly used to reproduce the effect of a protein environment.

2.4.4 Redox potential computations

Standard redox potential values have been obtained through the theoretical evaluation of the in-solvent free energy differences between oxidized and reduced species, following the basic equation:

$$\Delta G_{solv} = -nFE_{abs} \tag{2.4.1}$$

where n is the number of electrons involved in the redox process and F the Faraday constant (23.061 kcal/(mol·V). ΔG_{solv} is referred to the free energy difference between the in gas-phase optimized reduced and oxidized species, including solvent effects at a single-point level following the COSMO approach. Free energy (G) values have been obtained from the electronic SCF energy considering three contributions to the total partition function (Q), qtranslational, qrotational, qvibrational, assuming that Q can be written as the product of them.[286] To evaluate enthalpy and entropy contributions, the values for temperature and pressure have been set to 298.15 K and 1 bar, respectively. Because of the high values of the SCF wavenumbers arising from the harmonic approximation, a scaling factor was set to 0.9914 (default value in the TURBOMOLE) for BP86 functional,[277] to 0.965 for B3LYP and to 0.9818 for TPSS. In order to reproduce experiments (when necessary, Sections 3.1, 3.2, 3.3, and 3,5), the obtained potential values have been scaled by using the Fc^+/Fc couple as reference, whose potential, computed according to the same protocol at the BP86/TZVP/COSMO level, is -5.09 V, -5.20 V and -4.92 when considering CH_2Cl_2, THF and MeCN as solvents, respectively. Small variations from this protocol have been introduced in some of the presented works, and they will be discussed and justified in detail in the corresponding Sections.

Chapter 3

DFT investigation on key topics in the [FeFe] - hydrogenases biomimic research field

The [FeFe]-hydrogenase biomimic design/synthesis subject area is very wide and diversified. Figure 3.0.1 summarizes key active fields of research on synthetic systems, which ranges from electrocatalysis, photocatalysis and solid state devices, through hydride and mixed-valent systems, to the reproduction of fundamental H-cluster structural features.[127, 15, 160] As anticipated in section 1.4.3 , despite the numerous and ambitious goals reached in the last years, an intimate and complete knowledge of both steps and factors that control and modulate the activity of models is still missing. This requires a deep understanding of structural, redox, protonation and catalytic properties of these diiron auxiliaries, in view to be able to provide a low barrier reaction pathway without the the need of the proteic matrix. In this context, computational tools, especially QM based techniques, can turn extremely useful, or even necessary, to gain insights useful for the design of novel and always more efficient biomimics. In the present PhD work, DFT methods have been used to address a series of puzzling issues related to some of the research fields pictured in Figure 3.0.1. The overall research has thus been organized in a series of sub-projects: some of them have been approached purely from a computational standpoint, while others have implied collaborations with experimental international research groups. These sub-projects are related to the following general topics:

- The effect of dithiolate pendant nature on protonation/redox properties and catalytic performances of biomimics (sections 3.1 and 3.2)
- Implication on reactivity and electronic structure of the variation of Fe first coordination sphere (section 3.3)
- Reproduction of key active site structural features (sections 3.4 and 3.5).
- Oxidative behavior of biomimics towards dihydrogen (section 3.6)

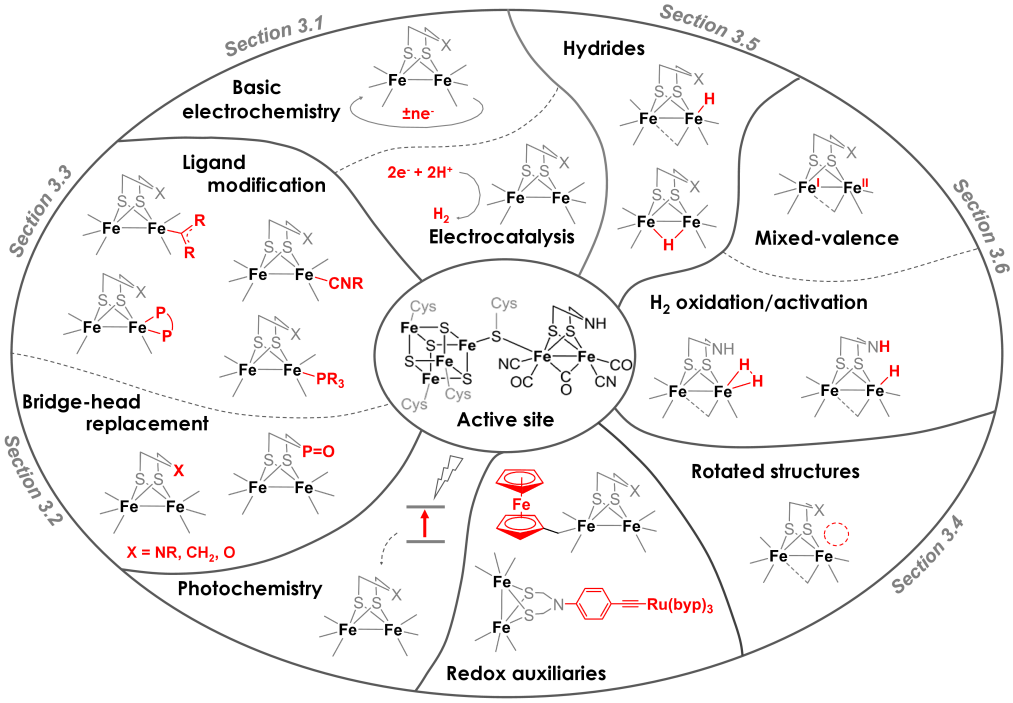

Figure 3.0.1: Summary of key areas of research on [FeFe]-hydrogenase synthetic systems. The projects addressed in the context of this thesis, which are related to the reported areas, are indicated with the number of the corresponding section.

3.1 Influence of the dithiolate bridge on the oxidative processes of diiron models related to the active site of [FeFe]-hydrogenases

In collaboration with P. Schollammer and C. Elleouet, Université de Bretagne Occidentale, France

3.1.1 Introduction

If the reduction of protons into dihydrogen at $Fe^{I}Fe^{I}$ systems has been widely studied, whereas, the one- and two-electron oxidation processes involving such diiron mimics have been comparatively less explored, despite the challenging perspective of activating efficiently H_2 at such a bimetallic site. $Fe^{I}Fe^{II}$ systems have served as models for H_{ox} state of [FeFe]-H_2ases active site and some aspects on their reactions, reactivity and geometry have been addressed.[192, 175, 174, 157, 150, 287, 156, 288, 206, 289] Only very recently, first examples of catalytic activation of H_2 by mixed valence diiron complexes, featuring pendant base in their coordination sphere, have

been reported.[206, 207, 290] As aforementioned, one of the goals, still to be achieved for the development of efficient bio-inspired electrocatalysts, is to address the question of the retention, by synthetic models, of the specific called rotated or inverted conformation, that is adopted by the H-cluster and which allows the efficient H^+/H_2 conversion by affording a free coordination site nearby the pendant amine of the azadithiolate cofactor. The stability of this conformation depends on different factors such as the steric behaviors of the dithiolate bridge, the oxidation states of iron atoms as well as the electron-donating power of terminal ligands and their sterical crowding (see section 3.4 for further details).[291, 176] Structural studies have revealed that mixed valence model $Fe^{I}Fe^{II}$ complexes adopt this inverted conformation but very rare examples of $Fe^{I}Fe^{I}$ systems with such a geometry have been reported and, among them only a single case shows simultaneous presence of rotated $Fe^{I}Fe^{I}$ core and adt as dithiolate linker. Indeed, very recently, P. Schollammer et al. described such case study: P. Schollammer et al. described the sole example to date of an azadithiolate $Fe^{I}Fe^{I}$ complex,$[Fe_2(CO)_4(\kappa^2-dmpe)(\mu-adt^{Bn})]$(**1**) ($adt^{Bn}$ = $(SCH_2)_2NCH_2C_6H_5$, dmpe = $(CH_3)_2PCH_2CH_2P(CH_3)_2$), which adopts a fully rotated structure in the solid state that appears slightly persistent in solution (its DFT optimized structure is reported in Figure3.1.3).[291, 292] In order to explore the effects of the redox changes on the behaviors and the geometry of **1**, its oxidation has been studied by electrochemical methods. The present work reveals, by comparison of the properties of **1** with those of the analogous species $[Fe_2(CO)_4(\kappa^2 - dmpe)(\mu - pdt)]$ (**2**) (pdt = propanedithiolate)[293], the strong influence of an amine functionality in the dithiolate bridge on the oxidative processes of diiron molecules $[Fe_2(CO)_4(\kappa^2 - chelate)(\mu - dithiolate)]$. DFT calculations have been performed with the aim to rationalize experimental results and to understand the cause of the differences in the oxidative processes involving adt and pdt species **1** and **2**.

3.1.2 Results and discussion

Experiments showed that complex **1** and **2** have a significantly different oxidative behavior. In fact, the shift of oxidation potentials of the two neutral complexes **1** and **2** is only of 60 mV, while the one associated to the monocationic forms $\mathbf{1}^+$ and $\mathbf{2}^+$ is of 290 mV. This difference is even more stressed when experiments are performed in the presence of CO. The oxidation of both **1** and **2** leads to the coordination of an exogenous CO molecule. However, only upon CO coordination to **1** a surprising inversion of oxidation potential is observed, being the **[1-CO]**$^+$ easier to be oxidized with respect to **1**. This has been rationalized on the basis of some possible structural rearrangements deriving from an interaction of adt with the diiron center. DFT (BP86/TZVP/COSMO, $\varepsilon = 8.93$) has been thus used to clarify which could be the possible intramolecular changes/rearrangements upon oxidation that can be considered responsible for the different behavior, both in the presence of N_2/Ar and in the presence of CO.

3.1.2.1 DFT investigations on the oxidative processes of 1 and 2 in the presence of N_2 or Ar

Previous computations at the DFT-BP86/TZVP level revealed that the lowest-energy isomer of **1** corresponds to its "rotated form" (**1rot**), experimentally observed at the solid state, while the unrotated isomer, featuring the phosphine ligands in dibasal position (**1unrot**), is predicted to be only 2.7 kcal/mol higher in energy (in CH_2Cl_2).[291] These two species result isoenergetic when thermal and entropic contributions are evaluated and included in computations, which is in line with experimental observations. Since the BP86/TZVP scheme has proven to be successful in reproducing both structural and spectroscopic (IR vCO) properties of **1**, it has also been adopted herein to study its oxidative behavior.

The study of **1** ad **2** oxidations in the presence of N_2 or Ar implied the structural assignment of both their monocationic and bicationic forms, which has been made through a preliminary conformational search of both species, followed by a comparison between computed and experimental first and second oxidation potentials.

The thermodynamic speciation of $\mathbf{1}^+$points out that, among all the different isomers obtained by the one-electron oxidation of the neutral complex, rotated species exposing sites for substrate binding are the lowest energy ones (Figure 3.1.1). Interestingly, $\mathbf{1}^+$ structures featuring an eclipsed geometry are predicted being not so distant in energy from rotated isomers. The (relatively) most stable ($\mathbf{1c}^+$) is in fact only 2.3 kcal/mol higher in energy with respect to the lowest energy minimum (in ΔG_{solv}). In these unrotated isomers the distance between one proton of the adt^{Bn} methylene group and the oxygen atom of the apical CO is about 2.5 Å. In general, the basal-apical orientation of dmpe is slightly unfavored with respect to the basal-basal one. Note that when the adt^{Bn} pendant points towards the unrotated $\{FeP_2\}$ moiety, the apical-basal orientation of dmpe is prevented for steric reasons. Only when rotation occurs at the $\{Fe(CO)_2\}$ moiety, an interaction between the N atom of adt^{Bn} and the Fe atom has been observed. Two different isomers, for each dmpe orientation (dibasal and apical-basal), have been found. They differ for the Fe-N distance, which is related to the strength of the interaction. The two dmpe apical-basal rotamers (not shown) are slightly higher in energy (∼2 kcal/mol) with respect to the corresponding two dibasal species. The most stable dibasal isomer has a coordination of N to the iron atom, with a computed Fe-N distance of 2.399 Å, while in the other energy minimum found this distance is elongated up to 2.466 Å. Both of them result ∼6 kcal/mol less stable than the lowest energy $\mathbf{1}^+$ isomer, suggesting that the formation of an additional Fe-N interaction is not favored after the first electron transfer. Remarkably, these structures featuring a Fe-N remote interaction are the only one characterized by an equatorial orientation of the pendant benzyl group.

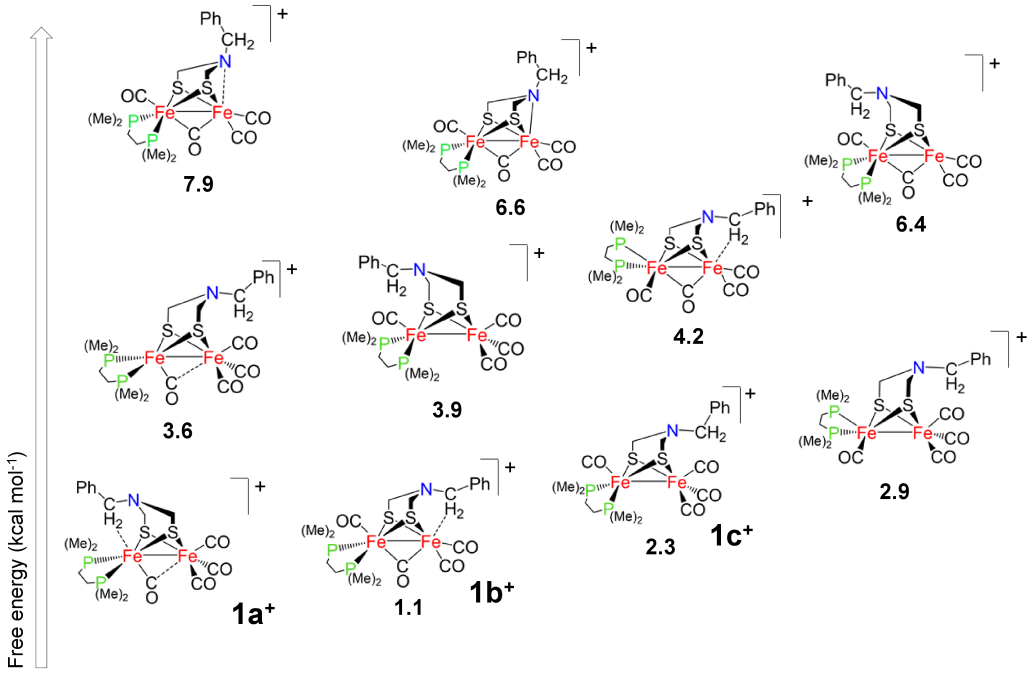

Figure 3.1.1: DFT energy minima computed for $\mathbf{1}^{+}$ (ΔG_{solv}, kcal/mol, T=273 K; P=1 atm).

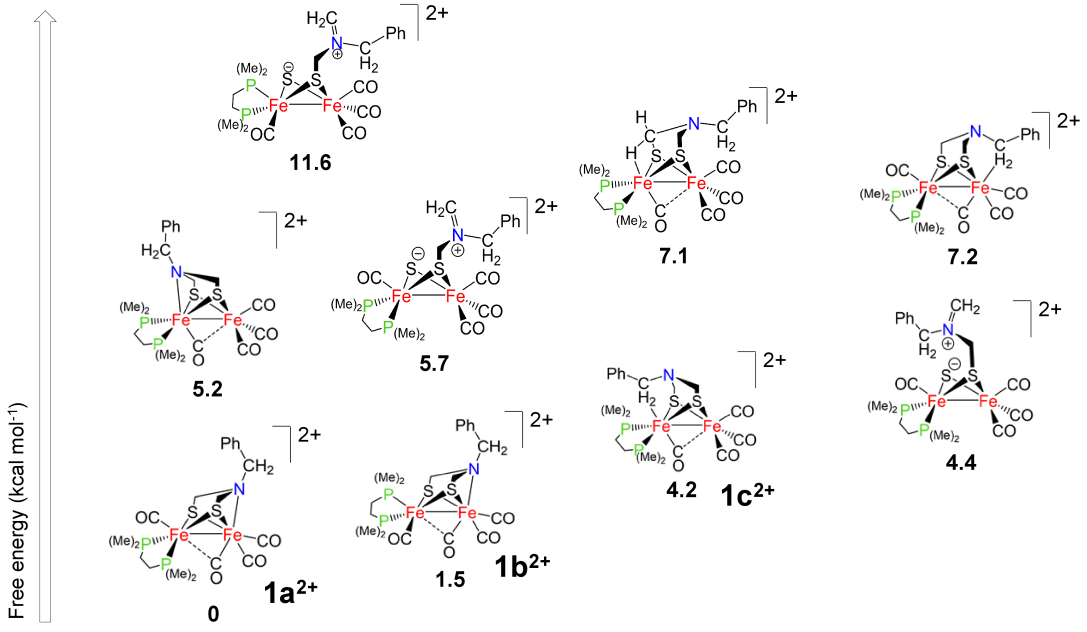

Figure 3.1.2: DFT energy minima computed for $\mathbf{1}^{2+}$ (ΔG_{solv}, kcal/mol, T=273 K; P=1 atm)

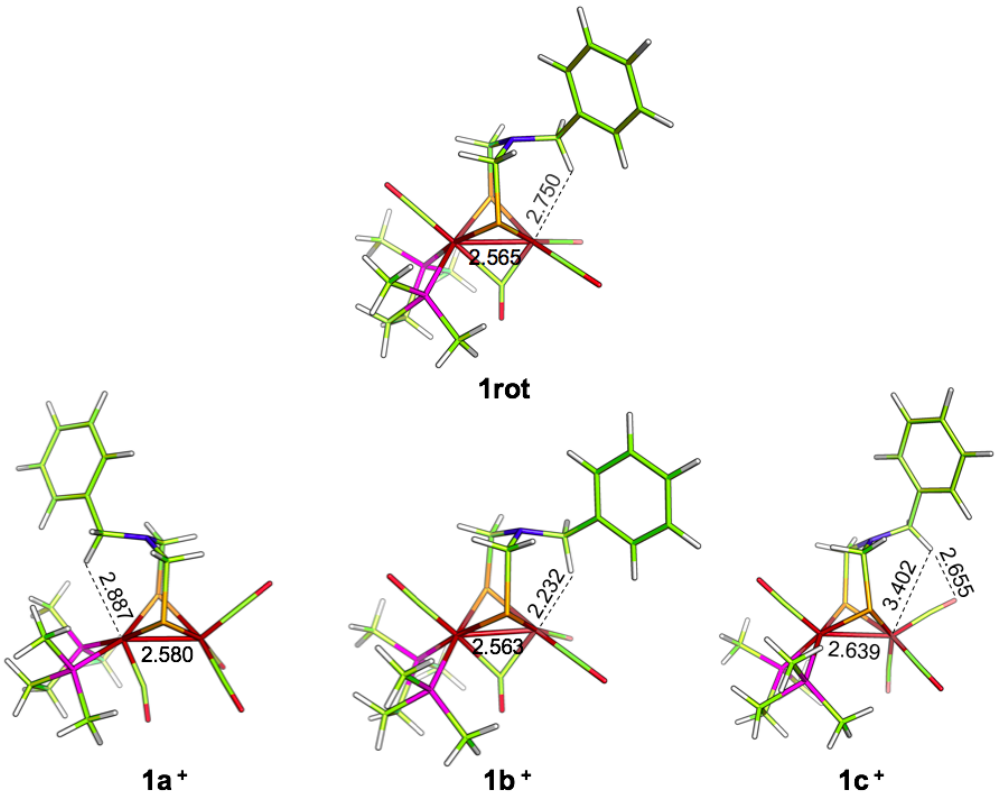

Figure 3.1.3: DFT optimized structure of **1rot** (up) and of the most stable cationic isomers, $\mathbf{1a}^+$, $\mathbf{1b}^+$ and $\mathbf{1c}^+$ (bottom). Selected distances in Å.

In all the other cases, in fact, the benzyl group rotates spontaneously to the axial position during the structure optimization, so that the methylene group slightly interacts with the apical CO (as described above in this section). The Fe-N coordination can actually trigger stability only upon the second oxidation, since the lowest energy $\mathbf{1^{2+}}$ isomers (namely $\mathbf{1a^{2+}}$ and $\mathbf{1b^{2+}}$) show a Fe-N bond (Figure 3.1.2). The Fe-N interaction is favored when the $\{Fe(CO)_2\}$ moiety is directly involved, particularly if dmpe is in dibasal disposition. Interestingly, the $\{Fe(CO)_2\}$ inverted pyramid evidently prefers interacting with the N lone pair than forming an agostic (or pseudo-agostic) interaction with the benzyl methylene group, while for the $\{FeP_2\}$ moiety the two resulting structures are almost energetically equivalent. If both Fe ions feature unrotated coordination environment, any kind of interaction with the adt^{Bn} pendant is impeded. As a result, one of the S-CH_2 bond breaks, so that the negative charge accumulated on S can balance the electron deficiency of iron centers. An additional structure featuring a peculiar agostic interaction between one Fe and one methylene proton of the adt bridge has been characterized and computed to be 7.1 kcal/mol higher in energy with respect to the ground state structure. An analogous interaction has already been observed in the dicationic form of the similar complex $Fe_2(CO)_3\{P(OMe)_3\}(\varkappa^2\text{-LL})(\mu\text{-pdt})$ with (LL = I_{Me}-CH_2-I_{Me} with I_{Me} = 1-methylimidazol-2-ylidene).[289]

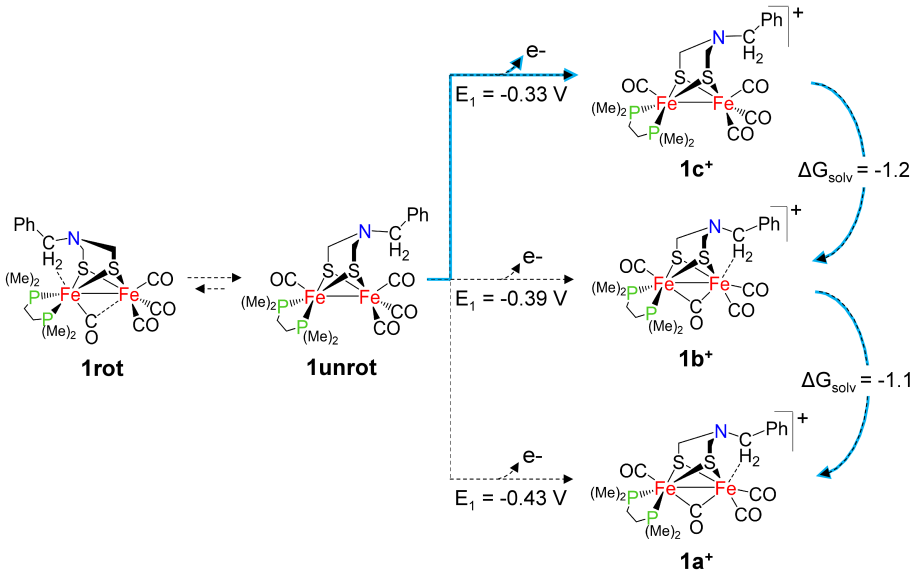

Figure 3.1.4: DFT E_{ox} values of the $\mathbf{1}^{+/0}$ couple. Free energy differences (kcal/mol) (T=273 K; P=1 atm) among $\mathbf{1}^{+}$ isomers are also reported. The pathway associated to with the computed E_1 that better matches the experimental value is highlighted with light blue arrows.

The DFT calculations suggest that unrotated→rotated rearrangements occur during the oxidative process (Figure 3.1.4). The isomer of **1** that most likely is involved in oxidation is the eclipsed **1unrot**, which is compatible with its major population in solution. The DFT oxidation potentials considering $\mathbf{1a}^{+}$, $\mathbf{1b}^{+}$ and $\mathbf{1c}^{+}$ as oxidation products are in a range of 30-130 mV of discrepancy with respect to the exp value of -0.30 V. The computed $E_{ox}^{+/0}$ value that provides the best match between experiments and theory is associated with the oxidation of **1unrot** to give the most stable eclipsed isomer $\mathbf{1c}^{+}$, which, however, would undergo isomerization to one of the lower energy rotated counterparts. The proposed DFT pathway is thus **1unrot**→$\mathbf{1c}^{+}$→$\mathbf{1a}^{+}$($\mathbf{1b}^{+}$). Such a rearrangement process fits well with the partial reversibility of the first oxidation, which is in line with the thermodynamically facile rearrangement $\mathbf{1c}^{+}$→$\mathbf{1b}^{+}$/$\mathbf{1a}^{+}$. However, it may also occur in parallel of the chemical step associated with the first oxidative process (EC) observed under N_2 for **1**.

The isomeric speciation of $\mathbf{1}^{2+}$ showed that the most stable species ($\mathbf{1a}^{2+}$) exhibits a Fe-N bond that involves the {$Fe(CO)_2$} core (Figure 3.1.2). Although the coexistence of $\mathbf{1a}^{+}$, and $\mathbf{1b}^{+}$, cannot be ruled out by DFT on a relative stability ground (also $\mathbf{1b}^{+}$ could be susceptible to further oxidation at the same potential of $\mathbf{1a}^{+}$), nevertheless the best match between theory (-0.17 V) vs experimental (-0.11 V) values for $E_{ox}^{2+/+}$ suggests the $\mathbf{1a}^{+}$→$\mathbf{1a}^{2+}$ pathway is that occurring during CV (Figure 3.1.2.1). When the product is supposed to feature an agostic interaction instead of Fe-N coordination (as in $\mathbf{1c}^{2+}$), the predicted oxidation potential is shifted towards much more positive values. These results are supportive of the idea that the second electron transfer leads to the formation of a Fe-N bond, a process that is in line with the irreversible oxidation step experimentally observed. Computations of the redox potential associated with

this second oxidative process (from cationic to bicationic species) have been performed adding explicitly the counterion PF_6^- in the models of both reactant and product. This approach is necessary to allow a fair comparison of all the different redox events, since computation of redox potentials is very sensitive to the overall charge of the system.

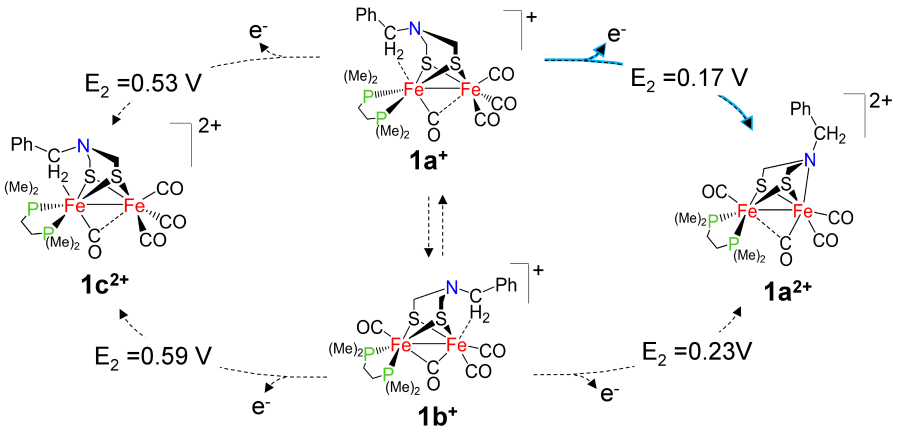

Figure 3.1.5: DFT E_{ox} values of the $\mathbf{1}^{2+/+}$ couple. The pathway associated to with the computed E_2 that better matches the experimental value is highlighted with light blue arrows.

The thermodynamic speciation of **2** points out that its ground state corresponds to an eclipsed structure featuring dmpe in dibasal position and pdt oriented towards the $\{FeP_2\}$ core. Its lowest energy monocationic form ($\mathbf{2a}^+$) is characterized by a rotated $\{FeP_2\}$ moiety and features pdt pointing towards the Fe vacant site. The flip of pdt yields $\mathbf{2b}^+$, predicted to be very close in energy to $\mathbf{2a}^+$ (only 1.0 kcal/mol less stable). The pyramidal inversion at the $\{Fe(CO)_2\}$ core is instead energetically unfavored, as already observed for the dppe analogous complex. The most stable among unrotated structures ($\mathbf{2c}^+$) lies 3.0 kcal/mol above $\mathbf{2a}^+$. The DFT oxidation potential for **2** is: -0.25 V, -0.20 V and -0.12 V if considering $\mathbf{2a}^+$, $\mathbf{2b}^+$ or $\mathbf{2c}^+$, respectively, as products. As the experimental oxidation potential is -0.24 V, the first electron transfer is expected to induce the rotation of the $\{FeP_2\}$ core. As emerged from previous studies (both experimental and theoretical) on the similar system $[Fe_2(CO)_3\{P(OMe)_3\}(\varkappa^2\text{-LL})(\mu\text{-pdt})$[289], the structural rearrangement occurring in the irreversible second electron transfer in this family of μ-pdt complexes is suggested to be associated with the formation of an agostic[294] interaction between one Fe and one methylene proton of pdt. Such kind of interaction is also present in the lowest energy isomer of $\mathbf{2}^{2+}$, and involves the $\{FeP_2\}$ moiety. In the present study, computed E_{ox} value is +0.45 V, starting from $\mathbf{2a}^+$ (+0.30 V starting from $\mathbf{2b}^+$), which could be assigned to the $\mathbf{2}^+$ irreversible oxidation experimentally detected at +0.40 V. The presence of the iron-pdt interaction must be a key structural feature of $\mathbf{2}^{2+}$ Indeed, because considering the lacking of such agostic interaction in the oxidation products of $\mathbf{2a}^+$ and $\mathbf{2b}^+$ the computed $E_{ox}^{2+/+}$

results (+0.86 V) is in complete full disagreement with experimental data. An agostic interaction has been postulated to exist in diferrous state of trisubstituted propane dithiolate $\{L_3(CO)_3$-pdt$\}$ species[288], although formed by central methylene. According to DFT, However, a similar interaction results very unstable in $\mathbf{2}^{2+}$. Computed $E_{ox}^{+/0}$ and $E_{ox}^{2+/+}$ peaks are shifted by 87 mV (exp. 60mV) and 217 mV (exp. 290 mV) when the adt^{Bn} bridge is replaced by pdt. These positive shifts are attributable to the different nature of the dithiolate bridged-head group in **1** vs **2**. The large shift of $E_{ox}^{2+/+}$ is likely due to the intramolecular agostic (or anagostic) interaction in $\mathbf{1a}^+$ and $\mathbf{1b}^+$ that makes Fe more electron rich, thus facilitating the second oxidative process. Similar arguments can be used to explain the limited shift occurring in $E_{ox}^{+/0}$ of the two derivatives: although weaker than that in $\mathbf{1}^+$ the benzyl-Fe remote agostic interaction observed in **1** could be responsible for a slightly electron richer Fe in **1** vs **2**. A nice compatibility can be noted between weaker interaction in **1** vs $\mathbf{1}^+$and $E_{ox}^{+/0}$ being far less than $E_{ox}^{2+/+}$. In addition, the speciation of $\mathbf{1}^{2+}$ shows that the Fe-N coordination is more stabilizing than the Fe-H_2C agostic interaction observed in $\mathbf{2}^{2+}$, which fairly correlates with different strength of a genuine coordination bond vs agostic (weaker) interaction. As a result, the shift of $E_{ox}^{2+/+}$peak, switching from adt^{Bn} to pdt, is larger than that of $E_{ox}^{+/0}$.

3.1.2.2 DFT investigations on the oxidative processes of 1 and 2 in the presence of CO

As aforementioned, experiments suggest that the first electron transfer in the presence of CO leads to coordination of an exogenous CO molecule to give the $\mathbf{1\text{-}CO}^+$ species.

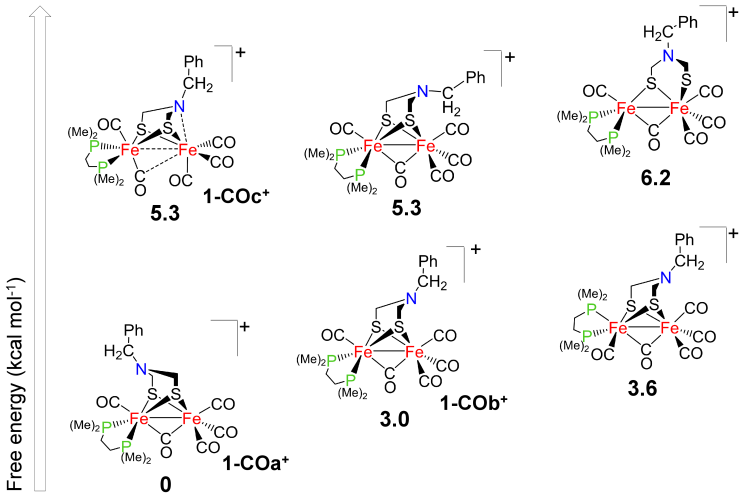

Figure 3.1.6: DFT energy minima computed for $\mathbf{1\text{-}CO}^+$ (ΔG_{solv}, kcal/mol, T=273 K; P=1 atm)

The occurrence of its further oxidation at a less positive potential than the first one, has been

rationalized on the basis of some possible structural rearrangements deriving from an interaction of adt with the diiron center. A preliminary isomeric speciation of both **1-CO**$^+$ and **1-CO**$^{2+}$ species has been carried out, in order to clarify whether the supposed amine interaction with Fe takes place before, during or after the second electron transfer. The two lowest energy isomers of **1-CO**$^+$, here referred to as **1-COa**$^+$ and **1-COb**$^+$, differ solely for the orientation of the adt^{Bn} pendant (Figure 3.1.6). They both exhibit a fully bridged CO and dmpe in dibasal position.

The only isomer detected featuring a Fe-N remote interaction (**1-COc**$^+$) is ∽5 kcal/mol higher in energy than the lowest energy isomer. In this case, the computed distance between N of adt and the Fe at the $\{Fe(CO)_2\}$ side is 2.587 Å, with concomitant shift of one CO to the $\{FeP_2\}$ side. The computed Fe-Fe distance of 3.498 Å is compatible with no intermetallic interaction, while the Fe-S-S-Fe dihedral angle of 145.8 ° reveals a smaller distortion of the Fe_2S_2 core than in the other isomers found (the computed Fe-S-S-Fe dihedral angle is 106.9° and 107.7° in **1-COa**$^+$and **1-COb**$^+$ respectively).

The binding of CO to **1a**$^+$ is predicted to be energetically highly favored (ΔE_{solv}=-14.1 kcal/mol). When considering also thermal and entropic contributions, however, ΔG_{solv} is -1.5 kcal /mol as expected from the associative nature of binding reactions involving small gaseous molecules (entailing evident loss of roto-translational entropy). Analogously, kinetic parameters $\Delta E_{solv}\neq$ and $\Delta G_{solv}\neq$ of CO to **1a**$^+$ are 9.7 kcal/mol and 17.8 kcal/mol respectively. Figure 3.1.9 shows structures and relative energies of transition states associated to CO binding, starting from relevant isomers of **1**$^+$. CO coordination in bridging position is energetically unfavorable compared to coordination to apical sites. Binding energy of CO to both Fe apical sites of **1a**$^+$ is quite similar, a result already obtained in the case of a analog $Fe_2CO_4L_2$ system.[289]

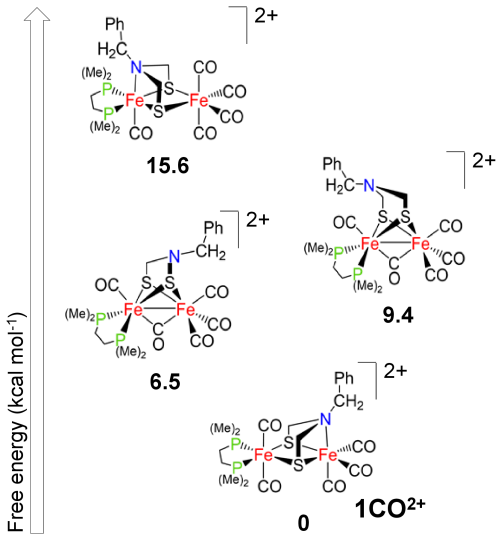

Figure 3.1.7: DFT energy minima computed for **1-CO**$^{2+}$ (ΔG_{solv}, kcal/mol, T=273 K; P=1 atm)

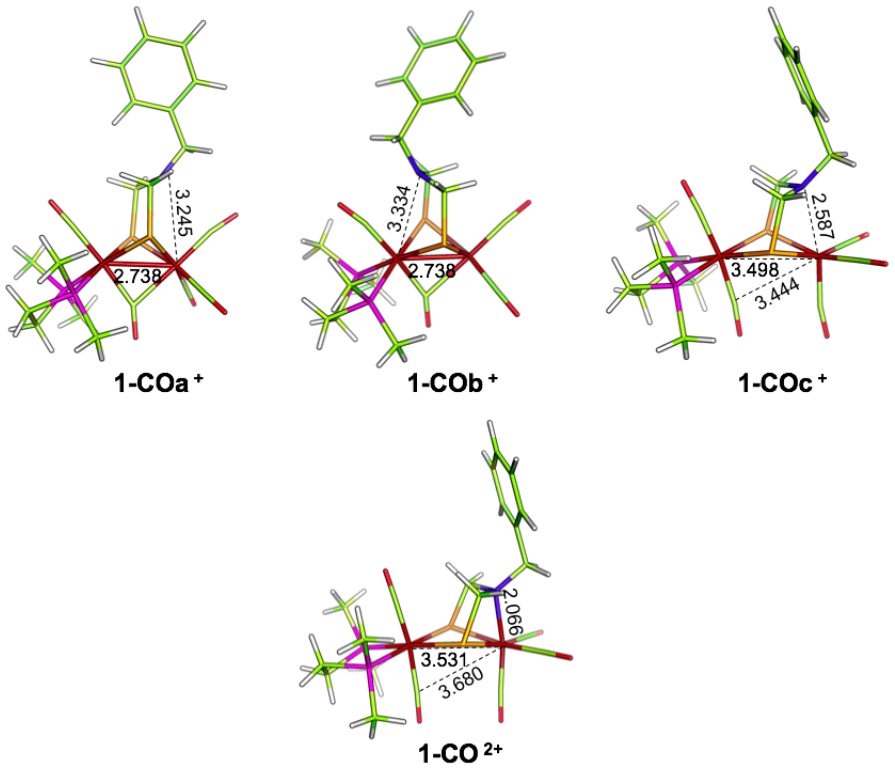

Figure 3.1.8: DFT optimized structure of **1-COa**$^+$, **1-COb**$^+$, **1-COc**$^+$(top) and of **1-CO**$^{2+}$(bottom). Selected distances in Å.

The structure if **1-CO**$^{2+}$ has been characterized at solid state and features the amine functionality coordinated to the {Fe(CO)$_2$} moiety. Also the DFT conformational search of **1-CO**$^{2+}$ confirms that **1-CO**$^+$ oxidation leads to the coordination of the amine to one Fe center, unambiguously that of the {Fe(CO)$_2$} moiety (Figure 3.1.7). Indeed, the structure with Fe-N bond involving the {FeP$_2$} center lies 15.6 kcal/mol above. The optimized **1-CO**$^{2+}$structure is presented in Figure **3.1.8**.

As experimentally observed: 1) each iron atom coordination sphere could be depicted as a distorted octahedral geometry, 2) the Fe-Fe distance (3.531 Å DFT vs 3.421(12) Å exp.) suggests no bonding interaction between metal centers, 3) the Fe$_2$S$_2$ core is close to planarity (Fe-S-S-Fe dihedral angle = 156.1° DFT vs 152.2° exp.) and 4) the dmpe P atoms are almost co-planar with the Fe$_2$S$_2$ core and with two equatorial CO's coordinated to the other Fe atom. Despite the fact that isomers featuring Fe...N interactions in **1-CO**$^+$ are calculated to be slightly less favored compared to other eclipsed isomers, DFT clearly indicates that a key for rationalizing the fact that the CO adduct **1-CO**$^+$ is easier to oxidize than **1**, (unlike **2**), lies in the nature of **1-CO**$^+$ and requires a Fe...N interaction. In fact, experiments revealed that **1-CO**$^+$ oxidation occurs at a potential $E_{ox1}^{1/2}$ < -0.30 V (Figure 3.1.2.2). Computations suggest that such a scenario is satisfied only when considering **1-COc**$^+$ (featuring Fe...N interaction) as starting point for oxidation ($E_{2(CO)}$ = -0.51 V). Indeed, $E_{2(CO)}$ values obtained starting from **1-COb**$^+$ and **1-COa**$^+$ (both lacking the Fe...N interaction) are -0.27 V and -0.20 V respectively, in contrast

with experimental observations. Moreover, when an electron donor (N lone pair) is present (in **1**), the final diferrous species (**1-CO^{2+}**) is stabilized by the Fe-N coordination so that the Fe-Fe interaction is no longer required to fulfill the 36e counting.[288, 181]

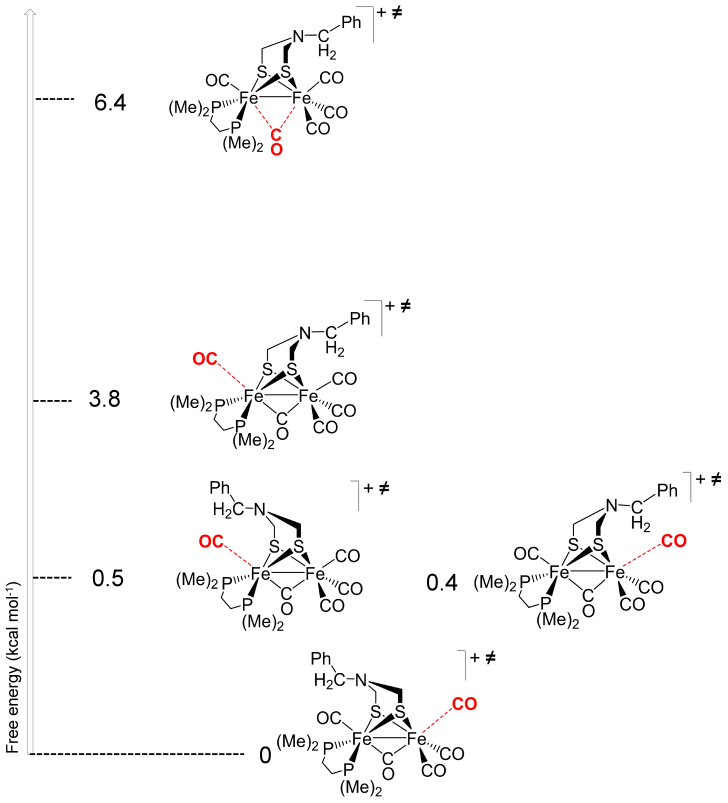

Figure 3.1.9: Transition states with relative free energy values (ΔG_{solv}) associated to the reaction between **1**$^{+}$and CO.

Moreover, CO binding to **2**$^{+}$is predicted to be exergonic, independently on which **2**$^{+}$ isomer is considered. In analogy with **1-CO**$^{+}$, also the most stable **2-CO**$^{+}$ rotamers feature dmpe in dibasal position (**2-COa**$^{+}$ and **2-COb**$^{+}$). Stability of the **2-CO**$^{+}$ adduct is not affected by the orientation of pdt. Concerning **2-CO^{2+}**, the two lowest energy isomers are both characterized by a coordination geometry with a bridging CO and dibasal dmpe. The most stable bis-cationic isomer (Figure 3.1.14, **2-COa^{2+}**) features pdt oriented towards the {Fe(CO)$_2$} unit (while the other pdt orientation –not shown- is less stable by 1.5 kcal/mol). Two structures presenting an agostic interaction (Fe-H$_2$C(pdt) has been found that lie 16.7 and 20.3 kcal/mol above **2-COa^{2+}**. Their structure resemble that of **1-CO^{2+}**, since: i) the Fe_2S_2 core is only slightly distorted (avg Fe-S-S-Fe dihedral angle = 151.6°), ii) the intermetallic bond is absent (avg Fe-Fe distance = 3.523 Å) and iii) dmpe lies in the equatorial plane containing the Fe_2S_2 subunit plus two CO (coordinated to the opposite Fe). They differ for the methylene group of pdt strap that donates C-H in the agostic interaction to Fe: in the most stable of the two (**2-COb^{2+}**, Figure 3.1.11) it is the central methylene group, while in the other structure –not shown- it is a

side methylene. Interestingly, and unlike **1-CO**$^{2+}$, any interaction between Fe centers and the pendant is disfavored, an observation confirmed by **2-CO**$^{+}$ DFT oxidation potentials. In fact, although both oxidations leading to **2-COa**$^{2+}$ and **2-COb**$^{2+}$ are predicted to occur at more positive potentials than the first one (-0.24V), in line with experiments, the best match with the experimental E_{ox} (0.05 V) is reached when the product does not show any agostic interaction (0.17 V).

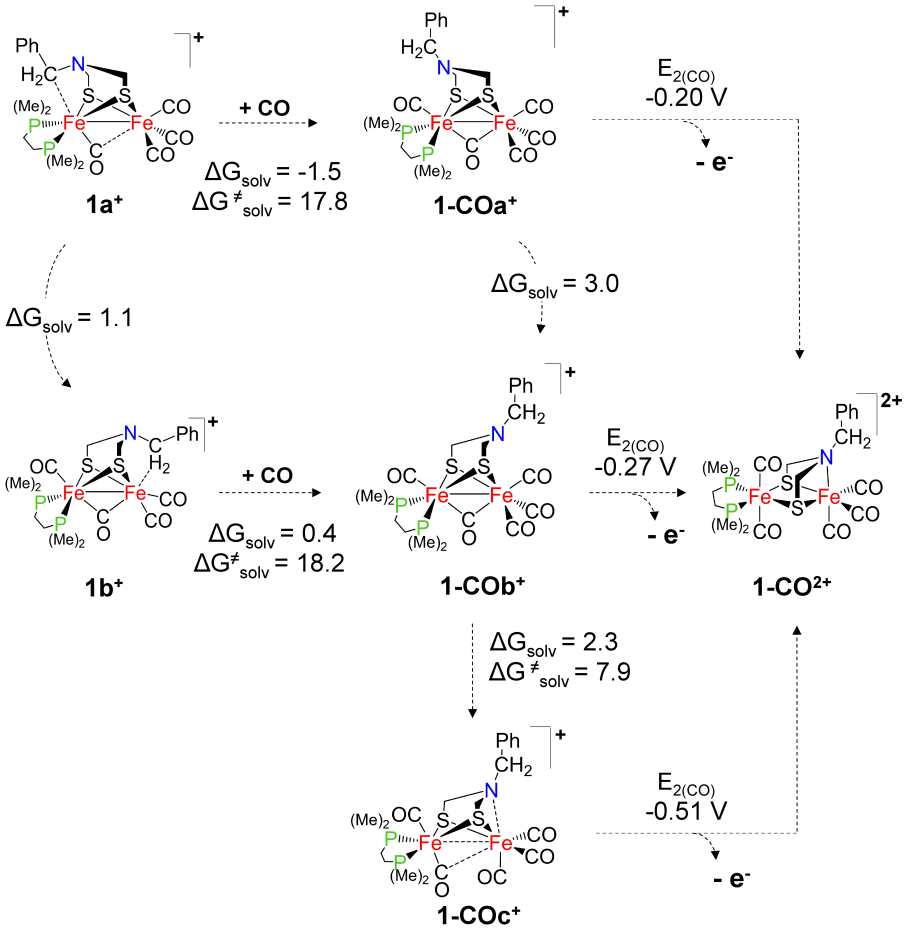

Figure 3.1.10: DFT mechanism of **1** oxidation under CO atmosphere. Solvent corrected free energies and redox potentials are reported in kcal/mol and V, respectively. As a note: a marginal inconsistency in thermodynamic closed cycles (i.e., among G values vertically reported and E° horizontally reported) is due to different modelling level employed to simulate the two: computational E° has actually required the explicit use of negative counterions to get acceptable match of experimental CV values. For simplicity, however, they have been omitted for simulating relative stability among isomers (as in such case their presence is less relevant).

Indeed, oxidation of **1** and **2** (showing a Fe-Fe bonding HOMO) causes an apparently unexpected shortening of the Fe-Fe distance and oxidation of **1**$^{+}$ and **2**$^{+}$ (showing an antibonding Fe-Fe HOMO) leads to the full break of the Fe-Fe bond. Such a behavior can be easily justified, however, by aforementioned electron-counting argumentation. The loss of the first electron is

balanced by a stronger Fe-Fe interaction in $Fe^{I}Fe^{II}$ forms (each Fe is a one electron donor), while eventual Fe...N or agostic interactions can stabilize the two electron deficiency in diferrous species without the necessity of invoking the intermetallic bond.

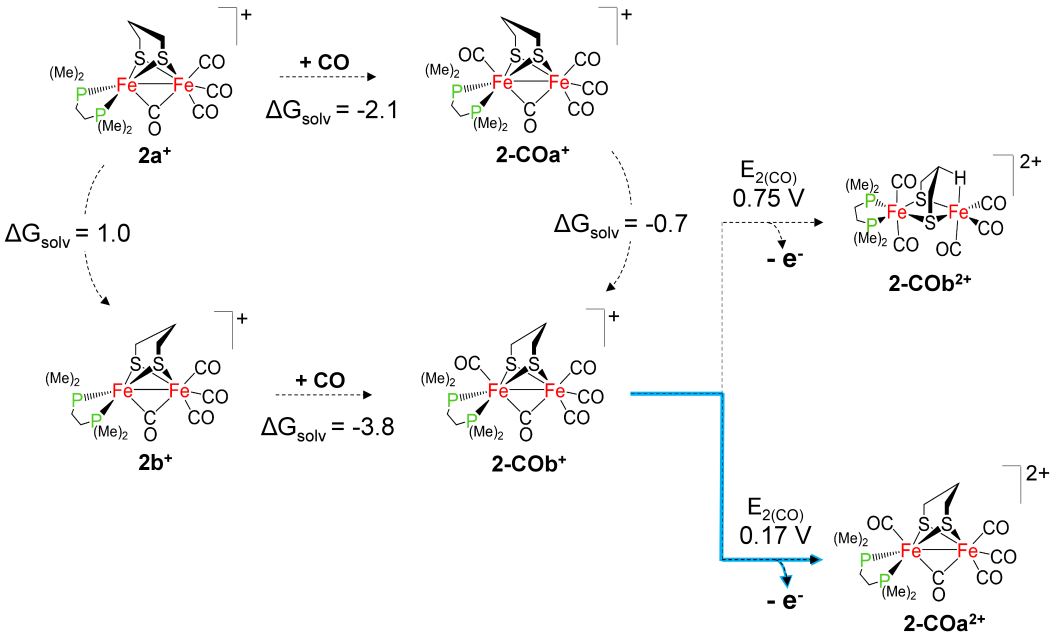

Figure 3.1.11: DFT mechanism of **2** oxidation under CO. Solvated free energy (T=273 K ; P=1 atm) and oxidation potentials are reported in kcal/mol and V, respectively. Light blue shows the pathway that better fits experimental CV features.

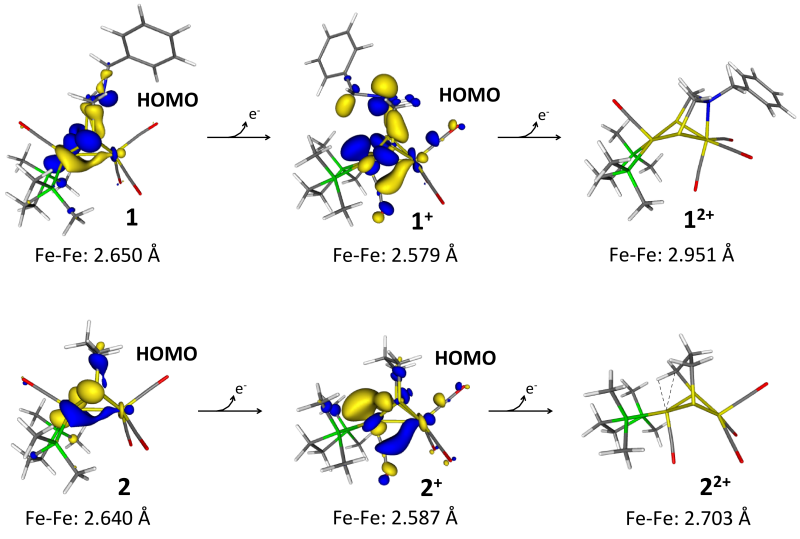

Figure 3.1.12: Fe-Fe bond behavior upon first and second reductions. HOMO cutoff 0.035 a.u.

3.1.3 Conclusions

In summary, the present study evidences the role of stabilizing interactions in the oxidative behavior of the first $Fe^{I}Fe^{I}$ derivative featuring the same rotated conformation present in the FeFe-hydrogenase active site. DFT provided insights on (experimentally) elusive cationic states and a possible mechanistic rationale underlying the different behavior of CV performed under N_2 vs CO. The oxidative mechanisms are summarized in Figure **3.1.13**. $\mathbf{1}^{+}$, as its neutral precursor **1**, is stabilized through an anagostic Fe...HC interaction between the Bn group and the iron center ($\mathbf{1a}^{+}$). Such an interaction, absent in the pdt analogue $\mathbf{2}^{+}$, is responsible for the easier oxidation of the nitrogen based $Fe^{I}Fe^{II}$ species (Figure 3.1.13 and 3.1.14, step B) that affords $\mathbf{1^{2}}^{+}$, featuring the amine coordinated to one iron atom. The role of a weak Fe...HC interaction in stabilizing the inverted (rotated) conformation of **1** was recently highlighted.[291] The present investigation indicates that such elusive interaction can also modulate redox properties of diiron dithiolates. In the presence of CO, the agostic interaction, is removed by the coordination of CO, giving the formation of $\mathbf{1\text{-}CO}^{+}$ (Figure 3.1.13, step C). That induces a flip of the nitrogen atom towards the $\{Fe(CO)_2\}$ moiety.[295] The oxidation of $\mathbf{2}^{+}$ also allows CO addition at the $Fe^{I}Fe^{II}$ core, affording $\mathbf{2\text{-}CO}^{+}$ (Figure 3.1.14, step C). One of the most relevant results is that oxidation of $\mathbf{1\text{-}CO}^{+}$ to $\mathbf{1\text{-}CO^{2}}^{+}$ is easier than that of **1** into $\mathbf{1}^{+}$ (Figure 3.1.13, step D), thus indicating an inversion of the potentials which is not observed with **2** (Figure 3.1.14, step D). Further, we have shown that a Fe...N interaction is not sufficient alone to explain the redox potential inversion. Indeed, the Fe-N coordination is predicted also in $\mathbf{1^{2}}^{+}$ (i.e. in the absence of CO) that is formed at a potential higher than that of $\mathbf{1}^{+}$ (Figure 3.1.13). Moreover, the absence of potential inversion in the case of **2** shows that also the coordination of CO to the diiron core is not a decisive point. All these observations led us to conclude that a Fe...N interaction should be present in the CO adduct already at the $Fe^{I}Fe^{II}$ stage, although in a less populated isomer (Figure 3.1.13, species $\mathbf{1\text{-}CO}^{+}$). All the illustrated results reveal the straight influence of the replacement of CH_2 with NR into the dithiolate bridge on the redox behavior of diiron models of [FeFe]-hydrogenase. A stabilizing effect of N-based pendant to the unsaturated diferrous centers of similar dithiolates has been previously discussed. Yet, for the first time we investigated by DFT all molecular details underlying an unpredicted reactivity, pointing out the role of the N---Fe interaction already at the $Fe^{I}Fe^{II}$ oxidation level, which, to the best of our knowledge, is unprecedented in the realm of [FeFe]-hydrogenase mimics. The observation of the potential inversion phenomenon only in the N-containing bridgehead species affords an interesting example of how to tailor the molecular scaffold of the diiron dithiolate so as to switch on or off a given redox property.

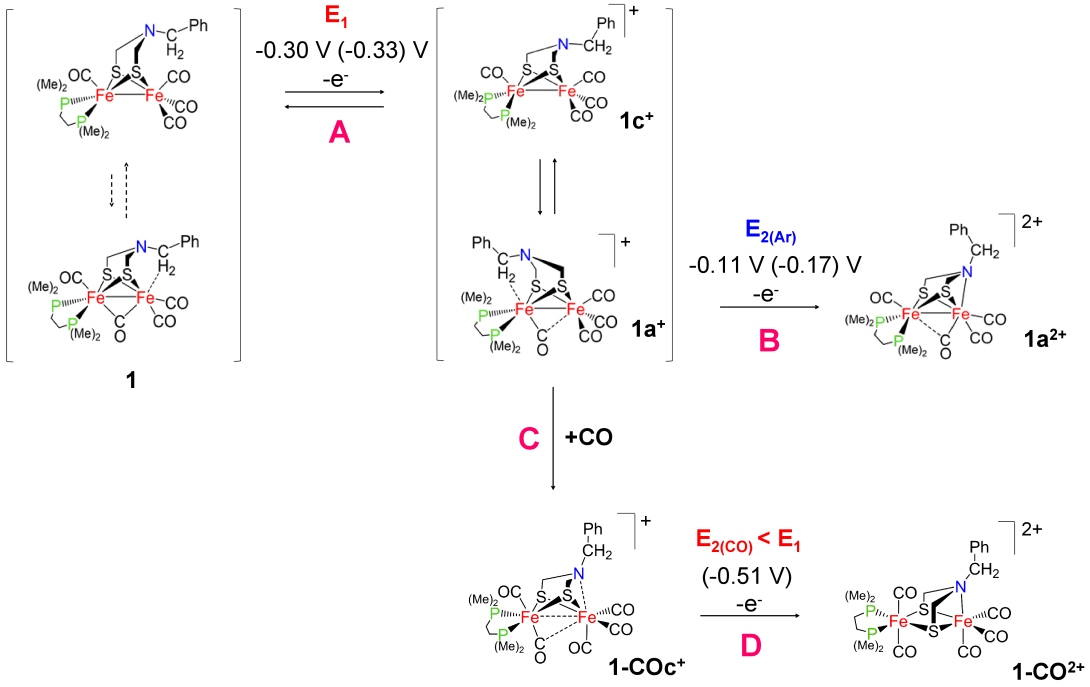

Figure 3.1.13: Oxidative process of $[Fe_2(CO)_4(\varkappa^2\text{-dmpe})(\mu\text{-}adt^{Bn})]$ (**1**). (Calculated redox potentials are in parenthesis).

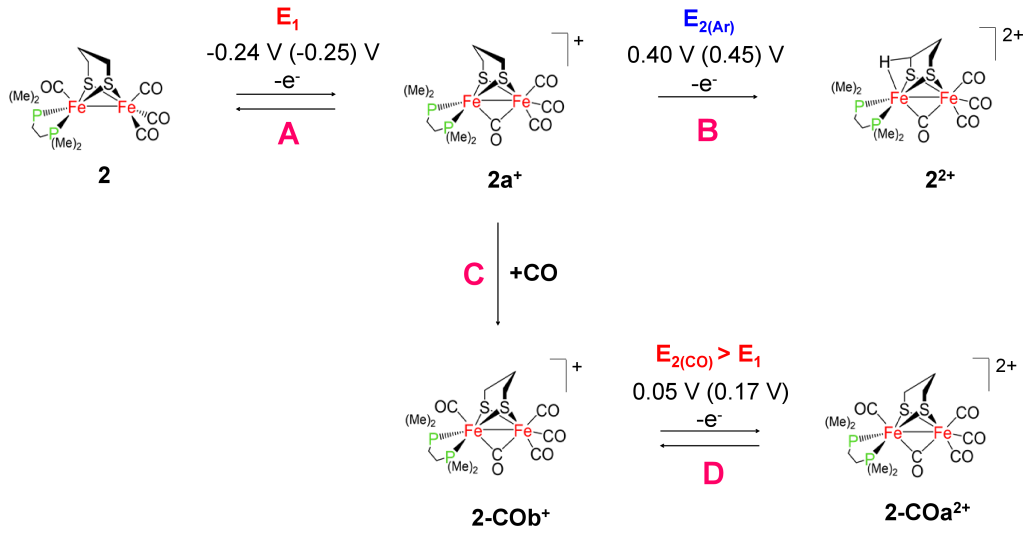

Figure 3.1.14: Oxidative process of $[Fe_2(CO)_4(\varkappa^2\text{-dmpe})(\mu\text{-}pdt)]$ (**2**). (Calculated redox potentials are in parenthesis).

3.2 Mechanisms of proton reduction catalyzed by $[Fe_2(CO)_6\{\mu\text{-}(SCH_2)_2(R)P{=}O\}]$ (R = Ph, Et) models

In collaboration with W. Weigand and L. Almazahareh, Jena University, Germany

3.2.1 Introduction

It is well known that, in the proton reduction process, a proton relay from the NH group to the vacant Fe_d site is a key mechanistic element, that results in the formation of terminal Fe_d-hydride species and, subsequently, in H_2 evolution. In the biological system, the azadithiolate cofactor is proposed to shuttle protons to and from the diiron core via an agostic or hydrido–proton interaction.[37, 44, 296] The same processes have also been observed in related biomimic compounds, where protonation of the iron centers to form terminal or bridging hydrides, as well as of the diothiolate bridge-head, is considered as a fundamental step in proton reduction catalysis.[297, 298, 281, 299, 300, 301] As a consequence, enhancing the system protophilicity would be a promising strategy to reach higher catalytic performances. Taking the simplest [FeFe]-hydrogenase model $[Fe_2(CO)_6(\mu\text{-adt})]$ as starting point, one can increase its protophilicity by substituting one or more CO's with donor groups (see section 3.3), affecting significantly not only acid/base properties but also reduction potentials (that yet become more unfavorable), or, alternatively, one can only act on the bridge-head by substituting adt with more basic dithiolate linkers. This second strategy is the one followed in this work.

Protonation of model systems of the active site at NR bridgehead groups as well as at N-containing pendant ligands (pyridine or amine functionality) that are either attached to the dithiolato linker or to mono- and bidentate phosphine ligands has been well investigated in several reports. However, protonation of the amine functionality by moderately strong acids (e.g. CF_3CO_2H) is only reported for tetrasubstituted model complexes. The protonation of the amine group of the hexacarbonyl complexes $[Fe_2(CO)_6\{\mu\text{-}(SCH_2)_2NR\}]$ requires very strong acids such as $HBF_4{\cdot}Et_2O$. Consequently, the catalytic reduction of moderately strong acids by $[Fe_2(CO)_6\{\mu\text{-}(SCH_2)_2NR\}]$ should start with reduction of the complex for the protonation to be accessible. W. Weigand and colleagues have recently described the synthesis and protonation of a novel type of the [FeFe]-hydrogenase models with phosphine oxide in the dithiolato linker, namely $[Fe_2(CO)_6\{\mu\text{-}(SCH_2)_2(Ph)P{=}O\}]$[302] (**1**) and $[Fe_2(CO)_6\{\mu\text{-}(SCH_2)_2(Et)P{=}O\}]$ (**2**) (Figure 3.2.1). While the RP=O functionality of **1** in CH_2Cl_2 solution can be protonated only in the presence of the strong $HBF_4{\cdot}Et_2O$, substitution of the R = Ph group by R = ethyl group in **2** results in a pronounced increase in protophilicity. In fact, **2** can be protonated by moderately strong acid (like trifluoroacetic acid, TFA), in contrast to analogous hexacarbonyl electrocatalysts.

DFT (BP86/TZVP/COSMO, ε = 8.93) has been used to address a series of issues in order to complement or rationalize experimental observation. Several aspects about **2** protonation and redox events have been described and clarified by computations. Additionally, the overall mechanism associated to H_2 evolution by **2** has been dissected.

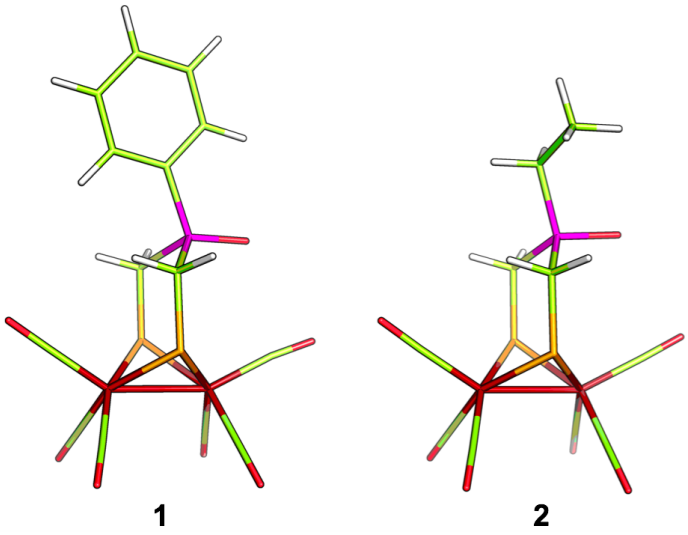

Figure 3.2.1: DFT optimized structures of **1** and **2**.

3.2.2 Results and discussion

3.2.2.1 Investigation of 2 reductive behavior in the absence of acid

Cyclic voltammetric experiments of **2** revealed that, analogously to **1**, its reduction occurs via two-electron transfers in a single step with potential inversion, a behavior already observed also for related hexacarbonyl systems (see section 1.4.1). Table 3.2.1 summarizes the redox properties of both **1** and **2** in different solvent. In CH_2Cl_2/NBu_4PF_6 solution, the half-wave potential of complex **2** ($E_{1/2}$ = -1.51 V) is slightly more negative than that of complex **1** ($E_{1/2}$ = -1.48 V), which reflects the stronger electron donating ability of the Et group in complex **2** compared to the Ph group in complex **1**. Similar trend is found in $MeCN/NBu_4PF_6$ solution. In comparison, the cathodic peak potentials (E_{pc}) of the P=O-systems in MeCN solution are less negative than those of various $[Fe_2(CO)_6\{\mu\text{-}(SCH_2)_2NR\}]$ models with -1.49 $\leq E_{pc} \leq$ -1.69 V. The oxidation potentials (MeCN solution) of the P=O-models are generally more positive than those of the $[Fe_2(CO)_6\{\mu\text{-}(SCH_2)_2NR\}]$ complexes (+0.46 $\leq E_{ox} \leq$ +0.73 V). In other words, the reduction of the P=O-complexes is generally easier than in the reduction of $[Fe_2(CO)_6\{\mu\text{-}(SCH_2)_2NR\}]$ whereas the oxidation is harder. This difference is related to the higher electron withdrawing nature of the $\mu\text{-}(SCH_2)_2(R)P{=}O$ compared to $\mu\text{-}(SCH_2)_2NR$.

DFT has been used to compute the first and the second reduction potentials separately, in order to characterize the elusive nature of mono- and bi-reduced species. Table 3.2.2.1 shows the main experimental/computed geometrical parameters of neutral, monoanionic and bianonic form isomers. The structural features of **2** are well reproduced at the in-vacuum BP86/TZVP level and DFT distances are only slightly overestimated with respect to the XRD values, as well as the average P-C-S angle (117.9° and 115.6° respectively).

Complex	solvent	E_{pc}	E_{pa}	$E_{1/2}$	E_{ox}
1	MeCN	-1.42	-1.23	-1.32	+0.78
	CH_2Cl_2	-1.52	-1.43	-1.48	+0.71
2	MeCN	-1.43	-1.34	-1.39	+0.74
	CH_2Cl_2	-1.57	-1.44	-1.51	+0.71

Table 3.2.1: Summary of the redox properties of 1 and 2. Potentials (in V vs. ferrocenium/ferrocene couple) are at 0.2 V s^{-1}.

Geometry optimizations have been performed in gas-phase and solvent effects have been included *a posteriori* at a single point level. Only CH_2Cl_2($\varepsilon = 8.53$) has been considered, since it has been subsequently used in dihydrogen evolution experiments.

	Distances (Å)					**ΔE (kcal/mol)**	
	Fe-Fe	Fe-S				$\varepsilon = 1$	$\varepsilon = 8.53$
2 XRD	2.511	2.260	2.259	2.253	2.255		
2	2.552	2.284	2.284	2.279	2.282	0	0
$\mathbf{2}_{eq}$	2.539	2.293	2.291	2.276	2.277	2.07	2.21
$\mathbf{2}_{rot}$	2.597	2.316	2.315	2.300	2.300	8.57	7.97
$\mathbf{2}^-$	2.829	2.321	2.322	2.323	2.320	2.00	0
$\mathbf{2}^-_{eq}$	2.819	2.365	2.304	2.326	2.321	0	0.16
$\mathbf{2}^-_{\mu-CO}$	2.557	2.286	4.343	2.280	2.306	0.79	0.43
$\mathbf{2}^-_{\mu-CO,eq}$	2.557	2.288	4.344	2.279	2.306	0.91	0.50
$\mathbf{2}^-_{rot}$	2.942	2.339	2.342	2.327	2.330	1.77	2.08
$\mathbf{2}^-_{eq,rot}$	2.919	2.340	2.323	2.348	2.324	6.44	5.99
$\mathbf{2}^{2-}_{\mu-CO}$	2.638	2.288	4.196	2.322	2.448	0	0
$\mathbf{2}^{2-}_{eq}$	3.471	2.371	2.371	2.334	2.337	10.51	12.73

Table 3.2.2: Main DFT optimized geometry parameters and relative energies of **2,** $\mathbf{2}^-$and $\mathbf{2}^{2-}$isomers.

Considering the relative energies of the different isomers (Table 3.2.2.1), the in-solvent optimized stereoisomer attaining the P=O moiety in equatorial position ($\mathbf{2}_{eq}$) is 2.07 kcal/mol less stable than the axial counterpart, while the rotated form, $\mathbf{2}_{rot}$, which shows a vacant site on an iron atom, is 8.12 kcal/mol higher than **2**. A similar trend is observed for gas-phase energies.

The monoanion lowest energy isomers are different if considering $\varepsilon = 1$ or $\varepsilon = 8.93$. In the gas-phase the most stable structure ($\mathbf{2}^-_{eq}$) presents an unrotated structure with P=O moiety in equatorial position, while in CH_2Cl_2 environment $\mathbf{2}^-_{eq}$ is almost isoenergetic to $\mathbf{2}^-$, in which the P=O group is in axial position (Figure 3.2.2). If considering solvent effect, only 0.43 kcal/mol higher than $\mathbf{2}^-$ we found an isomer in which a CO group is rotated to the bridging position and a

Fe-S bond is broken ($\mathbf{2}^{-}_{\mu-\mathrm{CO}}$, which is almost isoenergetic to its counterpart with equatorial P=O, namely $\mathbf{2}^{-}_{\mu-\mathrm{CO,eq}}$). The remaining less stable isomers ($\mathbf{2}^{-}_{\mathrm{rot}}$ and $\mathbf{2}^{-}_{\mathrm{eq,rot}}$) present both a rotated structure with a semibridging CO and differ only for the stereochemistry of the P=O functionality. The structural changes upon reduction can be rationalized on the basis of **2** LUMO, which is antibonding with respect to Fe-Fe and Fe-S distances. This result is in line with the general concomitant Fe-Fe and Fe-S bond weakening in the anionic isomers. In particular, in $\mathbf{2}^{-}$, $\mathbf{2}^{-}_{\mathrm{eq}}$ and $\mathbf{2}^{-}_{\mathrm{rot}}$, obtained from the reduction of **2**, $\mathbf{2}_{\mathrm{eq}}$ and $\mathbf{2}_{\mathrm{rot}}$ respectively, the Fe-Fe distances are increased on average by 0.301 Å with respect to the neutral form. The computed Fe-Fe and Fe-S distances of these minima are also comparable to the ones obtained for the isomer $\mathbf{2}^{-}_{\mathrm{eq,rot}}$. The only exception is given by $\mathbf{2}^{-}_{\mu-\mathrm{CO}}$, in which the additional electron leads to the break of a single Fe-S bond, while Fe-Fe and the remaining Fe-S distances are shorter than in the other minima, as a result of the shift of one CO group to the bridging position. The break of a Fe-S bond becomes energetically favored upon second reduction, since the ground state of the bianonic form is unambiguously $\mathbf{2}^{2-}_{\mu-\mathrm{CO}}$species, being 12.7 kcal/mol more stable (in solvent) then $\mathbf{2}^{2-}_{\mathrm{eq}}$ (Figure 3.2.3).

In order to reproduce experiments, the computed redox potentials presented in this work have been scaled by using the Fc^{+}/Fc as reference, whose potential, computed according to the same protocol, is -5.06 V (in CH_2Cl_2). Since redox potential computation is very sensitive to the overall charge of the system, counterions (K^{+}, Br^{-}) have been explicitly added during optimizations when needed. In this way, the comparison between all the different redox phenomena can be fair. Such a protocol was necessary to afford the closest match of theory versus experimental values.

Interestingly, computed redox potentials associated to first and second one-electron reductions of **2** involving the ground state structure of each redox state provided the bast match theory vs experiments. I fact, computed $E_{1(\mathrm{calc})}$ and $E_{2(\mathrm{calc})}$, related to $\mathbf{2} \rightarrow \mathbf{2}^{-}$ and $\mathbf{2}^{-} \rightarrow \mathbf{2}^{2-}_{\mu-\mathrm{CO}}$ are -1.67 V and -1.48 V respectively, so that, if considering the overall double reduction $E_{(\mathrm{calc})} = (E_{1(\mathrm{calc})}+E_{2(\mathrm{calc})})/2$ = -1.58 V, which is very close to the experimental value E_{pc}= -1.57 V vs Fc^{+}/Fc couple.

3.2.2.2 Protonation study

W. Weigand et al. previously reported protonation studies performed on **1**, indicating that i) it could be protonated only by strong acids such as $HBF_4{\cdot}Et_2O$ (∼100 equiv.), ii) its potonation occurs at the P=O functionality and iii) the carbonyl bands result shifted of ∼10 cm^{-1} to higher wavenumbers upon protonation.[302] The presence of 1-3 equiv. $HBF_4{\cdot}Et_2O$ in the CH_2Cl_2 solution of complex **2** did not affect its υ(CO) bands, which means that no reaction took place. The presence of 6.0-10 equiv. $HBF_4{\cdot}Et_2O$ resulted, instead, in an average shift of the carbonyl bands, Δυ(CO), by ∼8 cm^{-1}, which is comparable to that observed in case of complex **1** (∼10 cm^{-1}) and suggests protonation at the P=O functionality. Addition of 10-100 equiv. of TFA to the CH_2Cl_2 solution of complex **2** causes a Δυ(CO) of only ∼5 cm^{-1} to higher wavenumbers. The average shift of the υ(CO) bands upon protonation of the P=O functionality by TFA is thus less evident than that observed upon protonation of complex **1** (∼10 cm^{-1}) or **2** (∼8 cm^{-1}) by

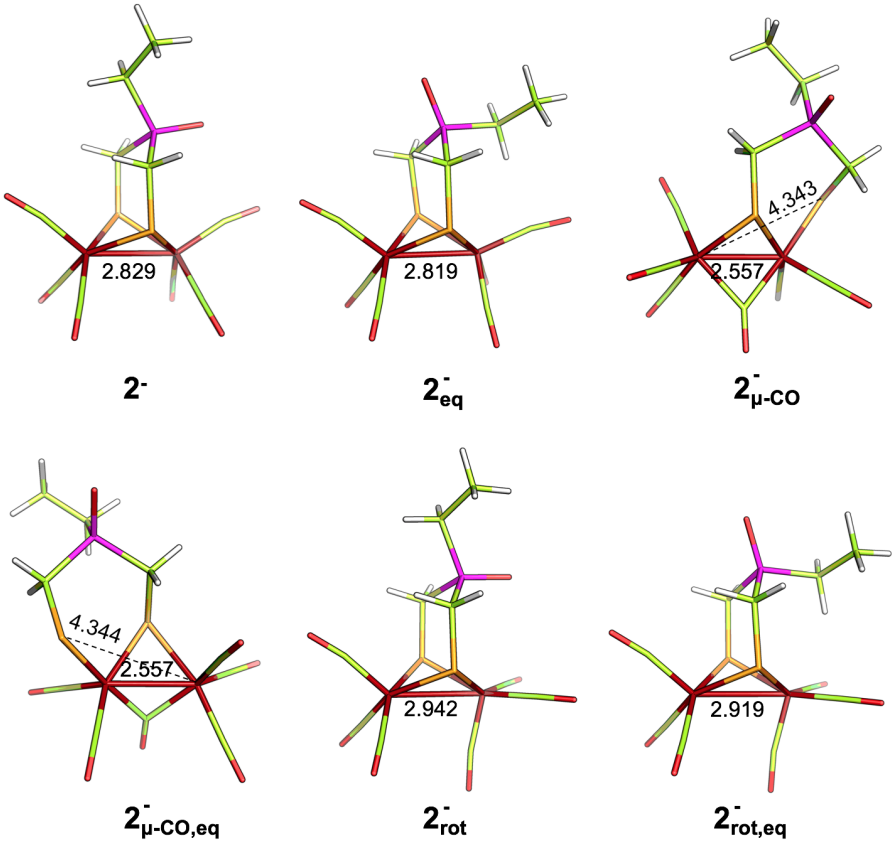

Figure 3.2.2: DFT optimized structures of $\mathbf{2}^-$ isomers. Selected distances are in Å.

$HBF_4{\cdot}Et_2O$, suggesting that the ion-pairing effect of TFA^- should be more significant than that of BF_4^-.

The regiochemistry of protonation at the P=O functionality in **2** has been confirmed by computations. Indeed, even the Fe-Fe μ-monoprotonated form results 8.79 kcal/mol higher in energy than the $P{=}OH^+$ adduct. The differences between **1** and **2** protonation properties, as well as ion-pairing effects of both TFA and HBF_4conjugate bases, have also been theoretically dissected. First of all, the increased proton affinity of complex **2** has been evaluated by NBO charges and by HOMO atomic population analysis of the P=O functionality. Although it could be noticed that on the P=O group of complex **2** is localized a slightly more negative charge and a higher HOMO population in comparison to complex **1**, such differences are too small to be sufficient to reliably rationalize the truly different behavior of the two systems. Indeed, a relative pK_A (referred to the P=O functionality) between the two complexes has been calculated.

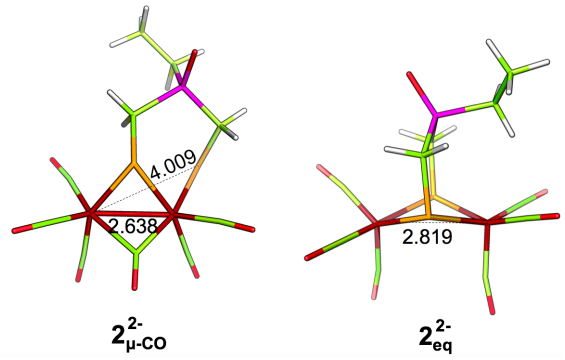

Figure 3.2.3: DFT optimized structures of $\mathbf{2}^{2-}$ isomers. Selected distances are in Å.

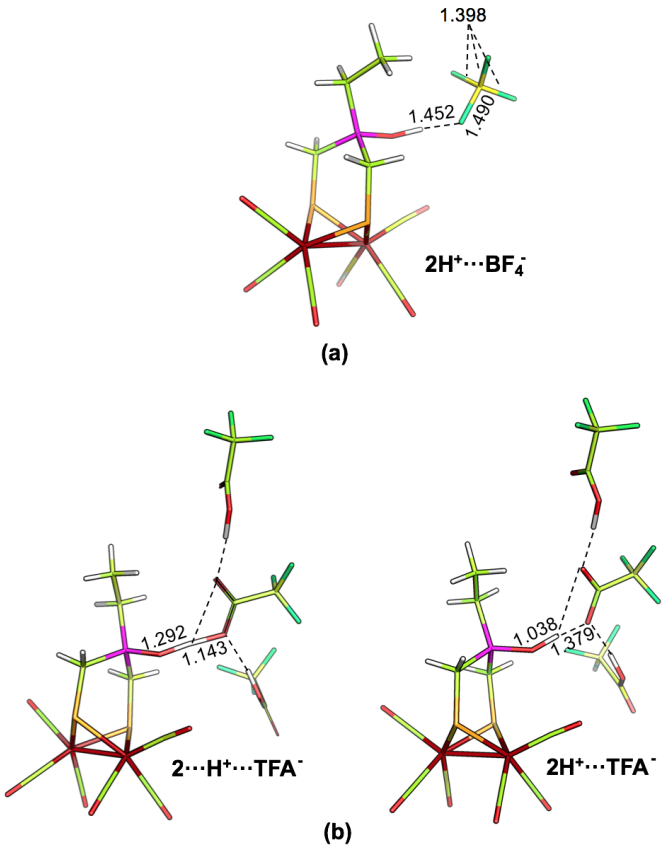

Figure 3.2.4: DFT optimized structures (ε = 8.93) of the $\mathbf{2H^+(O)}$ adducts with BF_4^- (top, panel **a**) and TFA- (bottom, panel **b**) as the conjugate base.

For each model we obtained the K_A values from the relation ΔG = -RT lnK_A, where T=298.15 K, R=1.987 cal/(mol·K) and where ΔG (kcal/mol) is the computed free energy difference between the P=O protonated species and the neutral one, without considering the free energy of the proton. In fact, what we are interested in is a variation of basicity (ΔpK_A = pK_A(**2**) - pK_A(**1**)) caused by the substitution of the phenyl group with an ethyl one, and in this way we don't need

to include the solvated G°(H^+) value in our computations. Our results reveal a ΔpK_A value of 1.44 units (in CH_2Cl_2), supporting a significant improved basicity in **2**.

Including explicit acid molecules (TFA and HBF_4) and their conjugate bases has allowed to study in a more detail the protonation of **2** and the different ion-paring effects of both TFA^- and BF_4^-. The optimized structures of the adduct of **2** protonated at P=O (hereafter referred as $\mathbf{2H^+(O)}$) with HBF_4 is reported in Figure 3.2.4(a). The analysis of BF_4^- counterion bond lengths in the adduct supports your hypothesis that the B-F bond involved in the H-bond with the P=OH^+ group is elongated with respect to the others. The H-bond between the anion and the P=OH^+ functionality weakens one of the B-F bonds and causes a distortion of the BF_4^- tetrahedral structure. In fact, if we consider the F-B-F average angle, considering the other three F atoms, we obtain a value of 112.1° higher than the expected 109.5° of the free anion. This result nicely agrees with experimental observation, since Our attempt to crystallize the protonated complex **2** by diffusion of dry pentane into dry CH_2Cl_2 solution of complex **2** in the presence of excess $HBF_4{\cdot}Et_2O$ under N_2 overnight led to the formation of a P=O---BF_3adduct through loss of a HF molecule. Such a behavior has been previously described by Beck et al. for the reaction between $HBF_4{\cdot}Et_2O$ and the complexes $CpML_2CN$ (M = Fe and L = dppe or M = Ru and L = PPh_3) in CH_2Cl_2 solution. Initially, the protonated complexes at the CN^- ligand are produced, then formation of the CN---BF_3 adducts occurs by loss of HF after 18–25 h stirring and precipitation of the product with Et_2O.

The picture of the $\mathbf{2H^+(O)}$ adduct with TFA^-, summarized in Figure 3.2.4(b), is more complicated. The simulation of 3 equiv. of TFA has been necessary to observe protonation. Computations indicate that the resulting adduct could be represented by two slightly different structures, that can be considered almost isoenergetic. In one of the two (referred as 2---H^+---TFA^-), the proton is "shared" between the P=O functionality and the acid molecule. The P=O---H^+ distance in too short to be considered a H-bond, which suggests the presence of a predominant covalent interaction, and thus an occurred protonation. In the second structure (referred to $2H^+$---TFA^-), instead, the P=O protonation is more evident. Interestingly, the adduct of **2** with TFA (referred to 2---TFA) is only slightly higher in energy with respect to protonation products at P=O. These results are indicative of a highly dynamic system, whose PES is characterized by the presence of these three different minima, which are separated by very small activation barriers. Among them, 2---H^+---$TFA^-$and $2H^+$---$TFA^-$are the most representative for the system. In both cases, the TFA–H+ distances are shorter than the BF4–H^+, resulting from a stronger ion-pairing effect in the first case. Ion-pairing effects in both TFA^- and BF_4^- adducts have also been quantified in terms of computed shifts of υ(CO) bands (for the TFA adduct the most stable 2---H^+---TFA^-structure has been considered). Remarkably, the computed Δυ(CO) for the TFA^- and BF_4^- adducts are 6 cm^{-1} and 11 cm^{-1} respectively, reproducing well the experimental IR spectra patterns upon protonation.

3.2.2.3 Proton reduction cycle catalyzed by 2: a mechanistic view

Figure 3.2.5 displays the suggested mechanisms for the electrocatalytic H_2 production by complex **2** (on the basis of CV) in CH_2Cl_2/NBu_4PF_6 solution and in the presence of TFA.

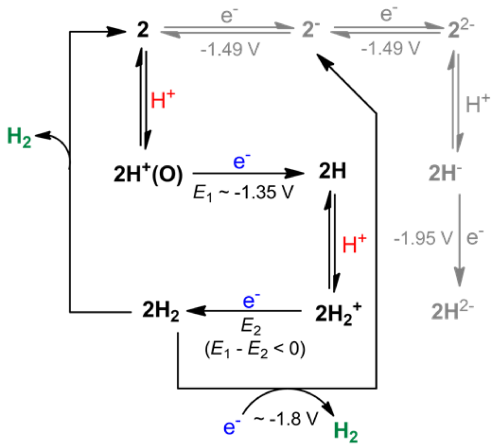

Figure 3.2.5: Proposed catalytic reduction of TFA by **2** on the basis of CV experiments (in CH_2Cl_2/NBu_4PF_6 solution). The grey path could be important only at acid equiv. < 4.

According to this scheme, catalysis entails a one-electron reduction after **2** protonation (black arrows). A secondary pathway, in which a two-electron reduction occurs prior protonation, is also feasible if the acid concentration is decreased (grey arrows). All the feasible proton reduction pathways catalyzed by **2** have been theoretically investigated, in order to unravel the nature of intermediates involved in the mechanism. A conformational search of the protonated form of both $\mathbf{2}^-$ and $\mathbf{2}^{2-}$ (Figure 3.2.6) revealed that the protonation of the P=O moiety becomes progressively more difficult going from $\mathbf{2}^-$ to $\mathbf{2}^{2-}$. That is due to the larger amount of electron density on both iron and sulfur upon reduction that makes them more reactive (compared to the P=O group) towards the incoming proton (data not shown). These results suggest that the P=O functionality could be involved in the proton reduction mechanism only when **2** protonation is the first step of the catalytic cycle.

A preliminary complete systematic search of all isomers of the intermediates possibly involved in the whole proton reduction process (along the main "black arrows" pathway, which is the one involved in H_2 evolution) has been carried out. Computational evaluation of kinetic barriers along with the comparison calcd vs exp redox potentials has then allowed to discern the most viable reaction pathways, whose energy profiles are presented in Figure 3.2.8 and 3.2.9. In Figure 3.2.6 and 3.2.2.3 are displayed the most stable isomeric forms of catalytic cycle intermediates. Among them, the ones that are predicted to be actually involved in the H_2 evolution mechanism are marked with their relative labels. Protonation step of **2** is practically barrierless (**2** $\rightarrow$ **TS1**: 0.2 kcal/mol), suggesting a fast proton transfer to the P=O moiety followed by $\mathbf{2H(O)}^+$ one-electron reduction (Figure 3.2.8). With the aim to verify whether reduction could lead spontaneously to proton relay from P=O to Fe, (as occurring in related hydrogenase models containing N-

bridgehead) the redox potential of the couple $\mathbf{2H(O)}^{+}/\mathbf{2H(Fe)}^{0}$ has also been computed (-1.11 V). However, the computed value that better compares to experiments (E_{1exp} = -1.35 V) is that referring to the reduction to **2H(O)**, ($\mathbf{2H(O)}^{+}/\mathbf{2H(O)}^{0}$ E = -1.30 V). Subsequently, **2H(O)** undergoes a second protonation which, however, may also be preceded by an oxygen-to-iron proton transfer to give another energetically accessible **2H** isomer (Figure 3.2.8, black profile). In fact, the proton transfer transition state (**TS2**), that yields the t-Fe(H) hydride **2H(b)**, is predicted to lie only 4.2 kcal/mol above the P=O protonated form. Interestingly, a direct protonation product of **2H(b)** "as is" has not been found. Indeed, the breaking of at least one Fe-S bond is a necessary requisite to find a stable protonated species. Such protonation is expected to occur on the sulfur coordinated to a single Fe ion. Nonetheless, we found no **2H** isomer with both Fe-S bond broken and a terminal hydride, which suggests that such process is not viable. Alternatively, the terminal hydride **2H(b)** could rearrange to a Fe-Fe bridging (**2H(a)**) hydride through an isomerization (consisting in a double step Ray-Dutt-like twist, a mechanism active in similar models of [FeFe] hydrogenase). [71] Activation barriers leading to isomerization are similar to those found in the previous study (∼17 kcal/mol (**2H(b)** → **TS3**).

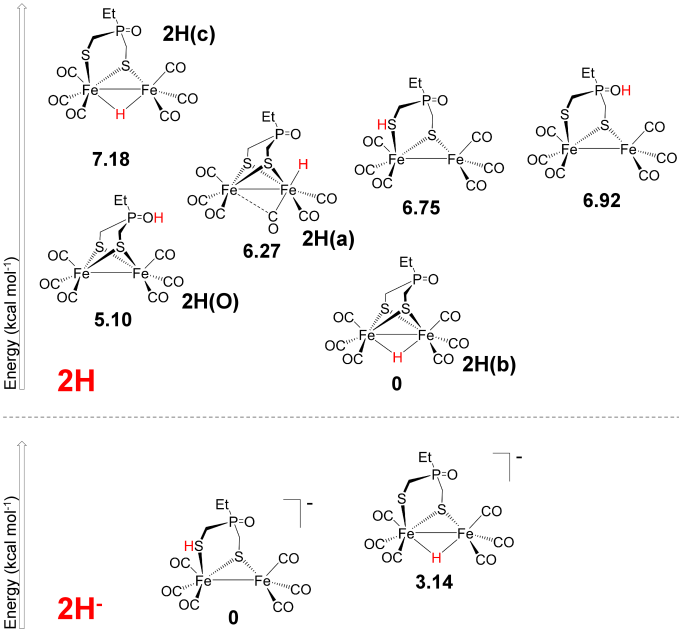

Figure 3.2.6: Thermodynamic speciation of monoprotonated intermediates **2H** and $\mathbf{2H}^{-}$. Relative in-solvent energies of the most relevant isomers are reported in kcal/mol.

Subsequently, this pathway proceeds through rather low barriers associated with the breaking of one Fe-S bond (**2H(a)** → **TS4**) and with the successive S protonation (**2H(c)** → **TS5**). Alternatively to isomerization, **2H(O)** can undergo two different direct protonation steps by TFA to the Fe_2 core: i) **2H(O)** can be protonated through **TS8** to give the terminal hydride $\mathbf{2H_2(b)}^{+}$ (Figure 3.2.8, green profile), or, ii) protonation of the Fe-Fe bond, that, however, resulted kinetically disfavored (see **2H(O)** → **TS9**) Figure 3.2.8, purple profile). Remarkably, the direct protonation

of **2H(O)** in terminal position is the most favorable process (even vs isomerization) as it has the lowest barrier (**2H(O)** → **TS8**, 13.7 kcal/mol). Besides aforementioned mechanisms, also H_2 formation through direct protonation of the Fe-H moiety has been tested, but resulting energy barriers are too high (>30 kcal/mol).

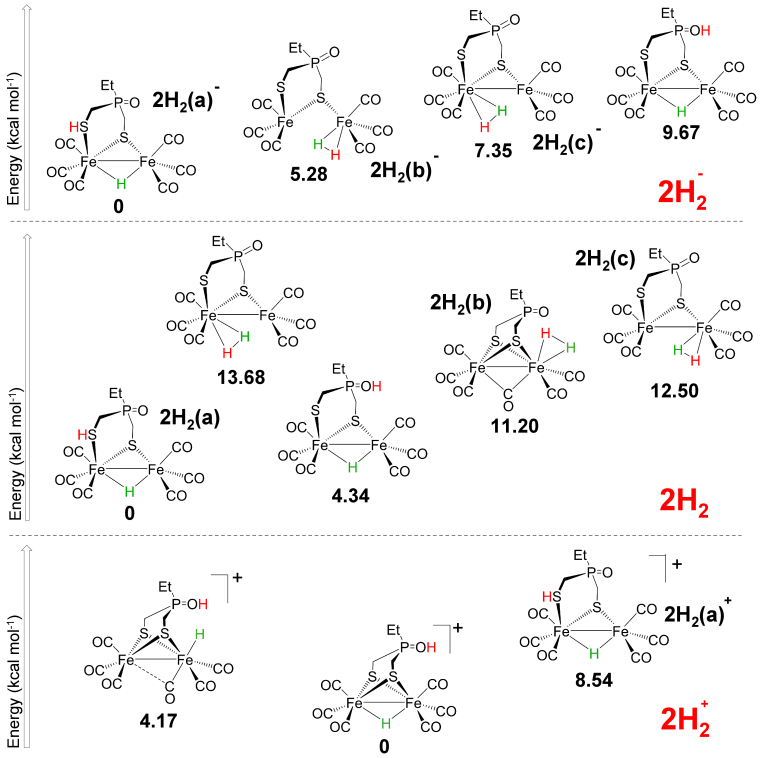

Figure 3.2.7: Thermodynamic speciation of monoprotonated intermediates **2H**$_2$, **2H**$_2^+$and **2H**$_2^-$. Relative in-solvent energies of the most relevant isomers are reported in kcal/mol.

Reduction potentials of both **2H$_2$(a)**$^+$ and **2H$_2$(b)**$^+$ ($E_{2(a)}$ and $E_{2(b)}$) are predicted to be around -0.3 V. The pathway for H_2 formation and release starting from **2H$_2$(a)** is more energetically costly than the one starting from **2H$_2$(b)**. In fact, the isomerization of **2H$_2$(a)** to the η^2-H_2 complex **2H$_2$(c)** and the recovery of **2** after H_2 loss (that can only take place at the Fe involved in the break of the Fe-S bond) require 12.7 and 14.0 kcal/mol respectively. One electron reduction of **2H$_2$(b)**$^+$, instead, is concomitant with oxygen-to-iron proton transfer and H_2 release from the so formed **2H$_2$(b)** is actually barrierless (0.2 kcal/mol). A catodic peak at -1.8 V has also been experimentally observed and it has been assigned to a further one-electron reduction of **2H$_2$**. Our calculations show that this reduction (E_3 = -1.80 V) is associated with the formation of **2H$_2$(a)**$^-$ starting from **2H$_2$(a)** (Figure 3.2.9). H_2 formation can then occur on both Fe atoms, since the two pathways result energetically similar. In both cases the RDS is associated with H^+ intramolecular migration to give the η^2-H_2 complexes **2H$_2$(b)**$^-$ and **2H$_2$(c)**$^-$, with **TS11** and **TS13** respectively 8.6 and 11.1 kcal/mol higher in energy than **2H$_2$(a)**$^-$. Comparing outlined

mechanisms, focusing on the same reduction level, it emerges that if isomerization of **2H(O)** is prevented, the overall energetic cost of catalysis is decreased.

3.2.3 Conclusions

A pre-condition for the successful design of an efficient and durable biomimetic compound is the knowledge of both structure and functioning of the related natural system. This could, in fact, address the synthesis of new compounds attaining the key structural features of an enzyme active site, with the hope of replicating also its reactivity. However, this strategy could also be unsuccessful. For example, in the [FeFe]-hydrogenase context, the lack of the protein scaffold in biomimic compounds, besides making difficult the reproduction of some fundamental active site feature (e.g. its rotated conformation), also impedes the practical use of cyanide ligands, whose introduction in synthetic systems becomes even deleterious for catalysis.[161, 162]

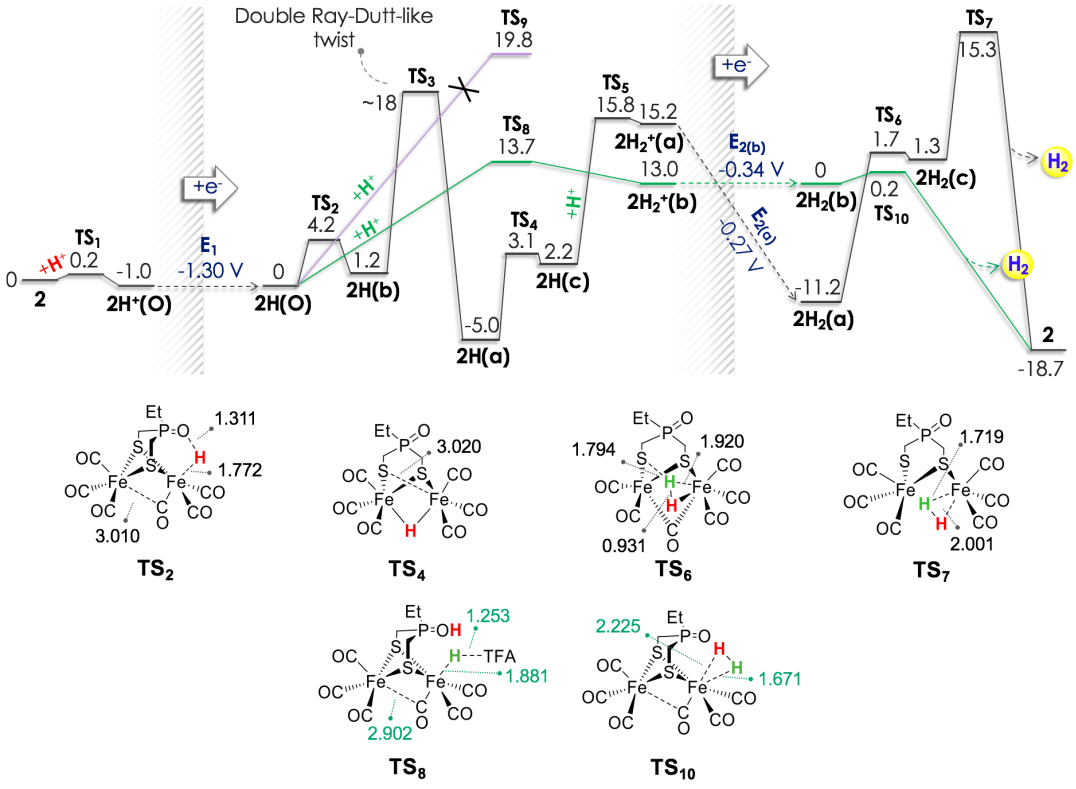

Figure 3.2.8: Top: energy profiles associated to proton reduction catalyzed by **2**. The solvent corrected energies (kcal/mol) have been computed with respect to the first intermediate formed per each redox state. Bottom: structures of a series of selected transition states involved in the proposed mechanism. Distances in Å.

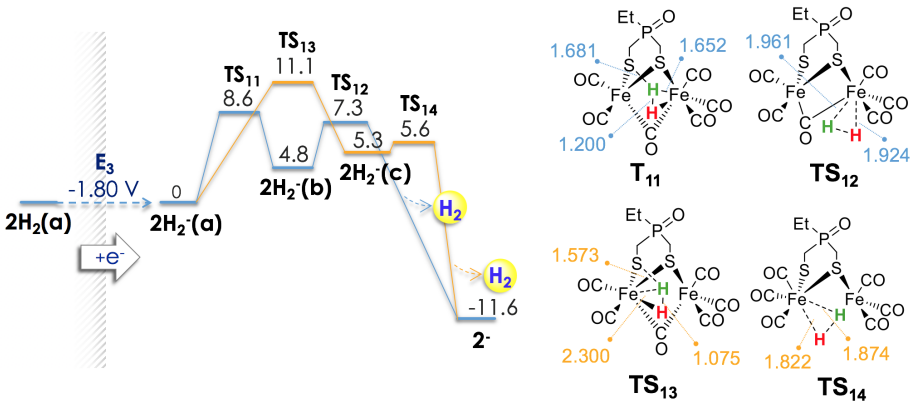

Figure 3.2.9: Top: energy profiles of $\mathbf{H}_2$ formation and release starting from $\mathbf{2H}_2$. The solvent corrected energies (kcal/mol) have been computed with respect to $\mathbf{2H}_2^-\mathbf{(a)}$. Bottom: structures of transition states involved in the proposed mechanism. Distances in Å.

The characterization of the adt cofactor in [FeFe]-hydrogenase has prompted the synthesis of a plethora of mimics with N-containing bridge-heads as acid/base cofactor.[15] However, the possibility of going beyond Nature, through the substitution of the amine group group (so far considered as a firm cornerstone in the hydrogenase modelling) by other functionalities, able to improve protonation and/or redox properties of synthetic systems, should not be ruled out.

To date, no hexacarbonyl model complex containing μ-$(SCH_2)_2$NR linker has been described to undergo N-protonation by moderately strong acids such as TFA and actually only strong acids (e.g. HBF_4.Et_2O) are able to protonate the N atom. Here, the first example of proton reduction catalyzed by an hexacarbonyl complex, in which the first protonation (by moderately strong acids) precedes the first electron transfer, is presented. Computed reaction pathways, associated with the possible H_2 release routes, suggest that the P=O moiety could play a crucial role in catalysis. Indeed, its protophilicity makes P=O the preferential protonation site and also hinders the formation of the μ-H isomer, that is known to represent a thermodynamic sink (or at least an obstacle) for H_2 production.[151] Also interesting is the P=O proximity to the hydride at the iron center in $\mathbf{2H_2(b)}^+$, that makes proton relay and H_2 release a spontaneous process upon reduction. These results would seem to point to the possibility of ameliorating some features that evolution has selected so far by suitably substituting what is considered a key active site functional group (adt). Additionally, relatively recent works have shown that upon oxidation of the diiron core, the central amine is able to coordinate to the metal, deactivating the system for catalysis. The substitution of the biologically relevant amine with abiological saturated and non-coordinating bridge-heads could thus be an intriguing strategy to overcome this issue. Finally, it is noteworthy that exactly like in Fe_2 azadithiolates, also with the proposed derivatives containing RP=O group, it is possible to properly tailor redox and acid/base properties of the catalyst by tuning the R nature, a versatile feature that can turn out useful in the design of improved synthetic models of hydrogenase.

3.3 Preparation and Protonation of $Fe_2(CNR)_6$(μ-pdt) Electron-Rich Analogues of $Fe_2(CO)_6$(μ-pdt)

In collaboration with T. B. Rauchfuss, University of Illinois at Urbana

3.3.1 Introduction

Over the preceding several years, compounds of the type $Fe_2(SR)_2(CO)_{6-x}L_x$ have been examined in considerable detail.[303] In contrast to the parent hexacarbonyls, the substituted derivatives are susceptible to oxidation and protonation[304, 305], two reaction modes characteristic of the hydrogenases.[14] Indeed, the work is mainly motivated by interest in the chemistry of the [FeFe]-hydrogenases, which feature a $Fe_2(SR)_2(CO)_3(CN)_2$(RSFe) active site. Synthetic analogues of this site most often include disubstituted species, e.g., $Fe_2(SR)_2(CO)_4L_2$, but tri- and tetrasubstituted derivatives have also been prepared. The tetrasubstituted species are often subject to significant steric congestion as is evident in the unusual acid-base properties of $Fe_2(CO)_2(dppv)_2$(μ-pdt) and $Fe_2(CO)_2(PMe_3)_4$(μ-pdt) (pdt = $CH_2(CH_2S^-)_2$, dppv = cis-$C_2H_2(PPh_2)_2$)[306, 307, 308]. In other works, bulky dithiolates have been shown to stabilize unusual, but biomimetic coordination geometry at one of the Fe centers.[309, 291, 176] These precedents point to the desirability of examining electron-rich analogues of $Fe_2(SR)_2(CO)_6$, but without the steric constraints imposed by phosphines and other bulky ligands. In this project, replicas of $Fe_2(CO)_6$(μ-pdt) have been sought, where the symmetry and noncongestion of the parent hexacarbonyl derivatives are preserved, but the basicity and redox properties are modified. A hypothetical electron-rich, nonbulky target is the acetonitrile complex $Fe_2(NCMe)_6$(μ-pdt). Such a species is unlikely to be isolable since even $Fe_2(CO)_5(NCMe)$(μ-pdt) is very labile.[310] One might also envision $[Fe_2(CN)_6(\mu\text{-pdt})]^{6-}$ since polyanionic cyanometallates are known, e.g., $[Ni(CN)_4]^{4-}$ and $\{[(NC)_5Co]_2C_2(CO_2Me)_2]\}^{6-}$.[311] Approaches to $[Fe_2(CN)_6(\mu\text{-pdt})]^{6-}$would necessarily need to be indirect since $[Fe_2(CO)_4(CN)_2(\mu\text{-pdt})]^{2-}$is unreactive toward cyanide, although the diferrous polycyanides may be more realistic targets.[171] For generating a hexasubstituted diiron dithiolate, isocyanides represent a compromise between cyanide and nitriles[312, 313], while also featuring a modest steric profile virtually isosteric with CO in the vicinity of the metal center. It is known that four CO ligands in $Fe_2(CO)_6$(μ-pdt) can be replaced by isocyanide ligands.[158, 314, 315, 316] Several poly(isocyanide) analogues of metal carbonyl complexes are known. These species include analogues of mono- and dimetallic carbonyls. A few clusters are also known, e.g., Ni_4(CNBu-t)$_7$ and Pt_7(CNBu-t)$_{12}$.[317] Studies on homoleptic and polyisocyanide complexes remain an active area,[318, 319, 320, 321] but the theme has not been applied to hydrogenase models. T. B. Rauchfuss et al. have proposed the synthesis of a set of hydrogenases biomimic compounds $Fe_2(CNR)_6$(μ-pdt) (R = Me, 4-$MeOC_6H_4$, 4-ClC_6H_4). Structural characterization, protonation reactions and oxidation properties have been addressed both experimentally and computationally. Calculations have been carried out on $Fe_2(CNMe)_6$(μ-pdt) (the smallest system under investigation, and thus the less computationally costly) as illustrative

study.

3.3.2 Results and discussion

3.3.2.1 Characterization of $[Fe_2(CNMe)_6(\mu\text{-pdt})]^z$, (z = 0/+1)

Crystallization of $Fe_2(CNMe)_6(\mu$-pdt) afforded X-ray quality crystals. The Fe(1)-Fe(2) distance of 2.540 Å compares well to other $Fe_2(CO)_{6-x}L_x(\mu$-pdt) species. The structure of $Fe_2(CNC_6H_4Cl)_6(\mu$-pdt) was also confirmed by X-ray crystallography. As shown in Table 3.3.1 the Fe-C bond lengths correlate with the expected trends in π-backbonding by these ligands. Both the Fe-S and Fe-Fe bond lengths in $Fe_2(CNMe)_6(\mu$-pdt) are slightly longer than those in $Fe_2(CNC_6H_4Cl)_6(\mu$-pdt) and $Fe_2(CO)_6(\mu$-pdt), consistent with the electron-donating ability of the MeNC ligands. The nonlinearity of the CNC cores of isocyanide ligands qualitatively indicates their participation in π-backbonding.[322] In both $Fe_2(CNC_6H_4Cl)_6(\mu$-pdt) and $Fe_2(CNMe)_6(\mu$-pdt), the CNC angles for the apical isocyanide ligands deviate only a few degree from linearity. More pronounced distortions are observed for the basal ligands (Table 3.3.1). The bending of the basal RNC ligands is consistent with the shortened Fe-C_{basal} distances, a difference that is more pronounced in these $(RNC)_6$ complexes than the parent hexacarbonyls.

DFT computations confirmed a striking aspect of the system, namely its close structural similarity to $Fe_2(CO)_6(\mu$-pdt), despite their highly differing chemical properties.[323, 67, 324] The interatomic distances are very similar. The fractional electronic occupations per single atom, including the 2-electron Fe-Fe bonding HOMO are also similar, as well as HOMO shapes (Figure 3.3.1, top). The NBO analysis revealed π-back-donation from Fe to CNMe, as is also indicated experimentally by short Fe-C distances and nonlinearity of the Me-N-C angles (Figure 3.3.1, bottom). Both features are reproduced computationally: the Fe-$C_{(basal)avg}$ distances are about 0.02 Å shorter than $C_{(apical)avg}$.

	$Fe_2(CO)_6(\mu\text{-pdt})$	$Fe_2(CNC_6H_4Cl)_6(\mu\text{-pdt})$	$Fe_2(CNMe)_6(\mu\text{-pdt})$
Fe-$C_{(apical)avg}$	1.802(1) [1.800]	1.812(12)	1.847(12) [1.808]
Fe-$C_{(basal)avg}$	1.799(2) [1.787]	1.807(5)	1.823(7) [1.790]
Fe-S_{avg}	2.252(3) [2.279]	2.261(2)	2.273(2) [2.292]
Fe-Fe	2.5103(11) [2.551]	2.530(2)	2.540(1) [2.562]
C-N-C_{apical}		165 (distal)[a]	177 (distal)[a] [165.1]
C-N-C_{basal}		172 (proximal)	173 (proximal)
		164, 175 (distal)[a]	176, 176 (distal)[a]
		166, 175 (proximal)	166, 166 (proximal) [150.3]

Table 3.3.1: Selected Distances (Å) and Angles (°) in $Fe_2(CO)_6(\mu$-pdt), $Fe_2(CNC_6H_4Cl)_6(\mu$-pdt), and $Fe_2(CNMe)_6(\mu$-pdt) (DFT-calculated values in brackets). [a]Distal Fe is adjacent to the C-CH_2-C center. Proximal is the other Fe. These definitions conform with the labeling of Fe_d and Fe_p in the [FeFe]-hydrogenases.

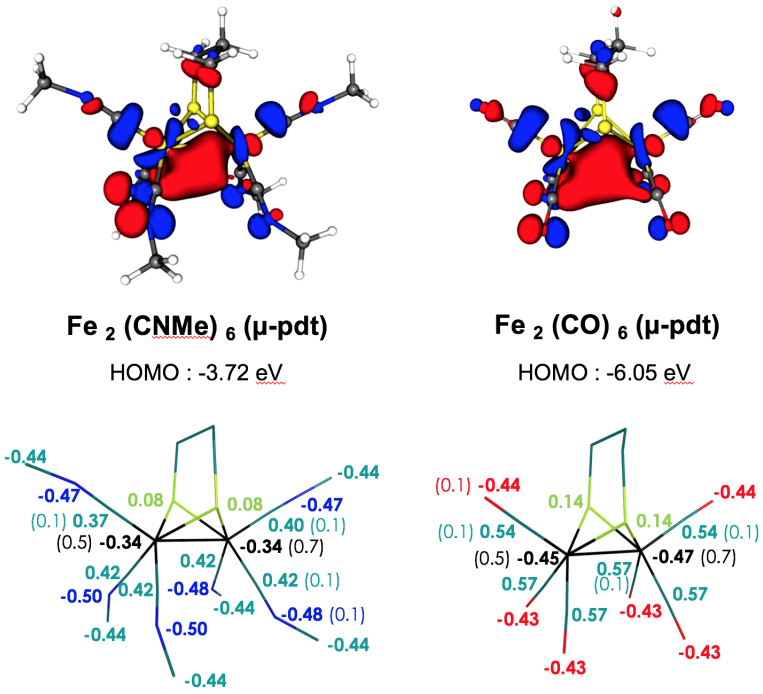

Figure 3.3.1: Top: HOMO (cutoff value: 0.035). Bottom: NBO partial charges (bold, next to atoms) and fractional atomic contributions to the HOMO (parentheses) of $Fe_2(CO)_6$(μ-pdt) and $Fe_2(CNMe)_6$(μ-pdt).

The atomic partial charges are qualitatively compatible with the reducing power and basicity for the considered system, as indicated by the greater electron density residing on the ligands. Complexes with strongly bent RNC ligands generally exhibit νCN bands near 1900 cm^{-1}[325], as seen for $Fe_2(CNMe)_6$(μ-pdt), whose IR spectrum was also computed at the BP86/TZVP level (Figure 3.3.2). IR simulations were performed with the same full-electron TZVP basis set that was employed to investigate energies and geometries of structures of interest, without need of using scaling factors (usually necessary for functionals other than BP86, to correct the harmonic potential shape). The frequency range associated with the νCN normal modes was computed to be 1983-2117 cm^{-1}, which is reasonably consistent with the observed spectrum. The good agreement of both structural and spectroscopic features between experimental and computed values proved that the BP86/TZVP scheme is suitable to describe the electronic structure of the system.

Using DFT, we investigated the possibility that the rotated isomer $Fe_2(CNMe)_5$(μ-CNMe)(μ-pdt), featuring a bridging CNMe ligand, exists in significant equilibrium concentrations at room temperature. The energy of this rotated isomer is elevated by only 2.2 kcal/mol with respect to the unrotated one, suggesting that it is indeed reasonable that it is populated in solution, or at least forms readily. Furthermore, rotated $Fe_2(CNMe)_5$(μ-CNMe)(μ-pdt) would be particularly susceptible to fast electron-transfer since it is preorganized in the geometry expected for $[Fe_2(CNMe)_6(\mu\text{-pdt})]^+$. In the optimized structure for $Fe_2(CNMe)_5$(μ-CNMe)(μ-pdt), the C-N-

Me angles reveal that the distorted Fe center is the stronger π-donor, with the average C-N-C(Me) angle of 141.8°. The NBO charges on Fe unrotated $Fe_2(CNMe)_6$(μ-pdt) are both -0.342, whereas for the rotated form, the values are -0.405 and -0.307 (rotated Fe center).

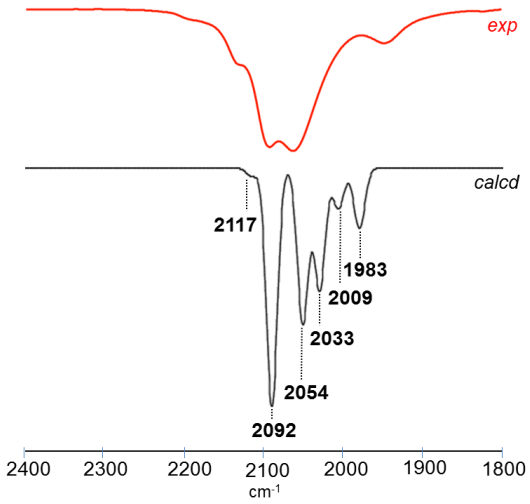

Figure 3.3.2: DFT-computed (black) and experimental (red) IR spectra of $Fe_2(CNMe)_6$(μ-pdt) in the νCN region.

Computations confirm that the most stable monocationic isomer contains a bridging isocyanide ligand, giving $[Fe_2(CNMe)_5(\mu\text{-}CNMe)(\mu\text{-pdt})]^+$. This structure is a typical rotated mixed-valence $Fe^{I}Fe^{II}$ species, often referred (as aforementioned) to as H_{ox} models.[173, 287, 157] The DFT-calculated structures highlight the greater bending of the C—N—Me ligands in rotated $Fe_2(CNMe)_5$(μ-CNMe)(μ-pdt) vs $[Fe_2(CNMe)_5(\mu\text{-}CNMe)(\mu\text{-pdt})]^+$. The Fe-μ-C(NMe) distances differ by 0.4 Å, vs ∼1 Å difference was observed for Fe-μ-C(O) bonds in the H_{ox} models of the type $[Fe_2(\mu\text{-}CO)L_5(\mu\text{-pdt}]^+$.[173] In the enzyme from D. desulfuricans, the Fe-μ-C distances differ by 0.7 Å.[44]

3.3.2.2 Oxidation reactions

Experiments revealed that the redox properties of the hexaisocyanide and hexacarbonyl compounds are very different. One clear indication is that the hexacarbonyls are unaffected by Fc^+, whereas treatment of hexaisocyanides with Fc^+ results in immediate reaction. Cyclic voltammetry (CV) studies showed that the oxidation processes of this class of compounds are complex, since secondary reactions, of unknown origin, have emerged. In particular, the CV of $Fe_2(CNMe)_6$(μ-pdt) shows an ostensible reversible couple near -1.2 V, but also smaller processes at -1.0 and -1.8 V. At slow scan rates (12.5 mV/s), the dominant feature at -1.2 V resolves into two overlapping processes, with $E_{1/2}$ = -1.2 and -1.3 V. The two redox couples are tentatively assigned as $[Fe_2(CNMe)_6(\mu\text{-pdt})]^{+/0}$ for its rotated and unrotated neutral isomers (see previous subsection), since their computed 1e oxidation potentials are -1.23 and -1.38 V, respectively. These results suggest that the rotated isomer would be a more potent reducing agent

than the parent by 0.15 V. However, since the CV complexity raised the possibility of coordination by solvent (THF, MeCN), the energies for the couple $[Fe_2(CNMe)_4(\mu\text{-}CNMe)(solvent)(\mu\text{-}pdt)]^+/Fe_2(CNMe)_5(solvent)(\mu\text{-}pdt)$ were also calculated. These results are summarized in Figure 3.3.2.2. The computations for the considered coupled have implied the thermodynamic speciation of each possible mono-substituted solvento-complex (featuring a solvent molecule in place of an apical or basal CNMe) for both neutral and cationic species and considering both THF and MeCN as solvents. Subsequently, every possible oxidation process, starting from each energetically accessible solvento-complex, have been considered for the evaluation of oxidation potentials. Interestingly, the computed oxidation potential shifts (in the presence of both solvents) are compatible with experimental observations, since they cover the range in which the peaks associated to eventual side-reactions fall.

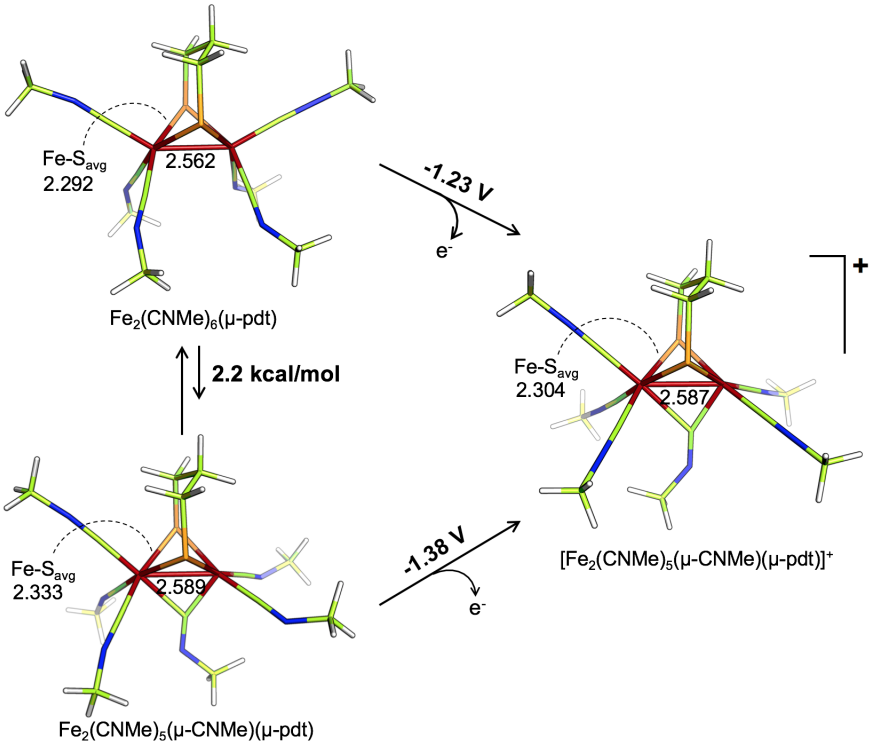

Figure 3.3.3: DFT structures of $Fe_2(CNMe)_6(\mu\text{-}pdt)$, $Fe_2(CNMe)_5(\mu\text{-}CNMe)(\mu\text{-}pdt)$ and $[Fe_2(CNMe)_6(\mu\text{-}pdt)]^+$. Relative energies between the two neutral rotamers are reported (in kcal/mol), as well as their relative DFT-calculated redox couples (in V). Selected distances in Å.

3.3.2.3 Protonation of $Fe_2(CNMe)_6(\mu\text{-}pdt)$

$Fe_2(CNMe)_6(\mu\text{-}pdt)$ is protonated with 1 equiv of $[HNEt_3]BAr^F_4$, a weak acid (pKa MeCN = 19)[326], which is unreactive toward the arylisocyanide systems, whose protonation requires the strong acid $[H(OEt)_2]BAr^F_4$ (Ar^F = 3,5-$(CF_3)_2C_6H_3$). The ^{1}H NMR spectrum of $Fe_2(CNMe)_6(\mu\text{-}pdt)$ protonation product is complex but can be fully assigned. A doublet and quasiquartet

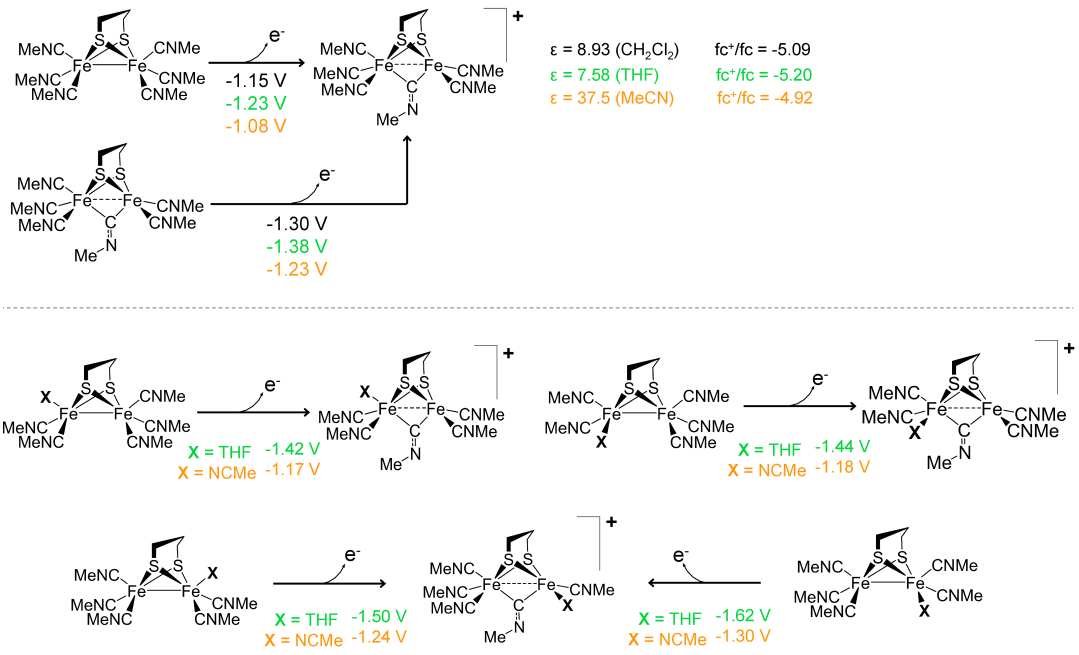

Figure 3.3.4: Top: DFT oxidation potentials of the couple $[Fe_2(CNMe)_6(\mu\text{-pdt})]^{+/0}$ in different solvents. Bottom: DFT oxidation potentials of the couple $[Fe_2(CNMe)_4(\mu\text{-CNMe})(\text{solvent})(\mu\text{-pdt})]^+$/ $Fe_2(CNMe)_5(\text{solvent})(\mu\text{-pdt})$ with solvent = THF, MeCN.

appear, respectively, at δ 3.34 and 8.33, with integrated intensity 3:1 and an apparent J_{HH} = 4.8 Hz. Comparable NMR shifts and couplings are observed for the aminocarbyne $[Cp_2Co_2(\mu\text{-}PMe_2)_2(\mu\text{-CNMe(H)})]^+$.[327] The lowfield portion of the $^{13}C\{^1H\}$ NMR spectrum displays a signal at δ 340 as well as resonances at δ 166, 165, and 164. The ^{13}C NMR signal at δ 340 is also consistent with a bridging aminocarbyne ligand[328, 329], indicating that protonation occurs at the MeNC ligand. The unmodified MeNC ligands upon protonation exhibit ^1H NMR resonances in the ratio 1:2:2. These data are consistent with the formulation $[Fe_2(CNMe)_5\{\mu\text{-CN(H)-Me}\}(\mu\text{-pdt})]^+$, which adopts a rotated structure. Unlike the situation for the unprotonated parent, turnstile rotation of the $Fe(CNMe)_3$ subunit in $[Fe_2(CNMe)_5\{\mu\text{-CN(H)-Me}\}(\mu\text{-pdt})]^+$ is inhibited even at 25 °C, as seen in oxidized species of the general formula $[Fe_2L_5(\mu\text{-CO})(\mu\text{-pdt})]_2^+$.

Upon warming its solutions to near room temperature, $[Fe_2(CNMe)_5\{\mu\text{-CN(H)-Me}\}(\mu\text{-pdt})]^+$ isomerizes to the hydride $[Fe_2(\mu\text{-H})(CNMe)_6(\mu\text{-pdt})]^+$. The structure of this species is indicated by its ^1H NMR spectrum, showing two peaks with a 1:2 ratio for FeCNMe and a hydride signal at δ −17.2, as expected.[316] In summary, the kinetic protonation product can be assigned to a N-protonated μ-CNMe ligand, while the thermodynamic one is a typical Fe-Fe bridging hydride. The kinetics for the conversion of the former in the latter were examined by monitoring the rate of the disappearance of $[Fe_2(CNMe)_5\{\mu\text{-CN(H)-Me}\}(\mu\text{-pdt})]^+$ by ^1H NMR spectroscopy. Over the course of hours, $[Fe_2(CNMe)_5\{\mu\text{-CN(H)-Me}\}(\mu\text{-pdt})]^+$ disappeared concomitant with the growth of the hydride. The isomerization to the hydride follows first-order behavior with a rate constant $k = 1.93(2) \times 10^{-4}\ s^{-1}$.

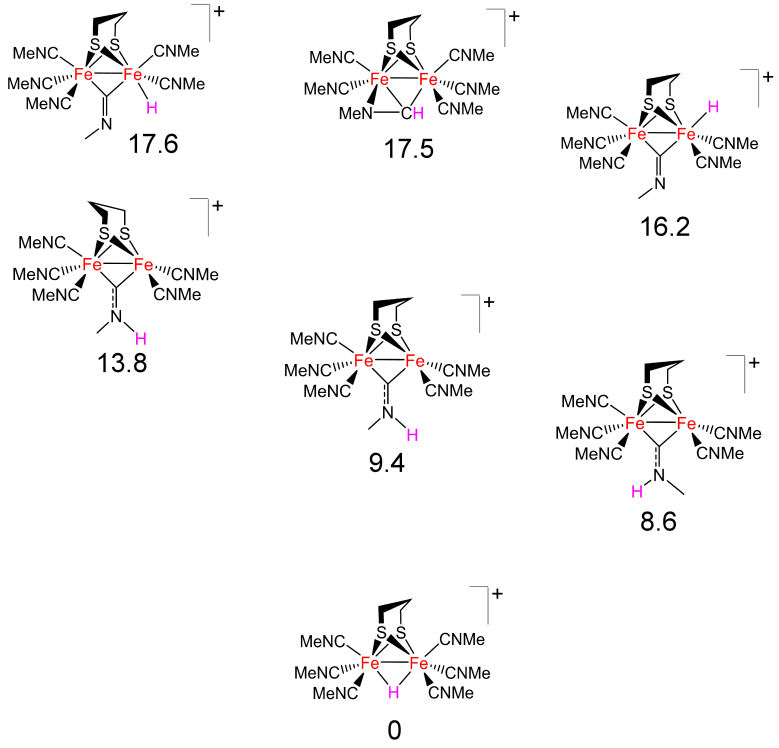

Figure 3.3.5: Structures (relative energy in kcal/mol) for seven low-energy isomers resulting from protonation of $Fe_2(CNMe)_6$(μ-pdt). The two lowest energy isomers were observed spectroscopically.

DFT has been used to address $Fe_2(CNMe)_6$(μ-pdt) protonation from both thermodynamic and kinetic standpoints. A conformational search of the protonated species led to the characterization of the isomers presented in Figure 3.3.5. They have been pinpointed by considering all putative basic sites. The two different orientations of the inner methylene of pdt have been taken into account only when required by symmetry considerations and only for moderately high in energy species. The C-protonated (except the one 28.0 kcal/mol) and the N-protonated structures (except those in which the iminoformyl or the amino-carbyne ligand is μ-coordinated to the Fe atoms) share the common feature of showing one of the Fe ions in a the trigonal bipyramidal coordination fashion. Looking at the energy data, one can conclude that the two "non-hydrido" species are the two unequivalent forms at 8.6 and 9.4 kcal/mol. The slight energy difference is probably due to the different methyl orientation and to its larger repulsive effect (with respect to H) with the nearby ligands.

Transition state structures (corresponding to all the possbile regiochemical sites for protonation) have been dissected, considering explicitly an acid molecule (HOTf) as source of protons (Figure 3.3.6). According to the calculations, N-protonation by HOTf would have a very low barrier, as is typical for protonation of amines and imines.[330] In contrast, protonation at Fe or at the Fe—Fe bond would be expected to proceed via a significant barrier due to higher reorganizational energies involved. The following barriers were calculated for protonation at Fe: apical (12.7

kcal/mol), basal position (11.5 kcal/mol), and Fe−Fe bond (7.8 kcal/mol). A higher barrier of ca. 14 kcal/mol is also indicated for C-protonation of an apical isocyanide. The overall picture is consistent with the experimental observation that the kinetic product of protonation is the aminocarbyne complex, and not a Fe-hydride species.

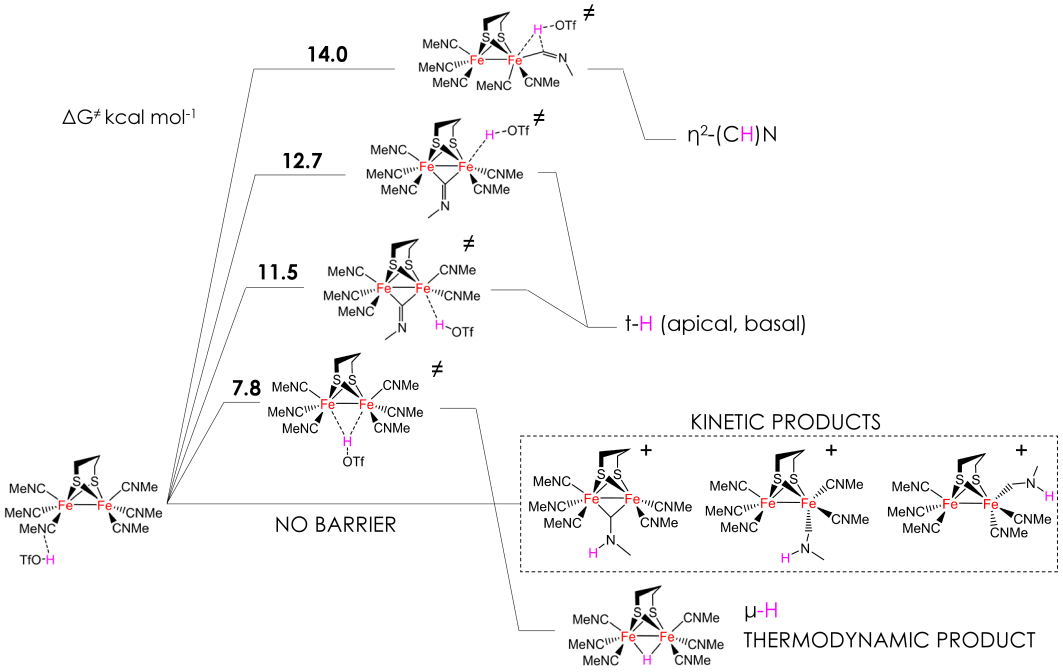

Figure 3.3.6: Comparative kinetic data (in kcal/mol) which correspond to the regiochemical sites for protonation of $Fe_2(CNMe)_6(\mu\text{-pdt})$ by HOTf. As a note: the ranking therein of protonation products is only of qualitative interest and for detailed information on thermodynamic speciation, refer to Figure 3.3.5.

Two scenarios can be envisioned for the conversion of the neutral derivative into the aminocarbyne product. N-protonation of a basal (bent) MeNC ligand in $Fe_2(CNMe)_6(\mu\text{-pdt})$ would produce a basal aminocarbyne, poised to migrate to the bridging site. The related migration of basal ligand to the bridging site has been found to be facile.[331] Alternatively, N-protonation could occur directly at the μ-CNMe ligand in the rotated isomer of $Fe_2(CNMe)_6(\mu\text{-pdt})$. Both processes give the same result. The protonation trans-$[Mo(CNMe)_2(\varkappa^2\text{-dppe})_2]$ proceeds analogously to $Fe_2(CNMe)_6(\mu\text{-pdt})$. The kinetic product is the aminocarbyne $[Mo(CNMe)\text{-}(CN(H)Me)(\varkappa^2\text{-dppe})_2]^+$, which subsequently rearranges to the hydride $[MoH(CNMe)_2(\varkappa^2\text{-dppe})_2]^+$.[325, 322]

In order to investigate on a possible mechanism which leads from the kinetic to the thermodynamic product, both intramolecular and intermolecular pathways for H^+ transfer have been searched. As an intermolecular H^+ shuttle, a neutral acid molecule has been employed. Two possible mechanisms for intramolecular H^+ transfer from N sites to Fe (without invoking the explicit acid) have been characterized (Figure 3.3.7, up). The energetically favored one features the assistance of a C atom in the transfer. Actually, it is the Fe-C bond which appears to undergo the attack, since no energy minimum structure can be located featuring a CH group coordinated

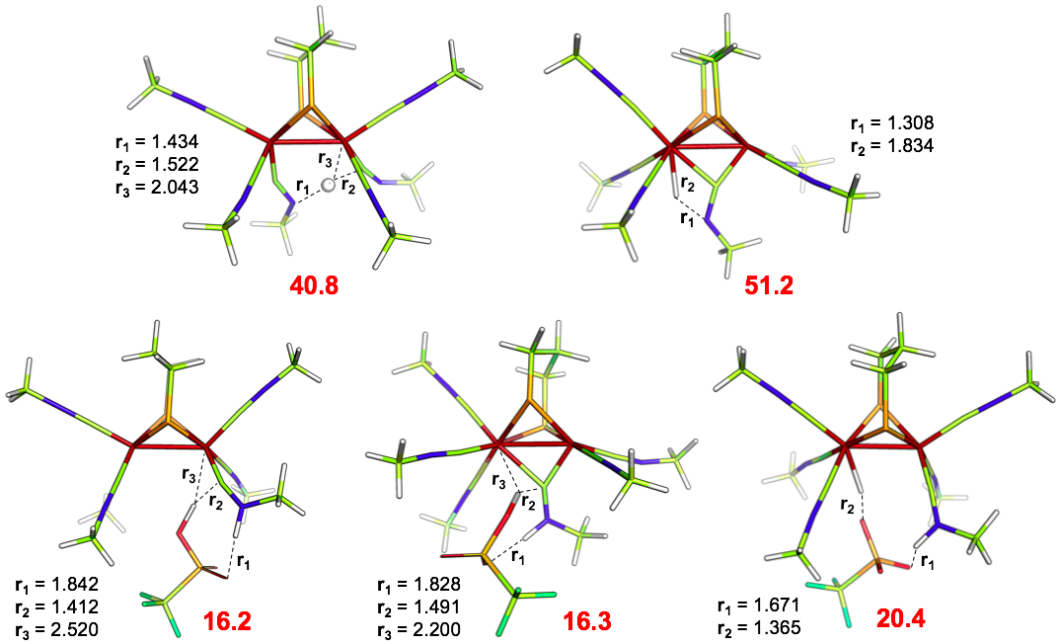

Figure 3.3.7: Selected lower-energy transition state structures associated to proton transfer, following both intramolecular (top) and intermolecular (bottom, with explicit triflic acid)) pathways. Distances (black values) in Å, $\Delta E^{\neq}_{solv}$ (red values) in kcal/mol.

in η-2 fashion to the Fe ion. Such a transition state structure (unlike the less stable one) entails the de-coordination of the μ-CNMe from one Fe while releasing the proton. Also, a concomitant turning back of the entire $Fe(CNMe)_3$ can be observed, when referring to the most stable found kinetic product. Also noteworthy is the different hydride character of the two located structures, as indicated by the different Fe-H distances. However, even the most stable between the two above mentioned intramolecular pathways requires a $\Delta E^{\neq}_{solv}$ = 40.8 kcal/mol. Remarkably, this activation barrier is significantly lowered if an intermolecular-acid-assisted pathway is considered. Three transition state structures involving an acid molecule as H^+ shuttle have been located (Figure 3.3.7, bottom).

3.3.2.4 Other Diiron Carbyne Complexes

The cation $[Fe_2(SMe)_2(CO)_3(PMe_3)_2(CCF_3)]^+$ represented the first reported carbyne derivative of a diiron dithiolate. Isolated as its $BF4^-$ salt, this species arises via a multistep pathway from the tetrafluoroethylene complex $Fe_2(SMe)_2(CO)_4(PMe_3)_2(C_2F_4)$, culminating in fluoride abstraction with BF_3.[332] This cation was described as a terminal carbyne complex (Figure 3.3.8, structure in the box), but our DFT calculations suggest otherwise. Since crystallographic studies of the related $Fe_2(SMe)_2(CO)_6(\mu\text{-}\eta^1,\eta^1\text{-}C_2F_4)$ and $Fe_2(SMe)_2(CO)_6(\mu\text{-}C(F)CF_3)$ complexes show that the SMe groups adopt the anti disposition, this conformation was adopted in our calculations.[332] There were 12 rotamers of $[Fe_2(SMe)_2(CO)_3(PMe_3)_2(CCF_3)]^+$ evaluated with attention to the orientation of the SMe groups. The energies of these isomers fall into three ranges: (1) In the

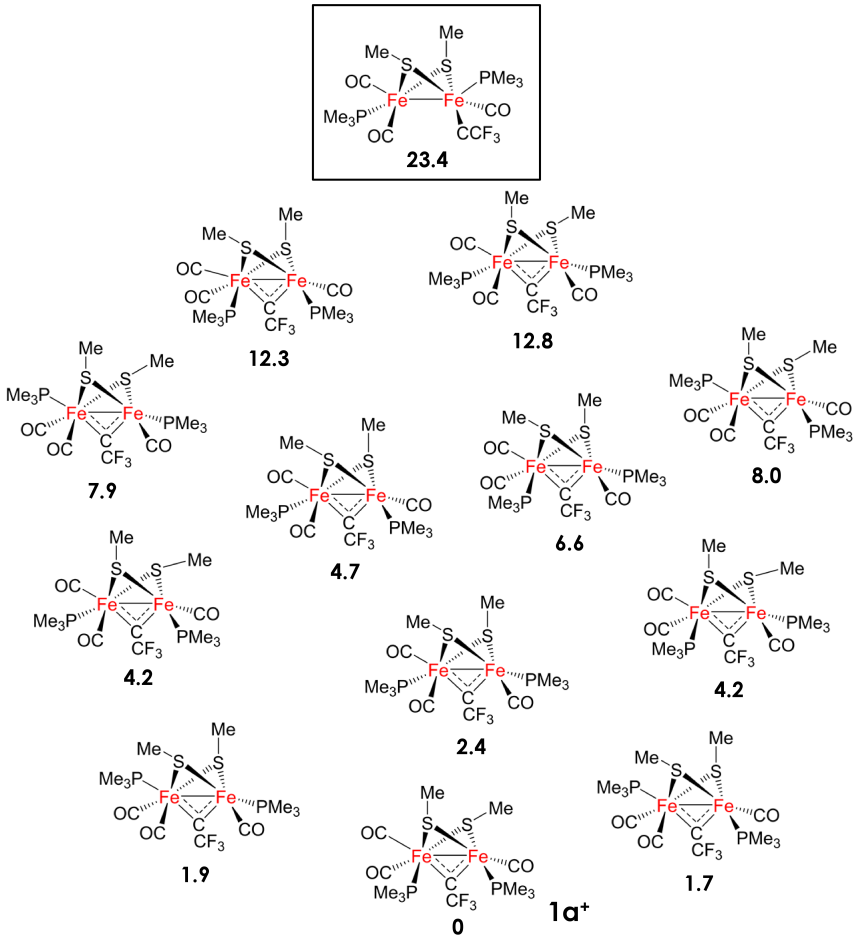

Figure 3.3.8: Thermodynamic speciation of $[Fe_2(SMe)_2(CO)_3(PMe_3)_2(CCF_3)]^+$. The structure reported in the box (top) is the one originally proposed, while the revised one is labeled $\mathbf{1a}^+$ (bottom).

range 0-6.5 kcal/mol are 10 isomeric μ-carbyne complexes with no obvious steric interactions between the ligand substituents. (2) At 12.3 and 12.7 kcal/mol are two μ-carbyne complexes with mutually cis PMe_3 ligands, which sterically clash with an equatorial SMe group. (3) At 24.3 kcal/mol is the terminal carbyne complex originally proposed. On the basis of these results, a revised ground state structure is assigned, featuring a bridging carbyne ligand and cis-basal PMe_3 groups ($\mathbf{1a}^+$, Figure 3.3.8).

3.3.3 Conclusions

Relative to $Fe_2(CO)_6$(μ-*pdt*), the complexes $Fe_2(CNR)_6$(μ-*pdt*) exhibit enhanced basicity, reducing power, and lability. These attributes are all desirable from the perspective of new reactivity. The electronic structure and stereodynamics are also instructive. In terms of its reducing power, the highly negative $[Fe_2(CNMe)_6(\mu\text{-pdt})]^{+/0}$ couple is noteworthy. To provide context, the oxi-

dation of $Fe_2(CO)_6$(μ-pdt) has only been achieved with $[N(C_6H_3$-2,4- $Br)_3]SbCl_6$ [333](E = 1.36 V [334]), and even then the cation abstracts chloride from $[SbCl_6]^-$, usually considered an inert anion. The $[Fe_2(CO)_5(CNMe)$(μ-pdt)$]^{+/0}$ couple is observed at 0.57 V, a shift of nearly 200 mV versus the $[Fe_2(CO)_6$(μ-pdt)$]^{+/0}$ couple.[335] Otherwise, the replacement of CO by MeNC shifts the redox potential by ca. 300 mV/substitution.[161] Similar trends in ΔEp are observed for the $Cr(CNR)_{6-x}(CO)_x$ complexes.[336] As established in this work, the electrochemistry of $Fe_2(CNR)_6$(μ-pdt) systems is complex, probably resulting from the involvement of ligand dissociation and formation of related solvento species, some of which have been previously identified. These protonation studies also revealed the lability of the MeNC ligand. In terms of its protonation, $Fe_2(CNMe)_6$(μ-pdt) behaves analogously to trans-$Mo(CNR)(L)(Ph_2PCH_2CH_2PPh_2)_2$ (L = CNR, N_2, CO).[337, 338] Both the Mo(0) and $[Fe(I)]_2$ species undergo kinetic protonation at RNC to give unstable aminocarbyne species, which isomerize to a thermodynamic hydrido complex. The conversion of the aminocarbyne to the hydride in $Fe_2(CNMe)_6$(μ-pdt) follows first-order kinetics and probably involves intramolecular rearrangement. DFT calculations provide insights into this pathway. Isomeric with $[Fe_2$(μ-H)$(CNMe)_6$(μ-pdt)$]^+$ is $[Fe_2$(t-H)(μ-CNMe)$(CNMe)_5$(μ-pdt)$]^+$, which contains a basal terminal hydride, and is only 8 kcal/mol higher in energy. The rearrangement of terminal hydrides, especially basal terminal hydrides, to μ-hydrides is known to be facile in related systems. Overall, the combined experimental and computational results highlight the indirect path followed in the conversion of the diiron(I) complex to its diiron(II) μ-hydride derivative. The following question arises: is such a pathway general? That is, do all diiron dithiolates protonate at ligands prior to formation of the μ-hydrides? Surely, the basicity of Fe-Fe bonds and steric distortions strongly influence the rate of μ-hydride formation.[335] In terms of the intimate details for protonation of $Fe_2(CO)_2(PMe_3)_4$(μ-pdt) at least, spectroscopic evidence indeed favors initial protonation at ligands prior to protonation at metal.[307] In one of the more striking findings, this work provides some guidance for the synthesis of reduced diiron dithiolato complexes with a biomimetic structure. Recall that the active site adopts a rotated structure wherein the two Fe sites are differentiated, leaving one Fe center with an open apical coordination site, poised for interaction with substrates. In the prototypical $Fe_2(CO)_6$(μ-pdt) and its simple substituted derivatives, the rotated structure is destabilized by 9-12 kcal/mol above the unrotated structure.[339] Early calculations suggested that electronic factors were modest, so most efforts to stabilize the rotated state have focused on steric effects.[291, 309, 176, 172] The rotated structure is only adopted in Fe^IFe^I species with a combination of bulky dithiolates, which do not exist in nature, and unsymmetrical substitution. The present work suggests that the rotated structure is stabilized by a collection of strong donor ligands.

3.4 Design of a $Fe^{I}Fe^{I}$ biomimic compound featuring a rotated ground state conformation

3.4.1 Introduction

The present work has been inspired by one of the most interesting finding emerged from the collaboration with prof. T. B. Rauchfuss, regarding the $Fe_2(CNMe)_6(\mu\text{-}pdt)$ species (section 3.3).[340] Calculations have in fact revealed that this system exists also in a low-energy $Fe^{I}Fe^{I}$ rotated form, which is surprisingly predicted to be accessible at room temperature. In the past years many attempts have been made in order to retain such a remarkable feature in biomimic compounds in their $Fe^{I}Fe^{I}$ state. In fact, if it is well established that the one-electron oxidation of $Fe^{I}Fe^{I}$ species into mixed valence $Fe^{I}Fe^{II}$ systems induces an inverted pyramidal conformation at one iron atom,[173, 172, 157, 42, 150, 175] very few examples of a fully rotated $Fe^{I}Fe^{I}$ system have been described.[291, 176] The first hydrogenases biomimic presenting a vacant site at one Fe center has been proposed by C. J. Pickett et al., consisting in a $4Fe6S^{2-}$ complex obtained through double reduction of its neutral parent.[341] This system is composed by a pair of dithiolate-bridged $Fe^{0}Fe^{II}$ subunits connected by two bridging thiolates, being much more reminiscent (from a structural view point) of the entire H-cluster than of the sole diiron subunit $[2Fe]_H$. The presence of a Fe-Fe bridging CO and thus of a vacant coordination site in one of the two connected 2Fe clusters has been assessed by means of infrared spectroscopy and theoretical considerations, but no XRD information is available. The fully rotated $Fe^{I}Fe^{I}$ dithiolate models $[Fe_2(CO)_4(\varkappa^2\text{-dmpe})\{\mu\text{-}(SCH_2)_2NBn\}]$ (dmpe = $Me_2PCH_2CH_2PMe_2$) and $[Fe_2(CO)_4(\varkappa^2\text{-dppv})(\mu\text{-}R_2pdt)]$ (dppv=cis-$C_2H_2(PPh_2)_2$, R=Me, Et, Ph) have been subsequently described and crystallized in their rotated form by P. Schollammer (see section 3.1)[291] and T. B. Rauchfuss groups[176], respectively. The common feature of these system is the sterical crowding of their dithiolate bridges: the formation of eventual remote anagostic or agostic interactions between the bulky susbtituents of the dithiolate bridge-head and one Fe center is able to induce a distorted geometry at the Fe atom. These rotated conformations are however short-living or not observable in solution. Interestingly, the role of hindering dithiolate bridges in the stabilization of the rotated conformation was previously observed in $Fe^{I}Fe^{II}$complexes. The same strategy has also been adopted in the synthesis of $[Fe_2(CO)_5(\varkappa^2\text{-dmpe})\{\mu\text{-}(SCHPh)_2SiPh_2\}]$, which features a sterically stabilized semi-rotated conformation.[309] The relevance of the discovery that $Fe_2(CNMe)_6(\mu\text{-pdt})$ exists in an energetically accessible rotated conformation at room temperature is thus evident, because it shows that is possible to tune the unrotated/rotated equilibrium without invoking any steric effect. Thus, the electron-rich $Fe_2(CNMe)_6(\mu\text{-pdt})$ has been taken as staring point of the present work. The iron atoms coordination spheres have been suitably modified by means of DFT modeling, in order to design a biomimic compound with a predicted rotated ground state conformation.

3.4.2 Results and discussion

The electronic effects connected with $Fe(CO)_3$rotation in (μ-SRS)$[Fe(CO)_3]_2$ systems have been theoretically discussed in previous works by M. Hall et al.[324] In particular, they showed that this process is predicted to induce the transfer of a partial electron density from the unrotated $Fe(CO)_3$ unit to the rotated $Fe(CO)_3$ unit. This subtle observation suggested that the complex de-symmetrization could be an exploitable factor to ease rotation of one Fe unit with respect to the other. Indeed, DFT calculations on monosubstituted complexes revealed that the replacement of one CO by a better donor ligand, L , facilitates the rotation of the $Fe(CO)_3$ unit and hinders the rotation of the $Fe(CO)_2$L unit, while the replacement of one CO by a poorer donor ligand than CO, L', facilitates the rotation of the $Fe(CO)_2$L' unit and hinders the rotation of the adjacent $Fe(CO)_3$ unit. Additionally, possible roles of the -SRS- pendant have been investigated. Remarkably, the nature of the pendant group attached to the central atom of the three-carbon S-to-S linker has proved to have a dramatic effect on difference in energy between the rotated and the unrotated structures. In particular, amine-functionalized bridges can lower the relative energy of the rotated structures by donating electron density to stabilize the "open site" created upon the Fe center by $Fe(CO)_3$ rotation. Furthermore, our results on the $Fe_2(CNMe)_6$(μ-pdt) system are indicative that the rotated conformation becomes more accessible if the electron-richness of the complex is increased. Although this last observation still needs a detailed electronic structure based justification, we decided to take $Fe_2(CNMe)_6$(μ-pdt) as starting point to perform a rational design of new compounds, inspired by the information collected by the previous Hall's theoretical works. The replacement of pdt with a nitrogen-based bridge-head led us to unravel the structure of complex $Fe_2(CNMe)_6$(μ-adt). The asymmetry of the system (avoiding at the same time the loss of electron-richness at the diiron core) has been achieved by introducing one CN^-in place of one CNMe ligand, giving the $[Fe_2(CNMe)_5(CN)(\mu\text{-pdt})]^-$ derivative. Also the effect of the combination of both amine functionalized bridge and asymmetric substitution of strong donor ligands in the same complex, namely $[Fe_2(CNMe)_5(CN)(\mu\text{-adt})]^-$, has been investigated.

As a note: the present work consists in a series of thermodynamic speciations of a selected set of compounds, in order to provide general information and hints for future synthesis. Thus, relative energies among different isomers have just been evaluated by means of their pure electronic energy, without thermal/entropic corrections or solvent treatment. Grimme empirical dispersion corrections[276] for density functional calculations have been also included.

The replacement of a CNR ligand with a cyanide group in $[Fe_2(CNMe)_5(CN)(\mu\text{-pdt})]^-$ and $[Fe_2(CNMe)_5(CN)(\mu\text{-adt})]^-$ required a complete conformational search of all the putative isomers (not shown) of these new models, in order to pinpoint the energetically favored ligand distribution in both rotated and unrotated forms. In both cases, the ground state unrotated form features the cyanide ligand in apical position, pointing towards the dithiolate bridge-head. In their most stable rotated structures, instead, the cyanide ligand is in apical position at the unrotated Fe unit, with pdt/adt flipped towards the rotated $Fe(CNMe)_3$ unit. The hindering of the R subtituents of the CNR moiety (especially in rotated isomers) led us to include also dispersion corrections in geometry optimizations. In this way, the long-range interactions between the alkyl groups are treated in a more accurate way. Figure 3.4.1 shows the most stable rotated

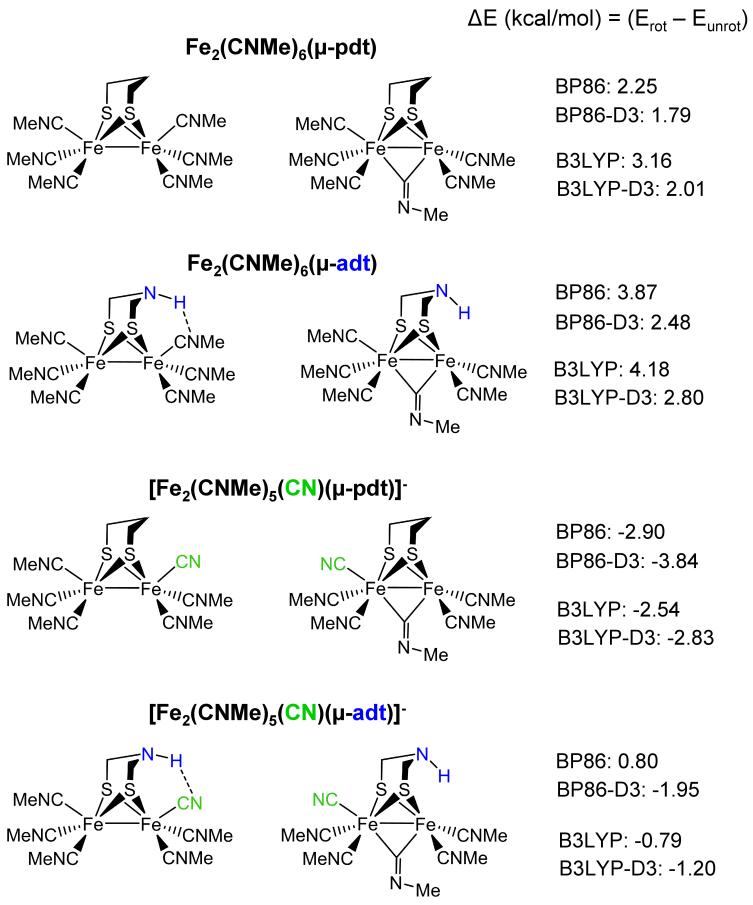

Figure 3.4.1: Computed in gas-phase relative energies between rotated and unrotated isomers [ΔE (kcal/mol) = (E_{rot} - E_{unrot})] of the set of compounds under investigation.

and unrotated isomers obtained per each model considered, together with their relative energies. Also a second functional (B3LYP) has been adopted (at a single point level, on BP86-optimized structures) in order to further validate results. The inclusion of Grimme dispersion corrections at both BP86 and B3LYP levels reduces ΔE = Erot - Eunrot, since in rotated isomers, in which the alkyl substituents of CNMe groups get closer than in the unrotated form, the London dispersion forces become stronger.

Regrettably (and in contrast with expectations), the introduction of the adt pendant entails the stabilization of the unrotated structure rather than of the rotated one. This is presumably due to the formation of a H-bond between one apical CNMe ligand and adt, allowed by the presence of a secondary amine as bridge-head. The de-symmetrization of the system by introducing a cyanide ligand, instead, proved to be a very powerful strategy to stabilize rotation, which is predicted to occur at the Fe(CNMe)3 moiety (as expected).). This is the first time that a full rotated conformation of a synthetic model of hydrogenase is predicted to be more stable than the unrotated isomer. Again, the presence of adt in $[Fe_2(CNMe)_5(CN)(\mu\text{-adt})]^-$is not functional for a further stabilization of the rotated form. Since the inclusion of a cyanide ligand causes

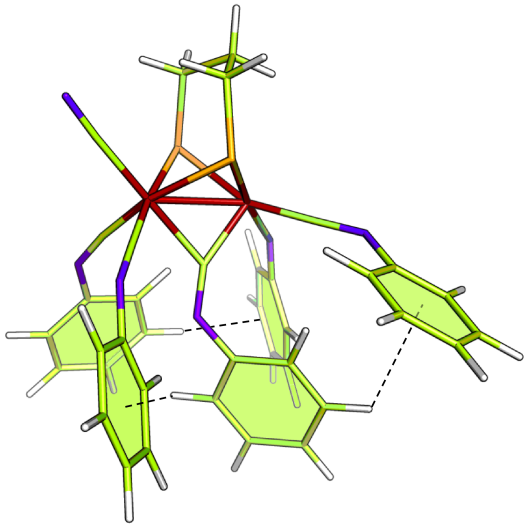

Figure 3.4.2: DFT-D3 optimized structure of the rotated isomer of $Fe_2(CNPh)_6$(μ-pdt). Stacking interactions among Ph rings are also highlighted.

the decrease of the overall charge, making the system anionic, we also simulated the same set of structures by including a counterion (K^+) to balance the negative charge. Reassuringly, no significant change of computed relative energies has been observed.

In order to fulfill synthetic requirements the Me substituents of CNMe have been subsequently replaced by Ph groups, since the derivative $Fe_2(CNPh)_6$(μ-pdt) could be easily handled from an experimental standpoint. Remarkably, this substitution led to a rotated structure (whose optimized structure at BP86-D3 level is presented in 3.4.2) in which a series of stacking interactions among the Ph groups contribute to lower Erot with respect to Eunrot (ΔE = -3.17 (BP86), -7.87 (BP86-D3), -2.22 (B3LYP), -9.81 B3LYP-D3).

3.4.3 Conclusions

Computed relative energies between rotated and unrotated forms of typical hydrogenases analogues (e.g. hexacarbonyl complexes) are usually in the range of 9-12 kcal/mol, in favor of the unrotated isomer.[323] Previous works indicated that this gap could be strongly reduced by the use of steric effects that stabilize the open site at rotated Fe.[176, 291] Alternatively, the inclusion of highly basic ligands in $Fe_2(CNMe)_6$(μ-pdt) has proved that rotated forms could also be stabilized through pure electronic factors (yet to be deeply unraveled), without the need of any steric hinder at metal centers.[340] Indeed, $Fe_2(CNMe)_5$(μ-CNMe)(μ-pdt) form has been detected by CV experiments as a populated isomer at room temperature.[340] With the present work we show that combining a set of electron-donor ligands with complex de-symmetrization could be (in a theoretical perspective) a successful strategy to obtain a ground state rotated conformation, holding great promise for mimicking such a key feature of the biological system. Complex $[Fe_2(CNPh)_5(CN)(\mu\text{-pdt})]^-$ is going to be synthesized and structurally characterized by Rauch-

fuss and coworkers, to verify its existence in a stable (both in solid state and solution) rotated conformation.

3.5 DFT dissection of the reduction step in H_2 catalytic production by [FeFe]-hydrogenase-inspired models: can the bridging hydride become more reactive than the terminal isomer?

3.5.1 Introduction

The reduction of protons, once these have bound the cofactor in its Fe^IFe^I redox state, is a key step in HER both in enzyme catalysis and in that performed by synthetic analogues. Therefore, the present study is specifically focused on the first reduction occurring during catalytic HER: $[Fe^{II}Fe^{II}]$-H + $e^- \rightarrow [Fe^IFe^{II}]$-H, with the H coordination mode being unspecified. The importance of mixed-valence $[Fe^IFe^{II}]$-H species resides in their likely intermediacy in both the enzyme turnover and also electrocatalysis performed by synthetic Fe^IFe^I analogues.[192, 342] It has been postulated that in the enzyme the proton binds in a terminal fashion on the vacant apical position of Fe_d, even though t-H has been reported to be thermodynamically less stable than the corresponding FeFe μ-H.[161, 152, 162, 280] Thus, it is conceivable that a mechanism of rearrangement could, in principle, turn the t-H isomer into the μ-H isomer. However, two $Fe_2(CN)_2$-enzyme (aforementioned) interactions are expected to hinder the isomerization at Fe_d, preventing the formation of a less reactive μ-hydride.[70] The importance of the key lysine anchoring one cyanide in Clostridium pasteurianum [FeFe]-hydrogenase is such that its replacement results in a complete loss of activity because of the missed fixing of the H-cluster to the enzyme active site.[43] Despite the biological relevance of t- Hs, their experimental detection in synthetic analogues has been rare, and it even requires special conditions because of their spontaneous tendency to isomerize to μ-Hs, as is generally and widely reported (vide infra for more specific cases).[304] An intimate mechanism of rearrangement from t-H to μ-H in some bioinspired compounds has been proposed in a density functional theory (DFT) computational investigation illustrating the energetic viability of the process.[71] Such viability has been predicted to be absent in the enzyme cofactor, in a recent work by Reiher's group.[70] These data reinforce the aforementioned idea that (too) stable bridging hydrides would form a thermodynamic sink also in the enzyme if a kinetic device was not present to freeze the t-H-to-μ-H isomerization. Terminal (or "single Fe") coordination of hydrides in synthetic mimics of the enzyme was first detected by Ezzaher et al. in solution at low temperature.[343] In these conditions, the isomerization process leading to bridging isomers is certainly slow to occur. In the same study, it was shown that protonation of the asymmetric complex $[Fe_2(CO)_4(\kappa^2\text{dppe})(\mu\text{-pdt})]$ [dppe = 1,2-$C_2H_2(PPh_2)_2$] at two different temperatures (−50 and −75 °C) led to the formation of two different t-Hs, on the $(CO)_3$ Fe atom or on the (CO)(dppe) Fe atom, respectively.[343] The first solid-state (X-ray diffraction) characterization of a terminal hydride of a diferrous complex was performed by the Rauchfuss' group.[184] t-Hs were also characterized spectroscopically for a family of complexes with bulky bis-phosphine ligands [dppv = 1,2-cis-$C_2H_2(PPh_2)_2$].[151, 308] In one of these studies, the persistence of the terminal isomer was such to allow its redox potential measurement, along with that of μ-H. Analysis on

pdt and adt derivatives of species investigated in the same study showed that t-Hs reduce at potentials of 100−200 mV less negative than their bridging counterparts (ΔE°t-H − μ-H > 0).[184] As observed by Pickett's group, the reduction potential gap could be correlated with the spin density distribution derived from DFT analysis: while in μ-H, the spin density is delocalized on both Fe atoms, in t-H, it is localized on the Fe atom with no hydride.[344] Finally, Zaffaroni et al. reported that the protonation of $[Fe_2(CO)_2(PMe_3)_4(\mu\text{-pdt})]$ yields only t-H as a result.[307] Aimed at working out the issue "stable/less reactive μ-H vs unstable/reactive t-H", one strategy has been adopted to date: the search for stable t-Hs, or at least able to persist in solution long enough to be reduced (and protonated again). The use of bulky electron-donor ligands of the Fe_2 core has allowed Rauchfuss' group to obtain a derivative functioning in this last sense. Nonetheless, also because of the aforementioned evergrowing interest toward hydrogenases[36, 304, 160], it may be worth exploring new strategies. Along this way, it can be remarked that a hydride in the bridging position between Ni and Fe atoms has been unequivocally identified by different spectroscopy techniques in [NiFe]-hydrogenases, and it has been demonstrated that it is a catalytically active intermediate.[14] Even outside the hydrogenase family, other outstanding examples of bioorganometallic clusters forming μ-hydrides are known, such as FeMo-co embedded in the nitrogenase active site.[16] This would suggest that, in nature, there is no intrinsic disadvantage for catalytic processes to pass through metal-metal bridging hydride forms. Thus, we have searched for the combination of ligands that afforded species with ΔE°t-H − μ-H < 0, thus indicating a higher (or at least as high as) redox reactivity of μ-H versus t-H. This would allow us to overturn the paradigm, valid certainly in the [FeFe]-hydrogenase modeling, that depicts μ-H as persistent-less reactive, whereas t-H is labile-reactive. Herein, by the term "reactive", we are meaning "provided with higher (less negative compared to other redox references) reduction potential". DFT results show that pushing simultaneously on both the basicity and bulk of diiron ligands affords a μ-H with a reduction potential more favorable than that of t-H. The electron richness of the Fe_2 core has been revealed to affect ΔE°t-H − μ-H, but the factor proven to be crucial in turning the sign of the redox gap in favor of t-H is the steric repulsion introduced by means of bulky tertiary phosphines. Because t-H and μ-H feature different bond patterns inside their molecular structure, they behave differently upon reduction, and this unravels the origin of the correlation that emerged between ΔE°t-H − μ-H and the ligand number/type.

3.5.2 Redox potential computation details

Aiming at computing theoretical values of standard reduction potentials (E°) that best reproduced those experimentally observed, we initially adopted a consensus protocol based on $\Delta G_{solv(SCF)}$ computation, according to which standard redox potentials can be calculated following the general equation 2.4.1. Because the experimental value is known for the gap of the standard reduction potential (ΔE°t-H − μ-H) associated with the species $[HFe_2(pdt)(CO)_2(dppv)_2]^+$ we have tested which method provided the best match of theory versus experiment, among the following: ΔE (gas-phase condition), ΔE_{solv} (structure optimization in COSMO CH_2Cl_2), $\Delta E_{solv(SCF)}$ (gas-phase value + single-point COSMO corrections, CH_2Cl_2), ΔG (ΔE + thermal/entropic cor-

$\Delta E^{\circ}{}_{\text{t-H}-\mu\text{-H}}$					
ΔE	ΔE_{solv}	$\Delta E_{solv(SCF)}$	ΔG	ΔG_{solv}	$\Delta G_{solv(SCF)}$
179	216	180	136	172	144

Table 3.5.1: $\Delta E^{\circ}{}_{\text{tH}-\mu\text{H}}$values (in mV) calculated for different levels of theory for $[HFe_2(pdt)(CO)_2(dppv)_2]^+$.

rections), ΔG_{solv} (ΔE_{solv} + thermal/entropic corrections), and $\Delta G_{solv(SCF)}$ ($\Delta E_{solv(SCF)}$ + thermal/entropic corrections). All results for ΔE° calculations are reported in Table 3.5.1. As aforementioned, $\Delta G_{solv(SCF)}$ represents in theory the formally correct approach because it includes entropic and thermal contributions and solvent effects as well. However, in the case under investigation, $\Delta E_{solv(SCF)}$ values afforded the closest match of theory versus experiment concerning ΔE°t-H − μ-H (exp value, 200 mV; computed value arising from $\Delta E_{solv(SCF)}$, 216 mV; value from $\Delta G_{solv(SCF)}$, 172 mV) Besides reproducing ΔE°t-H − μ-H, our computational model allowed us to obtain a fine match (max error = 0.14 V) of theory versus experiment of redox potentials referenced to electrodes employed experimentally (such as Fc^+/Fc). The better performance of ΔE versus ΔG in the present case is likely due to a cancellation error effect arising from approximations normally used to turn ΔE into ΔG (i.e., ideal gas approximation, separation into components of the total energy, harmonic approximation, etc.).

3.5.3 Results and discussion

To investigate the possibility of designing bridging hydrides that show more favorable reduction potentials than terminally coordinated congeners and implicitly unveil which factors are more relevant in making one electron reduction of t-H generally easier than that of bridging hydrides,[151, 308] we studied a series of [FeFe]-hydrogenases bioinspired derivatives. We first varied all carbonyl and cyanides ligands (L) but the apical one at [Fe_p] and the pdt chelate. Then, since the methylthiolate ligand has never been employed in biomimetic compounds, we investigated the effect of its replacement with other ligands (Y) employed in inorganic synthesis, such as CO, PMe_3, and N-heterocyclic carbene (NHC), with this latter already proven to be a good donor, similarly to the biological cyanide ligand. Finally, also the effects of switching (XDT) chelate to different forms have been investigated.

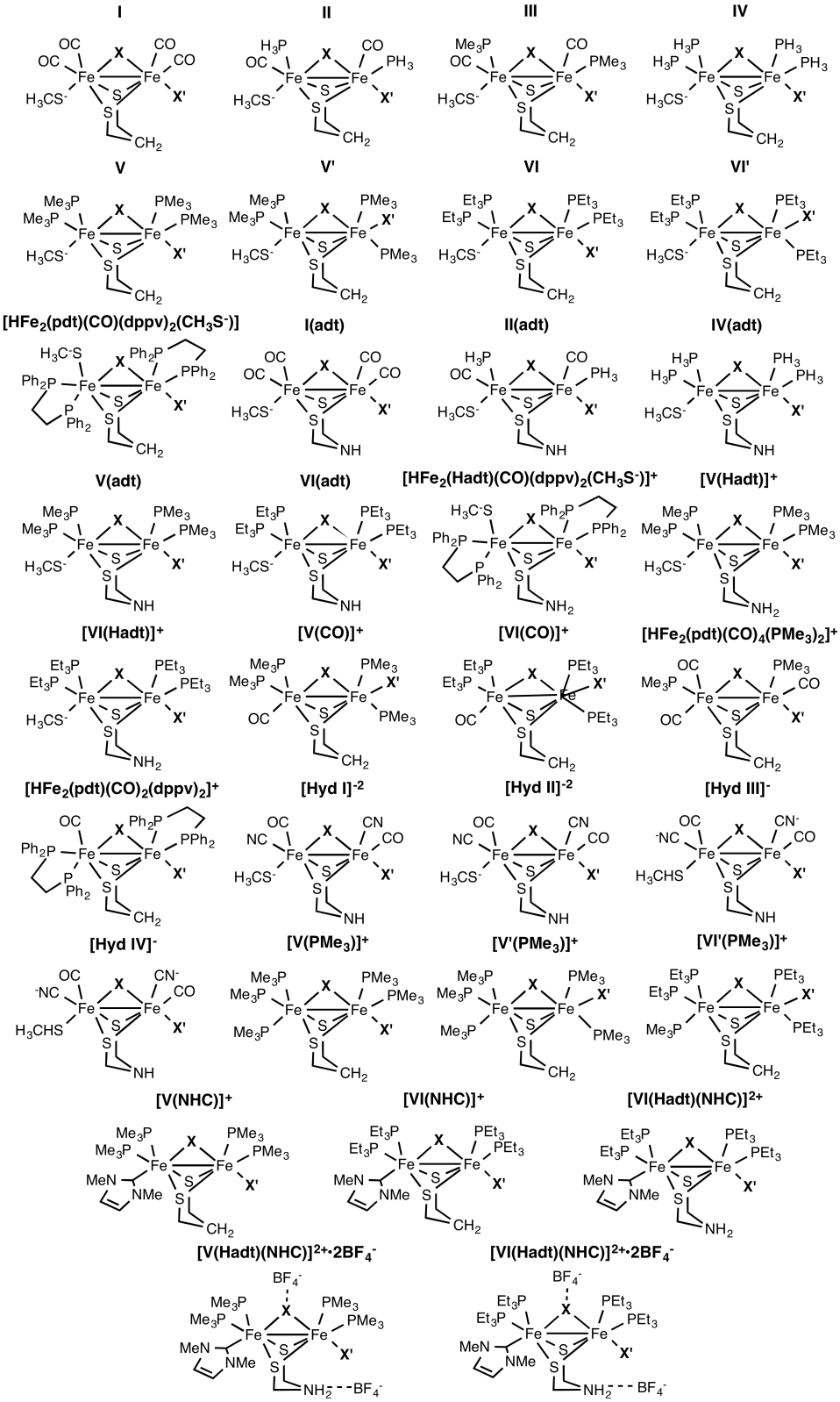

Figure 3.5.1: Full set of models investigated in the present study.

3.5.3.1 Effects of variations of L ligands

Because cyanides have been seldom used as iron ligands in the synthetic modeling of hydrogenases, due to their undesired proton affinity,[160] carbonyls and different types of phosphines[146, 147] have been used here as ligands of the [2Fe2S] center. Starting from the atomic coordinates of the PDB structure (PDB ID:1HFE), canonical H-cluster ligands were modified to obtain a series of compounds: $[HFe_2(PR_3)_x(CO_2)_{5-x}CH_3S(\mu\text{-pdt})]$ (with x = 0, 2, 4; R = H, Me, Et). The whole set of complexes is shown in Figure 3.5.1, with X/X' representing H and CO ligands switching relative positions in bridging (X=H^-, X'=CO) versus terminal hydrides (X=CO, X'=H^-). The H-cluster models investigated in the present study are: **[Hyd I]**$^{2-}$ = $[HFe_2(CO)_3(CN)_2(CH_3S)(\mu\text{-pdt})]^{2-}$, **[Hyd II]**$^{2-}$ = $[HFe_2(CO)_3(CN)_2\ (CH_3S)(\mu\text{-adt})]^{2-}$, **[Hyd III]**$^-$ = $[HFe_2(CO)_3(CN)_2(CH_3SH)(\mu\text{-pdt})]^-$, and **[Hyd IV]**$^-$ = $[HFe_2(CO)_3(CN)_2(CH_3SH)(\mu\text{-adt})]^-$. Only the lowest-energy stereoisomer (related to possible different rotamers at the $[Fe_d](X)_3$ group) of each species is shown in the picture (Figure 3.5.1). In **V**, **VI**, **[V(CO)]**$^+$, **[VI(CO)]**$^+$, **[V(PMe$_3$)]**$^+$, and **[VI(PMe$_3$)]**$^+$ species, the correct t-H disposition is to be obtained by rotating the $[Fe_d](X)_3$group by 120°. Upon reduction, the diiron core of μ-H and t-H is formally reduced from $[Fe^{II}Fe^{II}]$ to $[Fe^{II}Fe^{I}]$. Here, the values for $E^\circ_{\mu H}$ and E°_{tH} and $\Delta E^\circ_{tH-\mu H}$ have been referenced to the absolute redox potential of the Fc^+/Fc couple, commonly employed in electrochemical investigations related to [FeFe]-hydrogenases. The aim of systematically very the number and type of phosphines is to evaluate the role of their electron content and the steric bulk in modulating $\Delta E^\circ_{tH-\mu H}$. In addition, because the complexes in the model set contain an apical methylthiolate at $[Fe_p]$, this analysis has been done with the goal of modeling the role of the biogenic cysteine.

The results in Table 3.5.2 show that t-H is more easily reduced than μ-H, in all species considered (except **VI** and **VI**)', which is generally in line with the experimental data related to the biomimetic models investigated to date.[151] As expected, increasing the electronic density on the [2Fe] core of the various species implies more negative E°. Nonetheless, increasing the number of phosphines coordinated to the [2Fe] core does not appear to significantly affect the reduction potential gap, showing rather an irregular trend, going from **I** to **V**, with the last one featuring the clearest preference for t-H reduction. Unexpectedly, replacing PMe_3 with PEt_3 causes E° to become approximately equivalent in t-H versus μ-H ($\Delta E^\circ_{tH-\mu H} = -13$ mV).

Moreover, **VI** is also the only species showing a bridging form less stable than the terminal one, at both the $[Fe^{II}Fe^{II}]$-$[H^-]$ (by 4.4 kcal/mol) and $[Fe^{II}Fe^{I}]$-$[H^-]$ (by 4.1 kcal/mol) states. As for the **V'** and **VI'** μ-H species, they are isomers (with basal−apical disposition of PX_3 ligands at $[Fe_p]$) of **V** and **VI**, respectively. Reduction of these isomers has been investigated because they are very close in energy (within the DFT accuracy value) to the dibasal forms **V** and **VI**. Thus, both **V** and **VI** should be considered as two-component systems, denoted as **V**/**V**' and **VI**/**VI**', given a likely coexistence of both isomers in solution.

Compound	$E^{\circ}_{\mu H}$	E°_{tH}	$\Delta E^{\circ}_{tH-\mu H}$
I	-1.782	-1.589	193
II	-2.415	-2.230	185
III	-2.677	-2.478	199
IV	-2.990	-2.836	154
V	-3.451	-3.175	276
V'	-3.249	-3.175	74
VI	-3.185	-3.198	-13
VI'	-2.648	-3.198	-550

Table 3.5.2: Computed redox potentials (vs Fc^+/Fc) of μ-H and t-H for the series $[HFe_2(PR_3)_n(CO)_{5-n}CH_3S(\mu\text{-pdt})]$

Like **VI**, also **VI'** features a t-H more stable than μ-H by more than 2 kcal/mol at the [$Fe^{II}Fe^{II}$]-[H^-] state, whereas **V**/**V**' shows a preference for μ-H. This result is serendipitous, although particularly relevant, because stabilization of terminal versus bridging hydrides has been and still is to be considered a challenge from a synthetic standpoint.

Investigation of all of the reduced μ-H structures reveals that only VI features one [Fe_p]-H^- bond that is completely cleaved, to such an extent that H-coordination becomes terminal. In light of the reported higher reactivity toward protons of t-H form and because a second protonation is a requisite for the HER occurrence, the characteristics identified in **VI** could unravel interesting perspectives.

In particular, because $\Delta E^{\circ}_{tH-\mu H}$ associated with **VI** is near zero, whereas it is clearly > 0 for the very similar **V**, a proper tailoring of the second coordination sphere of the [2Fe] core could allow to tune such redox parameters. Curiously, however, the narrowing (and the sign inversion) of $\Delta E^{\circ}_{tH-\mu H}$ in **VI** is concomitant with the presence of a more stable t-H than μ-H so as to indicate the "classical" strategy and that pursued herein could be related.

It could be argued that PMe_3 and PEt_3 have so similar basic properties that the discrepancy that emerged between **V** and **VI** should be ascribed to steric repulsions possibly induced by the different bulk of R groups. It has to be noticed that going from electron-poorer to electronricher compounds, the number/type of P ligands does not clearly affect the E° gap, whose sign, yet, is even reverted in the presence of bulky Et groups on 4-P species. This would suggest that in a highly substituted diiron core, the creation of a conditions where bulky phospines induce an intramolecular steric effects can play a role and have an evident impact on $\Delta E^{\circ}_{tH-\mu H}$ modulation. The nonlinear trend outlined in Table 3.5.2 for $\Delta E^{\circ}_{tH-\mu H}$ shows that sign inversion occurs in an unpredictable way. This supports the fact that the number of σ-donors on the diiron derivative is not intrinsically a determinant factor, but it becomes a crucial prerequisite as it allows some peculiar effects to unveil their role on $\Delta E^{\circ}_{tH-\mu H}$ variation.

Even more surprisingly, not only the number of σ-donors but also the donor strength is not per

se sufficient to rationalize the observed picture. As previously extensively described, the PEt_3 group is a stronger donor ligand than PMe_3 is, even though other properties such as the pK_a 's of PMe_3 and PEt_3 are quite similar (8.65 for PMe_3 vs 8.69 for PMe_3). In addition, $E°_{\mu H}$ of V is more negative than that of **VI** and **VI'**, whereas the reversal is observed in t-H congeners of the same species. All such apparent anomalies must therefore be explained, invoking steric factors. The last statement is even reinforced considering that [Fe]-P(Et_3)) (2.392 Å, avg) bond distances are generally longer than those of [Fe]-P(Me_3) (2.327 Å, avg). This is another counterintuitive observation with respect to the outcome that had been figured out based on the stronger donor properties of PEt_3 versus PMe_3. To corroborate our hypothesis and to pinpoint the intimate reason underlying the **V** versus **VI** reductive behavior, a series of structural parameters have been analyzed in the **I**—**VI** set.

μ-H						
	$[Fe^{II}Fe^{II}]$			$[Fe^{I}Fe^{II}]$		
	Fe-Fe	Fe_p-H	Fe_d-H	Fe-Fe	Fe_p-H	Fe_d-H
I	2.600	1.644	1.721	2.779	1.593	1.854
II	2.598	1.641	1.739	2.690	1.626	1.765
III	2.615	1.640	1.750	2.799	1.589	1.893
IV	2.592	1.689	1.789	2.678	1.655	1.844
V	2.719	1.689	1.790	2.381	1.656	1.844
VI	2.837	1.751	1.823	3.419	1.545	2.963

t-H						
	$[Fe^{II}Fe^{II}]$			$[Fe^{I}Fe^{II}]$		
	Fe-Fe	Fe_p-C (CO)	Fe-C (CO)	Fe-Fe	Fe-C (CO)	Fe-C (CO)
I	2.526	2.000	1.978	2.704	1.990	1.998
II	2.505	1.976	1.953	2.661	1.960	1.973
III	2.501	1.978	1.938	2.664	1.961	1.966
IV	2.487	1.992	1.992	2.618	1.941	1.965
V	2.541	1.922	1.922	2.672	1.941	1.966
VI	2.573	1.995	1.931	2.723	1.943	1.978

Table 3.5.3: [Fe-Fe] and other selected distances (Å) in the μ-H and t-H isomers of the **I-VI** set.

Analysis of the data in Table 3.5.3 will be crucial to evaluating if and how a given structure is affected by intramolecular repulsive strain, that is the factor that will be shown to be decisive

to explain our results on $\Delta E^{\circ}_{tH-\mu H}$. The interatomic distances shown in Table 3.5.3 aim at monitoring structural variations upon reduction in the molecular region binding the hydride, throughout the **I**—**VI** set. This allows us to gain information on both the strength of the [Fe]-[Fe] interaction and the symmetry degree of the hydride coordination to iron (terminal vs bridging character), upon going from [$Fe^{II}Fe^{II}$] to [$Fe^{II}Fe^{I}$] states. From the data it is evident that **VI** has a peculiar feature, unique in the whole set: upon reduction, its μ-H species undergoes a complete breaking of the [Fe]-[Fe] bond with concomitant generation of relatively separated Fe subunits, the first containing a five-coordinated [Fe_d] and the second including a six-coordinated [Fe_p]. The last one is coordinated by hydride in a completely terminal fashion. **V** instead, even if very similar to **VI**, does not behave analogously once reduced. Indeed, **V** at [$Fe^{II}Fe^{I}$] redox state displays elongation of both [Fe]-[Fe] and [Fed]—H distances, but these are definitely moderate if quantitatively compared to those observed in **VI**. Such a different behavior in so similar derivatives occurring for only one of the two isomeric forms could help to explain the drop of $\Delta E^{\circ}_{tH-\mu H}$ observed in PEt_3 versus PMe_3 species. Otherwise stated, the cause of the structural differences for **V** versus **VI** in their reduced state could be at the ground of the sign inversion of $\Delta E^{\circ}_{tH-\mu H}$. Intramolecular steric repulsions are introduced by enlarging the R size of phosphine ligands upon going from **V** to **VI**, with the consequence of strain production (or destabilization) in [$Fe^{II}Fe^{II}$] redox state of **VI**, which is unique in the **I**—**VI** set of compounds. The destabilization affects both μ-H and t-H of **VI**, but reduction can alleviate repulsive interactions only in the bridging isomer but not in t-H, as emerged from a comparison of the structural parameters of **V** versus **VI**.

Thus, it becomes of primary importance to understand why reduction can separate the two Fe subunits of μ-H but not those of t-H in the case of VI. Some features being present exclusively in t-H may prevent the strain from being relaxed upon reduction. Indeed, all terminal-bound hydrides have a CO in the bridging position between the two Fe ions. Furthermore, the iron bridging CO is trans-oriented simultaneously to two strong electron donors (H^- and CH_3S^-): it is therefore predictable that, specifically in electron-rich derivatives, CO receives a large amount of electron density through a double π-back-donation from both Fe atoms. This implies the presence of two strong [Fe_p]-C(O)-[Fe_d] bonds (each with partial double-bond character), which can prevent dissociation of the two Fe subunits upon reduction. Bridging hydrides cannot show similar behavior because of the absence of π-acceptor properties by the H ligand. This results in μ-hydrido isomers of species affected by intramolecular destabilization (exactly as **VI**) being free to alleviate the strain thanks to reduction.

The observation of key distances associated with **V** (Table 3.5.3) brings to light that this derivative must not be affected by intramolecular strain, which implies that its reductive behavior should not deviate significantly from the other less substituted derivatives of Table 3.5.2. This indirectly indicates that, without steric factors influencing selectively the two hydrido forms of a given species, the observation of a more favorable redox potential associated with t-H must be governed by pure electronic factors. As aforementioned, the DFT isomer speciation showed (limited to **V** and **VI** in their [$Fe^{II}Fe^{II}$] state) that the two possible ligand dispositions at [Fe_d] (Pdibasal and Papical—basal) are so close in energy that DFT accuracy does not allow an unequivocal

resolution of their relative stability. Therefore, the two stereoisomers should be fairly predicted to coexist in a thermodynamically equilibrated solution. Redox potentials have therefore been calculated also for **V'** and **VI'**. Interestingly, reduction causes this time the loss of the apical PEt_3 from [Fe_d] coordination in the sole instance of **VI**, while **V** [[$Fe^{I}Fe^{II}$]] was still a bis-six-coordinated Fe species. The [Fe_d]−PEt_3 bond breaking upon reduction leads to a larger release of molecular strain compared to that observed for reduction of the dibasal isomer. Thus, dissociating a P ligand from Fe represents the other way that μ-Hs of strained/unstable species have for relaxing accumulated repulsions. Of course, because **VI** and **VI'** share the same t-H structure, the rationale that justifies why the strain release occurs only in μ-Hs is the same as that outlined previously. These results support quite incontrovertibly the idea that a proper modulation of the intramolecular sterics can influence the $\Delta E^{\circ}_{tH-\mu H}$ gap. Frontier molecular orbital (FMO) analysis has been then performed to pinpoint which electronic properties are mostly influenced by the structural difference in **V** versus **VI**. From inspection of the singly occupied molecular orbital (SOMO) in reduced states of **V** versus **VI**, shown in Figure 3.5.2 it is evident that the molecular strain affecting **VI** and (but not **V**) finds release upon reduction in μ-H, whereas in t-H, there is actually a strain retention. A comparison of ESOMO values shows that there is complete consistence with the more favorable reduction of t-H versus μ-H in **V** ($\Delta E^{\circ}_{tH-\mu H} > 0$; Table 3.5.2) and simultaneously with the reverse behavior in **VI** ($\Delta E^{\circ}_{tH-\mu H} < 0$). Also some differences are detectable in the atomic orbital composition (with consequential unequal distribution) of the two SOMOs in μ-hydrides of **V** versus **VI**, whereas such a parameter is practically unchanged when looking at the SOMO of t-Hs of the same species.

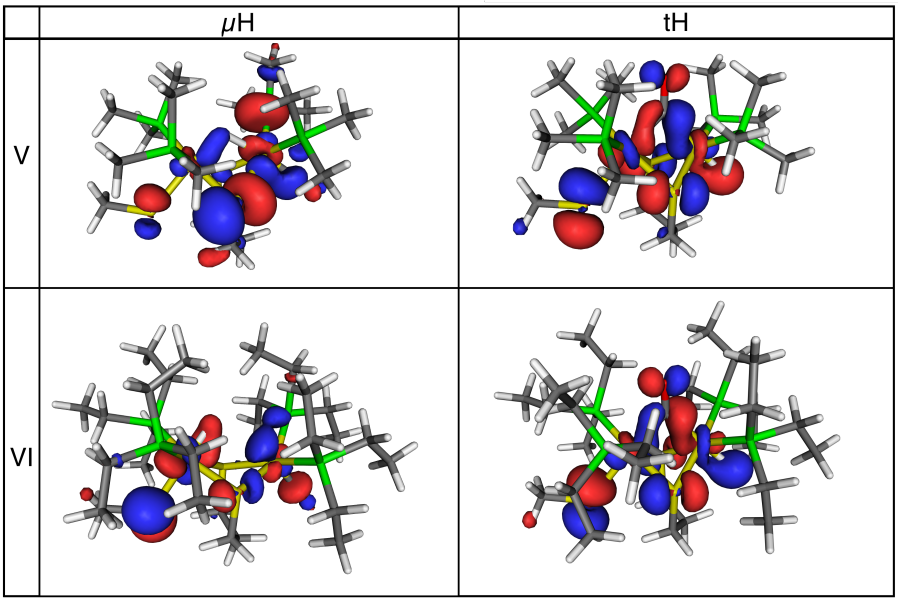

Figure 3.5.2: E_{SOMO}(eV) and electronic distribution in reduced states of both t-H and μ-H for derivatives **V** and **VI**. The isosurface cutoff value is 0.03 atomic units.

Compound	$E^{\circ}_{\mu H}$	E°_{tH}	$\Delta E^{\circ}_{tH-\mu H}$
[V(CO)]$^{+}$	-2.201	-2.022	179
[V(CO)]$^{+}$*	-2.649	-1.944	705
[V(PMe$_3$)]$^{+}$	-2.645	-2.353	292
[V'(PMe$_3$)]$^{+}$	-2.467	-2.354	114
[VI(PMe$_3$)]$^{+}$*	-1.467	-2.042	-566
[V(NHC)]$^{+}$	-2.840	-2.626	214
[VI(NHC)]$^{+}$	-2.523	-2.586	-45

Table 3.5.4: Computed redox potentials (vs Fc^{+}/Fc) of μ-H and t-H for the series $[HFe_2(PR_3)_n(CO)_{5-n}CH_3Y(\mu\text{-pdt})]$ (X=Me in **V**/**V**' and X=Et in **VI**/**VI**', Y=CO, PMe_3 and NHC). In complexes designated with an asterisk, the reduced form of μ-H loses an apical phosphine, originally trans-oriented to hydride, whereas $[V(NHC)]^{+}$ is the only 4-PEt_3 system in which the strain release occurs through breaking of Fe—Fe and one Fe—H bonds.

3.5.3.2 Effects of variations of Y ligand

Heretofore, have been considered complexes featuring the CH_3S^{-} ligand, a mimic of the cysteinyl sulfur bridge that links the [4Fe4S] cluster to the $[2Fe]_H$ center.[36, 38, 44] Nonetheless, has been already mentioned that CH_3S^{-} is not normally employed in the synthetic hydrogenases' chemistry.[345] Thus, has been set out to investigate the effect of replacing it with other ligands more routinely used synthetically, such as neutrally charged CO, PMe_3, and also NHC. The results showing E°, $\Delta E^{\circ}_{tH-\mu H}$, and all of those structural parameters that are useful to evaluating the strain release upon reduction of the various species are reported in Tables 3.5.4 and 3.5.5.

First, it is evident that the V-like versus VI-like comparison confirms the essential role of intramolecular repulsions and their release upon reduction for justifying the $\Delta E^{\circ}_{tH-\mu H}$ variation. The presence of the CO group in place of the methylthiol group makes $\Delta E^{\circ}_{tH-\mu H}$ significantly positive, indicative of μ-H reduction clearly disfavored versus t-H reduction. The importance of the simultaneous presence of two sv-donors trans-oriented to bridging CO in terminal hydrides has already been invoked as the reason that prevents strained t-H (of the **VI**/**VI'** system) from being energy-relaxed. Therefore, t-H isomer of **[VI(CO)]**$^{+}$ species can relax, as well as μ-H, thus not showing that different behavior upon reduction of t-H versus μ-H, which is necessary to observe $\Delta E^{\circ}_{tH-\mu H}$ inversion. Indeed, the true reason for which the oxidized **[VI(CO)]**$^{+}$-t-H is strained, despite the presence of two acceptors (with the CO replacing CH_3S^{-} and μ-CO), whereas, for example, **[VI(PMe$_3$)]**$^{+}$ is not strained is rather subtle and is more complicated than depicted here. It requires invoking electronic effects, which have been discussed in the following paragraphs. It was expected that substitution of CH_3S^{-} by PMe_3 (**[VI(PMe$_3$)]**$^{+}$) would lead to outcomes analogous to those of **VI**/**VI**'. These findings can be explained by the σ-donor nature of PMe_3 , which, although less strong compared to the thiolate, is well-known. In this peculiar case, it has been studied only one stereoisomer at $[Fe_d]$ because the other is very unstable (data not shown). **[VI(PMe$_3$)]**$^{+}$ actually shows strongly negative $\Delta E^{\circ}_{tH-\mu H}$ (see Table3.5.4, but the

μ-H				
	$[Fe^{II}Fe^{II}]$		$[Fe^{I}Fe^{II}]$	
	Fe-Fe	Fe_d-H	Fe-Fe	Fe_d-H
[V(CO)]$^+$	2.648	1.662	2.792	1.680
[VI(CO)]$^+$	2.689	1.675	2.692	1.695
[V(PMe$_3$)]$^+$	2.765	1.748	2.932	1.776
[V'(PMe$_3$)]$^+$	2.718	1.702	2.885	1.802
[VI(PMe$_3$)]$^+$	2.779	1.710	2.719	1.721
[V(NHC)]$^+$	2.711	1.702	2.873	1.846
[VI(NHC)]$^+$	2.881	1.790	3.527	3.011

t-H				
	$[Fe^{II}Fe^{II}]$		$[Fe^{I}Fe^{II}]$	
	Fe-Fe	Fe_d-C(CO)	Fe-Fe	Fe_d-C(CO)
[V(CO)]$^+$	2.641	1.529	3.093	2.999
[VI(CO)]$^+$*	2.674	2.513	3.179	2.989
[V(PMe$_3$)]$^+$	2.772	2.747	3.268	3.279
[V'(PMe$_3$)]$^+$	2.772	2.747	3.268	3.279
[VI(PMe$_3$)]$^+$*	2.920	2.921	3.379	3.297
[V(NHC)]$^+$	2.768	2.679	3.214	3.144
[VI(NHC)]$^+$	2.875	2.771	3.329	3.181

Table 3.5.5: [Fe-Fe] and other selected distances (Å) in the μ-H and t-H isomers of the **I-VI** set.

reason underlying this result requires application of the strain-release model in a slightly different way. Because the apical PMe_3 is a weaker donor than thiolate, it cannot trigger the formation of a $[Fe_p]$—C(O) bond (2.921 Å) as strong as in the case of CH_3S^--based species **VI**/**VI'** (1.995 Å), essential for preventing relaxation of molecular strain in terminal hydrides. This entails that t-H of **[VI(PMe$_3$)]$^+$** is not strained at all already at the oxidized level (see Figure 3.5.3), as is clearly evidenced from the structural parameter analysis presented in Table 3.5.5. $\Delta E^\circ_{tH-\mu H}$ values and structural parameters associated with **[VI(NHC)]$^+$** qualitatively confirm all results observed for **[VI(PMe$_3$)]$^+$**. The quantitative difference ($\Delta E^\circ_{tH-\mu H}$ of the PMe_3 species is clearly more negative than that in the NHC one) is explained by the fact that the **[VI(PMe$_3$)]$^+$** μ-H loses a phosphine upon reduction, while the **[VI(NHC)]$^+$** μ-H displays [Fe]—[Fe] and [Fed]—H bond breaking. This last reductive behavior has less impact on the E° gap (see also **VI** vs **VI**') from a quantitative standpoint. It may be argued at this point that also **[VI'(CO)]$^+$** should feature a $[Fe^{II}Fe^{II}]$ t-H repulsively unstrained, just like **[VI(PMe$_3$)]$^+$** and **[VI(NHC)]$^+$**.

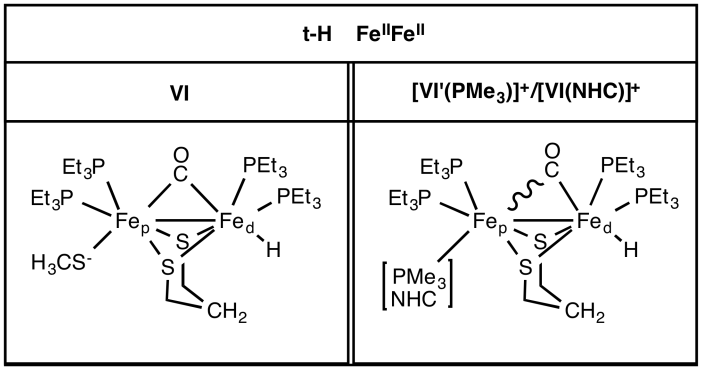

Figure 3.5.3: Neutrally charged apical donors implying a weakening of the [Fep]−C(O) bond in the cationic diferrous state of t-H: this causes **[VI(PMe$_3$)]**$^+$ and **[VI(NHC)]**$^+$ to be unstrained structures, unlike **VI** (bearing apical CH_3S).

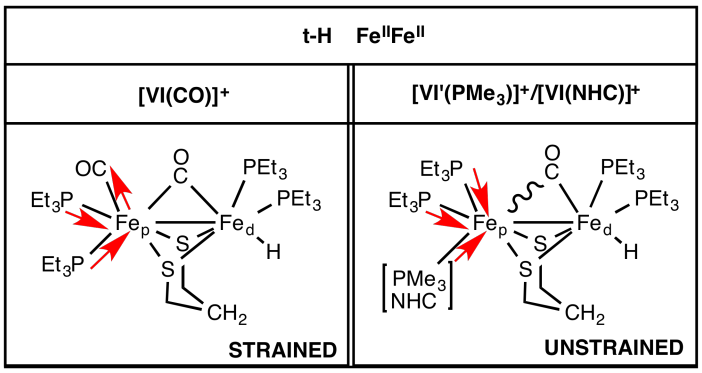

Figure 3.5.4: Schematic illustration of electronic factors underlying the presence of strain in t-H-**[VI'(CO)]**$^+$ and the absence of strain in t-H-**[VI(PMe$_3$)]**$^+$ and t-H-**[VI(NHC)]**$^+$.

The apical CO is actually expected to induce an even weaker [Fep]−C(O) bond trans to it, compared to those characterizing **[VI(PMe$_3$)]**$^+$ and **[VI(NHC)]**$^+$. As can be viewed in Table 3.5.5 (for example, focusing on the [Fe]−[Fe] bond), **[VI'(CO)]**$^+$ features structural parameters that are indicative of a strained oxidized state, at least more than the corresponding state in **[VI(PMe$_3$)]**$^+$ and **[VI(NHC)]**$^+$. That is due to a couple of factors, the first being the fact that the most stable rotameric disposition of **[VI'(CO)]**$^+$ at [Fe$_p$] is not $(CO)_{ap}$−Fe−$(PEt_3)_{2ba-ba}$ but instead $(PEt_3)_{ap}$−Fe−$(CO)_{ba}(PEt_3)_{ba}$. Such a result is probably due to the same aforementioned reason: two mutually trans-oriented CO's are less stable than that in a P−Fe−(CO) disposition. Thus, oxidized t-H-**[VI'(CO)]**$^+$ has actually a donor (P) ligand in the apical position at [Fe$_p$], just like **[VI(PMe3)]**$^+$ and **[VI(NHC)]**$^+$, so that the issue of the different strain (in the former vs the two latter species) remains unclear, unless electronic factors are invoked. To shed light on that, one has to consider that t-H-**[VI'(CO)]**$^+$ has a less electron-rich [2FeH] core than that of the other two species because of the presence of CO versus NHC and PMe_3. This means that in t-H-**[VI'(CO)]**$^+$ more electron density is drawn from the [2FeH] core compared to t-H-**[VI(PMe$_3$)]**$^+$ and t-H-**[VI(NHC)]**$^+$(see Figure 3.5.4).

	μ-H		t-H		
Compound	$[Fe^{II}Fe^{II}]$	$[Fe^{I}Fe^{II}]$	$[Fe^{II}Fe^{II}]$	$[Fe^{I}Fe^{II}]$	$\Delta E^{\circ}_{tH-\mu H}$
V/V'	US	US	US	US	> 0
VI/VI'	S	US	S	S	< 0
[V(CO)]$^+$	US	US	US	US	> 0
[VI(CO)]$^+$	S	US	S	US	> 0
[V/V'(PMe$_3$)]$^+$	US	US	US	US	> 0
[VI(PMe$_3$)]$^+$*	S	US	US	US	< 0
[V(NHC)]$^+$	US	US	US	US	> 0
[VI(NHC)]$^+$	S	US	US	US	< 0

Table 3.5.6: Strain pattern related to some key species described above.

Although the 18-electron rule formally requires the presence of the [Fe]−[Fe] bond in the investigated species, it is yet conceivable that, in very electron-rich di-iron cores such as those in t-H-**[VI(PMe$_3$)]$^+$** and t-H-**[VI(NHC)]$^+$**, each Fe ion is already electronically saturated, so that the [Fe]−[Fe] formation is less mandatory than that in t-H-**[VI'(CO)]$^+$**. On a more general level, it can thus be confidently concluded that what ultimately determines the sign of $\Delta E^{\circ}_{tH-\mu H}$ is not necessarily the presence of factors keeping strained t-Hs from relaxing, whereas corresponding μ-Hs are able to do that (as illustrated in the **VI/VI'** case). Indeed, the crucial point is the different reductive behavior of t-H versus μ-H of a given species, in whatever fashion it may occur. It is relevant that the model that has been devised to monitor the presence/absence of intramolecular strain remains valid in all of the instances investigated, with the only variation residing in the manner of application of the model itself. Identical behavior implies that t-Hs are reduced at potentials less negative than those of μ-Hs, whereas different behavior implies the opposite outcome. It has been stressed that herein the identical/different couple refers to how/if the t-H versus μ-H of a particular instance changes its features in terms of the repulsive strain model that has been set up and which could be coded as follows. Let 'S' stand for strained and 'US' for unstrained molecule: an identical reductive behavior t-H versus μ-H will be coded either by 'S/S vs S/S' or by 'US/US vs US/US' or finally by 'S/US vs S/US'. Any other combination of characters associated with the strain model will provide a different reductive behavior in the t-H/μ-H couple. This rationale can be schematically shown in Table 3.5.6, from which it is clear how a given pattern (the array of S/US characters) associated with the presence/absence of repulsive strain in both t-H and μ-H of each derivative entails a positive or negative sign of $\Delta E^{\circ}_{tH-\mu H}$. In light of the literature reporting that NHC and PMe_3 have been previously incorporated in diiron dithiolates modeling [FeFe]-hydrogenases, derivatives equipped with such ligands in the Fe apical position **[VI(PMe$_3$)]$^+$** and **[VI(NHC)]$^+$** could be potential candidates for the synthesis of new biomimetic compounds.

Compound	$\Delta E^{\circ}_{tH-\mu H}$
[HydI]$^-$	152
[HydII]$^-$	222
[HydIII]$^-$	478
[HydIV]$^-$	307

Table 3.5.7: $\Delta E^{\circ}_{tH-\mu H}$ associated with the $[2Fe]_H$ subunit of the H-Cluster (truncated at the cysteinyl thiolate).

3.5.3.3 Effects of protonation of CH_3S^- ligand

Further, it has been investigated the possibility of altering $\Delta E^{\circ}_{tH-\mu H}$ by decreasing the electron-donor character of the CH_3S^- group by protonating the S atom (which could mimic the electron-attracting character of the CO group and the presence of the cubane cluster). Such an effect has been tested on a set of computational models of the active site of [FeFe]-hydrogenase (here named **[Hyd X]**). Both dithiolate straps adt and pdt have been considered, a comparison anyway useful for the purposes of the present study, although the issue of the real identity of the X element in $-SCH_2XCH_2S-$ has been finally resolved in favor of nitrogen.[346] The presence of CH_3SH in place of the anionic CH_3S^- leads to an increase of $\Delta E^{\circ}_{tH-\mu H}$ by more than 300 mV in the model featuring pdt, while the augment is more limited in the case of the adt form (Table 3.5.7). An easier reduction of the t-H form fits well with the literature, which describes a scenario in which enzyme catalysis is characterized, among other factors, also by kinetic stabilization of the hydride in the terminal position at $[Fe_d]$. The t-H-to-μ-H rearrangement, active in all biomimetic compounds, is hindered in the enzyme through interaction between the ligand CN^- and a conserved lysine. In these conditions, the formation of a μ-H isomer would bring a less favored reductive event, probably impairing the catalytic efficiency.

3.5.3.4 Effect of variation of XDT chelate

The redox potentials of **[VI(NHC)]$^+$** for both hydride forms (-2.513 V for μ-H and -2.557 V for t-H vs Fc^+/Fc) still reveal overpotential (although less than that of CH_3S^--based species), as expected because of the large number of donor ligands coordinated to the [2FeH] center. A possible mitigation of this effect has been obtained by replacing pdt with adt. Indeed, the central amine of adt derivatives can be protonated in solutions by acids thus bearing an extra net positive charge in diiron dithiolate.[184] However, because hydride species bearing nonprotonated adt are also detected in the CH_2Cl_2 solution, $\Delta E^{\circ}_{tH-\mu H}$ has been computed also for some analogues of Table 3.5.2 in which pdt has been replaced with neutral azadithiolate. Moreover, two derivatives experimentally synthesized, $[HFe_2(CO)_2(dppv)_2(\mu\text{-pdt})]^+$ and $[HFe_2(CO)_4(PMe_3)_2(\mu\text{-pdt})]^+$ ($\Delta E^{\circ}_{tH-\mu H} = 188$ mV), have also been considered. These last two sets of calculations have served mainly as benchmarks for the present investigation. The obtained values confirm the same qualitative trend as that observed for pdt-based derivatives, even if a negative $\Delta E^{\circ}_{tH-\mu H}$ cannot be observed, probably because of a (N)H$-$[Fe] stabilizing interaction, which selectively favors t-H.

Compound	$\Delta E^{\circ}_{tH-\mu H}$
V(Hadt)]$^{+}$	576
VI(Hadt)]$^{+}$	399
[VI(Hadt)(NHC)]$^{2+}$	680
[V(Hadt)(NHC)]$^{2+}\cdot$ 2BF$_4^-$	218
[VI(Hadt)(NHC)]$^{2+}\cdot$ 2BF$_4^-$	84
[HFe$_2$(Hadt)(CO)(dppv)$_2$CH$_3$S]$^{+}$	455
[HFe$_2$(pdt)(CO)(dppv)$_2$CH$_3$S]	124

Table 3.5.8: Standard reduction potential gap (ΔE°tH−μH in mV) of derivatives containing Hadt as a dithiolate strap.

When switching to protonated (Hadt) derivatives, it can be noted that **[VI(NHC)(μ-Hadt)]$^{2+}$** shows, as expected, less negative E° values both in μ-H (−1.797 V vs Fc^{+}/Fc) and in t-H (−1.117 V vs Fc^{+}/Fc).

Regrettably, yet, this result goes to the detriment of the desired $\Delta E^{\circ}_{tH-\mu H}$ sign, as is observable in Table 3.5.3.4. The reasons for that can be found in a strong intramolecular NH(H)$^{2+}$−H[Fe] interaction (dihydrogen bonding), which selectively favors t-H versus μ-H, a feature recently illustrated also at the solid state in [HFe$_2$(CO)$_2$ (dppv)$_2$(μ-Hadt)]$^{2+}$ by Rauchfuss' group.[184] However, the strength of this interaction and also the doubly positive charge of [VI(NHC)(μ-Hadt)]$^{2+}$ could be overestimated by the previous calculations because of the absence of explicit counterions such as BF$_4^-$, which could be present near the electrode surface in buffers used in a real cyclic voltammetry experiment. In addition, it has been reported that BF$_4^-$ ions can alter a delicately balanced equilibrium existing between N and Fe-protonated isomers. The results show that adding explicit BF$_4^-$ ions in the simulation brings about an 8-fold decrease of $\Delta E^{\circ}_{tH-\mu H}$ with respect to the isolated bis-cation (see Table 3.5.3.4), which definitively points to a strong effect of the molecular charge on the redox gap. Although marked, however, the charge effect is not sufficient in this case to observe a μ-H reduction favored over that of t-H. It is worth recalling, nonetheless, that 84 mV (1.9 kcal/mol) is a value essentially very close to the precision limit of the employed computational method, thus indicating that a species may exist with t-H and μ-H with roughly the same reduction potential. The emerging scenario reveals that the amount of negative charge that is pushed into the diiron system is able to significantly affect $\Delta E^{\circ}_{tH-\mu H}$. This aspect is to be taken into appropriate consideration for fine-tuning a parameter, which could be relevant in the design of new catalysts. It becomes thus clear that a problem arises when pursuing the alternative strategy that have been herein explored, and that is thus worth recalling at this point: the design of a model species characterized by $\Delta E^{\circ}_{tH-\mu H} < 0$. This result is indeed achievable but only by very electron-rich derivatives, thus obviously characterized by reduction overpotential. Any attempt that has been made to decrease E° entails a $\Delta E^{\circ}_{tH-\mu H}$ shift toward more positive values. This point is confirmed also upon a comparison of [HFe$_2$(CO)(dppv)$_2$CH$_3$S(μ-Hadt)]$^{+}$ versus [HFe$_2$(CO)(dppv)$_2$CH$_3$S(μ-pdt)] (see Table 3.5.3.4), in which it has been probed the effect

of replacing a CO with CH_3S^- in Hadt and pdt derivatives, experimentally synthesized. CH_3S^- causes a $\Delta E^\circ_{tH-\mu H}$ shift toward less positive values (from 216 to 124 mV) in the pdt species, which is compatible with the role that has been described above for such a ligand. The case simulation of $[HFe_2(CO)(dppv)_2CH_3S(\mu\text{-pdt})]$ is also interesting in that it allows one to call back the importance of the repulsive strain factor, as defined previously: this derivative has the same overall charge as VI/VI, and all of these species share a common CH_3S^- bound at $[Fe_p]$.

Despite all similarities, however, $\Delta E^\circ_{tH-\mu H}$ is clearly positive in $[HFe_2(CO)(dppv)_2CH_3S(\mu\text{-pdt})]$ and negative in **VI** (strongly negative in **VI**'), a result that can be explained by the different intramolecular repulsive bumps that characterize these derivatives. In fact, phenyl rings of the dppv chelate can be observed to take on stabilization of T-shape orientations, at both the computational and X-ray crystallography level.[184] Also, in this case, however, upon switching to the Hadt species, a strong shift of $\Delta E^\circ_{tH-\mu H}$ is observed, as in all preceding cases, demonstrating (once again) how an unequivocal connection exists between absolute redox potentials and their gap in t-H versus μ-H isomers. A compromise between the reduction overpotential and the desired $\Delta E^\circ_{tH-\mu H}$ is therefore a probable key to design more efficient electrocatalysts. In such a sense, the tiny value computed for the redox gap value found for $[VI(NHC)(\mu\text{-Hadt})]^{2+}\cdot$ 2 BF_4^- could be considered stimulating.

3.5.4 Conclusions

Increasing the number of electron donors on the protonated [2FeH] core of [FeFe]-hydrogenases is predicted to alter $\Delta E^\circ_{tH-\mu H}$ in a nonlinear way, up to a substitution extent at which subtle steric factors come into play entailing a surprising modulation of the redox gap. Intramolecular steric repulsions among bulky PR_3 ligands of highly substituted ($Fe_2(PR_3)_4$) diiron dithiolates cause an unsuspected effect on $\Delta E^\circ_{tH-\mu H}$: an inversion of its sign, the target of this present investigation. Variation upon reduction of the structural and energetic parameters shows that such a result is due to a steric strain (or destabilization), which affects differently the μ-H and t-H isomeric forms. Thus, μ-H of highly substituted derivatives with bulky PR_3 in their oxidated $[Fe^{II}Fe^{II}]$ state is unstable toward reduction, compared to analogues with R of smaller size. The intramolecular strain thus generated can be released upon one-electron reduction in two ways depending on which one of the two rotational stereoisomers of μ-H is being reduced. The main point is that only μ-H shows release of the intramolecular strain because in t-H, a [Fe]-[Fe] bridging CO, which is strong π-acceptor and trans-oriented to two strong σ-donors, forms two strong [Fe]−C(O)−[Fe] bonds, preventing the two [Fe]-L_3 moieties from moving away from each other. Therefore, t-H of electron-rich species simultaneously bearing bulky PR_3 ligands cannot release the intramolecular strain, whereas μ-H does. This justifies the inversion of the $\Delta E^\circ_{tH-\mu H}$ sign observed in VI-like systems. In the case of neutrally charged σ-donors, less strong than the apical CH_3S^- (such as NHC), our results again show a $\Delta E^\circ_{tH-\mu H} < 0$, although t-H's of such derivatives show structural parameters indicating either [Fe]-$(P)R_3$ or [Fe]−[Fe]/[Fe]-H bond breaking. Justification of such a result requires therefore generalization of the model based on the strain presence/absence and on how/if it can be released upon reduction. The general factor underlying the positivity or

negativity of $\Delta E^{\circ}_{tH-\mu H}$ is the similarity or diversity of the reductive behavior by t-H versus μ-H of a given species. Therefore, in the case of species with NHC and PMe_3, their t-H is strain-free already at the oxidized state because two such ligands are not able to make sufficiently strong [Fe]−(C)O bonds, which would preserve the unstable configuration. By contrast, μ-H of the same species is affected by intramolecular repulsion at the oxidized state, reduction of which allows alleviation. This implies that the behavior of t-H versus μ-H is once again different, although according to another pattern compared to that emerged in CH_3S^--based species. It is worth pointing out that the possibility of replacing the anionic CH_3S^- with neutrally charged σ-donors is a relevant factor because it favors the lowering of the reduction overpotentials. Reducing the overall charge of the diiron dithiolates by, for instance, replacing neutral pdt with nitrogen-containing linkers that are susceptible to being protonated by acids, tends to favor t-H reduction over μ-H ($\Delta E^{\circ}_{tH-\mu H}$ is shifted toward more positive values). The same effect is observed when calculating $\Delta E^{\circ}_{tH-\mu H}$ after protonation of the apical CH_3S^- in models of the diiron core of the enzyme active site. These observations, along with the necessity of incorporating a large number of donor ligands in the diiron dithiolate, before the repulsive strain effect pops up, implies that non negligible overpotentials are to be taken into consideration. Therefore, a compromise that can balance the overpotential versus ΔE° competition has to be pursued.

3.6 Comparison of H_2 oxidation in [FeFe]-hydrogenases and biomimetic models highlights key stereoelectronic features for catalysis

3.6.1 Introduction

When considering the catalytic cycle in the direction of H_2 oxidation (Figure 3.6.1), the [FeFe]-hydrogenase form directly involved in H_2 binding is referred to as H_{ox}, where the redox state of the H-cluster can be formally described as $2Fe^{II}2Fe^{III}$-$Fe^{I}Fe^{II}$.[14] In addition, in H_{ox} a CO ligand bridges the two iron ions, and the Fed atom is five-coordinated. Due to the remarkable catalytic activity of [FeFe]-hydrogenases, the H_{ox} state has become a reference point for the design of biomimetic catalysts for H_2 oxidation. In fact, a variety of $Fe^{II}Fe^{I}$ complexes were synthesized and characterized in recent years.[15, 127] However, despite their similarity to the $[2Fe]_H$ subcluster, $Fe^{I}Fe^{II}$ complexes are unable to catalyze H_2 oxidation[15, 127], unless very few examples ([205, 181, 207]). In any case, the catalytic activity of such biomimetic complexes is much lower than that of the natural enzyme.

Thus, the design of a synthetic catalyst performing in conditions close to ideality, implies the ability to control the relative energies of all of the intermediates of a catalytic cycle.[347, 348] This, in turn, requires an understanding of the factors that determine the relative free energies of these catalytic intermediates and the development of predictive quantitative models. Indeed, general considerations about catalysis[347, 348] suggest that in an efficient catalyst for H_2 oxidation the energy difference between intermediate species should be small, because the formation of very stable or very unstable transient species is not compatible with a fast catalytic process. For analogous reasons, the oxidation potential of the catalyst-H_2 adduct and of the other intermediate species formed in the catalytic cycle should be as close as possible to the corresponding potential for the uncatalyzed reaction $H_2 \rightarrow 2H^+ + 2e^-$. In addition, the investigation of both [FeFe]-hydrogenases and synthetic complexes has revealed that the presence of a suitable pendant amine group, which can play the role of a base in the heterolytic cleavage of H_2, greatly increases catalytic activity[69, 346]. Finally, the oxidation potential of the catalyst-H_2 adduct must be less negative than for the isolated catalyst, because the oxidation of diiron biomimetic catalysts before H_2 binding can produce inactive species characterized by a Fe-N bond. In addition it should be noted that most synthetic models differ from the enzyme active site because they feature organo-phosphorous ligands, such as 1,2-C_2 H_2 (PPh_2)$_2$ (dppv) and PMe_3 in place of cyanide ligands.[160] This change allows to carry out mechanistic studies without the complications associated to CN^- reactivity, but its effect on the catalytic activity has been essentially unexplored.

With the aim of contributing to the design of novel and more efficient biomimetic catalysts for H_2 oxidation, we have used DFT to quantitatively compare four key reaction steps in the catalytic cycle of [FeFe]-hydrogenases and related biomimetic complexes[14, 15]: H_2 binding, one-electron oxidation of the H_2 adduct, H_2 cleavage, and intramolecular proton transfer following H_2

heterolytic cleavage (see Figure 3.6.1, red arrows). The comparison between natural and synthetic catalysts reveals key features for catalysis, which differentiate H-cluster models from synthetic analogues, and indirectly suggests new strategies to improve the catalytic activity of biomimetic complexes.

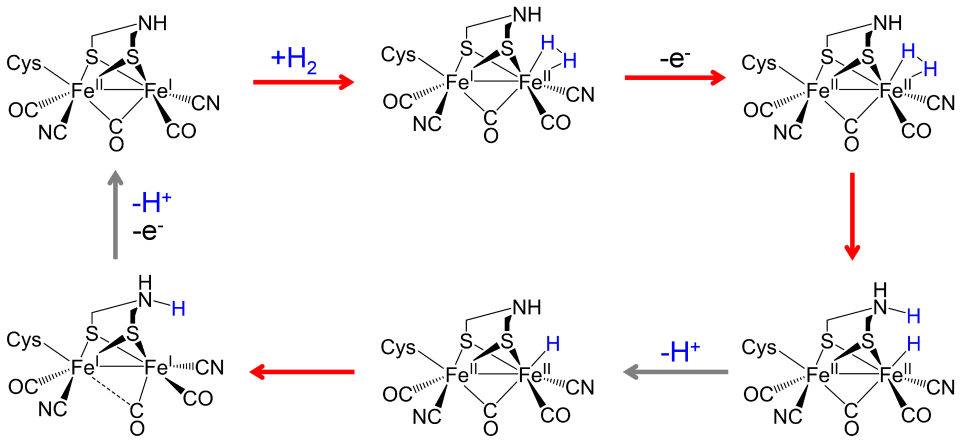

Figure 3.6.1: Schematic representation of the catalytic mechanism of H_2 oxidation in [FeFe]-hydrogenases. The reaction steps investigated in this study are in red.

3.6.2 Computational details

The standard absolute one-electron redox potentials (E°) have been computed following equation 2.4.1. An analysis on redox properties of a selected set of FeIIFeI models (Table 3.6.1) revealed that the inclusion of thermodynamic contributions (which were obtained setting temperature and pressure to 298.15 K and 1 bar, respectively) does not affect significantly E° values. Thus, in the present case, the E° values have been calculated by simply substituting ΔG_{solv} with ΔE_{solv} in equation 3.1.1. Analogously, also the energetic of the other investigated catalytic steps have been evaluated by means of pure electronic E_{SCF} energies. First of all, the energy changes observed upon intramolecular proton transfers and oxidation process (as above shown) are not predicted to be significantly altered by the addition of thermodynamic corrections. The only step in which their inclusion would be beneficial is H_2 binding, because of the loss of entropy associated with its associative nature. However, the approximation of neglecting the evaluation of entropic costs of the various catalytic steps is legitimate by the interest of the present work, which aims to highlight exclusively energetic trends observable upon ligand variations. Since the type of reaction involving each model investigated is exactly the same (at each step of the cycle), it is fairly expected that inclusion of entropic and thermal contributions would only entail a rigid shift of the same energy trend already observed considering pure (i.e., non-corrected) electronic energies. Effects due to the solvent, both for active site and biomimetic complexes, have been modeled using the COSMO approach[284, 285]. Geometry optimization of active site models have been carried out in a vacuum ($\varepsilon = 1$), and by considering a polarizable continuum medium characterized by $\varepsilon =$

4 (a value commonly used to reproduce the effect of a protein environment), whereas the solvent modeled in the calculations of biomimetic complexes is CH_2Cl_2 ($\varepsilon = 8.93$). The Broken Symmetry (BS) approximation[275], as introduced by Noodleman, has been used to theoretically treat spin-coupled systems (namely $\mathbf{H_{ox}}$**-full**$^{3-}$, $\mathbf{H_{ox}^{3-}}$, $\mathbf{10}^{2+}$ and $\mathbf{11}^{2+}$(see next section)). This approach allows to model antiferromagnetic interactions in the DFT single-determinant framework.

While in the optimized structures of the H_2 adducts the configuration of the NH group is always equatorial, in the reactant (i. e. before H_2 binding) both equatorial and axial configurations are possible. Since the configuration of the NH bond (equatorial or axial) of adt into the protein is unknown and expected to be affected by the protein environment (which has not been included in our models), for the sake of consistency we have considered only reactant structures featuring equatorial configuration of the NH group. To carry out an unbiased comparison, also when dealing with biomimetic complexes only isomers featuring equatorial configuration of the NH bond have been considered.

	$\mathbf{1}^+$	$\mathbf{2}^+$	$\mathbf{6}^+$	$\mathbf{9}^+$
E° = **-ΔE**$_{solv}$/nF	-5.99	-5.30	-4.52	-4.99
E° = **-ΔG**$_{solv}$/nF	-6.06	-5.36	-4.51	-5.07

Table 3.6.1: One-electron oxidation potentials of the couples $\mathbf{1}^{+/0}$, $\mathbf{2}^{+/0}$, $\mathbf{6}^{+/0}$ and $\mathbf{9}^{+/0}$ calculated for two different levels of theory setting $\varepsilon = 8.93$ (CH_2Cl_2).

3.6.3 Results

3.6.3.1 H_2 binding to the H_{ox} form of the H-cluster and to corresponding $Fe^{II}Fe^{I}$ biomimetic models

We have initially studied H_2 binding to a series of models of the H-cluster in the H_{ox} redox state ($2Fe^{II}2Fe^{III}$-$Fe^{I}Fe^{II}$). Model $\mathbf{H_{ox}}$**-full**$^{3-}$ differs from the real H-cluster only because the cysteine side chain bridging the $[4Fe4S]_H$ and the $[2Fe]_H$ subclusters is replaced by a methylthiolate group (Figure 3.6.2). Since in the enzyme the two CN^- groups of the H-cluster are involved in hydrogen bonding interaction with the peptide chain, two formamide molecules forming hydrogen bonds with the CN^- ligands have been also included in the $\mathbf{H_{ox}}$**-full**$^{3-}$ model. The slightly simpler model $\mathbf{H_{ox}^{3-}}$ differs from $\mathbf{H_{ox}}$**-full**$^{3-}$ only for the absence of the formamide molecules. In more simple models, the $[4Fe4S]_H$ subcluster is replaced by a H^+ (model $\mathbf{H_{ox}}$**-SHCH**$_3^-$) or is not present (model $\mathbf{H_{ox}}$**-SCH**$_3^{2-}$). Also a variant of the $\mathbf{H_{ox}}$**-SCH**$_3^{2-}$ model containing propanedithiolate (pdt) instead of adt has been studied (model $\mathbf{H_{ox}}$**(pdt)-SCH**$_3^{2-}$), to explicitly evaluate the effect on H_2 binding energy of the amine group in the dithiolate chelating ligand. The effect of protonation of the CN^- ligand coordinated to Fe_d was also evaluated (model $\mathbf{H_{ox}}$**-CNdH**$^-$), since in the enzyme such CN^- ligand interacts with a NH group of the peptide backbone but also with the NH_3^- group of a conserved lysine residue.[43]

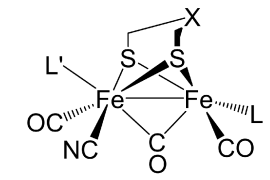

H_{ox}-full^{3-} : X = NH, L = SCH_3-4Fe4S, L' = CN^-
H_{ox}^{3-} : X = NH, L = SCH_3-4Fe4S, L' = CN^-
H_{ox}-SCH_3^{2-} : X = NH, L = SCH_3^-, L' = CN^-
H_{ox}(pdt)-SCH_3^{2-} : X = CH_2, L = SCH_3^-, L' = CN^-
H_{ox}-$SHCH_3^-$: X = NH, L = $SHCH_3$, L' = CN^-
H_{ox}-CNdH$^-$: X = NH, L = SCH_3^-, L' = CNH

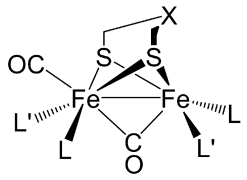

1$^+$: X = NH, L = L' = CO
1(pdt)$^+$: X = CH_2, L = L' = CO
2$^+$: X = NH, L = CO, L' = PMe_3
2(pdt)$^+$: X = CH_2, L = CO, L' = PMe_3
3$^+$: X = NH, L = L' = $P(OMe)_3$
4$^+$: X = NH, L = L' = PF_3
4(pdt)$^+$: X = CH_2, L = L' = PF_3
5$^+$: X = NH , L = L' = PH_3
6$^+$: X = NH, L = L' = PMe_3
6(pdt)$^+$: X = CH_2, L = L' = PMe_3
7$^+$: X = NH, L = L' = PEt_3

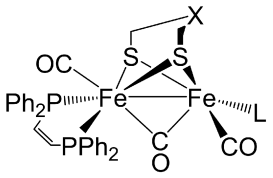

8$^+$: X = NH, L = CO
8(pdt)$^+$: X = CH_2, L = CO
9$^+$: X = NH, L = PMe_3
10$^+$: X = NH, L = Cp*Fe($C_5Me_4CH_2PMe_3$)
11$^+$: X = N(Bn), L = Cp*Fe($C_5Me_4CH_2PMe_3$)

Figure 3.6.2: Schematic structure of the [FeFe]-hydrogenase (top) and $Fe^{II}Fe^{I}$ biomimetic (bottom) models that have been investigated

In all models, H_2 binds in a non-classical way, and the H-H bond elongation is generally proportional to the binding affinity (Table 3.6.2). The BP86 computed binding energy of H_2 to the Fe_d atom of the $\mathbf{H_{ox}}$**-full**$^{3-}$ model is -2.3 kcal/mol (considering a dielectric constant = 1), whereas H_2 binding to the simplified models $\mathbf{H_{ox}^{3-}}$, $\mathbf{H_{ox}}$**-SHCH**$_3^-$ and $\mathbf{H_{ox}}$**-SCH**$_3^{2-}$ is endergonic (+0.9, +1.5 and +3.5 kcal/mol, respectively; Table 3.6.2). When considering $\mathbf{H_{ox}}$**-CNdH**$^-$, H_2 binding energy becomes even more unfavorable (+7.9 kcal/mol). The comparison of H_2 binding energies in $\mathbf{H_{ox}}$**-SCH**$_3^{2-}$ and $\mathbf{H_{ox}}$**(pdt)-SCH**$_3^{2-}$ reveals that the presence of the amino group in the chelating dithiolate ligand favorably contributes to H_2 binding (by about 2.6 kcal/mol; Table 3.6.2). Changing the dielectric constant from 1 to 4 (a value commonly used to model a generic and low polar protein environment) generally leads to slightly more favorable binding energies (by about 1 kcal/mol; Table 3.6.2).

To test the effect of the chosen functional on the reaction energies, we computed also H_2 binding energies using the B3LYP functional. Reassuringly, results are similar, even though H_2 binding is generally predicted to be slightly more endergonic(Table 3.6.2). The larger affinity of H_2 for $\mathbf{H_{ox}}$**-full**$^{3-}$ and $\mathbf{H_{ox}^{3-}}$, in comparison to diiron models of the active site, reveals that the presence of the 4Fe4S cluster affects substrate binding. In fact, binding of H_2 to all investigated models is concomitant with delocalization of the unpaired electron from Fe_d to Fe_p. In addition, in $\mathbf{H_{ox}}$**-full**$^{3-}$ and $\mathbf{H_{ox}^{3-}}$ partial electron transfer from the $[2Fe]_H$ to the 4Fe4S cluster (about 0.10 charge units) is also observed (see Figure 3.6.3). The binding energy difference between $\mathbf{H_{ox}}$**-full**$^{3-}$ and $\mathbf{H_{ox}^{3-}}$ reveals that also the H-cluster environment can affect substrate binding. In particular, the formation of H-bonds between the CN^- ligands and the environment decreases the electron density on the $[2Fe]_H$ subcluster, favoring H_2 binding.

As anticipated in section 1.4.1 (in the "H_2 Oxidation and bidiretional catalysis" subsection), the inactivity (or low activity) of H_{ox} models towards dihydrogen oxidation has been postulated to be associated with a low affinity for H_2, suggesting that the initial binding step could be the RDS of the entire catalysis. Thus, H_2 binding energies for a very extended series of biomimetic $Fe^{I}Fe^{II}$ complexes have been computed, in order to highlight in detail which are the relationships between complexes structure and H_2 affinity. Some of them, can be actually considered "virtual" H_{ox} models, since they do not have been isolated in their mixed-valence form. The considered mimics differ for the characteristics of the ligands coordinated to each Fe atom (complexes $\mathbf{1}^+$ to $\mathbf{9}^+$; Figure 3.6.2), and for the nature of the dithiolate chelating ligand (pdt instead of adt in complexes $\mathbf{1(pdt)}^+$, $\mathbf{2(pdt)}^+$, $\mathbf{4(pdt)}^+$, $\mathbf{6(pdt)}^+$, $\mathbf{8(pdt)}^+$). Complexes $\mathbf{1}^+$ to $\mathbf{7}^+$ are symmetric species in which the two Fe atoms are coordinated by the same set of ligands, whereas complexes $\mathbf{8}^+$ and $\mathbf{9}^+$ feature different ligands on the Fe atoms. In addition, we have studied also two variants of a recently reported synthetic complex[205], in which a decamethylferrocene derivative was linked to a diiron cluster ($[Fe_2(CO)_3(dppv)(Cp^*Fe(C_5Me_4CH_2PEt_2))(\mu\text{-adt})]^{2+}$; where $Cp^* = C_5Me_5$, referred to as model $\mathbf{10}^{2+}$, and , $([Fe_2(CO)_3(dppv)(Cp^*Fe(C_5Me_4CH_2PEt_2))(\mu\text{-adt}^{Bn})]^{2+}$; referred to as model $\mathbf{11}^{2+}$).

BP86 computed H_2 binding energies for the 'symmetric' diiron complexes $\mathbf{1}^+$-$\mathbf{7}^+$ (Table 3.6.2) range from exergonic (–3.2 kcal/mol; complex $\mathbf{1}^+$) to strongly endothermic (+8.3 kcal/mol; complex $\mathbf{7}^+$), and are inversely correlated to the number of phosphine ligands installed in the complexes, i.e. the more electron donor are the ligands, the lower is the affinity for H_2. Analogous results are obtained using the B3LYP functional, even though reaction energies are systematically shifted to more endothermic values (on average by about 4 kcal/mol; Table 3.6.2). The comparative analysis reveals that also in biomimetic complexes the NH group of adt contributes to H_2 binding, as deduced by the comparison of binding energies in corresponding adt- and pdt-containing complexes (Table 3.6.2). In addition, in most active site and biomimetic models, the H-H and NH....H_2 distances are inversely correlated (Table 3.6.2), indicating that the interaction between the N atom of adt and one of the two H atom of the coordinated H_2 molecule results in activation of the latter. Remarkably, and apparently in contradiction with the conclusions derived from the analysis of the symmetric complexes $\mathbf{1}^+$-$\mathbf{7}^+$ (few phosphine ligands correspond to high H_2 affinity, and viceversa), when considering asymmetric complexes ($\mathbf{8}^+$, $\mathbf{9}^+$, $\mathbf{10}^{2+}$ and $\mathbf{11}^{2+}$) the lowest energy H_2 adducts correspond to isomers in which the substrate binds to the Fe atom coordinated by the largest number of phosphine ligands. Indeed, when considering asymmetric complexes, two competing effects must be taken into account: on the one hand H_2 preferentially binds to the iron atom coordinated by the lowest number of phosphine ligands but, on the other hand, in the lowest energy reactant isomer the five-coordinated atom is bound by the highest number of phosphine ligands (see Figure 3.6.4). It turns out that the energy difference between the five-coordinated reactant isomers is so large that H_2 binds to the Fe atoms featuring the largest number of phosphine ligands.

When considering the biomimetic model $\mathbf{10}^{2+}$, which differs from $\mathbf{9}^+$ for the presence of the decamethylferrocene redox-active ligand, H_2 binding (in CH_2Cl_2) is computed to be slightly exergonic (-0.7 kcal/mol), and about 6 kcal/mol more favorable than in $\mathbf{9}^+$, indicating that the

presence of the ferrocenium moiety significantly affect H_2 binding. In $\mathbf{11}^{2+}$, which differs from $\mathbf{10}^{2+}$ because in the former the N atom of adt is linked to a benzyl group, and therefore is more basic than in adt, H_2 binding is even more favored (-3.3 kcal/mol). In fact, similarly to the scenario depicted investigating the active site models $\mathbf{H_{ox}\text{-}full}^{3-}$ and $\mathbf{H}_{ox}^{3-}$, H_2 binding to $\mathbf{10}^{2+}$ and $\mathbf{11}^{2+}$not only leads to delocalization of the unpaired electron from Fe_d to Fe_p (observed in all $Fe^{I}Fe^{II}$ complexes upon H_2 binding), but is also concomitant with partial electron transfer from the diiron moiety to the ferrocenium ligand. Therefore, in $\mathbf{10}^{2+}$ and $\mathbf{11}^{2+}$ the Fe_d atom is less electron-rich than in the corresponding models that do not feature a redox-active ligand, and consequently the H_2-Fe_d bond is stronger. To better characterize the chemical nature of the Fe-H_2 bond in the enzyme cofactor and in biomimetic models, we have carried out a Natural Bond Orbital (NBO) analysis of the H_2 adducts. As generally accepted, two factors can contribute to H_2 binding to a transition metal: donation from the H-H bond to an empty orbital on the metal ion, and back-donation from the metal ion to the antibonding σ^* orbital of H_2. NBO analysis reveals that the occupation of the H_2 σ-bond in the different complexes is significantly lower than 2 (from 1.47 to 1.62; not shown), indicating significant donation from H_2 to the metal ion. On the other hand, the H_2 σ^* populations are always negligible. In relation to the catalytic properties, it should be noted that a too high affinity of the catalyst for H_2would be detrimental, because the formation of very stable intermediate species necessarily implies large energy barriers in the next catalytic steps. On the other hand, a low affinity for the substrate, as computed in $\mathbf{6}^{+}$, $\mathbf{7}^{+}$, $\mathbf{8}^{+}$ and $\mathbf{9}^{+}$, implies that the catalytic process could take place efficiently only under high H_2 pressure. In line with these remarks, in the most complete enzymatic cofactor model ($\mathbf{H_{ox}\text{-}full}^{3-}$) the computed H_2 binding reaction energy is close to 0 kcal/mol. When considering biomimetic complexes, reaction energies close to 0 kcal/mol are obtained only for $\mathbf{10}^{2+}$ and $\mathbf{11}^{2+}$, and to a lesser extent for complexes $\mathbf{1}^{+}$and $\mathbf{4}^{+}$ (which however contain π-acceptor or electron-withdrawing groups that are expected to impact negatively on their stability and redox properties; vide infra). When comparing the enzyme cofactor and biomimetic models, it is also remarkable that the large negative charge of the H-cluster (-3), compared to biomimetic complexes (+1), does not impair H_2 binding. The apparently contradictory observation that H_2 binds via -donation to a highly anionic complex can be rationalized considering that only the five-coordinated iron atom of the metal cofactor must be sufficiently electron poor to allow H_2 binding. In fact, a relatively electron-poor five-coordinated Fe ion can be present also in highly anionic species (such as the H-cluster) when suitable electron acceptor ligands (such as CO, CN^- and 4Fe4S) are coordinated to the Fe ions.

Compound	ΔE (kcal/mol) BP86		ΔE (kcal/mol) B3LYP		d H-H (Å)	d NH···H (CH···H) (Å)
	ε = 1	ε = 4	ε = 1	ε = 4		
$\mathbf{H_{ox}}$**-full**$^{3-}$	-2.26	-1.70	1.50	1.67	0.825	2.131
$\mathbf{H_{ox}^{3-}}$	0.87	0.89	3.04	3.62	0.822	2.130
$\mathbf{H_{ox}}$**-SHCH**$_3^-$	1.46	0.42	3.80	2.54	0.816	2.192
$\mathbf{H_{ox}}$**-SCH**$_3^{2-}$	3.46	2.69	5.76	4.96	0.808	2.284
$\mathbf{H_{ox}(pdt)}$**-SCH**$_3^{2-}$	6.05	5.13	8.09	7.25	0.815	2.890
$\mathbf{H_{ox}}$**-CNdH**$^-$	7.93	9.03	5.93	6.08	0.814	2.213
	ε = 1	ε = 8.93	ε = 1	ε = 8.93		
1$^+$	-3.24	-4.73	2.10	0.74	0.839	1.842
2$^+$	0.95	1.66	4.33	4.95	0.819	1.980
3$^+$	-0.21	0.66	4.20	5.47	0.839	2.011
4$^+$	0.35	-0.98	4.49	2.39	0.848	1.833
5$^+$	1.81	2.42	6.23	6.44	0.819	2.010
6$^+$	6.16	6.54	10.0	10.6	0.814	2.049
7$^+$	8.25	8.73	12.5	13.4	0.816	2.038
8$^+$	4.46	3.17	5.63	4.40	0.849	1.822
9$^+$	6.89	6.87	11.6	10.9	0.826	1.977
10$^+$	2.64	-0.74	-1.16	-0.16	0.866	1.751
11$^+$	0.15	-3.26	-2.20	-0.81	0.857	1.759
1(pdt)$^+$	2.83	2.02	6.33	5.83	0.810	2.921
2(pdt)$^+$	4.87	4.65	8.04	8.22	0.797	2.823
4(pdt)$^+$	4.58	3.51	8.06	6.20	0.801	2.980
6(pdt)$^+$	7.50	6.98	10.4	10.6	0.800	3.094
8(pdt)$^+$	7.42	6.47	9.82	9.57	0.812	2.954

Table 3.6.2: H_2 binding energies (kcal/mol), computed with the BP86 and B3LYP functionals, and selected geometry parameters (from BP86 calculations) for models of the [FeFe]-hydrogenase active site and for $Fe^{II}Fe^{I}$ biomimetic models.

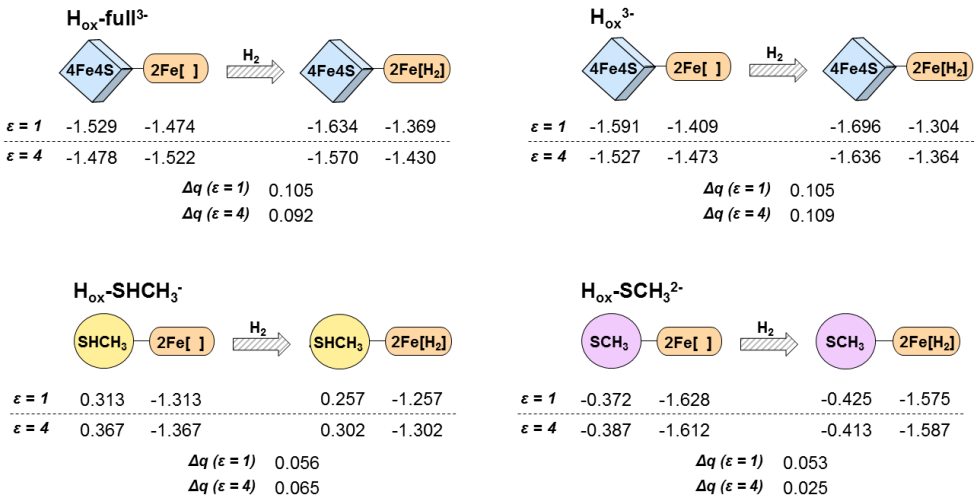

Figure 3.6.3: Computed NBO charge transfers from the 2Fe unit to 4Fe4S, SCH_3^- or $SHCH_3$ groups (according to the considered H-cluster model).

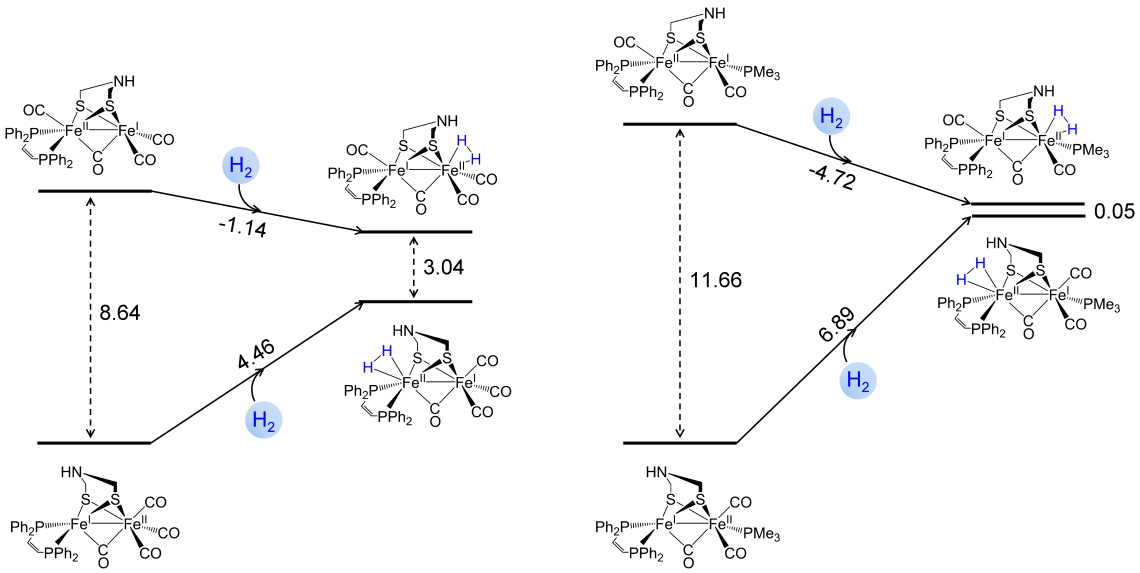

Figure 3.6.4: Energetics of H_2 binding to the asymmetric complexes $\mathbf{8}^+$ and $\mathbf{9}^+$, considering possible substrate binding to different isomers of the reactant.

3.6.3.2 Heterolytic cleavage of H_2 on H-cluster and biomimetic models

Heterolytic cleveage of H_2 can, at least in principle, occur either on Fe^IFe^{II} or $Fe^{II}Fe^{II}$ forms, and is expected to become energetically more favored as the overall oxidation state of the binuclear cluster increases.[4] Indeed, whereas heterolytic cleavage on Fe^IFe^{II} species is always strongly en-

dergonic when considering H-cluster models, in most of the $Fe^{I}Fe^{II}$ biomimetic complexes studied in this work H_2 cleavage would be already exergonic at the $Fe^{I}Fe^{II}$ redox level (Table 3.6.3). More specifically, heterolytic cleavage at the $Fe^{I}Fe^{II}$ redox state is strongly exergonic for the hexacarbonyl derivative $\mathbf{1}^{+}$, and becomes progressively less exergonic as COs are replaced by electron-donor phosphine ligands (as a note: the set of biomimic compounds considered hereafter has been reduced. In particular we selected the series of "homologous" complexes of type $Fe_2(CO)_{6-x}((PMe)_3)_x(\mu\text{-adt})$ with x = 0, 2, 4, namely complexes $\mathbf{1}^{+}$, $\mathbf{2}^{+}$ and $\mathbf{6}^{+}$. In addition, also the asymmetric synthetic complex $\mathbf{9}^{+}$ has been taken into account). The dielectric constant of the solvent strongly affects the energetics of the heterolytic cleavage, which becomes significantly more favored when increasing the value of ε. Such an observation can be rationalized considering the zwitterionic nature of the product, which features a protonated amine and a hydride coordinated to the metal atom. The computational investigation of H_2 reactivity on $Fe^{II}Fe^{II}$ model complexes (from $\mathbf{1\text{-}H_2^{2+}}$ to $\mathbf{9\text{-}H_2^{2+}}$) reveals that in all cases except $\mathbf{6\text{-}H_2^{2+}}$ (at B3LYP level) the H_2 adducts do not correspond to an energy minimum structure, and spontaneously evolve during optimization to species in which the H_2 molecule is heterolytically cleaved. In other words, when the iron ligands are not strong electron donor, H_2 cleavage is spontaneous and barrierless once the diiron complex is oxidized to $Fe^{II}Fe^{II}$. Also when considering diiron models of the H-cluster, oxidation from $Fe^{I}Fe^{II}$ to $Fe^{II}Fe^{II}$ favors H_2 heterolitic cleavage (models $\mathbf{H_{ox}\text{-}SCH_3{-}H_2^{-}}$ and $\mathbf{H_{ox}\text{-}SHCH_3{-}H_2}$; Table 3.6.3). However, in this case, both the H_2 adduct and the corresponding species in which H_2 is cleaved correspond to energy minimum structures. The reason for the different reactivity of Fe I Fe II biomimetic and H-cluster models can be revealed through a Born-Haber cycle in which the H_2 heterolytic cleavage reaction is decomposed into three steps (see Table 3.6.5): detachment of the H_2 molecule from diiron species, followed by proton binding to the amine group of adt and hydride binding to the iron atom. For the sake of brevity, we present only the comparison between one active site model ($\mathbf{H_{ox}\text{-}SHCH_3{-}H_2^{-}}$) and only one of the $Fe^{I}Fe^{II}$ biomimetic compounds ($\mathbf{2\text{-}H_2^{+}}$) under investigation. A comparison extended to the other investigated complexes (not shown) shows that the general outcome is substantially unchanged. Energetics of H_2 detachment (Table 3.6.5) is practically the same in enzyme vs biomimetic models (about 1 kcal/mol difference falls below the DFT precision limit and also the chemical accuracy). Proton binding is more favored in the H-cluster model, which is expectable due to its larger negative charge. However, the effects of the overall charge are much more evident when considering the energetics of the H^{-} binding step, which is strongly disfavored in diiron H-cluster models, when compared to the biomimetic model.

We have subsequently analyzed the energetics of H_2 heterolytic cleavage in enzyme and biomimetic models containing redox ligands (a 4Fe4S cluster and a ferrocenium moiety in $\mathbf{H_{ox}\text{-}full\text{-}H_2^{2-/3-}}$ and $\mathbf{10/11\text{-}H_2^{2+/+}}$, respectively). The cleavage results strongly affected by the presence of the redox-active ligand. Both cases in which the intramolecular electron transfer can occur concomitantly or not with H_2 heterolytic cleavage have been considered. Interestingly, a comparison of results obtained for $\mathbf{Fe^{I}Fe^{II}(NH)\text{-}H_2 \rightarrow Fe^{I}Fe^{II}(NH_2^{+})\text{-}H^{-}}$ vs $\mathbf{Redox\text{-}Fe^{I}Fe^{II}\text{-}H_2 \rightarrow Redox\text{-}Fe^{I}Fe^{II}\text{-}(H^{+},\ H^{-})}$ suggests that the presence of a redox cofactor is able to tune the energetic of H_2 heterolytic cleavage towards thermoneutrality. The high discrepancies between BP86 and

B3LYP computed ΔEs for the process **Redox-Fe^{I}Fe^{II}-H$_2$** → **Redox-Fe^{II}Fe^{II}-(H$^+$, H$^-$)** (Table 3.6.4) (considering **10-H$_2^{2+}$** and **11-H$_2^{2+}$**) arises from the fact that, actually, closed shell species of type **Redox-Fe^{II}Fe^{II}-(H$^+$, H$^-$)** are much higher in energy than those related to **Redox-Fe^{I}Fe^{II}-(H$^+$, H$^-$)** ones only at B3LYP level (while they are the most stable ones at BP86 level). These apparently unconsistent results can be rationalized on the basis of the different nature of the two density functionals. Indeed, it is well known that, (unlike BP86), the hybrid B3LYP functional tends to stabilize high spin states, because of the presence of 20% of non-local HF exchange contribution. However, since experiments detected the formation of a diamagnetic species concomitantly with or after the H_2 cleavage, we can conclude that B3LYP is not suited to properly describe the redox behavior of this class of compounds.

	BP86		B3LYP	
	ε=1	ε=8.93	ε=1	ε=8.93
Compound	**Fe^{I}Fe^{II}(NH)-H$_2$** → **Fe^{I}Fe^{II}(NH$_2^+$)-H$^-$**			
1-H$_2^+$/1-H$_2^{2+}$	-4.60	-12.71	-15.47	-22.40
2-H$_2^+$/2-H$_2^{2+}$	3.34	-3.70	-5.95	-12.51
6-H$_2^+$/6-H$_2^{2+}$	1.54	-3.38	-4.78	-8.79
9-H$_2^+$/9-H$_2^{2+}$	1.69	-3.67	-8.83	-13.4
H$_{ox}$-SCH$_3$−H$_2^{2-}$ / H$_{ox}$-SCH$_3$−H$_2^-$	15.90	7.42	18.79	10.08
H$_{ox}$-SHCH$_3$−H$_2^-$ / H$_{ox}$-SHCH$_3$−H$_2$	13.64	4.66	14.97	6.32
	Fe^{II}Fe^{II}(NH)-H$_2$ → **Fe^{II}Fe^{II}(NH$_2^+$)-H$^-$**			
1-H$_2^+$/1-H$_2^{2+}$	-	-	-	-
2-H$_2^+$/2-H$_2^{2+}$	-	-	-	-
6-H$_2^+$/6-H$_2^{2+}$	-	-	-1.81	-5.00
9-H$_2^+$/9-H$_2^{2+}$	-	-	-	-
H$_{ox}$-SCH$_3$−H$_2^{2-}$ / H$_{ox}$-SCH$_3$−H$_2^-$	4.78	-3.39	5.02	-3.47
H$_{ox}$-SHCH$_3$−H$_2^-$ / H$_{ox}$-SHCH$_3$−H$_2$	-0.61	-7.71	-0.29	-9.08

Table 3.6.3: Reaction energies computed for the heterolytic cleavage of H_2 on biomimetic and H-cluster models, considering both $Fe^{I}Fe^{II}$ and $Fe^{II}Fe^{II}$ redox states.

	Redox-$Fe^{I}Fe^{II}$-H_2 → Redox-$Fe^{I}Fe^{II}$-(H^+, H^-)			
Compound	Cleavage without intramolecular electron transfer			
	BP86		B3LYP	
10-H_2^{2+}	0.64 (ε = 1)	-0.72 (ε = 8.93)	1.03 (ε = 1)	-3.68 (ε = 8.93)
11-H_2^{2+}	-1.28 (ε = 1)	0.61 (ε = 8.93)	-2.63 (ε = 1)	-3.97 (ε = 8.93)
H_{ox}-full-H_2^{3-}	9.11 (ε = 1)	3.01 (ε = 4)	9.82 (ε = 1)	4.01 (ε = 4)
	Redox-$Fe^{I}Fe^{II}$-H_2 → Redox-$Fe^{II}Fe^{II}$-(H^+, H^-)			
	Cleavage concomitant to intramolecular electron transfer			
10-H_2^{2+}	-1.24 (ε = 1)	-8.67 (ε = 8.93)	20.96 (ε = 1)	4.43 (ε = 8.93)
11-H_2^{2+}	-6.07 (ε = 1)	-6.63 (ε = 8.93)	13.07 (ε = 1)	5.75 (ε = 8.93)
H_{ox}-full-H_2^{3-}	- (ε = 1)	- (ε = 4)	- (ε = 1)	- (ε = 4)
	Redox-$Fe^{II}Fe^{II}$-H_2 → Redox-$Fe^{II}Fe^{II}$-(H^+, H^-)			
H_{ox}-full-H_2^{2-}	2.46 (ε = 1)	-4.76 (ε = 4)	1.21 (ε = 1)	-5.28 (ε = 4)

Table 3.6.4: Reaction energies computed for the heterolytic cleavage of H_2 on biomimetic and H-cluster models featuring an intramolecular redox cofactor, considering both $Fe^{I}Fe^{II}$ and $Fe^{II}Fe^{II}$ redox states.

3.6.3.3 Effect of H_2 binding on the redox properties of the H-cluster and biomimetic models

Another key step of the H_2 $\rightarrow 2H^+/2e^-$ process as catalyzed by the diiron core of the [FeFe]-hydrogenase is the one-electron oxidation of the $Fe^{I}Fe^{II}$-H_2 adduct, which, as discussed in the previous section, could precede, be concomitant, or follow the heterolytic cleavage of H_2 . To evaluate the effect of H_2 binding on the redox properties of the diiron moiety of the catalysts, we have computed and analyzed the oxidation potentials of a subset of biomimetic models (**1**$^+$, **2**$^+$, **6**$^+$ and **9**$^+$) before and after H_2 binding . It must be underlined that the main purpose of these calculations is to investigate possible variations of redox potential of the various diiron species under study, upon H_2 binding. Indeed, while the comparison of computed absolute redox potentials for complexes characterized by different overall charge and structure is very challenging, due to the necessity to accurately describe short- and long-range environmental effects (in order to take properly into account the effects of counterions and solvent molecules), the comparison of redox potentials for complexes featuring analogous chemical structure and same overall charge is much less affected by the simplified description of the system. That implies that a possible

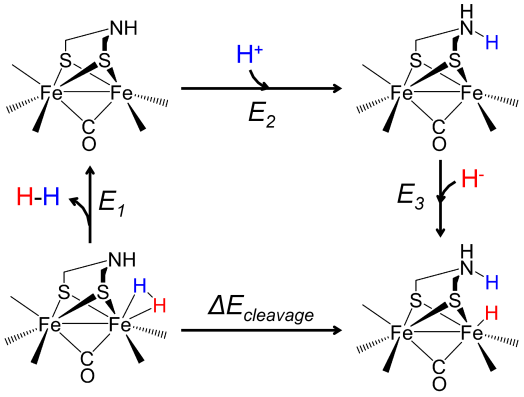

Compound	$\Delta E_{cleavage}$	E_1	E_2	E_3
$\mathbf{H}_{ox}$**-SCH**$_3^{2-}$ ($\varepsilon = 4$)	7.42	-2.69	-315.04	-413.88
$\mathbf{2}^+$ ($\varepsilon = 8.93$)	-3.70	-1.66	-254.22	-486.85
	$\Delta\Delta E_{cleavage}$ = 11.12	ΔE_1 = -1.03	ΔE_2 = -60.82	ΔE_3 = 673.97

Table 3.6.5: Born-Haber cycle (top) and relative energetics (in kcal/mol, bottom) associated to H_2 heterolytic cleavage.

and systematic inaccuracy (arising from the theory level) affecting the exact absolute value of the redox potential should not affect the validity of the comparative analysis. This last assertion is even more justified, in the light of no necessity at this stage to match computational values vs exp redox potentials. For such reason, DFT results are presented in the following as absolute oxidation potentials, which means that they have not been referenced to any other specific redox couple.

It is well known that H_2 binding is able to trigger the subsequent oxidation of the H-cluster. The oxidative behavior of active site models and biomimics is quite different. In general, the one-electron oxidation of active site models can yield two isomers, that only differ for the presence of a N_{adt}-Fe_dbond in one of the two minima. Two isomers have been also characterized for their corresponding oxidized $Fe^{II}Fe^{II}$-H_2 adducts, one with an elongated dihydrogen molecule coordinated to Fed, and the other in which H_2 has undergone heterolytic cleavage, yielding a hydride complex characterized by protonation of N_{adt}. A schematic illustration of these oxidative processes and chemical equilibria between oxidation products is presented in Figure 3.6.5, where the simplest active site model $\mathbf{H}_{ox}$**-SCH**$_3^{2-}$ is taken into account. Here, the labels "**a**" and "**b**" have been adopted to distinguish the two different structures arising from the one-electron oxidation of both model and its H_2-adduct. One electron oxidation of $\mathbf{H}_{ox}$**-SCH**$_3^{2-}$ can yield two isomers ($\mathbf{aH}_{ox}$**-SCH**$_3^-$ and $\mathbf{bH}_{ox}$**-SCH**$_3^-$), which differ for the presence of a N_{adt}-Fe_d bond in $\mathbf{bH}_{ox}$**-SCH**$_3^-$ (Figure 3.6.5). $\mathbf{aH}_{ox}$**-SCH**$_3^-$ is 2.6 kcal/mol lower in energy than $\mathbf{bH}_{ox}$**-SCH**$_3^-$. Two isomers have been characterized also for the corresponding oxidized $Fe^{II}Fe^{II}$-H_2 adduct $\mathbf{H}_{ox}$**-SCH**$_3$**−H**$_2^-$; one with an elongated dihydrogen molecule coordinated to Fe_d ($\mathbf{a(H}_{ox}$**-SCH**$_3$**−H**$_2$**)**$^-$), and the other, (3.4

kcal/mol lower in energy), in which H_2 has undergone heterolytic cleavage ($\mathbf{b(H_{ox}\text{-}SCH_3{-}H_2)^-}$, , affording a hydride species characterized by protonation of N_{adt} (Figure 3.6.5). The computed energy barrier for the transformation of $\mathbf{a(H_{ox}\text{-}SCH_3{-}H_2)^-}$ in $\mathbf{b(H_{ox}\text{-}SCH_3{-}H_2)^-}$ is lower than 1 kcal/mol, suggesting that at room temperature $\mathbf{b(H_{ox}\text{-}SCH_3{-}H_2)^-}$would be formed directly after H_2 binding and oxidation. BP86 computed absolute oxidation potentials ($E_{ox,abs}$) for $\mathbf{H_{ox}\text{-}SCH_3^{2-}}$ and $\mathbf{H_{ox}\text{-}SCH_3{-}H_2^{2-}}$ and their differences ($\Delta E_{ox,abs}$) are summarized in Figure 3.6.5. $E_{ox,abs}$ values are in the range -2.58/-2.14 V, depending on the coordination environment of the Fe_d atom. More relevantly, comparison of the two thermodynamically more favored oxidation pathways (from $\mathbf{H_{ox}\text{-}SCH_3^{2-}}$ to $\mathbf{aH_{ox}\text{-}SCH_3^-}$ and from $\mathbf{H_{ox}\text{-}SCH_3{-}H_2^{2-}}$ to $\mathbf{b(H_{ox}\text{-}SCH_3{-}H_2)^-}$) reveals that H_2 binding increases oxidation potential by about 330 mV. A very similar behavior has been observed also for the other considered active site models (data not shown).

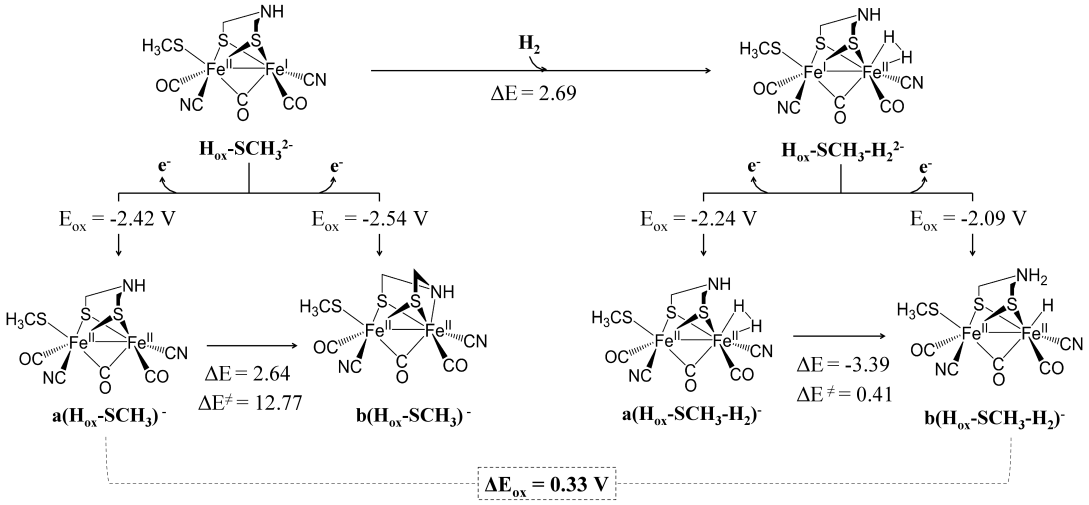

Figure 3.6.5: BP86 computed absolute oxidation potentials (Eox (V), red values) for $\mathbf{H_{ox}\text{-}SCH_3^{2-}}$ and for its H_2 adduct (energy values have been computed setting $\varepsilon = 4$, which is a value commonly used to simply mimic the presence of the protein environment). E and E≠ values are in kcal/mol.

Computed $E_{ox,abs}$ values for the biomimetic models $\mathbf{1}^+$, $\mathbf{2}^+$, $\mathbf{6}^+$ and $\mathbf{9}^+$, and for the corresponding H_2-adducts $\mathbf{1\text{-}H_2^+}$, $\mathbf{2\text{-}H_2^+}$, $\mathbf{6\text{-}H_2^+}$ and $\mathbf{9\text{-}H_2^+}$, are shown in Table 3.6.6. Focusing on biomimetic compounds, their oxidation always yields species featuring a N_{adt}-Fe_dbond, while oxidation of their H_2 adducts is concerted with H_2 heterolytic cleavage. Only when considering $\mathbf{6\text{-}H_2^{2+}}$ (with B3LYP), that is the more electron-rich model of the set, both isomers featuring cleaved and uncleaved H_2 correspond to energy minima (differing by less than 2 kcal/mol). Indeed, previously we have shown that when considering this series of biomimetic complexes H_2 cleavage is already exergonic at the Fe^IFe^{II} redox level. $E_{ox,abs}$ values for biomimetic complexes are much more negative than for active site models, as expected considering that $\mathbf{1}^+$, $\mathbf{2}^+$, $\mathbf{6}^+$ and $\mathbf{9}^+$, as well as their H_2 adducts, are cationic species, whereas the corresponding models of the enzyme cofactor are anionic. As expected, oxidation becomes easier and easier as a function of the number of

phosphine ligands, with absolute redox potentials ranging from -6.36 V in $\mathbf{1}^+$ to -4.52 V in $\mathbf{6}^+$. The H_2 binding makes all biomimetic complexes more reducing (with $\Delta E_{ox,abs}$ (i.e., the redox potential shift) in the range 640-1050 mV). Notably, the amount of shift ΔE caused by the H_2 binding to diiron compounds is also related to the number of phosphine ligands, and therefore to the electron richness of the diiron core: the more electron poor the complex is, the more significant is the quantitative effect of H_2 binding on oxidation potential. Therefore, the oxidation potential of the different biomimetic models becomes more similar after H_2 binding.

The above observation, can be rationalized by considering a simple four spin-orbital/three-electron model. Indeed, the two frontier singly occupied molecular orbitals (α-HOMO and β-LUMO) of each diiron compound (i.e., pre-H_2 binding) are very similar and mainly localized on the Fe_d atom, and are suitable to interact with the orbital of H_2 in a bonding and antibonding combination. such two MO's are suitable to interact with H_2 orbitals (by the classic bonding/antibonding coupling). A schematic diagram illustrating MO interactions is shown in in Figure 3.6.6 for the series of "homologous" species $\mathbf{1}^+$, $\mathbf{2}^+$and $\mathbf{6}^+$. The two bonding MO's of the H_2-adduct are occupied and much lower in energy than those of the separated molecules (i.e., H_2 and the diiron compound of interest),. Concomitantly, the antibonding orbitals (i.e., the HOMO-LUMO of the H_2-adduct) are higher in energy than the corresponding orbitals of diiron compounds pre-adduct formation, thus accounting for the increase of the oxidation potential after H_2 binding. The extent of this destabilization is a function of the energy difference between the FMO's of the two not interacting molecules; a smaller energy difference (in $\mathbf{1}^+$) is reflected in a larger destabilization of the HOMO (=electron is more easily removed from it) in $\mathbf{1}^+$ vs $\mathbf{6}^+$ after H_2 binding.

In summary, substrate binding favors one electron oxidation of the $Fe^{I}Fe^{II}$ core. In addition, oxidation of the H_2 adducts is concomitant with heterolytic cleavage of the H_2 molecule. The latter observation is relevant in the light of the H_2 binding step, which is associated with a reaction energy close to 0 kcal/mol even when considering the H-cluster.

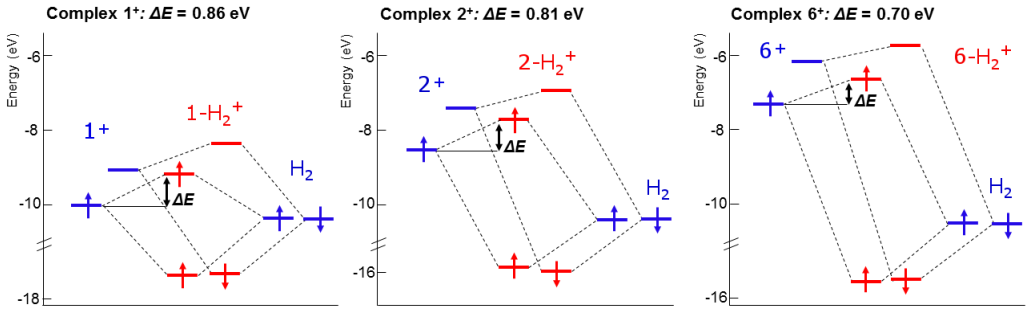

Figure 3.6.6: MOs diagram describing bonding and antibonding interactions between biomimics and dihydrogen.

Indeed, as already remarked, high affinity for H_2 would be deleterious for an efficient catalytic cycle, because it would cause formation of very stable and unreactive, intermediate species. On the other hand, a too low affinity for the substrate is also incompatible with catalysis. However, a moderately low affinity of the catalyst for H_2 can be beneficial for catalysis if H_2 binding is

	$\mathbf{E_{ox,abs}(V)}$ $\mathbf{Fe^{I}Fe^{II} \rightarrow Fe^{II}Fe^{II}}$		$\mathbf{E_{ox,abs}(V)}$ $\mathbf{Fe^{I}Fe^{II}(H_2) \rightarrow Fe^{II}Fe^{II}(H_2)}$		$\mathbf{\Delta E_{ox,abs}}$	
Compound	BP86	B3LYP	BP86	B3LYP	BP86	B3LYP
$\mathbf{1}^{+}$	-5.99	-5.66	-5.38	-4.97	0.98	0.70
$\mathbf{2}^{+}$	-5.30	-5.06	-4.66	-4.45	0.94	0.64
$\mathbf{6}^{+}$	-4.52	-4.35	-3.87	-3.81	0.66	0.54
$\mathbf{9}^{+}$	-4.99	-4.86	-4.50	-4.27	0.62	0.58

Table 3.6.6: Computed absolute one-electron oxidation potentials of a selected set of biomimics and their H_2-adducts.

simultaneous to one-electron oxidation, which leads to a H_2 cleavage step to occur barrierless.

3.6.3.4 Intramolecular proton transfer in the H-cluster and in biomimetic models

Finally, we have investigated the energetics of another crucial step in the H_2 oxidation catalytic cycle, i.e. proton transfer from the iron coordination environment to the pendant amine group (Figure 3.6.1; Table 3.6.7), which formally corresponds to a $Fe^{II}Fe^{II}$-H(R_2 NH) $\rightarrow Fe^{I}Fe^{I}$(R_2 NH_2^+) process. In an ideal catalyst, the reaction energy for such a step should be close to zero. In line with this observation, small proton transfer reaction energies are computed when considering the [FeFe]-hydrogenase models $\mathbf{H_{ox}}$**-full-**$\mathbf{H^{3-}}$ and $\mathbf{H_{ox}}$**-SHCH$_3$**$-\mathbf{H^{-}}$ (3.5 and -1.5 kcal/mol, respectively, when $\varepsilon = 4$). Note that the proton transfer reaction energy for the $\mathbf{H_{ox}}$**-SCH$_3$**$-\mathbf{H_2^{-}}$ model could not be computed, because the only stable isomer corresponds to the $Fe^{II}Fe^{II}$-H(R_2 NH) species. This result can be rationalized considering that the basicity of the FeFe core in the $\mathbf{H_{ox}}$**-SCH$_3$**$-\mathbf{H^{2-}}$ model is most likely overestimated, due to the large negative charge of the model (-2). In this context, $\mathbf{H_{ox}}$**-SHCH$_3$**$-\mathbf{H^{-}}$ and $\mathbf{H_{ox}}$**-full-**$\mathbf{H^{3-}}$ are more realistic models because in the former the charge is only -1, and in the latter, even if the overall charge is more negative (-3), the charge density is lower due to the large size of the model. When considering the diiron biomimetic models the reaction energy values are spread on a larger interval (Table 3.6.7). In particular, the proton transfer reaction is essentially irreversible, in the direction of adt protonation, in models characterized by a very electron poor diiron core, such as **1-**$\mathbf{H^{+}}$, whereas thee^{II}Fe^{II}-H(R_2 NH) species is strongly favoured in very electron rich models, such as **6-**$\mathbf{H^{+}}$. Remarkably, the reaction energy closer to zero is computed for **9-**$\mathbf{H^{+}}$, which corresponds to the scaffold of the biomimetic complex capable of catalysing H_2 oxidation proposed by Rauchfuss et al.[205] Indeed, in the real catalyst a benzyl group is linked to the nitrogen atom of adt; however, also considering this modification (model **9(adt$^{\mathbf{Bn}}$)-**$\mathbf{H^{+}}$) the absolute value of the proton transfer reaction energy remains below 3 kcal/mol (Table 3.6.7). As noted for the heterolytic cleavage step, also in this case the dielectric constant of the solvent significantly affects the energetics of the process, and again, proton transfer becomes more favorable when increasing the value of ε. This observation suggests that also the energetic of the proton transfer step can be somewhat modulated by a proper choice of the solvent.

	$Fe^{II}Fe^{II}$-H^- → $Fe^{I}Fe^{I}$-H^-			
Compound	BP86		B3LYP	
	$\varepsilon = 1$	$\varepsilon = 4$	$\varepsilon = 1$	$\varepsilon = 4$
$\mathbf{H_{ox}}$-**full**$^{3-}$	8.88	3.51	8.64	3.65
$\mathbf{H_{ox}^{3-}}$	5.76	-0.07	7.77	1.75
$\mathbf{H_{ox}}$-$\mathbf{SCH_3^{2-}}$	-	-	13.40	7.21
$\mathbf{H_{ox}}$-$\mathbf{SHCH_3^{-}}$	6.89	-1.53	10.01	0.36
	$\varepsilon = 1$	$\varepsilon = 8.93$	$\varepsilon = 1$	$\varepsilon = 8.93$
$\mathbf{1}^+$	-4.43	-16.03	-2.49	-13.58
$\mathbf{2}^+$	2.06	-6.27	4.18	-4.96
$\mathbf{6}^+$	9.81	2.74	12.29	5.77
$\mathbf{9}^+$	4.03	-3.91	5.03	-3.54
$\mathbf{9(adt^{Bn})}^+$	-1.37	-3.75	-0.90	-3.73
$\mathbf{10}^+$	9.76	1.45	9.64	-0.41
$\mathbf{11}^+$	6.23	1.83	5.53	0.51

Table 3.6.7: Computed energy variations upon intramolecular proton transfer in both H-cluster and biomimics compounds.

3.6.4 Conclusions

The catalytic cofactor of [FeFe]-hydrogenases, the so-called H-cluster, has inspired the synthesis of hundreds of biomimetic complexes.[15] In fact, the elucidation of structure-activity relationships in this class of iron coordination compounds is expected to drive the design of affordable catalysts for H^+ reduction and H_2 oxidation. In this respect, it is important to outline that recipies for the design of biomimetic complexes should take into account that the catalytic process is a multi-step process, and therefore the selection of the proper ligands should be aimed to 'optimize' all steps within the process.[348] Even if [FeFe]-hydrogenases generally catalyze H^+ reduction in physiological conditions, several of these enzymes can also catalyze H_2 oxidation with a high turnover frequency.[14] Notably, the same does not hold true for biomimetic catalysts: while several diiron complexes can catalyze H^+ reduction (in a few cases with high turnover frequency[331, 68, 308]), H_2 oxidation remained elusive until Rauchfuss and collaborators showed that the insertion of a suitable redox non-innocent ligand into a $Fe^{I}Fe^{II}$ biomimetic scaffold could be crucial for catalytic activity.[205] In fact, the presence of a redox-active group allows to couple H_2 binding with one electron oxidation of the bimetallic cluster. This coupling is crucial for two reasons: heterolytic cleavage of H_2 can easily take place on $Fe^{II}Fe^{II}$ species,[4] but oxidation of the $Fe^{I}Fe^{II}$ cluster must take place only after H_2 coordination, otherwise catalytically inactive forms in which the N atom of adt enters the coordination sphere of the Fe atom might be formed [[68, 349]]. In addition, since H_2 binding in the $Fe^{I}Fe^{II}$ state of the diiron core should not be too exergonic, because this would imply large activation energy barriers in the catalytic cycle, it is crucial that H_2 binding is

tightly coupled to one-electron oxidation. Even though the Rauchfuss' catalyst represented the first conceptual breakthrough in the field, its catalytic activity is relatively poor, indicating that additional stereoelectronic features are necessary to reach or at least get close to the catalytic efficiency of the enzyme. Prompted by these observations, and with the aim of disclosing other stereolectronic features possibly critical in catalysis, we have compared the energetics of three key steps in the H_2 oxidation catalytic cycle (H_2 binding, one electron oxidation of the H_2 adduct and intramolecular proton transfer) in the enzyme cofactor and in a series of diiron biomimetic complexes differing for the number and nature of phosphine ligands.

To date, all the H_{ox} models that have been synthesized and isolated feature hindering PMe_3, dppv or N-heterocyclic carbene ligands.[15, 127] However, the present work indicates that H_2 binding to highly substituted derivatives is predicted to be much more endoergonic than that related to electron-poorer biomimics or to H-cluster models. These results are in line with the experimental observation of difficult (or even impeded) H_2 binding/activation to synthetic H_{ox}models. In addition, another DFT result matching with experiments is that the presence of adt , in place of pdt, is able to lower H_2 binding energies.[206, 205] Indeed, the substitution of nitrogen-based with carbon-based bridge-heads has proved to entail the loss of any H_2 binding/activation ability by synthetic models. Interestingly, DFT results confirm that the NH /NR group is crucial not only for its well documented role as a base in H_2 heterolytic cleavage,[14] but also for tuning the H_2 affinity to the diiron cluster. In summary, our analysis highlights a very peculiar and functionally relevant trade-off which is operative in the H-cluster, where a sufficiently electron poor iron atom (allowing H_2 coordination) and a sufficiently electron rich coordination compound (allowing facile one electron oxidation) coexist. On the other hand, in biomimetic complexes containing phosphine ligands an increase in the electron donor properties of the ligand, which favors one electron oxidation, is accompanied by a too disfavored H_2 binding energy, and vice versa. In other words, the bimetallic cofactor in [FeFe]-hydrogenases is very electron rich and, after H_2 binding, is easily oxidized. in spite of an electron richness that is distributed onto the entire scaffold of the H-cluster, distal Fe can still bind H_2 due to the presence of electron accepting ligands (CO, CN^-) that make such Fe sufficiently Lewis acid so as to favor sigma-donation from H_2 to the metal atom.

Heterolytic cleavage is supposed to be exergonic at the Fe^IFe^{II} stage in biomimic compounds, while in H-cluster models it becomes favorable only after the first electron removal. This is another remarkable difference between biomimic compounds and active site, that could, at least in principle, have some implication also on the energetic of the following catalytic steps. Indeed, supposing that heterlotytic cleavage occurs prior to oxidation, the formation of relatively stable Fe^IFe^{II} species (that already underwent H_2 bond breaking) would make the subsequent oxidation potentials even more unfavorable than that reported in 3.6.6. In addition, H_2 binding is predicted to favor oxidation of active site models by less (~ 0.3V) than biomimic compounds ($\sim 0.6-1$V). Yet, very few examples of mimics show a proton transfer energy close to zero, in contrast to what has been observed for H-cluster models. All of these observations point out that the H-cluster is perfectly designed to behave as an ideal catalyst (in sharp contrast to biomimics), which is associated to an overall smooth energy profile, where each chemical transformation is

thermodynamically closer to $\Delta E = 0$, as well as each redox step more favored, with respect to those expected for mimics. Further investigations in the field of H_2 oxidation bioinspired compounds are still needed. Indeed it appears interesting the contribute by Sun et al[207] that demonstrate it is possible to observe moderate catalytic activity of H_2 oxidation even without including an intramolecular redox cofactor (Rauchfuss approach)

Chapter 4

DFT study of CO_2 activation catalyzed by a class of thiolate-bridged di-iron complexes with a [Cp*Fe(μ-SR)$_2$FeCp*] scaffold

4.1 Introduction

Thiolate-bridged diiron clusters have been widely synthesized and structurally determined especially in the form of Fe_2S_2 clusters, since their close similarity to hydrogenase active site.[15, 127] Diiron sulfide/thiolate systems without the typical $[2Fe]_H$ "butterfly" conformation and CO ligands have been less investigated, particularly for what concerns their reactivity towards nitrogenase-relevant substrates. An example of low-coordinate, sulfide-bridged diiron complex resembling a fragment of the FeMo-co, namely LFeSFeL (L = [HC(CMeN[2,6- diisopropylphenyl])2]-) was proposed by P. L. Holland and coworkers.[233] This system proved to bind nitrogen-donor substrates and to cleave the N-N single bond of phenylhydrazine. J. Qu et al. proposed instead a series of diiron-thiolate systems with Cp* ligands (Cp* = η^5-C_5Me_5) as FeMo-co mimics.[123, 239, 350, 238] The aim was to achieve a similar reactivity of the previously reported diruthenium counterparts (with two or three thiolate bridges), which provide a bimetallic reaction site for small molecules (alkyns, hydrazines, alkyl halides) activation and conversion, and, at the same time, to replicate the minimal functional subunit of nitrogenase active site. Among them, the species [Cp*Fe(μ-SEt)$_2$(μ,η^2-RN=NH)FeCp*] (R = Me, Ph) was the first to possess excellent catalytic activity toward N-N bond reductive cleavage of hydrazine and derivatives.[123] Such diiron species is directly obtained through chemical activation of a precursor containing three thiolate bridges ([Cp*Fe(μ-SEt)$_3$FeCp*]; (R = Me, Ph) which, remarkably, has proved to cleave carbon-halogen bonds[351]) plus hydrazine. The (formally) 32e [Cp*Fe^{II}(μ-SEt)$_2$Fe^{II}Cp*] species (hereafter **1**) has been proposed as an active intermediate, along the suggested mechanism of N_2H_4 reduction. Interestingly, also capability of N_2 activation by **1** has been investigated, although only theoretically.[237]

The electron-unsaturated nature of the metallic centers explains the instability (reactivity) of **1** as well as the need, for practical uses, of starting catalysis from species with higher coordination

Compound	Fe_1-Fe_1	Fe_1-S_1	Fe_1-S_2	Fe_2-S_1	Fe_1-S_2
1	2.905	2.190	2.189	2.203	2.204
2	2.820	2.147	2.152	2.297	2.295
2 XRD	2.780	2.148	2.152	1.298	2.300
3	2.867	2.206	2.206	2.210	2.211
3 XRD	2.843	2.214	2.213	2.220	2.222

Table 4.2.1: DFT and XRD main geometrical parameters of **1**, **2** and **3**.

numbers. In this direction, small variations in the second coordination sphere have been shown to stabilize the electron-poor core of **1**, retaining at the same time its reductive activity towards hydrazine. In fact, complexes **2** and **3** (Figure 4.2.1) have been synthesized and crystallized. In complex **2** the ethylthiolate pendants have been replaced by a benzene-1,2-dithiolate (bdt) ligand, which leans towards one iron atom and binds the di-iron core in a μ-η^2:η^4 manner. The so formed agostic interaction stabilizes the electron-deficient core. In complex **3**, instead, more hindering thiolates (bearing an aromatic moiety with a $-SiMe_3$ group) are introduced in place of the ethylthiolate groups.

The interest in this class of complexes stems from the fact that nitrogenase has proven to be a promiscuous enzyme, cable of catalyzing the reduction of many substrates, including CO_2.[18] The purpose of the present work is thus to understand if the same CO_2 reduction can be retained or exhibited by the biomimetic Fe_2S_2 systems.

A computational study of CO_2 binding to **1**, **2** and **3** is here reported. In a second stage, also the CO_2 activation on the three species is taken into consideration. In particular, a CO_2 binding modes analysis to the di-iron core will be first reported, in order to highlight the role that this class of complexes plays in CO_2 activation, and then putative CO_2reduction pathways to both CO and HCOOH will be proposed.

4.2 Results

4.2.1 Computational characterization of 1, 2 and 3

The TPSS/TZVP/COSMO (ε = 7.58) optimized structures of **1**, **2** and **3** are reported in Figure 4.2.1 while their main geometrical parameters are collected in Table 4.2.1. The reported absolute minima correspond to closed shell states but, particularly in complex **1** and **3** cases, the high spin configurations (S=1) are easily accessible, because of the presence of weak field ligands. The larger energy difference between singlet and triplet states in **2** is attributed to the Fe-bdt π-interaction, which favors the formation of a closed shell system.

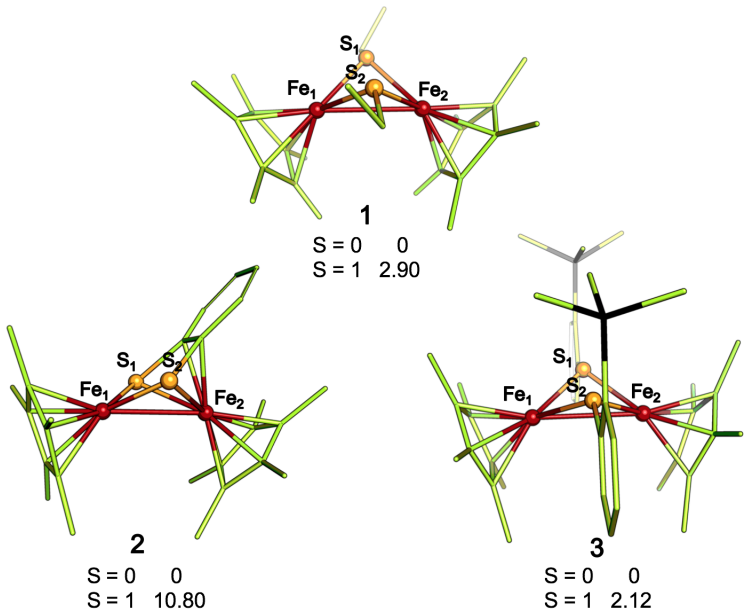

Figure 4.2.1: DFT-optimized structures of complex 1,2 and 3. The labels S_n and Fe_n are referred to Table 4.1, where the main geometrical parameters are collected. Energy differences between low spin and high spin solutions are reported (in kcal/mol). Higher spin multiplicity solutions have not been shown or discussed, since they are much higher in energy with respect to the ground state.

Even if the Fe-Fe distances are quite long in all complexes, the electron counting approach suggests the presence of an intermetallic bond, which would provide 17 d electrons for each Fe^{II} center. The weakness of the Fe-Fe interaction may be the result of the bulky Me groups on the Cp* ligands: such statement is supported by the observation of shorter Fe-Fe distances when Me groups are replaced by less bulky hydrogens both in complex **1** and **2** (a behavior also observed for Ni dimers featuring differently substituted Cp ligands). FMOs analysis of this class of compounds revealed that the HOMO has a metal d-orbital character in all complexes, while the LUMO has also a small component of ligand orbitals. The Fe-bdt interaction in **2** breaks the orbitals symmetry, with being in this case: i) the LUMO mainly located on the iron involved in the agostic interaction and ii) the HOMO on the other iron.

4.2.2 Analysis of CO_2 binding modes

DFT computations suggest that **1** is predicted to engage CO_2 in two ways (Figure 4.2.2). A regioselective behavior has been detected, in that the formation of a given product out of others depends on the "face" of the catalyst that interacts with CO_2. In fact, if we imagine a plane containing the Fe-Fe bond and parallel to the one containing the two S atoms, we can identify two different faces of the molecule. The first face includes the SEt pendants and the two iron ions are coordinated by CO_2 in a μ^2-(η^2C,O) fashion, to give the **1-CO_2(a)** and **1-CO_2(b)** modes, which differ only for the spatial orientation of the Et groups. The other face, hindered by the

presence of Cp* groups, binds CO_2 through a single-Fe coordination, in a side-on fashion, giving rise to **1-CO$_2$(c)** mode (Figure 4.2.2). In **1-CO$_2$(c)** the Fe-Fe bond is broken, while in both **1-CO$_2$(a)** and **1-CO$_2$(b)** it results shorter (vs **1**) by 0.26 and 0.33 Å, respectively. Interestingly, when the ethyl moiety points toward the μ^2-(η^2C,O) ligand, the binding becomes exergonic, suggesting that this long range interaction appears crucial for the stabilization of the interaction. $\Delta E^{\neq}$ values associated with side-on and μ^2-(η^2C,O) binding modes are 18.5 kcal/mol and 25.2 kcal/mol, respectively. Thus, **1-CO$_2$(a)** can be considered the thermodynamic product of CO_2 binding to **1**, while **1-CO$_2$(c)** is the kinetic one. A possible isomerization between the two forms has not yet been investigated.

In order to understand the nature of the catalyst-CO_2 interaction we have quantified possible charge variations involved in the binding (Table 4.2.2). NBO analysis of the atomic partial charges suggests that upon binding CO_2 receives electron density from the catalyst. This charge transfer, which is quite unexpected because of the presence of electron-deficient metallic centers, is sufficient to activate the CO_2 molecule. In fact, in all the resulting **1-CO$_2$** binding modes, the O-C-O angle is far less than 180° after coordination and the C-O distances are $>$ 1.17 Å (computed C-O distances of the free CO_2 at the TPSS/TZVP/COSMO level) (Table 4.2.6).

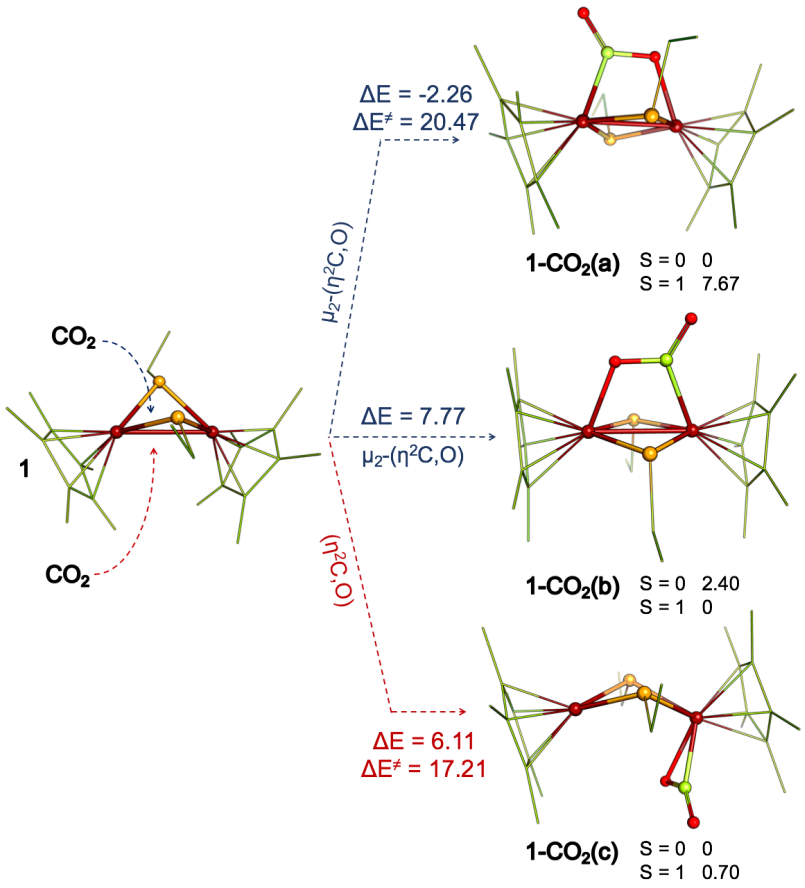

Figure 4.2.2: CO_2 binding modes to complex **1**. The binding energy values and the relative stability of the high and low spin species are also reported (kcal/mol).

NBO charge analysis	**1**	**1-CO_2(a)**	**1-CO_2(b)**	**1-CO_2(c)**
Fe(1)	0.092	-0.011	0.29	0.20
Fe(2)	0.091	0.24	0.49	0.17
$(SEt)_2$	-0.021	0.34	-0.088	0.10
$(Cp^*)_2$	-0.16	0.12	-0.055	0.10
	free CO_2			
C_{CO_2}	0.93	0.65	0.62	0.75
O_{CO_2}(1)	-0.46	-0.65	-0.62	-0.56
O_{CO_2}(2)	-0.46	-0.68	-0.67	-0.57
	ΔqCO_2	-0.67	-0.66	-0.58

Table 4.2.2: NBO charge analysis of **1** and the **1-CO_2** interaction modes. The Δq_{CO_2} values are referred to the variation of the CO_2 atomic partial charges upon coordination to **1**. Fe atoms are referred to as (1) or (2) according to Figure 4.2.1, while O (1) is the oxygen atom involved in the bond with the metal center.

		1	**1(Cp-OMe)**	**1(Cp)**	**1(Cp-Cl)**
Binding energies(kcal/mol)	μ^2-(η^2C,O)	-2.3	-0.6	5.8	7.4
	side-on	6.1	10.1	10.4	12.2
FMO energies(eV)	HOMO	-3.45	-3.76	-3.83	-4.69
	LUMO	-2.32	-2.83	-2.91	-3.63
	Gap	1.13	0.93	0.92	1.06

		2	**2(Cp-OMe)**	**2(Cp)**	**2(Cp-Cl)**
Binding energies(kcal/mol)	side-on	8.00	12.4	15.0	17.8
FMO energies(eV)	HOMO	-3.57	-3.83	-3.95	-4.17
	LUMO	-2.11	-2.37	-2.44	-2.63
	Gap	1.46	1.46	1.51	1.54

Table 4.2.3: : CO_2 binding energies to **1**, **1(Cp-OMe)**, **1(Cp)**, **1(Cp-Cl)** and **2**, **2(Cp-OMe)**, **2(Cp)**, **2(Cp-Cl),** with their related HOMO/LUMO energies. The reported μ_2 -(η^2C,O) binding energies are referred to the formation of the most stable **1-CO_2 (a)** product.

Probably due to the two vs one Fe coordination of CO_2, in **a** and **b** modes, the activation appears more pronounced than in **c** mode, as a consequence of a more significant charge transfer. However, the greater "structural" activation of CO_2 is not reflected quantitatively in binding energies. It's interesting that the electron transfer upon CO_2 binding is independent to the electron deficiency of the system, while it is driven by the relative energy of FMOs of both CO_2 and catalyst. In this regard, CO_2 binding mainly involves the interaction of its LUMO with the HOMO of the complex. In order to corroborate this observation, we have modified **1** so as

to obtain a series of homologous species, differing by the type of substituents on Cp rings. In this way it is possible to evaluate if the stereo-electronic properties of some Fe ligands are able to tune the energetic of CO_2 binding, as well as its coordination mode. The series considered is: [Cp*Fe(μ-SR)$_2$FeCp*] (**1**), [OMe-CpFe(μ-SR)$_2$FeCp-OMe] (**1Cp-OMe**), [CpFe(μ-SR)2FeCp] (**1Cp**), [Cl-CpFe(μ-SR)$_2$ FeCp-Cl] (**1Cp-Cl**) (ordered from the more electron-donating (ED) to the more electron-withdrawing (EW) Cp substituents). No change in coordination modes was observed, but an intriguing correlation has been found between the basicity of Cp groups and CO_2 binding energies. In fact, the more electron-rich the Cp ligands are (and thus, the more destabilized the FMOs are) the more the computed binding energies decrease (see Table 4.2.3), supporting the postulated $LUMO_{CO_2}$-$HOMO_{cat}$ interaction.

The presence of a chelating bdt ligand in complex **2**, allows CO_2 binding to occur only at one of the two catalyst faces, leading to **2-CO$_2$(a)**, with the CO_2 molecule side-on coordinated to the iron atom not involved in the agostic interaction. **2-CO$_2$(a)** looks like **1-CO$_2$(c)**. In fact, also a μ^2-(η^2C,O) coordination mode entailing breaking of the Fe-bdt agostic bond has been observed, but it is estimated to be ∼10 kcal/mol less stable with respect to the side-on form. Such results nicely agree with the previous frontier molecular orbital analysis, which suggests that HOMO of **2** is almost completely confined to a single Fe center. Interestingly, the computed binding energy is very close to that obtained for the side-on coordination in **1**. Differently from the **1** case, the μ^2-(η^2C,O) binding of carbon dioxide to **2** occurs on the same face of the catalyst where the side-on binding mode occurs, thus leading to Fe-Fe bond breaking.

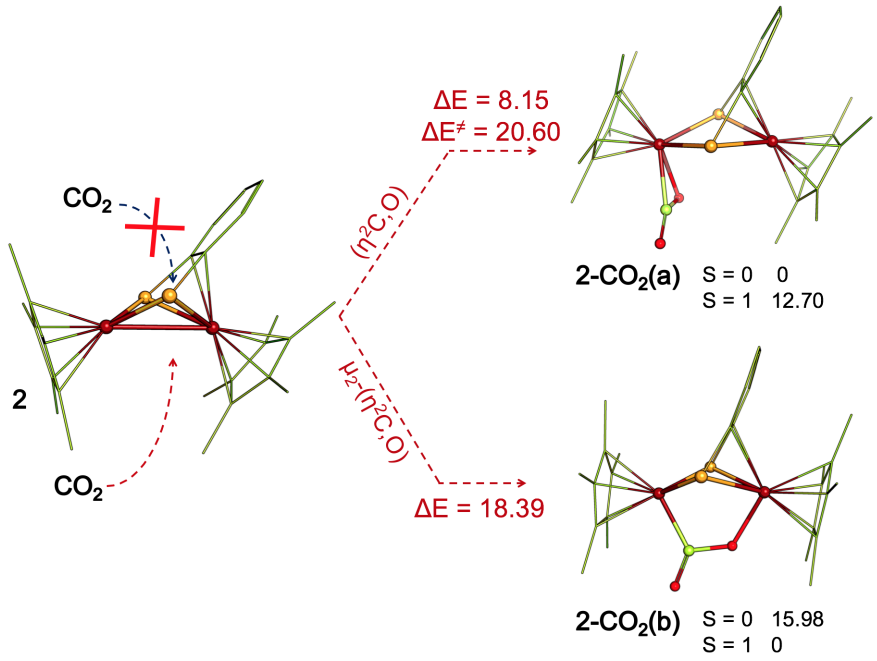

Figure 4.2.3: CO_2 binding modes to complex **2**. The binding energy values and the relative stability of the high and low spin species are also reported (kcal/mol).

NBO charge analysis	**2**	**2-CO_2(a)**	**2-CO_2(b)**
Fe(1)	0.040	0.10	0.32
Fe(2)	0.070	0.17	0.53
$(SEt)_2$	-0.014	-0.16	-0.25
$(Cp^*)_2$	-0.022	0.22	-0.051
	free CO_2		
C_{CO_2}	0.93	0.76	0.60
$O_{CO_2}(1)$	-0.46	-0.54	-0.60
$O_{CO_2}(2)$	-0.46	-0.55	-0.66
	ΔqCO_2	-0.34	-0.66

Table 4.2.4: NBO charge analysis of **2** and the **2-CO_2** interaction modes. The Δq_{CO_2} values are referred to the variation of the CO_2 atomic partial charges upon coordination to **2**. Fe atoms are referred to as (1) or (2) according to Figure 4.2.1, while O (1) is the oxygen atom involved in the bond with the metal center.

NBO charge analysis	**3**	**3-CO_2(a)**	**3-CO_2(b)**	**3-CO_2(c)**
Fe(1)	0.11	0.05	0.12	0.25
Fe(2)	0.11	0.27	0.23	0.55
$(SEt)_2$	-0.14	0.13	-0.24	-0.17
$(Cp^*)_2$	-0.077	0.18	0.22	0.05
	free CO_2			
C_{CO_2}	0.93	0.64	0.75	0.61
$O_{CO_2}(1)$	-0.46	-0.62	-0.58	-0.62
$O_{CO_2}(2)$	-0.46	-0.66	-0.57	-0.68
	ΔqCO_2	-0.64	-0.39	-0.69

Table 4.2.5: NBO charge analysis of **3** and the **3-CO_2** interaction modes. The Δq_{CO_2} values are referred to the variation of the CO_2 atomic partial charges upon coordination to **3**. Fe atoms are referred to as (1) or (2) according to Figure 4.2.1, while O (1) is the oxygen atom involved in the bond with the metal center.

NBO charge analysis evidences (like in **1**) a charge transfer from the Fe2 center to CO_2 (Table 4.2.2). Therefore, the same strategy has been adopted that we used in the previous case. Also, CO_2 binding energies have been evaluated in comparison to a set of homologous complexes (of **2**) bearing different Cp substituents. Further, possible correlations have been searched between the computed $\Delta E_{binding}$ values and the FMOs energies (Table 4.2.3).

In analogy with **1**, the trend of the binding energy correlates with the HOMO energy variations, confirming that the substitution of the SEt moieties with a bdt ligand, necessary for stabilization

of the di-iron core, does not change its reactivity. Kinetics of the CO_2 side-on binding to **2** is very similar to that computed for **1**, since the obtained energy barrier is 21.6 kcal/mol.

CO_2 binding modes to **3** are summarized in Figure 4.2.4. The absence of a chelating dithiolate in **3** allows CO_2 binding to both its faces, leading in one case only to a μ^2-(η^2C,O) interaction (as already observed for **1**), and on in the other case, to both bridging and side-on coordination, with concomitant breaking of the Fe-Fe bond (in analogy with complex **2**). Interestingly, in this system the formation of a bridging CO_2 mode is predicted to be thermodynamically favored compared to the side-on mode. The energy barriers necessary to obtain **3-CO$_2$(a)**, **3-CO$_2$(b)** and **3-CO$_2$(c)** are 18.9, 17.9 and 17.4 kcal/mol respectively. This trend suggests that the **3-CO$_2$(c)** mode corresponds both to the kinetic product of the binding process and also to the thermodynamic product.

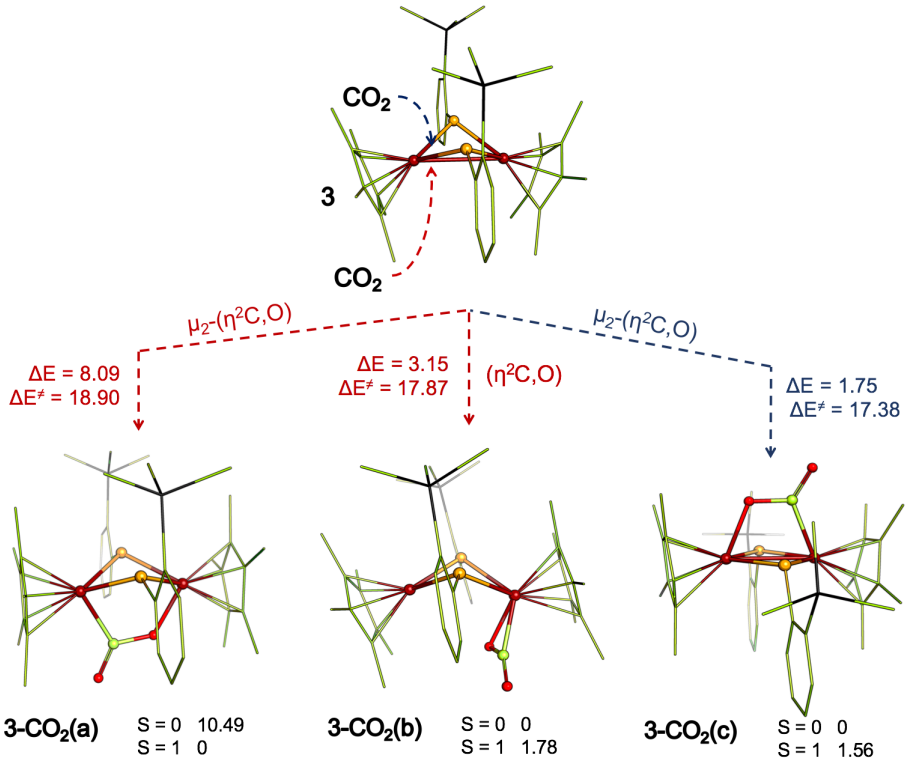

Figure 4.2.4: CO_2 binding modes to complex **3**. The binding energy values and the relative stability of the high and low spin species are also reported (kcal/mol).

4.2.3 Viable CO_2 reduction pathways

In a second stage of the study, we investigated pathways leading from Fe_2-CO_2 adducts to HCOOH and CO. With **1** as a reference system, DFT pathways are illustrated in Figures 4.2.5 and 4.2.6. Energetics associated with protonation and one-electron reduction has been computed considering the $LutH^+$/Lut and Cp_2Co^+/Cp_2Co couples, respectively, being 2,6-lutidine the proton source

	Fe-Fe (Å)	Fe-C (Å)	C-O(1) (Å)	C-O(2) (Å)	O-C-O°
1-CO_2(a)	2.570	2.001	1.333	1.233	122.5
1-CO_2(b)	2.741	2.019	1.321	1.231	121.9
1-CO_2(c)	3.294	1.947	1.256	1.121	141.1
2-CO_2(a)	3.422	1.976	1.254	1.203	143.1
2-CO_2(b)	3.233	2.009	1.355	1.222	117.2
3-CO_2(a)	2.739	2.026	1.320	1.230	122.5
3-CO_2(b)	3.229	1.967	1.257	1.209	139.8
3-CO_2(c)	3.189	2.003	1.363	1.227	116.7

Table 4.2.6: Relevant DFT geometry parameters related to the entire set investigated (**1**-**3**). Distances in Å.

and cobaltocene the reductive agent experimentally employed. Figure 4.2.5 shows a CO_2 reduction pathway proceeds via initial protonation at the CO_2 carbon atom, followed by the first one-electron reduction. At this point, a second protonation of one of CO_2 oxygen is feasible and, after the income of a second electron, HCOOH could be formed and released. If catalysis starts from a μ^2-(η^2C,O) coordination, instead, both protonation events reasonably take place on the same CO_2 oxygen atom, leading to the release of a water molecule, giving a very stable intermediate with a μ-CO ligand (Figure 4.2.6). Also the possibility of formation of a hydroxyl ligand, previously reported for di-ruthenium systems, has been considered. Release of HCOOH and CO from reduced and protonated **1** are exergonic: -13.6 and 40.8 kcal/mol, respectively.

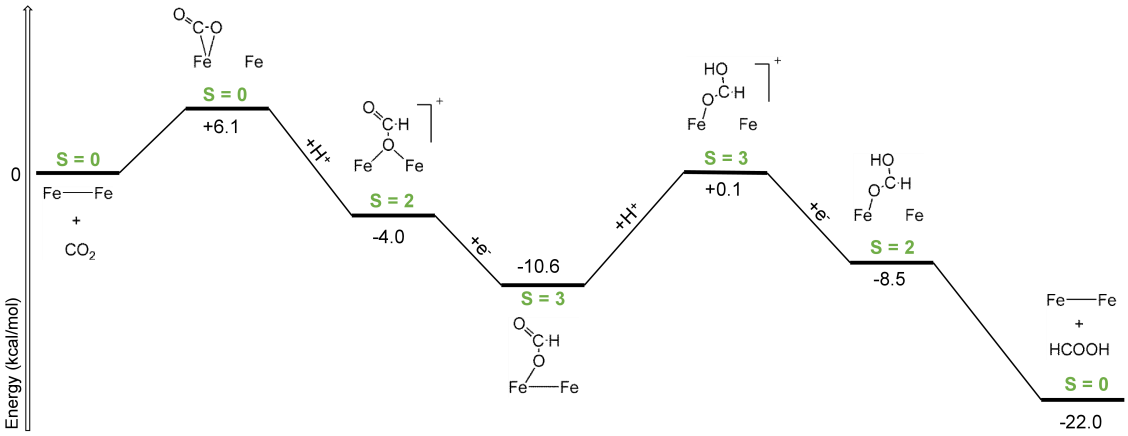

Figure 4.2.5: Proposed CO_2 reduction mechanism to HCOOH. Energy differences are computed in kcal/mol with respect to starting point. Spin state of each intermediate are also reported (in green).

Thus catalytic production of HCOOH can be anticipated whereas the formation of CO_2/H_2O is energetically prohibitive. These results are quite preliminary, since complete energy profiles, comprehensives of the kinetic barriers and entropic corrections, and alternative reaction mechanisms

(e.g. one-electron reduction occurring prior to the first protonation) are still under investigation. However, some relevant information could be deduced by this early analysis: i) a given CO_2 binding mode to the di-iron core is able to address the mechanism towards the formation of a single product and ii) the energy demanding CO release, which seems to prevent the catalyst recovering, suggests that these system could be employed to selectively reduce CO_2 to HCOOH.

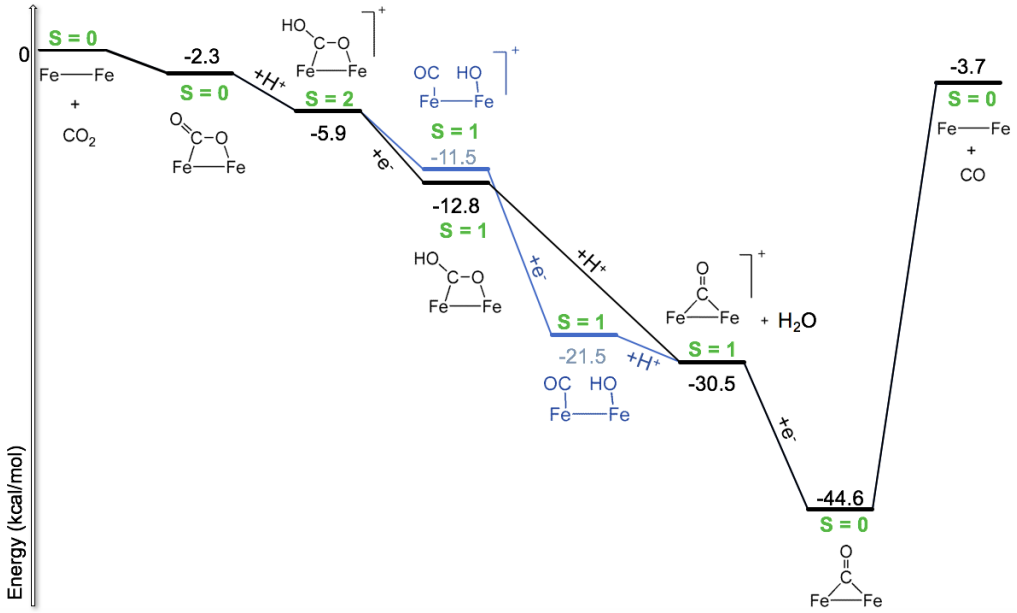

Figure 4.2.6: Proposed CO_2 reduction mechanism to CO. Energy differences are computed in kcal/mol with respect to starting point. Spin state of each intermediate are also reported (in green).

4.2.4 Activation of H_2 and CO_2 hydrogenation

The structural similarity between the systems under investigation and the hydrogenase di-iron core, led us to unravel the reactivity of **1** towards dihydrogen. In particular we computed the H_2 binding energies to **1**, associated to the different pinpointed coordination modes. Binding energy values for the two **1-H$_2$** adducts are reported in Table 4.2.7, together with their main geometrical parameters. Again, the activation of the small molecule occurs in a different manner according to the face of the catalyst involved in the reaction, leading on the one hand to a H_2 σ-complex (**1-H$_2$(a)**) and on the other to a bis-μ-hydride (**1-H$_2$(b)**), which is the thermodynamic product. In both cases low-spin solutions are much more stable than high-spin ones ($\sim$ 10kcal/mol).

From a kinetic point of view the paths leading to **1-H$_2$(a)** and **1-H$_2$(b)** are both viable, since the computed activation barriers of H_2 binding are 13.5 and 14.6 kcal/mol respectively, which corresponds to a too small difference for the resolution power of the present DFT methods. Our outcome suggests that the activation of H_2 via σ-complex is kinetically feasible, and would allow the coordination of CO_2 to the iron atom not involved in the Fe-H_2 interaction. This last observation is of great interest if we consider the possibility of reducing CO_2 using H_2 as the

reductant. Thus, we decided to study the role of the catalyst in the activation of both substrate and reductant by comparing the activation energies associated to H_2 and CO_2 binding. We also considered the possibility of the formation of a **1-CO_2,H_2** product, in which the Fe_2S_2 scaffold activates simultaneously H_2 and CO_2. The obtained results, summarized in Figure 4.2.7, suggest that 1) the activation of H_2 is predicted to be kinetically preferred than the one of CO_2 and 2) the formation of the **1-CO_2,H_2** species is downhill starting from both **1-CO_2(a)** and **1-H_2(a)** adducts. In order to highlight the nature of the Fe-H_2 interaction in both **1-H_2(a)** and **1-H_2(b)**, we analyzed the NBO charges before and after H_2 binding (Table 4.2.8). Interestingly, the catalyst behavior towards H_2 is different from the one already observed in the CO_2 case, since H_2 activation is predicted to occur through a ligand-to-metal charge transfer. Thus, we expect that the binding of dihydrogen could trigger the subsequent CO_2 coordination. However, the activation barriers to give the **1-CO_2,H_2** adduct starting from **1-CO_2(a)** and **1-H_2(a)** are still under investigation.

	1-H_2(a)	**1-H_2(b)**
Fe-Fe	3.14	2.45
Fe-$H_{(avg)}$	1.66	1.67
H-H	0.84	1.54
Binding energies (kcal/mol)	11.27	-3.57

Table 4.2.7: Binding energies (in kcal/mol) of H_2 to **1** and main geometrical parameters of **1-H_2(a)** and **1-H_2(b)** minima. Distances in Å.

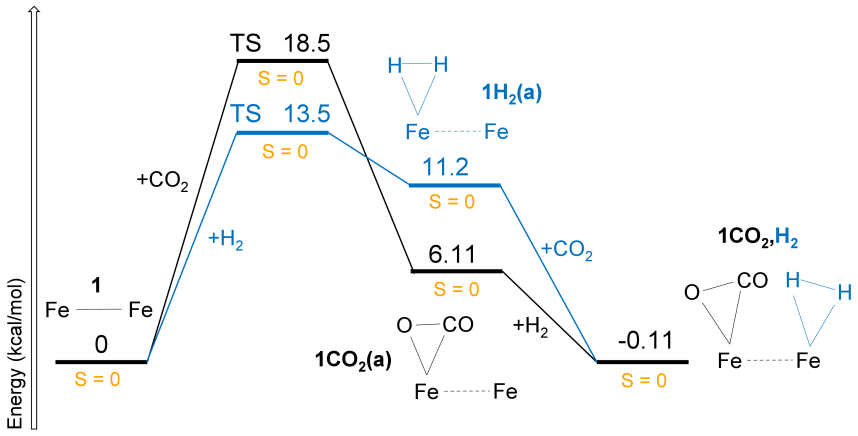

Figure 4.2.7: Comparison between H_2 and CO_2 binding to **1** and formation of the **1-CO_2 ,H_2** species. Energy differences are computed in kcal/mol with respect to starting point. Spin states of each intermediate are also reported (orange values).

NBO charge analysis	**1**	**1-H_2(a)**	**1-H_2(b)**
Fe(1)	0.092	-0,098	-0,026
Fe(2)	0.091	-0,098	0,164
$(SEt)_2$	-0.021	-0,134	-0.246
$(Cp^*)_2$	-0.160	0,030	0,094
	free H_2		
H	0	0,150	0,099
H	0	0,150	0,099
	ΔqH_2	0,300	0,201

Table 4.2.8: NBO charge analysis of **1** and the **1-H_2** interaction modes. The Δq_{H_2} values are referred to the variation of the H_2 atomic partial charges upon coordination to **1**.

4.3 Conclusions

The interest in structural and functional mimicking of nitrogenase by synthetic diiron models is rapidly growing. Most of the efforts has been devoted to achieve a biomimetic activation and conversion of nitrogenase natural substrates (e.g. dinitrogen-containing species). The recently emerged substrate promiscuity towards carbon-based small molecules, e.g CO_2, is surely one of the most powerful kind of reactivity performed by nitrogenases. Regrettably, to date, none of the proposed nitrogenase biomimic compounds has been tested towards CO_2 binding, activation and/or conversion. We presented here a theoretical study about CO_2 binding to a class of both nitrogenase-like (and, interestingly, also hydrogenase-like) models with scaffold Fe_2S_2, as well as its possible conversion to either CO or HCOOH. The presented results have been presently undergoing refinement process (i.e., inclusion of entropic contributions and dispersion corrections). A more accurate treatment of dispersive contributions would be of great interest in the study of CO_2 binding. A more accurate treatment of dispersion contributions would be of great interest in the study of CO_2 binding to complex 3, a process that has (theoretically) proven to be influenced and triggered by long-range interactions with the ligands. Additionally, characterization of transition states associated with the presented CO_2 conversion pathways are still ongoing. However, although the proposed results are quite preliminary, some useful general information about the reactivity of these class of compounds towards CO2 has arisen, as well as some hints to enhance the affinity of biomimcs vs CO_2 . First of all, DFT computed CO_2 binding energies suggest that, starting from the reactive 32e species **1**, it is possible to stabilize the di-iron core with suitable ligand modifications, preserving reactivity. The important variation of CO_2 geometrical parameters upon coordination are coherent with a significant activation of the molecule. Interestingly, the catalyst scaffold is predicted to bind CO_2 through a charge transfer from the HOMO of the catalyst to the LUMO of CO_2. Thus, the more electron releasing the ligands are, the more thermodynamically favored the binding is. Long-range interactions with the thiolate pendants are predicted to stabilize CO_2 coordination products and trigger its binding, particularly in the μ^2-

(η^2C,O) interaction. A remarkable feature of these systems is that CO_2 binding mode is affected by the face of the catalyst involved in new interaction. Hence, it is possible, at least in principle, to selectively obtain a single coordination product with the introduction of a suitable chelating ligand (e.g in complex **2** case). Characterization of putative reduction mechanisms has suggested that the formation of CO vs HCOOH is addressed by CO_2 coordination mode. The computed energy profiles associated to CO_2 reduction pinpoint a possible reaction selectivity to HCOOH formation. The preliminary study on CO_2 hydrogenation suggests that the catalyst scaffold is also predicted to bind the reductant, whose activation occurs through a ligand-to-metal charge transfer and is kinetically favored with respect to CO_2 activation. In addition, the formation of a H_2 σ-complex would allow the subsequent CO_2 activation, which could also be mediated by the Fe atom which is not involved in the Fe-H_2 interaction.

Concluding remarks

The work described in the present thesis has been devoted to the investigation of diiron dithiolate compounds, that are structurally and functionally related to [FeFe]-hydrogenase and nitrogenase active sites. DFT computations provided relevant insights for a better understanding of the chemistry of these systems, at the same time raising new questions and hints for future prospects.

The core of the thesis is dedicated to [FeFe]-hydrogenase biomimics, whose structures and reactivity have been theoretically addressed by various standpoints. Several gaps concerning the activity of these systems still need to be filled. Indeed, besides catalyzing proton reduction at moderate rates (usually accompanied to high overpotentials), synthetic analogues of [FeFe]-hydrogenases are not reversible catalysts, i.e. they cannot oxidize dihydrogen catalytically (except very few examples). When dealing with H_2 oxidation, which is one of the most problematic yet less explored topics in this research area, a detailed analysis of the factors underlying the oxidative behavior of biomimics is clearly indispensable. The present work highlights that the oxidation mechanisms and energetics of synthetic compounds are not only simply function of ligand basicity and/or complex overall charge. Oxidation processes can be affected by more subtle effects, such as the chemical nature of central group of the dithiolate FeFe-linker. Indeed, experiments revealed that the replacement of a nitrogen-based bridge-head with a propandithiolate unit is reflected in a significant variation of oxidation potential values. This observation has been theoretically rationalized on the basis of the formation of intramolecular interactions, such as N-to-Fe full or "partial" coordination and agostic/anagostic interactions, that could form upon oxidation(s). The more remarkable consequence of this finding is that, if one knows at a mechanistic level how (and at which stage of oxidation) the formation of these intramolecular interaction occurs, he could also use them to modulate the oxidation properties of a certain system.

However, the understanding of how to tune redox properties of biomimic compounds is necessary but not sufficient to reach the activity of the native system. Indeed, a detailed dissection of the four main steps in the H_2 oxidation direction catalytic cycle (H_2 binding, H_2 heterolytic cleavage, the subsequent one-electron oxidation and intramolecular proton transfer) highlighted a crucial difference in the reactivity of H-cluster models vs biomimic compounds. In particular, it emerged that the H-cluster behaves as an ideal catalyst (in sharp contrast to biomimics), in that it follows a smooth overall free energy profile, where each intermediate species is thermodynamically neither too stable nor too unstable. This is a fundamental characteristic to ensure both high performances and reversibility in catalysis.

For what concerns proton reduction catalysis, two of the main issues are surely the protophilicity of the system and its regiochemistry of protonation. These aspects are also related to the formation of terminally coordinated (a reactive isomer) vs bridging (a less reactive isomer) Fe hydrides. It is well known that the bridging hydride is a thermodynamic sink (or at least an obstacle) for H_2 production in many of [FeFe]-hydrogenase synthetic models. This issue can in principle be overcome by following different strategies. One of them, which represents a classical paradigm for chemists operating in the hydrogenase modelling, consists in, slowing down the isomerization of the terminal-hydride (often the kinetic product of protonation) to bridging hydride. In this context, we studied the catalytic behavior of an hexacarbonyl model compound, in which a highly protophilic bridge-head pendant has proved to play a crucial role in the hindering of bridging hydride formation. Remarkably, the enhancement of system protophilicity (with respect to its analogues) has been reached with the introduction of an a-biological bridge-head, featuring a P=O moiety instead of a secondary amine. This result hints to the possibility of improving some fundamental feature for catalysis also without sticking to the examples provided by Nature.

An alternative strategy to the hindering of bridging hydride formation, instead, consists in overturning the terminal vs bridging hydride reactivity. This could be done by making the bridging isomer more reactive than the terminal one towards chemical reduction. This aspect has been theoretically investigated, and key information, regarding the stereoelectronic ingredients necessary to achieve this switch of reactivity has been provided.

Among the main structural features of the H-cluster, surely the rotated conformation is one of the most relevant to entail a hydrogenase-like reactivity. Regrettably, in bioinspired compounds the rotated conformation has been achieved only transiently and by means of pure steric hindering. Here we presented, instead, a well-designed model compound in which a suitable iron coordination sphere is predicted to stabilize a vacant coordination site without the need of any steric effect. Indeed, DFT computations pointed out that a rotated ground state geometry could be obtained by properly combining electron-rich ligands and complex asymmetry. The proposed system thus represents the first example of synthetic compound which is theoretically predicted to resemble the actual Fe's coordination geometry of the natural system.

A Fe_2S_2 scaffold has also been proposed as the core of a set of biomimic compounds that aims to perform nitrogenase activity. These compounds are indeed able to activate and convert nitrogenase-relevant substrates, e.g nitrogen-donor molecules, into ammonia. It is remarkable that the same functional unit has been investigated in the biomimicry of both hydrogenases and nitrogenases, reproducing some aspects of the reactivity of both natural systems. It would be of great interest finding a linkage between hydrogenase and nitrogenase- like reactivity of the Fe_2S_2 scaffold, also considering its role in the activation of other substrates, such as carbon dioxide. In the last part of the presented PhD research, a first step in this direction has been made. In this context, we have proposed a preliminary study regarding CO_2 activation and conversion performed by diiron dithiolates as nitrogenase functional analogues. Our results provided some useful and general information about the reactivity of these class of compounds towards CO_2, as well as some clues to favor CO_2 binding and activation.

List of publications

This thesis led to the following publications:

- F. Arrigoni, S. Mohamed Bouh, L. De Gioia, C. Elleouet, F. Y.Pétillon, P. Schollhammer, and G. Zampella, "Influence of the Dithiolate Bridge on the Oxidative Processes of Diiron Models related to the Active Site of [FeFe]-Hydrogenases", *Chemistry - A European Journal*, **2016**, accepted for publication.

- L. R. Almazahreh, F. Arrigoni, L. Bertini, H. Görls, G. Zampella, J. Talarmin, L. De Gioia, P. Schollhammer and W. Weigand, "Mechanisms of Proton Reduction Catalyzed by $[Fe_2(CO)_6\{\mu\text{-}(SCH_2)_2(R)P{=}O\}]$ (R = Ph, Et) Models", in preparation.

- X. Zhou, F. Arrigoni, B. E. Barton, G. M. Chambers, G. Zampella and T. B. Rauchfuss, "Preparation and Protonation of $Fe_2(pdt)(CNR)_6$, Electron-Rich Analogues of $Fe_2(pdt)(CO)_6$", *Inorganic Chemistry*, **2016**, 55 (7), 3401-3412.

- G. Filippi, F. Arrigoni, L. Bertini, L. De Gioia, and Giuseppe Zampella, "DFT Dissection of the Reduction Step in H_2 Catalytic Production by [FeFe]-Hydrogenase-Inspired Models: Can the Bridging Hydride Become More Reactive Than the Terminal Isomer?", *Inorganic Chemistry*, **2015**, 54 (19), 9529–9542.

- F. Arrigoni, L. Bertini, G. Filippi, L. De Gioia and G. Zampella, "Comparison of H_2 oxidation in [FeFe]-hydrogenases and biomimetic models highlights key stereoelectronic features for catalysis", in preparation.

- L. Bertini, M. Alberto, F. Arrigoni, L. De Gioia and G. Zampella, "On the photochemistry of $Fe_2(CO)_4(PMe_3)_2(\mu\text{-pdt})$, a [FeFe]-hydrogenase model. A DFT/TD-DFT investigation", *Physical Chemistry Chemical Physics*, **2016**, submitted.

Other publications:

- C. Greco, S. Sicolo, M.o Bruschi, L. Bertini, G. Zampella, G. Filippi, F. Arrigoni, L. De Gioia, "Towards biomimetic models of the reduced [FeFe]-hydrogenase that preserve the key structural features of the enzyme active site; a DFT investigation", *International Journal of Hydrogen Energy*, **2014**, 39 (32), 18565-18573.

- M. Bruschi, R. Breglia, F. Arrigoni, P. Fantucci, L. De Gioia, "Computational approaches to the prediction of the redox potentials of iron and copper bioinorganic systems", *International Journal of Quantum Chemistry*, **2016**, 116 (22), 1695–1705.
- W. Y. Chu, F. Arrigoni, C. P. Richers, E. R. Kahle, G. Zampella and T. B. Rauchfuss, "Imine-Centered Reactions in Imino-Phosphine Complexes of Iron Carbonyls", *Organometallics*, **2016**, 35 (17), 2782–2792.
- G. M. Chambers, F. Arrigoni, G. Zampella and Thomas B. Rauchfuss, "Effect of Pyramidalization of the $M_2(SR)_2$ Center: The Case of $(C_5H_5)_2Ni_2(SR)_2$", *Organometallics*, **2016**, 35 (5), 836–846.

List of abbreviations

adt^{Bn}	Benzyl azadithiolate
adt	Azadithiolate
bdt	Benzodithiolate
edt	Ethanedithiolate
odt	Oxadithiolate
pdt	Propanedithiolate
dmpe	1,2-Bis(dimethylphosphino)ethane
dppe	1,2-Bis(diphenylphosphino)ethane
dppv	1,2-Bis(diphenylphosphino)vinyl
PMe_3	Trimethylphosphine
PEt_3	Triethylphosphine
$POMe_3$	Trimethyl phosphite
NHC	1,3-Dimethyl-2,3-dihydro-1H-imidazole
CNMe	Methyl isocyanide
Fc	Ferrocene
Fc*	Decamethylferrocene
TFA	Trifluoroacetic acid
THF	Tetrahydrofuran
MeCN	Acetonitrile
HOTf	Triflic acid

Bibliography

[1] R. H. Holm and E. I. Solomon. Introduction : Bioinorganic Enzymology II. *Chemical Reviews*, 114:3367–3368, 2014.

[2] K. J. Waldron and N. J. Robinson. How do bacterial cells ensure that metalloproteins get the correct metal? *Nature reviews. Microbiology*, 7(1):25–35, 2009.

[3] A. J. Thomson and H. B. Gray. Bio-inorganic chemistry. *Current Opinion in Chemical Biology*, 2(2):155–158, 1998.

[4] J. C. Gordon and G. J. Kubas. Perspectives on how nature employs the principles of organometallic chemistry in dihydrogen activation in hydrogenases. *Organometallics*, 29(21):4682–4701, 2010.

[5] A. M. Appel, J. E. Bercaw, A. B. Bocarsly, H. Dobbek, D. L. Dubois, M. Dupuis, J. G. Ferry, E. Fujita, R. Hille, P.J A Kenis, C.A. Kerfeld, Robert H. Morris, Charles H F Peden, Archie R. Portis, Stephen W. Ragsdale, Thomas B. Rauchfuss, Joost N H Reek, Lance C. Seefeldt, Rudolf K. Thauer, and Grover L. Waldrop. Frontiers, opportunities, and challenges in biochemical and chemical catalysis of CO2 fixation. *Chemical Reviews*, 113(8):6621–6658, 2013.

[6] F. Meyer and W. B. Tolman. Forums on Small-Molecule Activation: from biological principles to energy applications. *Inorganic Chemistry*, 54(11):5039–5039, 2015.

[7] W. Lubitz and W. Tumas. Hydrogen: An overview. *Chemical Reviews*, 107(10):3900–3903, 2007.

[8] M. Z. Jacobson. Cleaning the Air and Improving Health with Hydrogen Fuel-Cell Vehicles. *Science*, 1901(2005):1901–5, 2014.

[9] J. C. Jones. Energy-return-on-energy-invested for hydrogen fuel from the steam reforming of natural gas. *Fuel*, 143(December 2014):631, 2015.

[10] M. Winter and R. J. Brodd. What are batteries, fuel cells, and supercapacitors? *Chemical Reviews*, 104(10):4245–4269, 2004.

[11] X. Cheng, Z. Shi, N. Glass, L. Zhang, J. Zhang, D. Song, Z. S. Liu, H. Wang, and J. Shen. A review of PEM hydrogen fuel cell contamination: Impacts, mechanisms, and mitigation. *Journal of Power Sources*, 165(2):739–756, 2007.

[12] J. A. Turner. Sustainable hydrogen production. *Science*, 305(5686):972–974, 2004.

[13] W. Lubitz, E. Reijerse, and M. van Gastel. [NiFe] and [FeFe] hydrogenases studied by advanced magnetic resonance techniques. *Chemical Reviews*, 107(10):4331–4365, 2007.

[14] W. Lubitz, H. Ogata, O. Rodiger, and E. Reijerse. Hydrogenases. *Chemical Reviews*, 114(8):4081–4148, 2014.

[15] C. Tard and C. J. Pickett. Structural and functional analogues of the active sites of the [Fe]-, [NiFe]-, and [FeFe]-hydrogenases. *Chemical Reviews*, 109(6):2245–2274, 2009.

[16] B. M. Hoffman, D. Lukoyanov, Z. Y. Yang, D. R. Dean, and L. C. Seefeldt. Mechanism of nitrogen fixation by nitrogenase: The next stage. *Chemical Reviews*, 114(8):4041–4062, 2014.

[17] J. M. Modak. Haber process for ammonia synthesis. *Resonance*, 7(8):69–77, 2002.

[18] Yi. Hu, C. C. Lee, and M. W. Ribbe. Vanadium nitrogenase: A two-hit wonder? *Dalton Transactions*, 41(4):1118–1127, 2012.

[19] K. R. Fixen, Y. Zheng, D. F. Harris, S. Shaw, Z. Y. Yang, D. R. Dean, L. C. Seefeldt, and C. S. Harwood. Light-driven carbon dioxide reduction to methane by nitrogenase in a photosynthetic bacterium. *Proceedings of the National Academy of Sciences of the United States of America*, 113(36):10163–10167, 2016.

[20] J. Qiao, Y. Liu, F. Hong, and J. Zhang. *A review of catalysts for the electroreduction of carbon dioxide to produce low-carbon fuels.*, volume 43. 2014.

[21] A. J. Martín, G. O. Larrazábal, and J. Pérez-Ramírez. Towards sustainable fuels and chemicals through the electrochemical reduction of CO2: lessons from water electrolysis. *Green Chem.*, 17(12):5114–5130, 2015.

[22] Q. Liu, L. Wu, R. Jackstell, and M. Beller. Using carbon dioxide as a building block in organic synthesis. *Nature communications*, 6:5933, 2015.

[23] P. G. Jessop, F. Joó, and C. Ch. Tai. Recent advances in the homogeneous hydrogenation of carbon dioxide. *Coordination Chemistry Reviews*, 248(21-24):2425–2442, 2004.

[24] M. Fontecave and V. Artero. Bioinspired catalysis at the crossroads between biology and chemistry: A remarkable example of an electrocatalytic material mimicking hydrogenases. *Comptes Rendus Chimie*, 14(4):362–371, 2011.

[25] L. C. Seefeldt, B. M. Hoffman, and D. R. Dean. Mechanism of Mo-dependent nitrogenase. *Annual Review of Biochemistry*, (78):701–722, 2009.

[26] J. C. Fontecilla-Camps, A. Volbeda, C. Cavazza, and Y. Nicolet. Structure/function relationships of [NiFe]- and [FeFe]-hydrogenases. *Chemical Reviews*, 107(10):4273–4303, 2007.

[27] J. Meyer. [FeFe] hydrogenases and their evolution: A genomic perspective. *Cellular and Molecular Life Sciences*, 64(9):1063–1084, 2007.

[28] P. M. Vignais. Classification and phylogeny of hydrogenases. *FEMS Microbiology Reviews*, 25, 2001.

[29] P. M. Vignais and B. Billoud. Occurrence, classification, and biological function of hydrogenases: an overview. *Chemical Reviews*, 107(10):4206–4272, 2007.

[30] C. Zirngibl, W. Van Dongen, B. Schworer, R. Von Bünau, M. Richter, A. Klein, and R. K. Thauer. H2-forming methylenetetrahydromethanopterin dehydrogenase, a novel type of hydrogenase without iron-sulfur clusters in methanogenic archaea. *European journal of biochemistry / FEBS*, 208(2):511–20, 1992.

[31] J. C Fontecilla-Camps, P. Amara, C. Cavazza, Y. Nicolet, and A. Volbeda. Structure-function relationships of anaerobic gas-processing metalloenzymes. *Nature*, 460(7257):814–22, 2009.

[32] D. Barford, K. Das, and M. P. Egloff. The structure and mechanism of protein phosphatases: insights into catalysis and regulation. *Annual Review of Biophysics and Biomolecular Structure*, 27(1):133–164, 1998.

[33] C. Madden, M. D. Vaughn, I. Díez-p, K. A. Brown, P. W. King, D. Gust, Ana L Moore, and Thomas A Moore. Catalytic turnover of [FeFe]hydrogenase based on single-molecule imaging. pages 1577–1582, 2012.

[34] M. Demuez, L. Cournac, O. Guerrini, P. Soucaille, and L. Girbal. Complete activity profile of Clostridium acetobutylicum [FeFe]-hydrogenase and kinetic parameters for endogenous redox partners. *FEMS Microbiology Letters*, 275(1):113–121, 2007.

[35] M. Winkler, J. Esselborn, and T. Happe. Molecular basis of [FeFe]-hydrogenase function An insight into the complex interplay between protein and catalytic cofactor. *Biochimica et Biophysica Acta - Bioenergetics*, 1827(8-9):974–985, 2013.

[36] J. W. Peters, W. N. Lanzilotta, B. J. Lemon, and L. C. Seefeldt. X-ray Crystal Structure of the Fe-Only Hydrogenase (Cpl) from Clostridium pasteurianum to 1.8 Angstrom Resolution. *Science*, 282(4):1853–1858, 1998.

[37] Y. Nicolet, B.J. Lemon, J. C. Fontecilla-Camps, and J. W. Peters. A novel FeS cluster in Fe-only hydrogenases. *Trends in Biochemical Sciences*, 25(3):138–143, 2000.

[38] Y. Nicolet, C. Piras, P. Legrand, C. E. Hatchikian, and J. C. Fontecilla-Camps. Desulfovibrio desulfuricans iron hydrogenase: The structure shows unusual coordination to an active site Fe binuclear center. *Structure*, 7(1):13–23, 1999.

[39] D. W. Mulder, E. M. Shepard, J. E. Meuser, N. Joshi, P. W. King, M. C. Posewitz, J. B. Broderick, and J. W. Peters. Insights into [FeFe]-hydrogenase structure, mechanism, and maturation. *Structure*, 19(8):1038–1052, 2011.

[40] S. T. Stripp, G. Goldet, C. Brandmayr, O. Sanganas, K. A. Vincent, M. Haumann, F. A. Armstrong, and T. Happe. How oxygen attacks [FeFe] hydrogenases from photosynthetic organisms. *Proceedings of the National Academy of Sciences of the United States of America*, 106(41):17331–6, 2009.

[41] A. J. Pierik, M. Hulstein, W. R. Hagen, and S. P. J. Albracht. A low-spin iron with CN and CO as intrinsic ligands forms the core of the active site in [Fe]-hydrogenases. *European Journal of Biochemistry*, 258(2):572–578, 1998.

[42] M. Bruschi, C. Greco, P. Fantucci, and L. De Gioia. Structural and electronic properties of the [FeFe] hydrogenase H-cluster in different redox and protonation states. A DFT investigation. *Inorganic Chemistry*, 47(13):6056–6071, 2008.

[43] P. Knorzer, A. Silakov, C. E. Foster, F. A. Armstrong, W. Lubitz, and T. Happe. Importance of the protein framework for catalytic activity of [FeFe]-hydrogenases. *Journal of Biological Chemistry*, 287(2):1489–1499, 2012.

[44] Y. Nicolet, A. L. De Lacey, X. Vernde, V. M. Fernandez, E. C. Hatchikian, and J. C. Fontecilla-Camps. Crystallographic and FTIR spectroscopic evidence of changes in Fe coordination upon reduction of the active site of the Fe-only hydrogenase from Desulfovibrio desulfuricans. *Journal of the American Chemical Society*, 123(8):1596–1601, 2001.

[45] D. Sezer, M. J. Prandolini, and T. F. Prisner. Dynamic nuclear polarization coupling factors calculated from molecular dynamics simulations of a nitroxide radical in water. *Physical chemistry chemical physics*, 11(31):6626–6637, 2009.

[46] M. Winkler, S. Kawelke, and T. Happe. Light driven hydrogen production in protein based semi-artificial systems. *Bioresource Technology*, 102(18):8493–8500, 2011.

[47] D. S. Patil, J. J. Moura, S. H. He, M. Teixeira, B. C. Prickril, D. V. DerVartanian, H. D. Peck, J. LeGall, and B. H. Huynh. EPR-detectable redox centers of the periplasmic hydrogenase from Desulfovibrio vulgaris. *Journal of Biological Chemistry*, 263(35):18732–18738, 1988.

[48] A. J. Pierik, W. R. Hagen, J. S. Redeker, R. B G Wolbert, M. Boersma, M. F J M Verhagen, H. Grande, C. Veeger, P. H A Mutsaers, R. H. Sands, and W. R. Dunham. Redox properties of the iron-sulfur clusters in activated Fe-hydrogenase from Desulfovibrio vulgaris. *European Journal of Biochemistry*, 209(1):63–72, 1992.

[49] Z. Liu and P. Hu. A Density Functional Theory study on the active center of Fe-only hydrogenase: Characterization and electronic structure of the redox states. *Journal of the American Chemical Society*, 124(15):5175–5182, 2002.

[50] C. E. Foster, T. Krämer, A. F. Wait, A. Parkin, D. P. Jennings, T. Happe, J. E. McGrady, and F. A. Armstrong. Inhibition of [FeFe]-hydrogenases by formaldehyde and wider mechanistic implications for biohydrogen activation. *Journal of the American Chemical Society*, 134(17):7553–7557, 2012.

[51] A. S. Pereira, P. Tavares, I. Moura, J. J G Moura, and B. H. Huynh. Mossbauer characterization of the iron-sulfur clusters in Desulfovibrio vulgaris hydrogenase. *Journal of the American Chemical Society*, 123(12):2771–2782, 2001.

[52] A. Silakov, E. J. Reijerse, S. P. J. Albracht, E. C. Hatchikian, and W. Lubitz. The electronic structure of the H-cluster in the FeFe] -hydrogenase from Desulfovibrio desulfuricans. *J. Am. Chem. Soc.*, 129(2):11447–11458, 2007.

[53] B. J. Lemon and J. W. Peters. Binding of exogenously added carbon monoxide at the active ste of the iron-only hydrogenase (CpI) from Clostridium pasteurianum. *Biochemistry*, 38(40):12969–12973, 1999.

[54] W. Roseboom, A. L. De Lacey, V. M. Fernandez, E. C. Hatchikian, and S. P. J. Albracht. The active site of the [FeFe]-hydrogenase from Desulfovibrio desulfuricans. Redox properties, light sensitivity and CO-ligand exchange as observed by infrared spectroscopy. *Journal of Biological Inorganic Chemistry*, 11(1):102–118, 2006.

[55] A. Adamska, A. Silakov, C. Lambertz, O. Rüdiger, T. Happe, E. Reijerse, and W. Lubitz. Identification and characterization of the "super-reduced" state of the H-cluster in [FeFe]-hydrogenase: a new building block for the catalytic cycle? *Angewandte Chemie - International Edition*, 51(46):11458–11462, 2012.

[56] A. Silakov, C. Kamp, E. Reijerse, T. Happe, and W. Lubitz. Spectroelectrochemical characterization of the active site of the [FeFe] hydrogenase HydA1 from Chlamydomonas reinhardtii. *Biochemistry*, 48(33):7780–7786, 2009.

[57] D. W. Mulder, M. W. Ratzloff, E. M. Shepard, A. S. Byer, S. M. Noone, J. W. Peters, J. B. Broderick, and P. W. King. EPR and FTIR analysis of the mechanism of H2 activation by [FeFe]-hydrogenase hyda1 from chlamydomonas reinhardtii. *Journal of the American Chemical Society*, 135(18):6921–6929, 2013.

[58] O. F. Erdem, L. Schwartz, M. Stein, A. Silakov, S. Kaur-Ghumaan, P. Huang, S. Ott, E. J. Reijerse, and W. Lubitz. A model of the [FeFe] hydrogenase active site with a biologically relevant azadithiolate bridge: a spectroscopic and theoretical investigation. *Angewandte Chemie - International Edition*, 50(6):1439–1443, 2011.

[59] M. Bruschi, G. Zampella, P. Fantucci, and L. De Gioia. DFT investigations of models related to the active site of [NiFe]- and [Fe]-hydrogenases. *Coordination Chemistry Reviews*, 249(15-16 SPEC. ISS.):1620–1640, 2005.

[60] S. J. Borg, J. W. Tye, M. B. Hall, and S. P. Best. Assignment of molecular structures to the electrochemical reduction products of diiron compounds related to [FeFe]-hydrogenase : a combined experimental and Density Functional Theory study. *Structure*, 46(2):384–394, 2007.

[61] I. Dance. Structural variability of the active site of Fe-only hydrogenase and its hydrogenated forms. *Chemical Communications (Cambridge)*, 17(17):1655–1656, 1999.

[62] Z. Cao and M. B. Hall. Modeling the active sites in metalloenzymes. Density functional calculations on models for [Fe]-hydrogenase: Structures and vibrational frequencies of the observed redox forms and the reaction mechanism at the diiron active center. *Journal of the American Chemical Society*, 123(16):3734–3742, 2001.

[63] C. V. Popescu and E. Münck. Electronic structure of the H-cluster in [FeFe]-hydrogenases. *Journal of the American Chemical Society*, 121(5):15054–15061, 1999.

[64] M. Bruschi, P. Fantucci, and L. De Gioia. DFT investigation of structural, electronic, and catalytic properties of diiron complexes related to the [2Fe]-hydrogenases active site. *Inorganic Chemistry*, 41(6):138–143, 2002.

[65] M. Bruschi, P. Fantucci, and L. De Gioia. Density functional theory investigation of the active site of [Fe]-hydrogenases: effects of redox state and ligand characteristics on structural, electronic, and reactivity properties of complexes related to the [2Fe]H subcluster. *Inorganic chemistry*, 42(15):4773–81, 2003.

[66] T. B. Rauchfuss. Diiron azadithiolates as models for the [FeFe]-hydrogenase active site and paradigm for the role of the second coordination sphere. *Accounts of Chemical Research*, 48(7):2107–2116, 2015.

[67] M.Y. Darensbourg, E. J. Lyon, X. Zhao, and I. P. Georgakaki. The organometallic active site of [Fe]hydrogenase: models and entatic states. *Proceedings of the National Academy of Sciences of the United States of America*, 100(7):3683–8, 2003.

[68] T. B. Rauchfuss. Diiron azadithiolates as models for the [FeFe]-hydrogenase active site and paradigm for the role of the second coordination sphere. *Accounts of Chemical Research*, 48(7):2107–2116, 2015.

[69] C. J. Curtis, A. Miedaner, R. Ciancanelli, W. W. Ellis, B. C. Noll, M. R. DuBois, and D. L. DuBois. [Ni(Et2PCH2NMeCH2PEt2)2]2+ as a functional model for hydrogenases. *Inorganic Chemistry*, 41(1):216–227, 2003.

[70] A. R. Finkelmann, M.T. Stiebritz, and M. Reiher. Inaccessibility of the μ-hydride species in [FeFe] hydrogenases. *Chemical Science*, 5(1):215–221, 2013.

[71] G. Zampella, P. Fantucci, and L. De Gioia. DFT characterization of the reaction pathways for terminal- to mu-hydride isomerisation in synthetic models of the [FeFe]-hydrogenase active site. *Chemical Communications*, 46(46):8824–8826, 2009.

[72] S. J. Ferguson. Nitrogen cycle enzymology. *Current Opinion in Chemical Biology*, 2(2):182–193, 1998.

[73] B. A. MacKay and M. D. Fryzuk. Dinitrogen coordination chemistry: on the biomimetic borderlands. *Chemical Reviews*, 104(2):385–401, 2004.

[74] H. P. Jia and E. A. Quadrelli. Mechanistic aspects of dinitrogen cleavage and hydrogenation to produce ammonia in catalysis and organometallic chemistry: relevance of metal hydride bonds and dihydrogen. *Chemical Society Reviews*, 43(2):547–564, 2014.

[75] B. Thamdrup. New pathways and processes in the global nitrogen cycle. *Annual Review of Ecology, Evolution, and Systematics*, 43(1):407–428, 2012.

[76] D. E. Canfield, A. N. Glazer, and P. G. Falkowski. The evolution and future of earth's nitrogen cycle. *Science*, 330(6001):192–196, 2010.

[77] Q. Cheng. Perspectives in biological nitrogen fixation research. *Journal of Integrative Plant Biology*, 50(7):786–798, 2008.

[78] P. C. Dos Santos, Z. Fang, S. W. Mason, J. C. Setubal, and R. Dixon. Distribution of nitrogen fixation and nitrogenase-like sequences amongst microbial genomes. *BMC Genomics*, 13(1):162, 2012.

[79] S. E. McGlynn, E. S. Boyd, J. W. Peters, and V. J. Orphan. Classifying the metal dependence of uncharacterized nitrogenases. *Frontiers in Microbiology*, 3(JAN):1–8, 2012.

[80] D. Burk, H. Lineweaver, and C. K. Horner. The specific influence of acidity on the mechanism of nitrogen fixation by azotobacter. *Journal of bacteriology*, 27(4):325–40, 1934.

[81] D. Burk. Azotase and nitrogenase in azotobacter. *Ergebnisse Enzym- forsch.*, 3:23–56, 1934.

[82] N. Gruber and J. N. Galloway. An Earth-system perspective of the global nitrogen cycle. *Nature*, 451(7176):293–6, 2008.

[83] R. R. Eady. Structureâfunction relationships of alternative nitrogenases. *Chemical Reviews*, 96(7):3013–3030, 1996.

[84] B. K. Burgess and D. J. Lowe. Mechanism of molybdenum nitrogenase. *Chemical Reviews*, 96(7):2983–3012, 1996.

[85] J. Kim, D. Woo, and D. C. Rees. X-ray crystal structure of the nitrogenase molybdenum-iron protein from Clostridium pasteurianum at 3.0 resolution. *Biochemistry*, 32(28):7104–7115, 1993.

[86] J. Kim and D. C. Rees. Structural models for the metal centers in the nitrogenase molybdenum-iron protein. *Science*, 257(5077):1677–82, 1992.

[87] J. S. Kim and D.C. Rees. Crystallographic structure and functional implications of the nitrogenase molybdenum iron protein from Azotobacter-Vinelandii. *Nature*, 360(6404):553–560, 1992.

[88] M. K. Chan, J. Kim, and D. C. Rees. The nitrogenase FeMo-cofactor and P-cluster pair: 2.2 A resolution structures. *Science*, 260(5109):792–794, 1993.

[89] D. Rehder. Vanadium nitrogenase. *Journal of Inorganic Biochemistry*, 80(1-2):133–136, 2000.

[90] L Mortenson. Components of cell-free extracts of clostridium pasteurianum required for ATP-dependent H2 evolution from dithionite and for N2 fixation. *Biochimica et Biophysica Acta*, 127(1):18–25, 1966.

[91] W. A. Bulen and J. R. LeComte. The nitrogenase system from Azotobacter: two-enzyme requirement for N2 reduction, ATP-dependent H2 evolution, and ATP hydrolysis. *Proceedings of the National Academy of Sciences of the United States of America*, 56(3):979–86, 1966.

[92] R. V. Hageman and R. H. Burris. Nitrogenase and nitrogenase reductase associate and dissociate with each catalytic cycle. *Proceedings of the National Academy of Sciences of the United States of America*, 75(6):2699–702, 1978.

[93] T. Spatzal, S. L. A. Andrade, and O. Einsle. The iron-molybdenum cofactor of nitrogenase. *Iron-Sulfur Clusters in Chemistry and Biology*, 90(8):89–106, 2014.

[94] V. K. Shah and W. J. Brill. Isolation of an iron-molybdenum cofactor from nitrogenase. *Proceedings of the National Academy of Sciences of the United States of America*, 74(8):3249–3253, 1977.

[95] D. R. Dean, J. T. Bolin, and L. Zheng. Nitrogenase metalloclusters: structures, organization, and synthesis. *Journal of Bacteriology*, 175(21):6737–6744, 1993.

[96] L. Ma, M. A. Brosius, and B. K. Burgess. Construction of a form of the MoFe protein of nitrogenase that accepts electrons from the Fe protein but does not reduce substrate. *Journal of Biological Chemistry*, 271(18):10528–10532, 1996.

[97] D. J. Lowe, K. Fisher, and R. N. Thorneley. Klebsiella pneumoniae nitrogenase: pre-steady-state absorbance changes show that redox changes occur in the MoFe protein that depend on substrate and component protein ratio; a role for P-centres in reducing dinitrogen? *Biochemical Journal*, 292(Pt 1):93–98, 1993.

[98] S. Duval, K. Danyal, S. Shaw, A. K. Lytle, D. R. Dean, B. M. Hoffman, E. Antony, and L. C. Seefeldt. Electron transfer precedes ATP hydrolysis during nitrogenase catalysis. *Proceedings of the National Academy of Sciences of the United States of America*, 110(41):16414–9, 2013.

[99] L. C. Seefeldt, B. M. Hoffman, and D. R. Dean. Electron transfer in nitrogenase catalysis. *Current Opinion in Chemical Biology*, 16(1-2):19–25, 2012.

[100] M. C. Durrant. An atomic-level mechanism for molybdenum nitrogenase. Proton reduction, inhibition of dinitrogen reduction by dihydrogen, and the HD formation reaction. *Biochemistry*, 41(47):13946–13955, 2002.

[101] B. Hinnemann and J. K. Norskov. Chemical activity of the nitrogenase FeMo cofactor with a central nitrogen ligand: Density Functional study. *Journal of the American Chemical Society*, 126(12):3920–3927, 2004.

[102] J. B. Varley and J. K. Nørskov. First-principles calculations of Fischer-Tropsch processes catalyzed by nitrogenase enzymes. *ChemCatChem*, 5(3):732–736, 2013.

[103] T. Lovell, T. Liu, D. A. Case, and L. Noodleman. Structural, spectroscopic, and redox consequences of a central ligand in the femoco of nitrogenase: A density functional theoretical study. *Journal of the American Chemical Society*, 125(27):8377–8383, 2003.

[104] F. Neese. The Yandulov/Schrock cycle and the nitrogenase reaction: Pathways of nitrogen fixation studied by density functional theory. *Angewandte Chemie - International Edition*, 45(2):196–199, 2005.

[105] T. V. Harris and R. K. Szilagyi. Comparative assessment of the composition and charge state of nitrogenase FeMo-cofactor. *Inorganic Chemistry*, 50(11):4811–4824, 2011.

[106] T. Spatzal, M. Aksoyoglu, L. Zhang, S. L. A. Andrade, E. Schleicher, S. Weber, D. C. Rees, and O. Einsle. Evidence for Interstitial Carbon in nitrogenase FeMo cofactor. *Science*, 334(November):940–940, 2011.

[107] K. M. Lancaster, M. Roemelt, P. Ettenhuber, Y. Hu, M. W. Ribbe, F. Neese, U. Bergmann, and S. DeBeer. X-ray emission spectroscopy evidences a central carbon in the nitrogenase iron-molybdenum cofactor. *Science*, 334(6058):974–977, 2011.

[108] K. M. Lancaster, Y. Hu, U. Bergmann, M. W. Ribbe, and S. Debeer. X-ray spectroscopic observation of an interstitial carbide in FeMoco precursor. *Journal of the American Chemical Society*, 135(2):610–612, 2013.

[109] J. A. Wiig, C. C. Lee, Y. Hu, and M. W. Ribbe. Tracing the interstitial carbide of the nitrogenase cofactor during substrate turnover. *Journal of the American Chemical Society*, 135(13):4982–4983, 2013.

[110] T. C. Yang, N. K. Maeser, M. Laryukhin, H. I. Lee, D. R. Dean, L. C. Seefeldt, and B. M. Hoffman. The interstitial atom of the nitrogenase FeMo-cofactor: ENDOR and ESEEM evidence that it is not a nitrogen. *Journal of the American Chemical Society*, 127(37):12804–12805, 2005.

[111] T. V. Harris and R. K. Szilagyi. Comparative assessment of the composition and charge state of nitrogenase FeMo-co. *Inorganic Chemistry*, 50(Iv):4811–4824, 2011.

[112] W. H. Orme-Johnson, W. D. Hamilton, T. L. Jones, M. Y. Tso, R. H. Burris, V. K. Shah, and W. J. Brill. Electron paramagnetic resonance of nitrogenase and nitrogenase components from Clostridium pasteurianum and Azotobacter vinelandii. *Proceedings of the National Academy of Sciences of the United States of America*, 69(11):3142–3145, 1972.

[113] R. R. Eady. Current status of structure function relationships of vanadium nitrogenase. *Coordination Chemistry Reviews*, 237(1-2):23–30, 2003.

[114] A. W. Fay, M. A. Blank, C. C. Lee, Y. Hu, K. O. Hodgson, B. Hedman, and M.W. Ribbe. Characterization of isolated nitrogenase FeVco. *Journal of the American Chemical Society*, 132(36):12612–12618, 2010.

[115] P. C. Dos Santos, R. Y. Igarashi, H. I. Lee, B. M. Hoffman, L. C. Seefeldt, and D. R. Dean. Substrate interactions with the nitrogenase active site. *Accounts of Chemical Research*, 38(3):208–214, 2005.

[116] L. C. Seefeldt, B. M. Hoffman, and D. R. Dean. Mechanism of Mo-dependent nitrogenase. *Annual Review of Biochemistry*, 78:701–722, 2009.

[117] B. M. Hoffman, D. R. Dean, and L. C. Seefeldt. Climbing nitrogenase: Toward a mechanism of enzymatic nitrogen fixation. *Accounts of Chemical Research*, 42(5):609–619, 2009.

[118] P. E. Wilson, A. C. Nyborg, and G. D. Watt. Duplication and extension of the Thorneley and Lowe kinetic model for Klebsiella pneumoniae nitrogenase catalysis using a MATHEMATICA software platform. *Biophysical Chemistry*, 91(3):281–304, 2001.

[119] P. M. Vignais, A. Colbeau, J. C. Willison, and Y. Jouanneau. Hydrogenase, nitrogenase, and hydrogen metabolism in the photosynthetic bacteria. *Advances in Microbial Physiology*, 26:155–234, 1985.

[120] B. M. Hoffman, D. Lukoyanov, D. R. Dean, and L. C. Seefeldt. Nitrogenase: A draft mechanism. *Accounts of Chemical Research*, 46(2):587–595, 2013.

[121] L. C. Seefeldt, Z. Y. Yang, S. Duval, and D. R. Dean. Nitrogenase reduction of carbon-containing compounds. *Biochimica et Biophysica Acta - Bioenergetics*, 1827(8-9):1102–1111, 2013.

[122] C. C. Lee, Y. Hu, and M. W. Ribbe. Vanadium Nitrogenase Reduces CO. *Science*, 329(5992):642, 2010.

[123] C. C. Lee, Y. Hu, and M. W. Ribbe. Unique features of the nitrogenase VFe protein from Azotobacter vinelandii. *Proceedings of the National Academy of Sciences*, 106(23):9209–9214, 2009.

[124] Z. Y. Yang, V. R. Moure, D. R. Dean, and L. C. Seefeldt. Carbon dioxide reduction to methane and coupling with acetylene to form propylene catalyzed by remodeled nitrogenase. *Proceedings of the National Academy of Sciences*, 109(48):19644–19648, 2012.

[125] J. G. Rebelein, Y. Hu, and M. W. Ribbe. Widening the product profile of carbon dioxide reduction by vanadium nitrogenase. *ChemBioChem*, 16(14):1993–1996, 2015.

[126] Y. Hu. Extending the carbon chain: hydrocarbon formation catalyzed by vanadium/molybdenum nitrogenases. *Science*, (August):753–756, 2011.

[127] T. R. Simmons, G. Berggren, M. Bacchi, M. Fontecave, and V. Artero. Mimicking hydrogenases: from biomimetics to artificial enzymes. *Coordination Chemistry Reviews*, 270-271(1):127–150, 2014.

[128] J. Hwang, Y. Jeong, J. M. Park, K. H. Lee, J. W. Hong, and J. Choi. Biomimetics: Forecasting the future of science, engineering, and medicine. *International Journal of Nanomedicine*, 10:5701–5713, 2015.

[129] J. F. V. Vincent, O. A. Bogatyreva, N. R. Bogatyrev, A. Bowyer, and A. Pahl. Biomimetics: its practice and theory. *Journal of the Royal Society, Interface / the Royal Society*, 3(9):471–82, 2006.

[130] S. Groysman and R. H. Holm. Biomimetic chemistry of iron, nickel, molybdenum, and tungsten in sulfur-ligated protein sites. *Biochemistry*, 48(11):2310–2320, 2009.

[131] S. Kaur-Ghumaan and M. Stein. [NiFe] hydrogenases: how close do structural and functional mimics approach the active site? *Dalton Transactions*, 43(25):9392, 2014.

[132] S. Canaguier, V. Artero, and M. Fontecave. Modelling [NiFe]-hydrogenases: nickel-based electrocatalysts for hydrogen production. *Dalton Transactions*, 25(3):315–325, 2008.

[133] Y. Oudart, V. Artero, J. Pe, and M. Fontecave. [Ni(xbsms)Ru(CO)2Cl2]: A bioinspired nickelâruthenium functional model of [NiFe] hydrogenase. *Society*, 45(11):4334–4336, 2006.

[134] Y. Oudart, V. Artero, J. Pécaut, C. Lebrun, and M. Fontecave. Dinuclear nickel-ruthenium complexes as functional bio-inspired models of [NiFe] hydrogenases. *European Journal of Inorganic Chemistry*, 18(18):2613–2626, 2007.

[135] M. A. Reynolds, T. B. Rauchfuss, and S. R. Wilson. Ruthenium derivatives of NiS2N2 complexes as analogues of bioorganometallic reaction centers. *Organometallics*, 22(8):1619–1625, 2003.

[136] S. Ogo, K. Ichikawa, T. Kishima, T. Matsumoto, H. Nakai, K. Kusaka, and T. Ohhara. A functional [NiFe]hydrogenase mimic that catalyzes electron and hydride transfer from H2. *Science*, 339(6120):682–4, 2013.

[137] T. Liu, D. L. Dubois, and R. M. Bullock. An iron complex with pendent amines as a molecular electrocatalyst for oxidation of hydrogen. *Nature chemistry*, 5(3):228–233, 2013.

[138] H. Reihlen, A. Gruhl, and G. Hessling. Uber den photochemischen und oxydativen Abbau von Carbonylen. *Justus Liebigs Annalen der Chemie*, 472(1):268–287, 1929.

[139] D. Seyferth, G. B. Womack, M. K. Gallagher, M. Cowie, B. W. Hames, J. P. Fackler Jr., and M. Mazany. Novel anionic rearrangements in hexacarbonyldiiron complexes of chelating organosulfur ligands. *Organometallics*, 6(2):283–294, 1987.

[140] W. Hieber and P. Spacu. Uber metallcarbonyle. XXVI. Einwirkung organischer schwefelverbindungen auf die carbonyle von eisen und kobalt. *Zeitschrift fur anorganische und allgemeine Chemie*, 4:353–364, 1937.

[141] K. Fauvel, R. Mathieu, and R. Poilblanc. Protonation of the metal-metal bond in [mu-(SCH3)Fe(CO)2L]2 complexes (L = P(CH3)3-x(C6H5)x). Experimental evidence of the variation of nucleophilicity of the metal-metal bond with donor properties of phosphorus ligands. *Inorganic Chemistry*, 15(4):976–978, 1976.

[142] E. J. Lyon, I. P. Georgakaki, J. H. Reibenspies, and M. Y. Darensbourg. Carbon monoxide and cyanide ligands in a classical organometallic complex model for Fe-only hydrogenase. *Angewandte Chemie - International Edition*, 38(21):3178–3180, 1999.

[143] R. Ch, M. Schmidt, S. M. Contakes, and T. B. Rauchfuss. First generation analogues of the binuclear site in the Fe-only hydrogenases: Fe2(mu-SR)2(CO4)(CN)22-. *Journal of the American Chemical Society*, 121(13):9736–9737, 1999.

[144] A. Le Cloirec, S. P. Best, S. Borg, S. C. Davies, D. J. Evans, L. Hughes, and C. J. Pickett. A di-iron dithiolate possessing structural elements of the carbonyl/cyanide sub-site of the H-centre of Fe-only hydrogenase. *Chemical Communications*, 1(c):2285–2286, 1999.

[145] J. D. Lawrence, H. Li, T. B. Rauchfuss, M. Bonard, and M. M. Rohmer. Diiron azadithiolates as models for the iron-only hydrogenase active site: Synthesis, structure, and stereoelectronics. *Angewandte Chemie - International Edition*, 40(9):1768–1771, 2001.

[146] L. C. Song, Z. Y. Yang, H. Z. Bian, and Q. M. Hu. Novel single and double diiron oxadithiolates as models for the active site of [Fe]-only hydrogenases. *Organometallics*, 23(13):3082–3084, 2004.

[147] Z. Wang, J. H. Liu, C. J. He, S. Jiang, B. Åkermark, and L. C. Sun. Azadithiolates cofactor of the iron-only hydrogenase and its PR3-monosubstituted derivatives: synthesis, structure, electrochemistry and protonation. *Journal of Organometallic Chemistry*, 692(24):5501–5507, 2007.

[148] W. B. Dong, M. Wang, X. Y. Liu, K. Jin, G. H. Li, F. J. Wang, and L. C. Sun. An insight into the protonation property of a diiron azadithiolate complex pertinent to the active site of Fe-only hydirogenases. *Chemical Communications*, 2(3):305–307, 2006.

[149] G. Si, W. G. Wang, H. Y. Wang, C. H. Tung, and L. Z. Wu. Facile synthesis and functionality-dependent electrochemistry of Fe-only hydrogenase mimics. *Inorganic Chemistry*, 47(18):8101–8111, 2008.

[150] A. K. Justice, L. De Gioia, M. J. Nilges, T. B. Rauchfuss, S. R. Wilson, and G. Zampella. Redox and structural properties of mixed-valence models for the active site of the [FeFe]-hydrogenase: Progress and challenges. *Inorganic Chemistry*, 47(16):7405–7414, 2008.

[151] B. E. Barton and T. B. Rauchfuss. Terminal hydride in [FeFe]-hydrogenase model has lower potential for H2 production than the isomeric bridging hydride. *Inorganic Chemistry*, 47(7):2261–2263, 2008.

[152] F. Gloaguen, J. D. Lawrence, T. B. Rauchfuss, M. Bénard, and M. M. Rohmer. Bimetallic carbonyl thiolates as functional models for Fe-only hydrogenases. *Inorganic Chemistry*, 41(25):6573–6582, 2002.

[153] R. Mejia-Rodriguez, D. Chong, J. H. Reibenspies, M. P. Soriaga, and M. Y. Darensbourg. The hydrophilic phosphatriazaadamantane ligand in the development of H2 production electrocatalysts: Iron hydrogenase model complexes. *Journal of the American Chemical Society*, 126(38):12004–12014, 2004.

[154] G. A. N. Felton, A. K. Vannucci, J. Chen, L. T. Lockett, N. Okumura, B. J. Petro, U. I. Zakai, D. H. Evans, R. S. Glass, and D. L. Lichtenberger. Hydrogen generation from weak acids: Electrochemical and computational studies of a diiron hydrogenase mimic. *Journal of the American Chemical Society*, 129(41):12521–12530, 2007.

[155] N. Wang, M. Wang, T. Liu, P. Li, T. Zhang, M. Y. Darensbourg, and L. Sun. CO-migration in the ligand substitution process of the chelating diphosphite diiron complex (mu-pdt)[Fe(CO)3][Fe(CO){(EtO) 2PN(Me)P(OEt)2}]. *Inorganic Chemistry*, 47(15):6948–6955, 2008.

[156] M. T. Olsen, B. E. Barton, and T. B. Rauchfuss. Hydrogen activation by biomimetic diiron dithiolates. *Inorganic Chemistry*, 48(16):7507–7509, 2009.

[157] C. M. Thomas, T. Liu, M. B. Hall, and M. Y. Darensbourg. Series of mixed valent Fe(II)Fe(I) complexes that model the Hox state of [FeFe] hydrogenase : redox properties, Density-Functional Theory investigation , and reactivities with extrinsic CO. *Inorganic Chemistry*, 47(15):7009–7024, 2008.

[158] J. D. Lawrence, T. B. Rauchfuss, and S. R. Wilson. New class of diiron dithiolates related to the Fe-only hydrogenase active site: Synthesis and characterization of [Fe2(SR)2(CNME)7]2+. *Inorganic Chemistry*, 41(24):6193–6195, 2002.

[159] J. W. Tye, J. Lee, H. W. Wang, R. Mejia-Rodriguez, J. H. Reibenspies, M. B. Hall, and M. Y. Darensbourg. Dual electron uptake by simultaneous iron and ligand reduction in an N-heterocyclic carbene substituted [FeFe] hydrogenase model compound. *Inorganic Chemistry*, 44(16):5550–5552, 2005.

[160] F. Gloaguen and T. B. Rauchfuss. Small molecule mimics of hydrogenases: hydrides and redox. *Chemical Society Reviews*, 38(1):100–108, 2009.

[161] F. Gloaguen, J. D. Lawrence, and T. B. Rauchfuss. Biomimetic hydrogen evolution catalyzed by an iron carbonyl thiolate. *Journal of the American Chemical Society*, 123(38):9476–9477, 2001.

[162] X. Zhao, I. P. Georgakaki, M. L. Miller, J. C. Yarbrough, and M. Y. Darensbourg. H/D exchange reactions in dinuclear iron thiolates as activity assay models of Fe-H2ase. *Communications*, (17):9710–9711, 2001.

[163] M. K. Harb, T. Niksch, J. Windhager, H. Gorls, R. Holze, L. T. Lockett, N. Okumura, D. H. Evans, R. S. Glass, D. L. Lichtenberger, M. El-khateeb, and W. Weigand. Synthesis and characterization of diiron diselenolato complexes including Iron Hydrogenase models. *Organometallics*, 28(4):1039–1048, 2009.

[164] M. K. Harb, U. P. Apfel, J. Kübel, H. Görls, G. A. N. Feiton, T. Sakamoto, D. H. Evans, R. S. Glass, D. L. Lichtenberger, M. El-khateeb, and W. Weigand. Preparation and characterization of homologous diiron dithiolato, diselenato, and ditellurato complexes: [FeFe]-hydrogenase models. *Organometallics*, 28(23):6666–6675, 2009.

[165] M. K. Harb, J. Windhager, D. Ahmad, H. Gorls, L. T. Lockett, N. Okumura, D. H. Evans, R. S. Glass, D. L. Lichtenberger, M. El-khateeb, and W. Weigand. Phosphane- and phosphite-substituted diiron diselenolato complexes as models for [FeFe]-hydrogenases. *European Journal of Inorganic Chemistry*, (23):3414–3420, 2009.

[166] M. K. Harb, H. Görls, T. Sakamoto, G. A. N. Felton, D. H. Evans, R. S. Glass, D. L. Lichtenberger, M. El-Khateeb, and W. Weigand. Synthesis and characterization of [FeFe]-hydrogenase models with bridging moieties containing (S, Se) and (S, Te). *European Journal of Inorganic Chemistry*, 3(25):3976–3985, 2010.

[167] U. Apfel, D. Troegel, Y. Halpin, S. Tschierlei, U. Uhlemann, H. Görls, M. Schmitt, J. Popp, P. Dunne, M. Venkatesan, M. Coey, M. Rudolph, J. G. Vos, R. Tacke, and W. Weigand. Models for the active site in [FeFe]-hydrogenase with iron-bound ligands derived from bis-, tris-, and tetrakis(mercaptomethyl)silanes. *Inorganic Chemistry*, 49(21):10117–10132, 2010.

[168] E. S. Donovan, J. J. McCormick, G. S. Nichol, and G. A. N. Felton. Cyclic voltammetric studies of chlorine-substituted diiron benzenedithiolato hexacarbonyl electrocatalysts inspired by the [FeFe]-hydrogenase active site. *Organometallics*, 31(23):8067–8070, 2012.

[169] P. E. M. Siegbahn, J. W. Tye, and M. B. Hall. Computational studies of [NiFe] and [FeFe] hydrogenases. *Chemical Reviews*, 107(10):4414–4435, 2007.

[170] C. A. Boyke, T. B. Rauchfuss, S. R. Wilson, M. Rohmer, M. Be, and Louis Pasteur. [Fe2(SR)2(mu-CO)(CNMe)6]2+ and analogues: a new class of diiron dithiolates as structural models for the Hox(air) state of the Fe-only hydrogenase. 2(6):268–275, 2004.

[171] C. A. Boyke, J. I. Van Der Vlugt, T. B. Rauchfuss, S. R. Wilson, G. Zampella, and L. De Gioia. Diferrous cyanides as models for the Fe-only hydrogenases. *Journal of the American Chemical Society*, 127(31):11010–11018, 2005.

[172] M. L. Singleton, N. Bhuvanesh, J. H. Reibenspies, and M. Y. Darensbourg. Synthetic support of de novo design: sterically bulky [FeFe]-hydrogenase models. *Angewandte Chemie*, 120(49):9634–9637, 2008.

[173] A. K. Justice, M. J. Nilges, T. B. Rauchfuss, S. R. Wilson, L. De Gioia, and G. Zampella. Diiron dithiolato carbonyls related to the Hox(CO) state of [FeFe]-hydrogenase. *Journal of the American Chemical Society*, 130(15):5293–5301, 2008.

[174] A. K. Justice, T. B. Rauchfuss, and S. R. Wilson. Unsaturated, mixed-valence diiron dithiolate model for the Hox state of the [FeFe] hydrogenase. *Angewandte Chemie - International Edition*, 46(32):6152–6154, 2007.

[175] T. Liu and M. Y. Darensbourg. A mixed-valent, Fe(II)Fe(I), diiron complex reproduces the unique rotated state of the [FeFe]hydrogenase active site. *Journal of the American Chemical Society*, 129(22):7008–7009, 2007.

[176] W. Wang, T. B. Rauchfuss, C. E. Moore, A. L. Rheingold, L. De Gioia, and G. Zampella. Crystallographic characterization of a fully rotated, basic diiron dithiolate: model for the Hred state? *Chemistry - A European Journal*, 19(46):15476–15479, 2013.

[177] S. Munery, J. F. Capon, L. De Gioia, C. Elleouet, C. Greco, F. Y. Pétillon, P. Schollhammer, J. Talarmin, and G Zampella. New FeI-FeI complex featuring a rotated conformation related to the [2Fe]H subsite of [Fe-Fe] hydrogenase. *Chemistry - A European Journal*, 19(46):15458–15461, 2013.

[178] P. Li, M. Wang, L. Chen, J. H. Liu, Z. B. Zhaoa, and L. C. Sun. Structures, protonation, and electrochemical properties of diiron dithiolate complexes containing pyridyl-phosphine ligands. *Dalton Transactions*, 2(11):1919–1926, 2009.

[179] Y. Wang, Z. Li, X. Zeng, X. Wang, C. Zhan, Y. Liu, X. Zeng, Q. Luo, and X. Liu. Synthesis and characterisation of three diiron tetracarbonyl complexes related to the diiron centre of [FeFe]-hydrogenase and their protonating, electrochemical investigation. *New Journal of Chemistry*, 33:1780–1789, 2009.

[180] S. Ezzaher, J. F. Capon, F. Gloaguen, F. Y. Petillon, P. Schollhammer, J. Talarmin, and N. Kervarec. Influence of a pendant amine in the second coordination sphere on proton transfer at a dissymmetrically disubstituted diiron system related to the [2Fe]H subsite of [FeFe]H2ase. *Inorganic Chemistry*, 48(1):2–4, 2009.

[181] D. Zheng, M. Wang, L. Chen, N. Wang, and L. Sun. Redox reactions of [FeFe]-hydrogenase models containing an internal amine and a pendant phosphine. *Inorganic Chemistry*, 53(3):1555–1561, 2014.

[182] J. L. Stanley, Z. M. Heiden, T. B. Rauchfuss, S. R. Wilson, L. De Gioia, and G. Zampella. Desymmetrized diiron azadithiolato carbonyls: a step toward modeling the iron-only hydrogenases. *Organometallics*, 27(1):119–125, 2008.

[183] B. E. Barton, M. T. Olsen, and T. B. Rauchfuss. Aza- and oxadithiolates are probable proton relays in functional models for the [FeFe]-hydrogenases. *Journal of the American Chemical Society*, 130(50):16834–16835, 2008.

[184] J. I. Van Der Vlugt, T. B. Rauchfuss, C. M. Whaley, and S. R. Wilson. Characterization of a diferrous terminal hydride mechanistically relevant to the Fe-only hydrogenases. *Journal of the American Chemical Society*, 127(46):16012–16013, 2005.

[185] G. Zampella, P. Fantucci, and L. De Gioia. Unveiling how stereoelectronic factors affect kinetics and thermodynamics of protonation regiochemistry in [FeFe] hydrogenase synthetic models: A DFT investigation. *Journal of the American Chemical Society*, 131(31):10909–10917, 2009.

[186] B. E. Barton, M. T. Olsen, and T. B. Rauchfuss. Artificial hydrogenases. *Current Opinion in Biotechnology*, 21(3):292–297, 2010.

[187] J. F. Capon, F. Gloaguen, P. Schollhammer, and J. Talarmin. Electrochemical proton reduction by thiolate-bridged hexacarbonyldiiron clusters. *Journal of Electroanalytical Chemistry*, 566(2):241–247, 2004.

[188] K. W. Kramarz and J. R. Norton. Slow proton-transfer reactions in organometallic and bioinorganic chemistry. *Progress in Inorganic Chemistry*, 42:1–65, 2014.

[189] S. A. Lerke, D. H. Evans, and S. W. Feldberg. Digital simulation of the square scheme in cyclic voltammetry. A comparison of methods. *Journal of Electroanalytical Chemistry*, 296(2):299–315, 1990.

[190] A. Darchen, H. Mousser, and H. Patin. Two-electron transfer catalysis of carbon monoxide exchange with a ligand in hexacarbonyl di-iron compounds. *Journal of the Chemical Society, Chemical Communications*, (968):968–970, 1988.

[191] L. C. Song, Z. Y. Yang, H. Z. Bian, Y. Liu, H. T. Wang, X. F. Liu, and Q. M. Hu. Diiron oxadithiolate type models for the active site of iron-only hydrogenases and biomimetic hydrogen evolution catalyzed by Fe2(mu-SCH2OCH2S-mu)(CO)6. *Organometallics*, 24(25):6126–6135, 2005.

[192] M. Razavet, S. J. Borg, S. J. George, S. P. Best, S. Fairhurst, and C. J. Pickett. Transient FTIR spectroelectrochemical and stopped-flow detection of a mixed valence (Fe(I)-Fe(II)) bridging carbonyl intermediate with structural elements and spectroscopic characteristics of the di-iron sub-site of all-iron hydrogenase. *Chemical communications (Cambridge, England)*, (7):700–701, 2002.

[193] G. Eilers, L. Schwartz, M. Stein, G. Zampella, L. De Gioia, S. Ott, and R. Lomoth. Ligand versus metal protonation of an iron hydrogenase active site mimic. *Chemistry - A European Journal*, 13(25):7075–7084, 2007.

[194] J. Ekstrom, M. Abrahamsson, C. Olson, J. Bergquist, F. B. Kaynak, L. Eriksson, S. C. Licheng, H. C. Becker, B. Akermark, L. Hammarstrom, and S. Ott. Bio-inspired, side-on attachment of a ruthenium photosensitizer to an iron hydrogenase active site model. *Dalton Transactions*, (38):4599–4606, 2006.

[195] D. Coucouvanis. Visible light-driven electron transfer and hydrogen generation catalysed by bio-inspired [2Fe2S] complexes. *Evolution*, 3(7):1–4, 2008.

[196] L. C. Song, M. Y. Tang, S. Z. Mei, J. H. Huang, and Q. M. Hu. The active site model for iron-only hydrogenases coordinatively bonded to a metalloporphyrin photosensitizer. *Organometallics*, 26(7):1575–1577, 2007.

[197] L. Sun and S. Ott. Iron hydrogenase active site mimics in supramolecular systems aiming for light-driven hydrogen production. *Coordination Chemistry Reviews*, 249(15-16):1653–1663, 2005.

[198] C. Tard, X. Liu, S. K. Ibrahim, M. Bruschi, L. De Gioia, S. C. Davies, X. Yang, L. Wang, G. Sawers, and C. J. Pickett. Synthesis of the H-cluster framework of iron-only hydrogenase. *Nature*, 433(7026):610–3, 2005.

[199] C. Gimbert-Suriach, M. Bhadbhade, and S. B. Colbran. Bridgehead hydrogen atoms are important: Unusual electrochemistry and proton reduction at iron dimers with ferrocenyl-substituted phosphido bridges. *Organometallics*, 31(9):3480–3491, 2012.

[200] J. Zhao, Z. Wei, X. Zeng, and X. Liu. Three diiron complexes bearing an aromatic ring as mimics of the diiron subunit of [FeFe]-hydrogenase: synthesis, electron transfer and coupled chemical reactions. *Dalton transactions*, 41(36):11125–33, 2012.

[201] X. Zeng, Z. Li, Z. Xiao, Y. Wang, and X. Liu. Using pendant ferrocenyl group(s) as an intramolecular standard to probe the reduction of diiron hexacarbonyl model complexes for the sub-unit of [FeFe]-hydrogenase. *Electrochemistry Communications*, 12(3):342–345, 2010.

[202] Y. C. Liu, T. H. Yen, Y. J. Tseng, C. H. Hu, G. H. Lee, and M. H. Chiang. Electron delocalization from the fullerene attachment to the diiron core within the active-site mimics of [FeFe]hydrogenase. *Inorganic Chemistry*, 51(11):5997–5999, 2012.

[203] Y. Si, K. Charreteur, J. F. Capon, F. Gloaguen, F. Y. Pétillon, P. Schollhammer, and J. Talarmin. Non-innocent bma ligand in a dissymetrically disubstituted diiron dithiolate related to the active site of the [FeFe] hydrogenases. *Journal of Inorganic Biochemistry*, 104(10):1038–1042, 2010.

[204] S. Roy, T. L. Groy, and A. K. Jones. Biomimetic model for [FeFe]-hydrogenase: asymmetrically disubstituted diiron complex witha redoz active 2,2'-bipyridil ligand. *Dalton Transactions*, 42(11):3843, 2013.

[205] J. M. Camara and T. B. Rauchfuss. Combining acid-base, redox and substrate binding functionalities to give a complete model for the [FeFe]-hydrogenase. *Nature Chemistry*, 4(1):26–30, 2012.

[206] J. M. Camara and T. B. Rauchfuss. Mild redox complementation enables H2 activation by [FeFe]-hydrogenase models. *Journal of the American Chemical Society*, 133(21):8098–8101, 2011.

[207] N. Wang, M. Wang, Y. Wang, D. Zheng, H. Han, M. S. G. Ahlquist, and L. Sun. Catalytic activation of H2 under mild conditions by an [FeFe]-hydrogenase model via an active mu-hydride species. *Journal of the American Chemical Society*, 135(37):13688–13691, 2013.

[208] K. C. MacLeod and P. L. Holland. Recent developments in the homogeneous reduction of dinitrogen by molybdenum and iron. *Nature Chemistry*, 5(7):559–565, 2013.

[209] N. Hazari. Homogeneous iron complexes for the conversion of dinitrogen into ammonia and hydrazine. *Chemical Society Reviews*, 39(11):4044–4056, 2010.

[210] W. Weigand and P. Schollhammer. Binding substrates to synthetic Fe-S-based clusters and the possible relevance to nitrogenases. In *Bioinspired Catalysis: Metal-Sulfur Complexes*, pages 289–323. 2015.

[211] H. C. Heim, T. M. Bernhardt, and S. M. Lang. The challenge of genrating iron-sulfur clusters. *International Journal of Mass Spectrometry*, 387:56–59, 2015.

[212] D. Sellmann, W. Soglowek, F. Knoch, and M. Moll. Nitrogenase model compounds: [muN2H2{Fe(NHS4)}2], the prototype for the coordination of diazene to iron sulfur centers and its stabilization through strong N-H-S hydrogen bonds. *Angewandte Chemie International Edition in English*, 28(9):1271–1272, 1989.

[213] H. C. Heim, T. M. Bernhardt, S. M. Lang, R. N. Barnett, and U. Landman. Interaction of ironâsulfur clusters with N2: biomimetic systems in the gas phase. *The Journal of Physical Chemistry C*, 120(23):12549–12558, 2016.

[214] A. D. Allen. Nitrogenopentammineruthenium(II) complexes. *Journal of the Chemical Society, Chemical Communications*, 24:621., 1965.

[215] B. A. MacKay and M. D. Fryzuk. Dinitrogen coordination chemistry: on the Biomimetic borderlands. *Chemical Reviews*, 104(2):385–402, 2004.

[216] R. R. Schrock and V. D. Yandulov. Catalytic reduction of dinitrogen to ammonia at a single molybdenum center. *Science*, 301(5629):76–78, 2003.

[217] R. R. Schrock. Catalytic reduction of dinitrogen to ammonia at well-defined single metal sites. *Philosophical Transactions of the Royal Society A: Mathematical, Physical and Engineering Sciences*, 363(1829):959–969, 2005.

[218] K. Tanifuji, N. Sickerman, C. C. Lee, T. Nagasawa, K. Miyazaki, Y. Ohki, K. Tatsumi, Y. Hu, and M. W. Ribbe. Structure and reactivity of an asymmetric synthetic mimic of nitrogenase cofactor. *Angewandte Chemie - International Edition*, 55(50):15633–15636, 2016.

[219] E. Block and G. Ofori-Okai. Catalytic disproportionation and reduction of hydrazine by sulfur-ligated molybdenum(IV) complexes. Characterization of the catalytic precursor. *Journal of the American Chemical Society*, 114(16):758–759, 1992.

[220] R. A. Henderson, G. J. Leigh, and C. J. Pickett. The chemistry of nitrogen fixation and models for the reactions of nitrogenase. *Advances in Inorganic Chemistry*, 27(C):197–292, 1983.

[221] W. C. Chu, C. C. Wu, and H. F. Hsu. Catalytic reduction of hydrazine to ammonia by a vanadium thiolate complex. *Inorganic Chemistry*, 45(8):3164–3166, 2006.

[222] D. Coucouvanis. Use of preassembled Fe/S and Fe/Mo/S clusters in the stepwise synthesis of potential analogues for the Fe/Mo/S Site in nitrogenase. *Accounts of chemical research*, 24(1):1–8, 1991.

[223] K. D. Demadis and D. Coucouvanis. Synthesis, structural characterization, and properties of new single and double cubanes containing the MoFe3S4 structural unit and molybdenum-bound polycarboxylate ligands. *Inorganic Chemistry*, 34(2):436–448, 1995.

[224] E. Nordlander, S. C. Lee, W. Cen, Z. Y. Wu, C . R. Natoli, A. Di Cicco, A. Filipponi, B. Hedman, K. O. Hodgson, and R. H. Holm. The heterometal cuboidal clusters MFe4S6(PEt3)4Cl (M=V,Mo): synthesis, structural analysis by crystallography and EXAFS, and relevance to the structure of the iron-molybdenum cofactor of nitrogenase. *J. Am. Chem. Soc.*, 115(13):5549–5558, 1993.

[225] J. S. Anderson, J. Rittle, and J. C. Peters. Catalytic conversion of nitrogen to ammonia by an iron model complex. *Nature*, 501(7465):84–7, 2013.

[226] T. J. Del Castillo, N. B. Thompson, and J. C. Peters. A synthetic single-site Fe nitrogenase: high turnover, freeze-quench 57Fe Mossbauer data, and a hydride resting state. *Journal of the American Chemical Society*, 138(16):5341–5350, 2016.

[227] G. Ung and J. C. Peters. Low-temperature N2 binding to two-coordinate L2Fe0 enables reductive trapping of L2FeN2â and NH3 generation. *Angew. Chem. Int. Ed.*, 54:531–535, 2014.

[228] P. J. Hill, L. R. Doyle, A. D. Crawford, W. K. Myers, and A. E. Ashley. Selective catalytic reduction of N2 to N2H4 by a simple Fe complex. *Journal of the American Chemical Society*, 138(41):13521–13524, 2016.

[229] Z. Ouyang, J. Cheng, L. Li, X. Bao, and L. Deng. High-spin iron(I) and iron(0) dinitrogen complexes supported by N-heterocyclic carbene ligands. *Chemistry - A European Journal*, 22(40):14162–14165, 2016.

[230] K. Arashiba, Y. Miyake, and Y. Nishibayashi. A molybdenum complex bearing PNP-type pincer ligands leads to the catalytic reduction of dinitrogen into ammonia. *Nature Chemistry*, 3(2):120–125, 2011.

[231] J. Rittle, C. C. L. McCrory, and J. C. Peters. A 106-fold enhancement in N2-binding affinity of an Fe2(mu-H)2core upon reduction to a mixed-valence FeIIFeIstate. *Journal of the American Chemical Society*, 136(39):13853–13862, 2014.

[232] S.E. Creutz and J. C. Peters. Catalytic reduction of N2 to NH3 by an FeâN2 complex featuring a C-atom anchor. *Journal of the American Chemical Society*, 136(3):1105–1115, 2014.

[233] J. Vela, S. Stoian, C. J. Flaschenriem, E. Mu, and P. L. Holland. A sulfido-bridged diiron(II) compound and its reactions with nitrogenase-relevant substrates. *Journal of the American Chemical Society, Communications*, 126(Ii):4522–4523, 2004.

[234] I. Coric, B. Q. Mercado, E. Bill, D. J. Vinyard, and P. L. Holland. Binding of dinitrogen to an ironâsulfurâcarbon site. *Nature*, 526(7571):96–99, 2015.

[235] K. Yoshimoto, T. Yatabe, T. Matsumoto, V. H. Tran, A. Robertson, H. Nakai, K. Asazawa, H. Tanaka, and S. Ogo. Inorganic clusters with a [Fe2 MoOS3] core: a functional model for acetylene reduction by nitrogenases. *Dalton Transactions*, 45(37):14620–14627, 2016.

[236] Y. Y. Li, B. Wang, Y. Luo, D. Yang, P. Tong, J. Zhao, L. Luo, Y. Zhou, S. Chen, F. Cheng, and J. Qu. Ammonia formation by a thiolate-bridged diiron amide complex as a nitrogenase mimic. *Nature Chemistry*, 5(4):320–6, 2013.

[237] Y. Luo, Y. Li, H. Yu, J. Zhao, Y. Chen, Z. Hou, and J. Qu. DFT studies on the reduction of dinitrogen to ammonia by a thiolate-bridged diiron complex as a nitrogenase mimic. *Organometallics*, 31(1):335–344, 2012.

[238] Y. Chen, L. Liu, Y. Peng, P. Chen, Y. Luo, and J. Qu. Unusual thiolate-bridged diiron clusters bearing the cis-HN=NH ligand and their reactivities with terminal alkynes. *Journal of the American Chemical Society*, 133(5):1147–1149, 2011.

[239] M. Yuki, Y. Miyake, and Y. Nishibayashi. Synthesis of sulfur- and nitrogen-bridged diiron complexes and catalytic behavior toward hydrazines. *Organometallics*, 31(8):2953–2956, 2012.

[240] C. Ziebart, C. Federsel, P. Anbarasan, R. Jackstell, W. Baumann, A. Spannenberg, and M. Beller. Well-defined iron catalyst for CO2 hydrogenation. *Journal of the American Chemical Society*, 134(51):20701–20704, 2012.

[241] R. Langer, Y. Diskin-Posner, G. Leitus, L. J. W. Shimon, Y. Ben-David, and D. Milstein. Low-pressure hydrogenation of carbon dioxide catalyzed by an iron pincer complex exhibiting noble metal activity. *Angewandte Chemie - International Edition*, 50(42):9948–9952, 2011.

[242] C. M. Zall, J. C. Linehan, and A. M. Appel. A molecular copper catalyst for hydrogenation of CO2 to formate. *ACS Catalysis*, 5(9):5301–5305, 2015.

[243] A. Szabo and N. S. Ostlund. *Modern Quantum Chemistry.* 1989.

[244] C. J. Cramer. *Essentials of computational chemistry. Theories and models.* 2003.

[245] C. Moller and M. S. Plesset. Note on an approximation treatment for many-electron systems. *Physical Review*, 66:618, 1934.

[246] C. D. Sherrill and H. F. Schaefer. The configurational interaction method: advances in highly correlated approaches. *Advances in Quantum Chemistry*, 34:143–269, 1999.

[247] I. Shavitt and R. J. Bartlett. *Many-body methods in chemistry and physics: MBPT and coupled-cluster theory.* 2009.

[248] P. G. Szalay and R. J. Bartlett. Multi-reference averaged quadratic coupled-cluster method: a size-extensive modification of multi-reference CI. *Chemical Physics Letters*, 214(5):481–488, 1993.

[249] W.D. L. A Bartlett and J. Rodney. A multi-reference coupled-cluster method for molecular application. *Chemical Physics Letters*, 1984.

[250] P. Hohenberg and W. Kohn. The inhomogeneous electron gas. *Physical Review*, 136(3B):B864, 1964.

[251] L. H. Thomas. The calculation of atomic fields. *Mathematical Proceedings of the Cambridge Philosophical Society*, 23(05):542–548, 1927.

[252] E. Fermi. *Un Metodo Statistico per la Determinazione di alcune Prioprietà dell'Atomo.*, volume 6. 1927.

[253] W. Kohn and L. J. Sham. Self-consistent equations including exchange and correlation effects. *Physical Review*, 140(4A):A1134–A1138, 1965.

[254] R. G. Parr and W. Yang. *Density functional theory of the electronic structure of molecules.*, volume 46. 1995.

[255] J P Perdew and A Zunger. Self-interaction correction to density functional approximations for many electron systems. *Physical Review B*, 23:5048, 1981.

[256] S. H. Vosko, L. Wilk, and M. Nusair. Accurate spin-dependent electron liquid correlation energies for local spin density calculations: a critical analysis. *Canadian Journal of Physics*, 58(8):1200–1211, 1980.

[257] J. P. Perdew and Y. Wang. Accurate and simple analytic representation of the electron-gas correlation energy. *Physical Review B*, 45(23):13244–13249, 1992.

[258] A. D. Becke. Density-Functional exchange-energy approximation with corrects asymptotic-behavior. *Physical Review A*, 38(6):3098–3100, 1988.

[259] C. Adamo and V. Barone. Exchange functionals with improved long-range behavior and adiabatic connection methods without adjustable parameters: The mPW and mPW1PW models. *Journal of Chemical Physics*, 108(2):664–675, 1998.

[260] N. C. Handy and A. J. Cohen. Left-right correlation energy. *Molecular Physics*, 99(5):403–412, 2001.

[261] X. Xu and W. A. Goddard. The X3LYP extended density functional for accurate descriptions of nonbond interactions, spin states, and thermochemical properties. *Proceedings of the National Academy of Sciences of the United States of America*, 101(9):2673–2677, 2004.

[262] J. P. Perdew, K. Burke, and M. Ernzerhof. Generalized Gradient Approximation made simple. *Physical Review Letters*, 77:3865–3868, 1996.

[263] D. J. Lacks and R. G. Gordon. Pair interactions of rare-gas atoms as a test of exchange-energy-density functionals in regions of large density gradients. *Physical Review A*, 47(6):4681–4690, 1993.

[264] C. Adamo and V. Barone. Physically motivated density functionals with improved performances: The modified PerdewâBurkeâErnzerhof model. *Journal of Chemical Physics*, 116:5933, 2002.

[265] J. P Perdew. Unified theory of exchange and correlation beyond the local density approximation. *Electronic Structure of Solids '91*, 17:11–20, 1991.

[266] C. Lee, W. Yang, and R. G. Parr. Development of the Colle-Salvetti correlation-energy formula into a functional of the electron density. *Physical Review B*, 37(2):785 – 789, 1988.

[267] O. Salvetti and R. Colle. Approximate calculation of the correlation energy for the closed and open shells. *Theoretica Chimica Acta*, 53(1):55–63, 1975.

[268] J. Tao, J. P. Perdew, V. N. Staroverov, and G. E. Scuseria. Climbing the density functional ladder: non-empirical meta-generalized gradient approximation designed for molecules and solids. *Physical Review Letters*, 91(14):146401, 2003.

[269] J. Krieger, J. Chen, G. Iafrate, and S. Kurth. Improved calculation of correlation energies employing an electron gas with a gap. *APS Meeting Abstracts*, 2000.

[270] T. V. Voorhis and G. E. Scuseria. A novel form for the exchange-correlation energy functional. *The Journal of Chemical Physics*, 109:400, 1998.

[271] K. Burke, M. Ernzerhof, and J. P. Perdew. The adiabatic connection method: a non-empirical hybrid. *Chemical Physics Letters*, 265:115–120, 1997.

[272] H. Hellmann. Einfuhrung in die Quantenchemie. In *Leipzig: Franz Deuticke. p. 285.* 1937.

[273] R. M. Dreizler and E. K. U. Gross. *Density Functional Theory. An approach to quantum many body problem.* 2012.

[274] P. J. Hay and W. R. Wadt. Ab initio effective core potentials for molecular calculations. Potentials for the transition metal atoms Sc to Hg. *The Journal of Chemical Physics*, 82(1):270, 1985.

[275] L. Noodleman, D. A. Case, and A. Aizman. Broken symmetry analysis of spin coupling in iron-sulfur clusters. *Journal of the American Chemical Society*, 110(4):1001–1005, 1988.

[276] S. Grimme. Density functional theory with London dispersion corrections. *Wiley Interdisciplinary Reviews: Computational Molecular Science*, 1(2):211–228, 2011.

[277] F. Furche, R. Ahlrichs, C. Hättig, W. Klopper, M. Ierka, and F. Weigend. Turbomole. *Wiley Interdiscip. Rev. Comput. Mol. Sci*, 4:91–100, 2014.

[278] J. P. Perdew. Density-Functional approximation for the correlation energy of the inhomogenous electron gas. *Physical Review B*, 33(12):8822–8824, 1986.

[279] A. SchaÌfer, C. Huber, and R. Ahlrichs. Fully optimized contracted Gaussian basis sets of triple zeta valence quality for atoms Li to Kr. *The Journal of Chemical Physics*, 100(8):5829, 1994.

[280] M. Bruschi, C. Greco, M. Kaukonen, P. Fantucci, U. Ryde, and L. De Gioia. Influence of the [2Fe]H subcluster environment on the properties of key intermediates in the catalytic cycle of [FeFe] hydrogenases: Hints for the rational design of synthetic catalysts. *Angewandte Chemie - International Edition*, 48(19):3503–3506, 2009.

[281] G. Zampella, C. Greco, P. Fantucci, and L. De Gioia. Proton reduction and dihydrogen oxidation on models of the [2Fe]H cluster of [Fe] hydrogenases. A density functional theory investigation. *Inorganic Chemistry*, 45(10):4109–4118, 2006.

[282] K. Eichkorn, F. Weigend, O. Treutler, and R. Ahlrichs. Auxiliary basis sets for main row atoms and transition metals and their use to approximate Coulomb potentials. *Theoretical Chemistry Accounts*, 97(1-4):119–124, 1997.

[283] J. Baker. An algorithm for the location of transition-states. *J outnal of Computational Chemistry*, 7:385–395, 1986.

[284] A. Klamt. Conductor-like Screening Model for Real Solvents: a new approach to the quantitative calculation of solvation phenomena. *Journal of Physical Chemistry*, 99(7):2224–2235, 1995.

[285] A. Klamt. Calculation of UV spectra in solution. *Journal of Physical Chemistry*, 100:3349–3353, 1996.

[286] F. Jensen. *Introduction to Computational Chemistry Computational Chemistry*. 2007.

[287] C. M. Thomas, M. Y. Darensbourg, and M. B. Hall. Computational definition of a mixed valent Fe(II)Fe(I) model of the [FeFe] hydrogenase active site resting state. *Journal of Inorganic biochemistry*, 101(11-12):1752–1757, 2007.

[288] M. T. Olsen, T. B. Rauchfuss, and S. R. Wilson. Role of the azadithiolate cofactor in models for [FeFe]-hydrogenase: Novel structures and catalytic implications. *Journal of the American Chemical Society*, 132(50):17733–17740, 2010.

[289] D. Chouffai, G. Zampella, J. F. Capon, L. . De Gioia, A. Le Goff, F. Y. Pétillon, P. Schollhammer, and J. Talarmin. Electrochemical and theoretical studies of the impact of the chelating ligand on the reactivity of [Fe2(CO) 4(k2- LL)(mu-pdt)]+ complexes with different substrates (LL = IMe-CH 2-I Me, dppe; IMe = 1-methylimidazol-2-ylidene). *Organometallics*, 31(3):1082–1091, 2012.

[290] S. Ghosh, G. Hogarth, N. Hollingsworth, K. B. Holt, S. E. Kabir, and B. E. Sanchez. Hydrogenase biomimetics: Fe 2(CO)4(mu-dppf)(mu-pdt) (dppf= 1,1'-bis(diphenylphosphino)ferrocene) both a proton-reduction and hydrogen oxidation catalyst. *Chemical Communications*, 50(8):945–947, 2014.

[291] S. Munery, J. F. Capon, L. Degioia, C. Elleouet, C. Greco, F. Y. Pétillon, P. Schollhammer, J. Talarmin, and G. Zampella. New FeI-FeI complex featuring a rotated conformation related to the [2Fe]H subsite of [Fe-Fe] hydrogenase. *Chemistry - A European Journal*, 19(46):15458–15461, 2013.

[292] L. De Gioia, C. Elleouet, S. Munery, F. Y. Pétillon, P. Schollhammer, J. Talarmin, and G. Zampella. Reductive behavior of [Fe2 (CO)4(k2-dmpe){mu-(SCH2) 2NBn}]: effect of symmetrization on the rotated conformation in FeI-FeI models of [2Fe]H subsite of [Fe-Fe]ÂH2ases. *European Journal of Inorganic Chemistry*, 2014(22):3456–3461, 2014.

[293] S. Ezzaher, J. F. Capon, F. Gloaguen, N. Kervarec, F. Y. Pétillon, R. Pichon, P. Schollhammer, and J. Talarmin. Diiron chelate complexes relevant to the active site of the iron-only hydrogenase. *Comptes Rendus Chimie*, 11(8):906–914, 2008.

[294] M. Brookhart, M. L. H. Green, and G. Parkin. Agostic interactions in transition metal compounds. *Proceedings of the National Academy of Sciences*, 104(17):6908–6914, 2007.

[295] S. Puhua, Y. Dawei, L. Ying, Z. Yahui, S. Linan, W. Baomin, and Q. Jingping. Thiolate-bridged nickelâiron and nickelâruthenium complexes relevant to the CO-inhibited state of [NiFe]-hydrogenase. *Organometallics*, 35(5):751–757, 2016.

[296] Y. Nicolet, C. Cavazza, and J. C. Fontecilla-Camps. Fe-only hydrogenases: Structure, function and evolution. *Journal of Inorganic Biochemistry*, 91(1):1–8, 2002.

[297] Z. Wang, W. Jiang, J. Liu, W. Jiang, Y. Wang, B. Åkermark, and L. Sun. Pendant bases as proton transfer relays in diiron dithiolate complexes inspired by [Fe-Fe] hydrogenase active site. *Journal of Organometallic Chemistry*, 693(17):2828–2834, 2008.

[298] J. A. Wright and C. J. Pickett. Protonation of a subsite analogue of [FeFe]-hydrogenase: mechanism of a deceptively simple reaction revealed by time-resolved IR spectroscopy. *Chemical Communications*, (38):5719–21, 2009.

[299] T. Zhou, Y. Mo, A. Liu, Z. Zhou, and K. R. Tsai. Enzymatic mechanism of Fe-only hydrogenase: density functional study on H-H making/breaking at the diiron cluster with concerted proton and electron transfers. *Inorganic Chemistry*, 43(3):923–930, 2004.

[300] C. Liu, J. N. T. Peck, J. A. Wright, C. J. Pickett, and M. B. Hall. Density functional calculations on protonation of the [FeFe]-hydrogenase model complex Fe2(mu-pdt)(CO)4(PMe3)2 and subsequent isomerization pathways. *European Journal of Inorganic Chemistry*, 2(7):1080–1093, 2011.

[301] M. G. I. Galinato, C. M. Whaley, D. Roberts, P. Wang, and N. Lehnert. Favorable protonation of the (mu-edt)Fe2(PMe3)4(CO)2(H-terminal)]+ hydrogenase model complex over its bridging mu-H counterpart. *European Journal of Inorganic Chemistry*, 2(7):1147–1154, 2011.

[302] L. R Almazahreh, U. Apfel, W. Imhof, M. Rudolph, H. Go, J. Talarmin, P. Schollhammer, M. El-khateeb, and W. Weigand. A Novel [FeFe]-hydrogenase model with a (SCH2)2P=O moiety. *Organometallics*, (Figure 1), 2013.

[303] J. C. Lansing, B. C. Manor, and T. B. Rauchfuss. *Encyclopedia of inorganic and bioinorganic chemistry*. 2011.

[304] S. Tschierlei, S. Ott, and R. Lomoth. Spectroscopically characterized intermediates of catalytic H2 formation by [FeFe] hydrogenase models. *Energy & Environmental Science*, 4(7):2340–2352, 2011.

[305] G. A. N. Felton, C. A. Mebi, B. J. Petro, A. K. Vannucci, D. H. Evans, R. S. Glass, and D. L. Lichtenberger. Review of electrochemical studies of complexes containing the Fe2S2 core characteristic of [FeFe]-hydrogenases including catalysis by these complexes of the reduction of acids to form dihydrogen. *Journal of Organometallic Chemistry*, 694(17):2681–2699, 2009.

[306] G. Filippi, F. Arrigoni, L. Bertini, L. De Gioia, and G. Zampella. DFT dissection of the reduction step in H2 catalytic production by [FeFe]-hydrogenase-inspired models: can the bridging hydride become more reactive than the terminal isomer? *Inorganic Chemistry*, 54(19):9529–9542, 2015.

[307] R. Zaffaroni, T. B. Rauchfuss, D. L. Gray, L. De Gioia, and G. Zampella. Terminal vs bridging hydrides of diiron dithiolates: Protonation of Fe2(dithiolate)(CO)2(PMe3)4. *Journal of the American Chemical Society*, 134(46):19260–19269, 2012.

[308] M. E. Carroll, B. E. Barton, T. B. Rauchfuss, and P. J. Carroll. Synthetic models for the active site of the [FeFe]-hydrogenase: Catalytic proton reduction and the structure of the doubly protonated intermediate. *Journal of the American Chemical Society*, 134(45):18843–18852, 2012.

[309] R. Goy, L. Bertini, C. Elleouet, H. Gorls, G. Zampella, J. Talarmin, L. De Gioia, P. Schollhammer, U. P. Apfel, and W. Weigand. A sterically stabilized Fe(I)-Fe(I) semi-rotated conformation of [FeFe] hydrogenase subsite model. *Dalton transactions*, 44(4):1690–9, 2014.

[310] A. E. Mack and T. B Rauchfuss. *Inorganic syntheses*. 2011.

[311] K. D. Grande, A. J. Kunin, L. S. Stuhl, and B. M. Foxman. A Sterically crowded Oorganopentacyanocobaltate: single-crystal X-ray structure determination and reactivity study of K6(NC)5CoC(COOCH3)=C(COOCH3)Co(CN)5)-6H20. *Inorganic Chemistry*, (7):1791–1794, 1983.

[312] J. Chatt, G. J. Leigh, and C. J. Pickett. Transition-metal binding sites and ligand parameters. *Dalton Transactions*, (232):2032–2038, 1980.

[313] B. P. Lever. Electrochemical parametrization of metal complex redox potentials, using the ruthenium(III)/ruthenium(II) couple to generate a ligand electrochemical series. *Inorganic Chemistry*, 29(17):1271–1285, 1990.

[314] L. C. Song, Z. Y. Yang, Y. J. Hua, H. T. Wang, Y. Liu, and Q. M. Hu. Diiron thiadithiolates as active site models for the iron-only hydrogenases: synthesis, structures, and catalytic H2 production. *Organometallics*, 26(8):2106–2110, 2007.

[315] J. Hou, X. Peng, J. Liu, Y. Gao, X. Zhao, S. Gao, and K. Han. A binuclear isocyanide azadithiolatoiron complex relevant to the active site of Fe-only hydrogenases: Synthesis, structure and electrochemical properties. *European Journal of Inorganic Chemistry*, (22):4679–4686, 2006.

[316] J. L. Nehring and D. M. Heinekey. Dinuclear iron isonitrile complexes: Models for the iron hydrogenase active site. *Inorganic Chemistry*, 42(14):4288–4292, 2003.

[317] L. Weber. Homoleptic isocyanide metalates. *Angewandte Chemie (International ed. in English)*, 37(11):1515–1517, 1998.

[318] C. C. Mokhtarzadeh, G. W. Margulieux, A. E. Carpenter, N. Weidemann, C. E. Moore, A. L. Rheingold, and J. S. Figueroa. Synthesis and protonation of an encumbered iron tetraisocyanide dianion. *Inorganic chemistry*, 54(11):5579–87, 2015.

[319] W. Sattler, M. E. Ener, J. D. Blakemore, A. A. Rachford, P. J. Labeaume, J. W. Thackeray, J. F. Cameron, J. R. Winkler, and H. B. Gray. Generation of powerful tungsten reductants by visible light excitation. *Journal of the American Chemical Society*, 135(29):10614–10617, 2013.

[320] M.V. Barybin, Wi. W. Brennessel, B. E. Kucera, M. E. Minyaev, V. J. Sussman, V. G. Young, and J. E. Ellis. Homoleptic isocyanidemetalates of 4d- and 5d-transition metals: [Nb(CNXyl)6]-, [Ta(CNXyl)6]-, and derivatives. *Journal of the American Chemical Society*, 129(5):1141–1150, 2007.

[321] T. J. Morsing, J. Bendix, H. Weihe, and A. Dossing. Oxo-bridged dinuclear chromium(III) complexes: Correlation between the optical and magnetic properties and the basicity of the oxo bridge. *Inorganic Chemistry*, 53(6):2996–3003, 2014.

[322] A. J. L. Pombeiro, M. F. Guedes Da Silva, and R. A. Michelin. Aminocarbyne complexes derived from isocyanides activated towards electrophilic addition. *Coordination Chemistry Reviews*, 218:43–74, 2001.

[323] L. Bertini, C. Greco, P. Fantucci, and L. De Gioia. TDDFT modeling of the CO-photolysis of Fe2(S2C3H6)(CO)6, a model of the [FeFe]-hydrogenase catalytic site. *International Journal of Quantum Chemistry*, 114(13):851–861, 2014.

[324] J. W. Tye, M. Y. Darensbourg, and M. B. Hall. De novo design of synthetic di-iron(I) complexes as structural models of the reduced form of iron-iron hydrogenase. *Inorganic Chemistry*, 45(4):1552–1559, 2006.

[325] M. F. N. N. Carvalho, M. T. Duarte, A. M. Galvao, and A. J. L. Pombeiro. Cyanide and methylisocyanide complexes of rhenium(l) [NBu4][ReX(CN)(dppe)2] (X = Cl or CN; dppe = Ph2PCH2CH2PPh2) and trans-[ReX(CNMe)(dppe)2] (X = H, F, Cl or CN): crystal structures of trans-[ReX(CNMe)(dppe)2] (X = H or Cl). *Journal of Organometallic Chemistry*, 469(1):79–87, 1994.

[326] K. Izutsu. *Dissociation constants in dipolar aprotic solvents*. 1990.

[327] H. Werner, R. Zolk, and W. Hofmann. Metallkomplexe mit verbrückenden dimethylphosphidoliganden : offnung der hydridobrucke im [(C5H5Co)2(mu-PMe2)2(mu-H)]+-kation durch Lewis-basen und bildung von mu-formimidoyl-komplexen uber hydrido(isonitril)- und mu-aminocarbinverbindungen als zwisch. *Journal of Organometallic Chemistry*, 302(1):65–86, 1986.

[328] F. Marchetti, S. Zacchini, and V. Zanotti. Coupling of isocyanide and μ-aminocarbyne ligands in diiron complexes promoted by hydride addition. *Organometallics*, 33(15):3990–3997, 2014.

[329] K. Boss, C. Dowling, A. R. Manning, D. Cunningham, and P. McArdle. The reaction of [Fe2(eta-C5H5)2(CO)(CNMe)(mu-CO)(mu-CNMe2)]+ and related salts with trifluoromethanesulphonic acid, HOSO2CF3: structure of cis-[Fe2(eta-C5H5)2(CO)2(mu-CNMe)(mu-CNMe2)] [BPh4]. *Journal of Organometallic Chemistry*, 579:252–268, 1999.

[330] K. W. Norton and J. R. Kramar. Slow proton-transfer reactions in organometallic and bioinorganic chemistry. In *Progress in Inorganic Chemistry*. 2007.

[331] W. Wang, T. B. Rauchfuss, L. Zhu, and G. Zampella. New reactions of terminal hydrides on a diiron dithiolate. *Journal of the American Chemical Society*, 136(15):5773–5782, 2014.

[332] J. J. Bonnet, R. Mathieu, R. Poilblanc, and J. A. Ibers. Insertion of tetrafluoroethylene into the iron-iron bond of (mu-(SCH3)Fe(CO)3)2, its thermal rearrangement to a bridging carbene ligand, and the transformation of the carbene to a perfluoromethylcarbyne ligand. Structures of mu-(SCH3)2mu-(C2F4)Fe2(CO)6. *Journal of the American Chemical Society*, 101(25):7487–7496, 1979.

[333] S. L. Matthews and D. M. Heinekey. An oxidized active site model for the FeFe hydrogenase: Reduction with hydrogen gas. *Inorganic Chemistry*, 50(17):7925–7927, 2011.

[334] N. G. Connelly and W. E. Geiger. Ox-und Redmittel in der Chemie Co(cp)2. *Chemical Reviewseviews*, 96(2):877–910, 1996.

[335] A. JablonskytÄ, L. R. Webster, T. R. Simmons, J. A. Wright, and C. J. Pickett. Electronic control of the protonation rates of Fe-Fe bonds. *Journal of the American Chemical Society*, 136(37):13038–13044, 2014.

[336] J. A. Connor, E. M. Jones, and G. K. McEwen. Isonitrile complexes of chromium(0) and molybdenum(0): characterisation and reactivity. *Dalton Transactions*, (1246):1246–1253, 1971.

[337] A. J. L. Pombeiro and R. L. Richards. Reactivity of Carbyne and Carbene Complexes of Molybdenum and Tungsten. *Transition Metal Chemistry*, 5:55–59, 1980.

[338] R. W. Stephany, M. J. A. De Bie, and W. Drenth. A 13C NMR and IR study of isocyanides and some of their complexes. *Organic Magnetic Resonance*, 6(1):45–47, 1974.

[339] L. Bertini, C. Greco, L. De Gioia, and P. Fantucci. DFT/TDDFT exploration of the potential energy surfaces of the ground state and excited states of Fe2(S2C3H6)(CO)6: a simple functional model of the [FeFe] hydrogenase active site. *Journal of Physical Chemistry A*, 113(19):5657–70, 2009.

[340] X. Zhou, B. E. Barton, G. M. Chambers, T. B. Rauchfuss, F. Arrigoni, and G. Zampella. Preparation and protonation of Fe2(pdt)(CNR)6 , electron-rich analogues of Fe2(pdt)(CO)6. *Inorganic Chemistry*, 2:acs.inorgchem.5b02789, 2016.

[341] H. C. Mun, C. Tard, S. J. Borg, X. Liu, S. K. Ibrahim, C. J. Pickett, and S. P. Best. Modeling [Fe-Fe] hydrogenase: Evidence for bridging carbonyl and distal iron coordination vacancy in an electrocatalytically competent proton reduction by an iron thiolate assembly that operates through Fe(0)-Fe(II) levels. *Journal of the American Chemical Society*, 129(36):11085–11092, 2007.

[342] D. Chong, I. P. Georgakaki, R. Mejia-Rodriguez, J. Sanabria-Chinchilla, M. P. Soriaga, and M. Y. Darensbourg. Electrocatalysis of hydrogen production by active site analogues of the iron hydrogenase enzyme: structure/function relationships. *Dalton Transactions*, (21):4158–4163, 2003.

[343] S. Ezzaher, J. F. Capon, F. Gloaguen, F. Y. Pétillon, P. Schollhammer, J. Talarmin, R. Pichon, and N. Kervarec. Evidence for the formation of terminal hydrides by protonation of an asymmetric iron hydrogenase active site mimic. *Inorganic Chemistry*, 46(9):3426–3428, 2007.

[344] A. Jablonskyte, J. A. Wright, S. A. Fairhurst, J. N. T. Peck, S. K. Ibrahim, V. S. Oganesyan, and C. J. Pickett. Paramagnetic bridging hydrides of relevance to catalytic hydrogen evolution at metallosulfur centers. *Journal of the American Chemical Society*, 133(46):18606–18609, 2011.

[345] I. A. De Carcer, A. DiPasquale, A. L. Rheingold, and D. M. Heinekey. Active-site models for iron hydrogenases: reduction chemistry of dinuclear iron complexes. *Inorganic Chemistry*, 45(20):8000–8002, 2006.

[346] G. Berggren, A. Adamska, C. Lambertz, T. R. Simmons, J. Esselborn, M. Atta, S. Gambarelli, J. M. Mouesca, E. Reijerse, W. Lubitz, T. Happe, V. Artero, and M. Fontecave. Biomimetic assembly and activation of [FeFe]-hydrogenases. *Nature*, 499(7456):66–69, 2013.

[347] S. Kozuch and S. Shaik. Combined kineticâquantum mechanical model for assessment of catalytic cycles. Application to cross-coupling and heck reactions. *Journal of the American Chemical Society*, 128(10):3355–3365, 2006.

[348] S. Kozuch and S. Shaik. How to conceptualize catalytic cycles? The energetic Span model. *Accounts of Chemical Research*, 44(2):101–110, 2011.

[349] T. Miyake, M. Bruschi, U. Cosentino, C. Baffert, V. Fourmond, C. Léger, G. Moro, L. De Gioia, and C. Greco. Does the environment around the H-cluster allow coordination of the pendant amine to the catalytic iron center in [FeFe] hydrogenases? Answers from theory. *Journal of Biological Inorganic Chemistry*, 18(6):693–700, 2013.

[350] Y. Chen, Y. Zhou, P. Chen, Y. Tao, Y. Li, and J. Qu. Nitrogenase model complexes [Cp*Fe(mu-SR1)2(mu-eta2-R 2NNH)FeCp*] (R1= Me, Et; R 2= Me, Ph; Cp* = eta5-C5Me 5): synthesis, structure, and catalytic NâN Bond cleavage of hydrazines on diiron centers. *Journal of the American Chemical Society*, 130(46):15250–15251, 2008.

[351] Y. Chen, Y. Zhou, and J. Qu. Synthesis and reactions of novel triply thiolate-bridged diiron complexes [Cp*Fe(mu-SR)3FeCp*] (Cp* = eta5-C5Me5 ; R = Et, Ph). *Organometallics*, 27(4):666–671, 2008.